HORSETOOTH RESERVOIR MODELING REPORT

FINAL

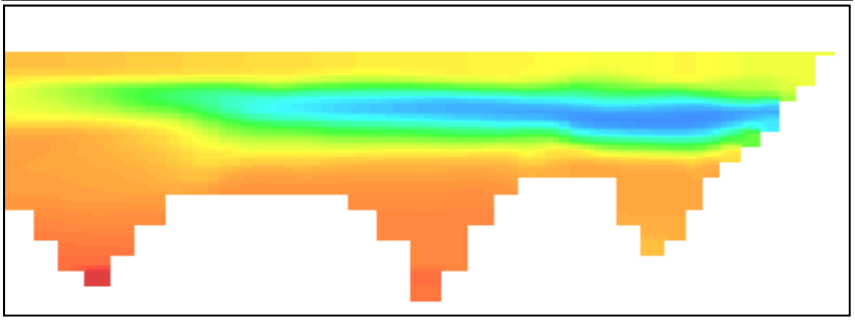

Prepared for:

Northern Colorado Water Conservancy District
Tri-Districts Soldier Canyon Filter Plant
The City of Fort Collins
The City of Greeley

Prepared by:

Christine Hawley

Jean Marie Boyer

Hydros Consulting

1731 Fifteenth St., Suite 103
Boulder, CO 80302

March 14, 2013

TABLE OF CONTENTS

LIST OF FIGURES

LIST OF TABLES

ACRONYMS AND ABREVIATIONS

AF	Acre-ft
AME	Absolute mean error
C	Celsius
C-BT	Colorado-Big Thompson
Chl *a*	Chlorophyll *a*
cfs	Cubic feet per second
CSU	Colorado State University
DBP	Disinfection by-products
DO	Dissolved oxygen
DOAP	Dissolved oxygen algal photosynthesis flux term
DOAR	Dissolved oxygen respiration flux term
DODOM	Dissolved oxygen dissolved organic matter decay flux term
DOM	Dissolved organic matter
DONITR	Dissolved oxygen nitrification flux term
DOOM	Dissolved oxygen organic matter decay flux term
DOPOM	Dissolved oxygen particulate organic matter decay flux term
DOREAR	Dissolved oxygen reaeration flux term
DOSOD	Dissolved oxygen sediment oxygen demand flux term
DUWS	Direct-use water supply
DWR	State of Colorado Division of Water Resources
EPA	U.S. Environmental Protection Agency
FCWTF	Fort Collins Water Treatment Facility
ft	Feet
F	Fahrenheit
GIS	Geographic Information System
HFC	Hansen Feeder Canal
L	Liter
LDOM	Labile dissolved organic matter
LPOM	Labile particulate organic matter
m	Meters

mg	Milligrams
Mn	Manganese
mph	Miles per hour
ND	Non-detect
NH3	Ammonia
NH4	Ammonium
NO2	Nitrite
NO3	Nitrate
NOAA	National Oceanographic and Atmospheric Administration
OM	Organic matter
PO4	Orthophosphate
RDOM	Refractory dissolved organic matter
RMSE	Root mean squared error
RPOM	Refractory particulate organic matter
SCFP	Tri-Districts Soldier Canyon Filter Plant
SOD	Sediment oxygen demand
TKN	Total Kjeldahl Nitrogen
TN	Total Nitrogen
TOC	Total Organic Carbon
TP	Total Phosphorus
TSS	Total Suspended Solids
ug	Micrograms
USBR	U.S. Bureau of Reclamation
USGS	U.S. Geological Survey
WQCD	Water Quality Control Division
WWTP	Wastewater Treatment Plant
WY	Water Year
Yr	Year

ACKNOWLEDGMENTS

Hydros Consulting would like to offer thanks to Northern Water for the opportunity to develop and apply this model of Horsetooth Reservoir. We would also like to thank the members of the technical committee that participated in project meetings and provided helpful direction and suggestions, including Judy Billica and Esther Vincent of Northern Water, Jill Oropeza of the City of Fort Collins, staff from the Tri-Districts Soldier Canyon Filter Plant, John McCutchan of the City of Greeley, Jesse Lepack of the Colorado Parks and Wildlife, George Parrish of the US EPA, Andrew Gilmore of the US Bureau of Reclamation, and Zack Shelley of the Big Thompson Watershed Forum. Finally, without direct support from Judy Billica, Esther Vincent, and Jen Stephenson in system conceptualization, water balance development, and data compilation, development of this model would not have been possible.

1 INTRODUCTION AND BACKGROUND

This report, sponsored and supported by Northern Water, the City of Fort Collins, the City of Greeley, and the Soldier Canyon Filter Plant, documents development and preliminary application of a dynamic, two-dimensional hydrodynamic and water-quality model for Horsetooth Reservoir. Water-quality concerns in the reservoir include metalimnetic and hypolimnetic low dissolved oxygen, manganese, total organic carbon, and occasional geosmin[1] outbreaks. Development of a water-quality model was commissioned to improve understanding of water-quality dynamics in the reservoir, and to provide a tool for use in simulation of any proposed future modifications to operations or inflow water quality. This document describes model construction, calibration, validation, and the results of preliminary scenarios. The following subsections provide a description of the reservoir and water-quality concerns, the project objectives, and the organization of this report.

1.1 SITE DESCRIPTION AND WATER-QUALITY CONCERNS

Horsetooth Reservoir is a terminal, off-stream storage reservoir for the Colorado-Big Thompson (C-BT) Project. Horsetooth Reservoir serves as a resource for public water supply, agricultural water supply, industrial water supply, and recreation. The reservoir, located in Larimer County at the edge of the foothills west of the City of Fort Collins, covers three canyons and was constructed between 1946 and 1949 with installation of four dams. The reservoir is over six miles long, flowing roughly north-northwest along its axis. It has a total capacity of 156,700 acre-ft (AF), and a maximum water depth of 188 ft. The Reservoir also has a number of distinct coves and bays on its south end and west side. Figure 1 shows the reservoir, bays and coves, and the location of the four dams.

[1] Geosmin is a compound produced by some species of cyanobacteria that causes taste and odor problems in drinking water.

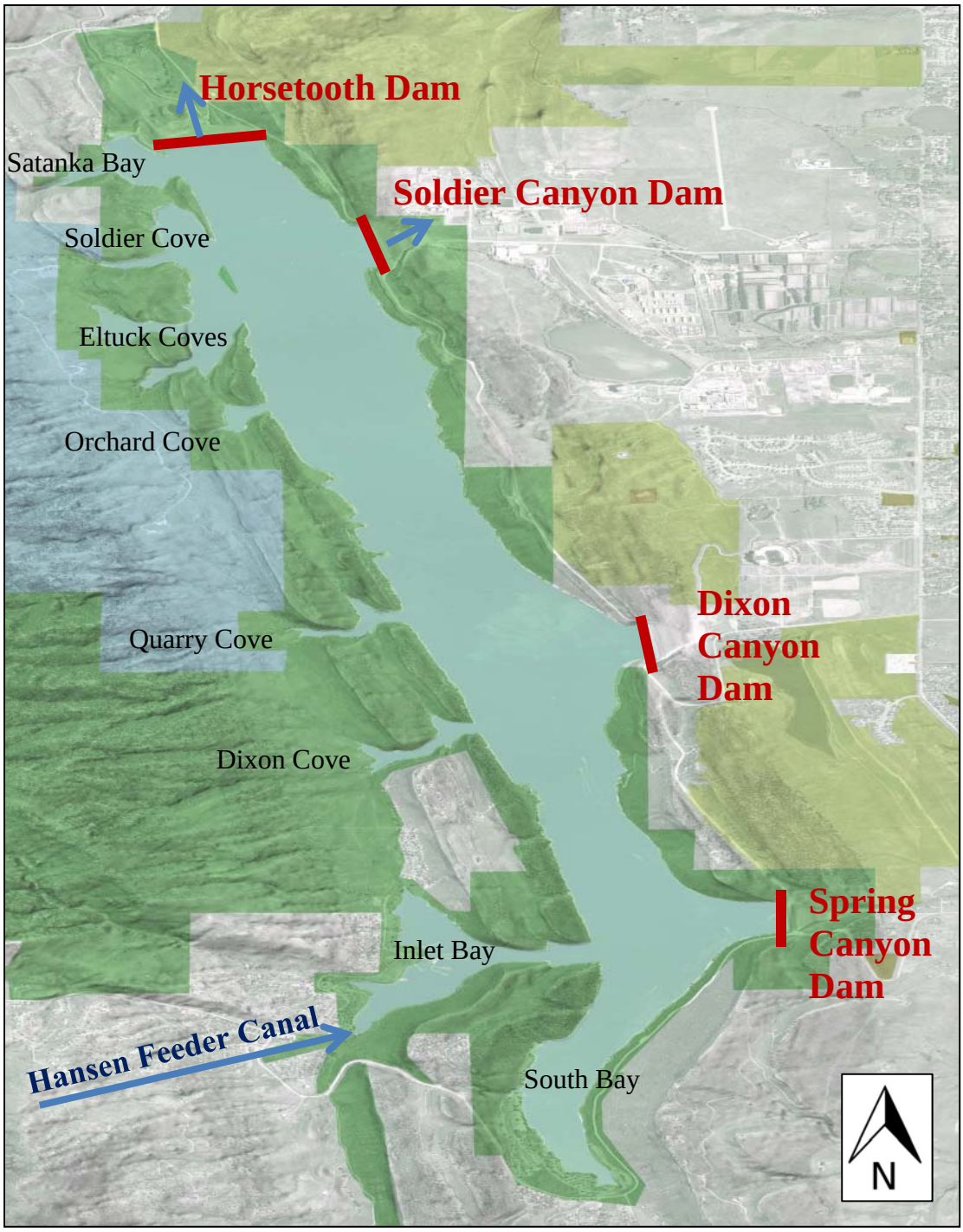

Figure 1. Horsetooth Reservoir

Water enters the reservoir via the Hansen Feeder Canal (Figure 1), which is managed as part of the C-BT Project. Water in the Hansen Feeder Canal is comprised of a mixture of native water from the Big Thompson watershed and water from the west slope Three Lakes System (via the trans-basin diversion structure, the Adams Tunnel). The water quality of these two sources varies seasonally and relative to one another. As such, the managed relative contribution from each source determines inflow water quality to Horsetooth Reservoir. The direct watershed is relatively small, with a 17 square mile area west of the reservoir providing direct runoff. Water is released from the reservoir through outlet works in the Soldier Canyon Dam and the Horsetooth Dam. Water released from Soldier Canyon Dam is routed to the Fort Collins Water Treatment Facility (FCWTF) and the Tri-Districts Soldier Canyon Filter Plant (SCFP). Water released from the Horsetooth Dam to the Hansen Supply Canal supplies the Greeley-Bellvue Water Treatment Plant and agricultural water users. The reservoir is presented in longitudinal profile in Figure 2 with the locations of the Hansen Feeder Canal, the outlets, and the basins associated with each canyon indicated.

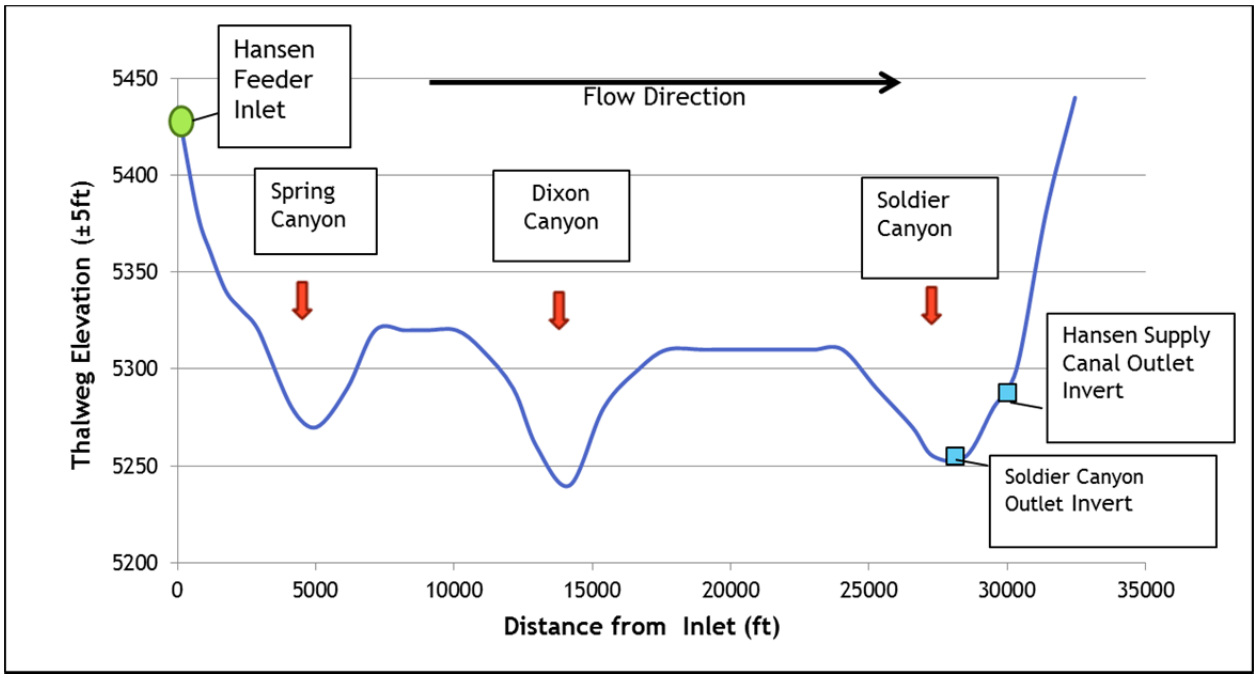

Figure 2. Lengthwise Profile of Horsetooth Reservoir

Several water-quality issues have been identified and studied in Horsetooth Reservoir (Jassby and Goldman, 1998; Jassby and Goldman, 1999; Johnson et al. 2006; Haby and Loftis, 2007; Lieberman, 2008; Billica and Oropeza, 2010). In 2006, Horsetooth Reservoir was added to the 303(d) list[2] due to frequently documented low dissolved oxygen (DO) concentrations (< 6 mg/l), particularly in the metalimnion. The noted concern in this listing was for the health of aquatic life. That listing has since been removed (CDPHE 2012a) due to changes in the assessment approach; however, the water quality in the reservoir has not changed significantly. The reservoir is currently on the 303(d) list for mercury (in fish tissue), copper, and arsenic concentrations (CDPHE 2012a).

In addition to dissolved oxygen concerns in the metalimnion, hypoxic (defined here as DO <2 mg/L) and anoxic conditions are observed in some areas at the bottom of the reservoir each year, typically in the late fall. Such conditions can lead to release of nutrients and other constituents such as manganese from the reservoir sediments. High manganese concentrations are problematic for water treatment. The outlet at Soldier Canyon Dam is a hypolimnetic withdrawal and elevated concentrations at the reservoir bottom can feed directly into the treatment facilities.

Total organic carbon (TOC) concentrations in this direct-use drinking water supply have also been a concern. Elevated concentrations of TOC can lead to the formation of disinfection by-products by reaction with chlorine during water treatment processes. TOC in the water column can also contribute to dissolved oxygen depletions through its degradation. Studies (Haby and Loftis, 2007; Hydros, 2011) have shown statistically-significant trends of increasing TOC concentrations in water at the east end of the Adams Tunnel. Haby and Loftis (2007) also found an increasing trend in TOC concentrations in water entering Horsetooth Reservoir from the Hansen Feeder Canal; however, the subsequent study by Hydros (2011) found no significant trend at this location for the longer period of record from 2000 through 2009.

Another water-quality concern is the occasional occurrence of geosmin (Billica et al., 2010). A geosmin outbreak in 2008 resulted in numerous taste and odor complaints. Geosmin is produced by certain cyanobacteria and actinomycetes. The City of Fort Collins now has a geosmin monitoring plan in place to act as an early warning system and to better understand geosmin-producing locations (in-reservoir and in the watershed) and conditions suitable to geosmin production.

[2] The 303(d) list is a list of water bodies or stream/river segments where water-quality concerns indicate that technology-based effluent limitations and other required controls alone are not stringent enough to allow the segment to meet standards. The list is required by Section 303(d) of the federal Clean Water Act and identifies segments for which Total Maximum Daily Loads (TMDLs) must be developed.

1.2 PROJECT OBJECTIVES

The primary objective of this project is to improve the understanding of what causes the observed water-quality in Horsetooth Reservoir. The focus is on key water-quality concerns of dissolved oxygen and total organic carbon; however, this will also require an understanding of stratification patterns, nutrient dynamics, and algal growth patterns. In addition to advancing the conceptualization of the system, there is a need to develop a numerical modeling tool that can simulate operational and inflow water-quality scenarios. Based on this, the following project goals were defined:

1. Develop a dynamic, numerical model that can simulate the following observed conditions from 2005 through September 2010:
    - Reservoir hydrodynamics,
    - Reservoir thermal stratification patterns,
    - Dissolved oxygen depletions in the metalimnion and hypolimnion across the length of the reservoir, and
    - Total organic carbon concentrations, particularly at the Soldier Canyon outlet.
2. Apply the model to a set of preliminary scenarios to develop a better understanding of:
    - Mechanisms causing metalimnetic and hypolimnetic low dissolved oxygen conditions,
    - The role of hydrodynamics and residence time on water quality, and
    - The role of inflow water quality in determining algal, dissolved oxygen, and TOC concentrations.

This report summarizes the work completed to meet these objectives. This work includes a review of existing data, development and testing of a numerical model, completion of a limited dissolved oxygen sensitivity analysis, and simulation of preliminary hypothetical scenarios to further investigate key system responses. It is anticipated that this investigation represents a first step in application and ongoing development of this modeling tool.

1.3 REPORT ORGANIZATION

This report is organized into six main report sections, with four appendices presenting the supporting figures and tables. The main report is organized as follows:

- Section 1 is the introductory section.
- Section 2 presents an overview of the findings from the review of existing relevant hydrologic, meteorological, and water-quality data.

- Model development and testing are documented in Section 3. This section includes a description of the modeling software and model construction steps taken. Additionally, this section presents calibration and validation of the model.
- Preliminary scenario simulation results are described in Section 4. This includes simulations to evaluate dissolved oxygen sensitivity and response as well as simulations varying residence time and inflow concentrations.
- Section 5 summarizes the findings and recommendations generated in the investigation.
- Finally, Section 6 provides references cited.

The supporting appendices are organized as follows:

- Appendix A presents temperature profiles of observed and simulated data for calibration and validation simulation periods.
- Appendix B presents water-quality plots of observed and simulated data for the combined calibration and validation period.
- Appendix C presents dissolved oxygen profiles of observed and simulated data for the combined calibration and validation period.
- Appendix D provides tabular summaries of preliminary scenario simulation results for key parameters.
- Appendix E presents the CE-QUAL-W2 control file for the full calibration and validation run.

2 REVIEW OF EXISTING DATA

Hydrologic, meteorological, and water-quality data were reviewed in detail to provide a conceptual system understanding to serve as a basis for model development. Review of existing data focused on the six year period of 2005 through September 2010. This period of record was selected for its completeness at the time of the start of this project and its timing relative to the reservoir drawdown. Between 2000 and 2004, Horsetooth Reservoir was drawn down to 4% of its normal volume to allow for maintenance work on the dams (Figure 3). Data from the drawdown period are not expected to reflect current operating conditions, and data prior to this period are sparse. In addition to review of existing data, the following studies of the reservoir were also reviewed:

- Studies by Ecological Research Associates for City of Fort Collins Utilities (Ecological Research Associates, 1996; Jassby and Goldman, 1998; and Jassby and Goldman, 1999);
- Physical Chemical and Biological Characteristics of Horsetooth Reservoir (Lieberman, 2008);
- Ecosystem Monitoring During Horsetooth Refilling (Johnson et al., 2006);
- Horsetooth Reservoir Water Balance and TOC Evaluation (INTERA and CH2MHill, 2006);
- Haby and Loftis (2007); and
- 2009 Horsetooth Water Quality Monitoring Report (Billica and Oropeza, 2010).

Photo: Ben Alexander, taken from Johnson et al., 2006

Figure 3. Aerial Image of Horsetooth Reservoir during Dam-Maintenance Drawdown

Key findings from the review of existing site data are discussed in the following subsections. Presentation of the complete detailed analysis and full dataset is beyond the scope of this report. Northern Water is currently preparing a report on hydrology and water quality in lakes and reservoirs including Horsetooth Reservoir, which will be issued in 2013 (Personal Communication, Billica, 2013).

Additionally, these flow and water-quality data are available at the Northern Water website (http://www.northernwater.org/).

2.1 HYDROLOGY

Hydrologic data were compiled from the following sources by Northern Water to create a water balance for Horsetooth for the focus period of record (2005 through September 2010):

- U.S. Bureau of Reclamation (USBR),
- State of Colorado Division of Water Resources (DWR),
- Northern Water,
- City of Fort Collins,
- Tri-Districts Soldier Canyon Filter Plant,
- Colorado State University (CSU; precipitation data),
- Colorado's Decision Support System (CDSS), and
- City of Greeley.

Inflows to Horsetooth Reservoir include Hansen Feeder Canal flows, precipitation, and runoff from the direct watershed. Water flows into the reservoir via the Hansen Feeder Canal throughout the year, typically with a two week hiatus in the fall. Flow rates are variable, ranging from 10 cfs to 500 cfs, as shown on Figure 4. As discussed previously, this water is a mixture of water from the Adams Tunnel and from the Big Thompson watershed. Typically, water from the Big Thompson River comprises the majority of inflows during the snowmelt runoff season (Billica and Oropeza, 2010).

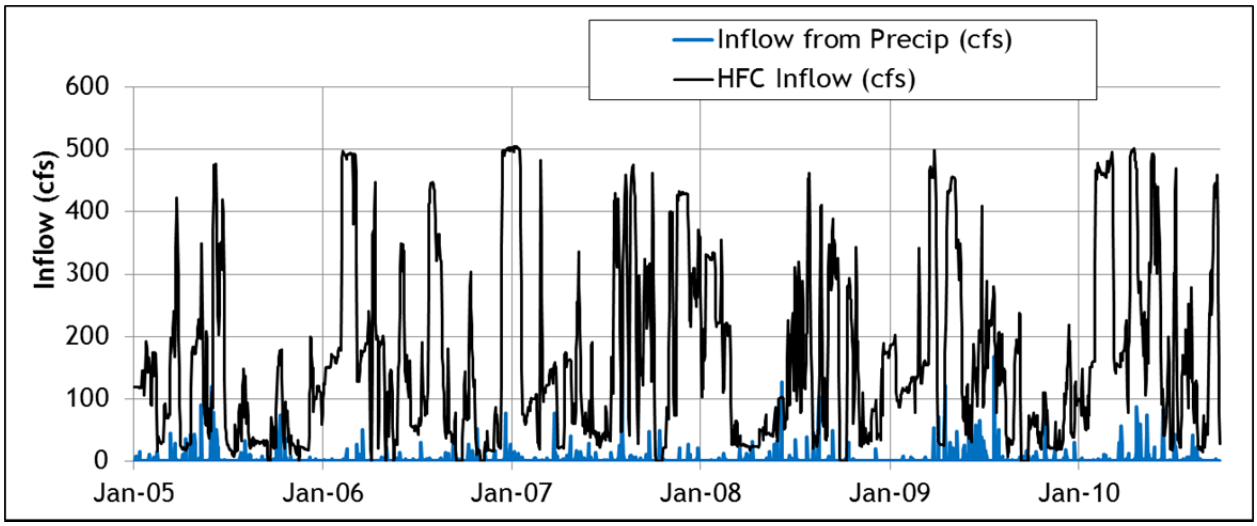

Figure 4. Daily Inflow Record to Horsetooth Reservoir

On average, direct precipitation comprises approximately 1.8% of the total reservoir inflow, and direct runoff from the small direct watershed was assumed to be negligible for the purposes of the water balance. Total inflow to the reservoir can vary widely from year to year in response to operations driven by hydrology and demands. Figure 5 presents total annual (calendar year) inflow to Horsetooth from the Hansen Feeder Canal and direct precipitation from 2005 through 2010 (Note: 2010 includes only January through September).

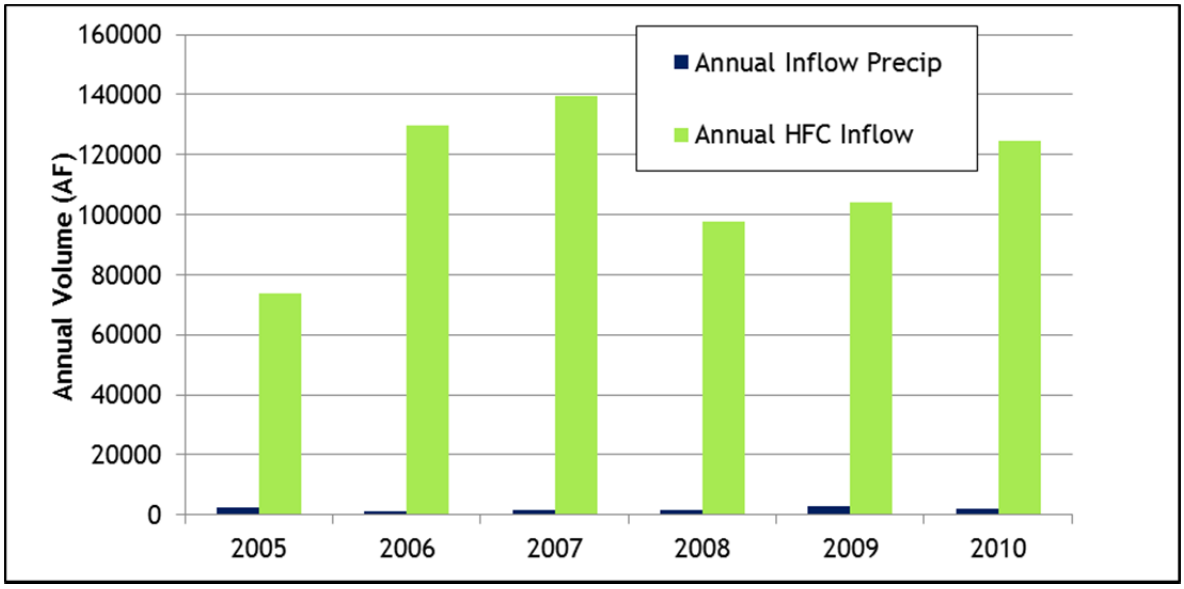

Figure 5. Annual (Calendar Year) Total Inflows to Horsetooth Reservoir (2005 through September 2010)

Outflows and losses from Horsetooth Reservoir include managed releases at Soldier Canyon, managed releases at Horsetooth Dam to the Hansen Supply Canal, seepage, and lake evaporation. Water is released at Soldier Canyon year round, with higher flow rates typically between March and November. The Hansen Supply Canal typically only receives water from Horsetooth from May through October, though flow rates are much higher than those out of Soldier Canyon. Figure 6 presents the daily outflows from Horsetooth based on the water balance from 2005 through September 2010. The seepage estimate is a constant 7 acre-ft/day, and lake evaporation is 0.73 times pan evaporation rates.

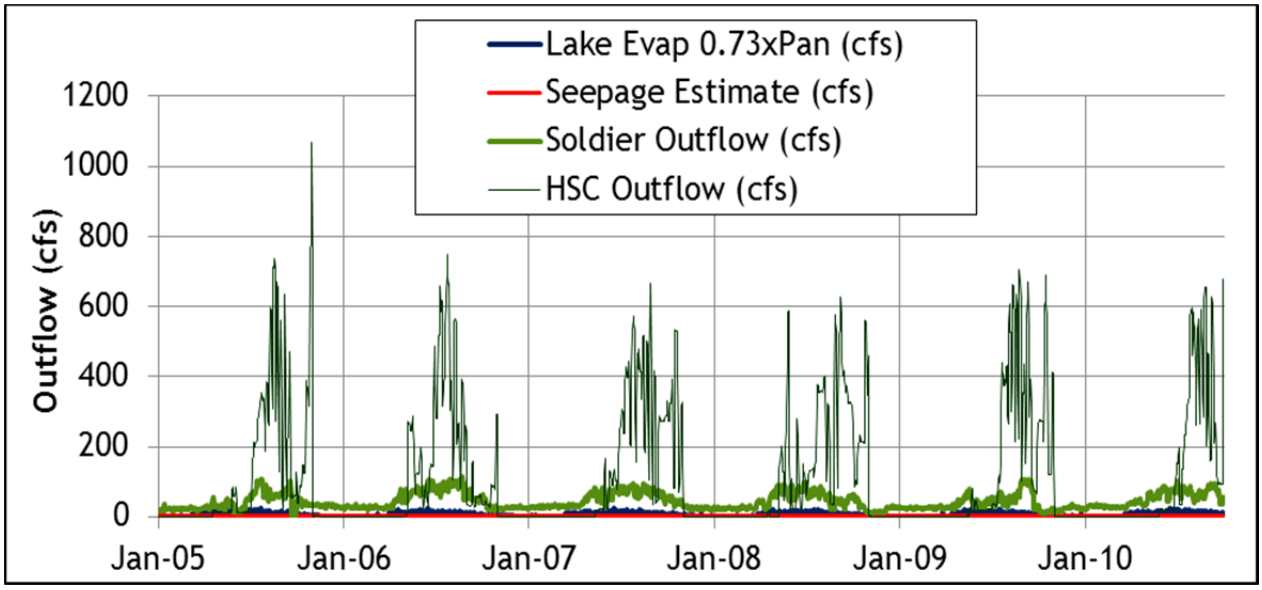

Figure 6. Daily Outflow Record to Horsetooth Reservoir

On an annual basis, flow out of Horsetooth Dam to the Hansen Supply Canal is typically more than twice the total flow out at Soldier Canyon. Evaporation and seepage make up a small percentage of the water balance, averaging 4% and 2% of outflows, respectively. Figure 7 presents total annual (calendar year) outflow volumes from Horsetooth for each of these water balance terms from 2005 through 2010 (Note: 2010 includes only January through September).

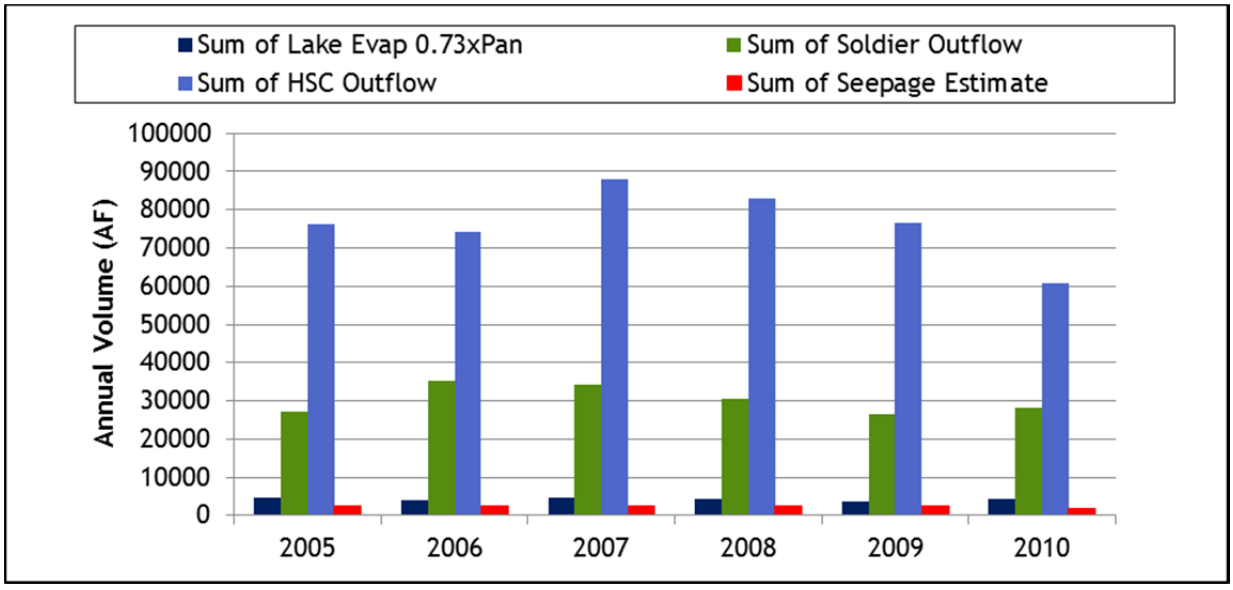

Figure 7. Annual (Calendar Year) Total Outflow Volumes from Horsetooth Reservoir (2005 through September 2010)

Water levels in Horsetooth Reservoir vary annually by roughly 40 and 60 ft for this period of record. The filling pattern causes water levels to be lowest in the winter and highest in the summer. Figure 8 shows the water surface elevation record from 2005 through September 2010.

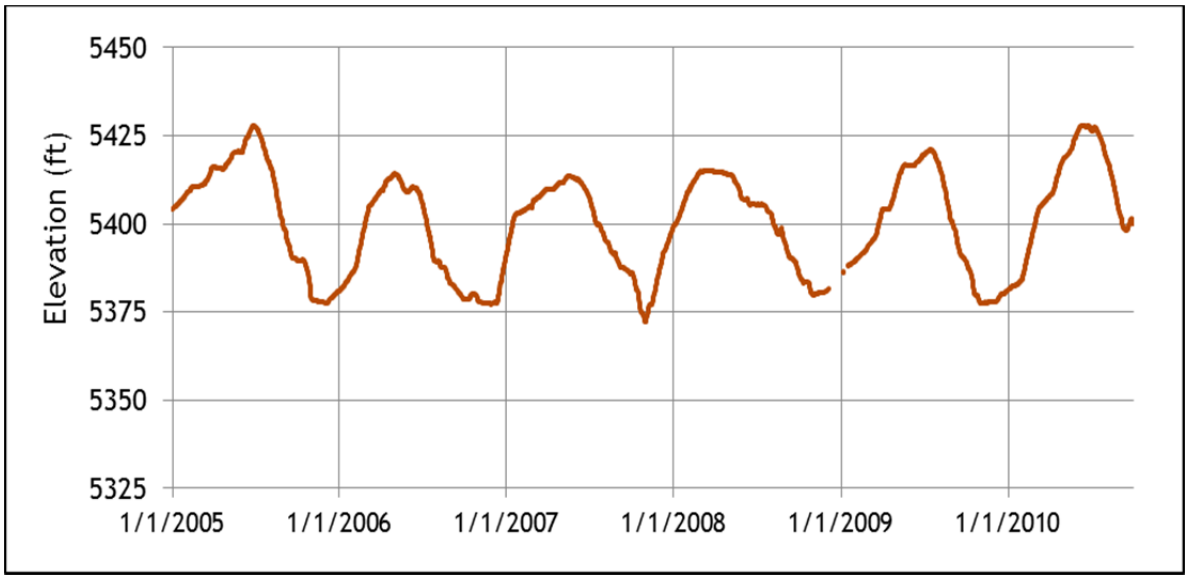

Figure 8. Water Surface Elevation Record for Horsetooth Reservoir

This operating range is shown in profile view on Figure 9. Based on the elevation-area-volume curves for the reservoir bathymetry, this variation range (shown in red on Figure 10) is in a fairly linear range of the surface area-to- elevation and volume-to-elevation curves.

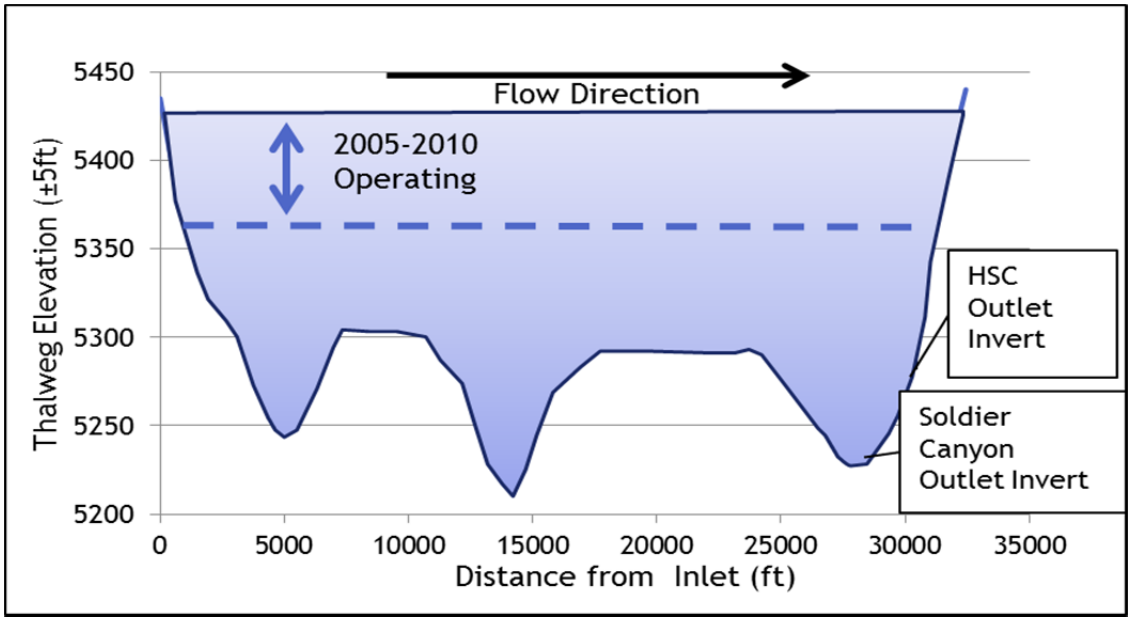

Figure 9. Profile View of Water Surface Elevation Range, 2005 through September 2010

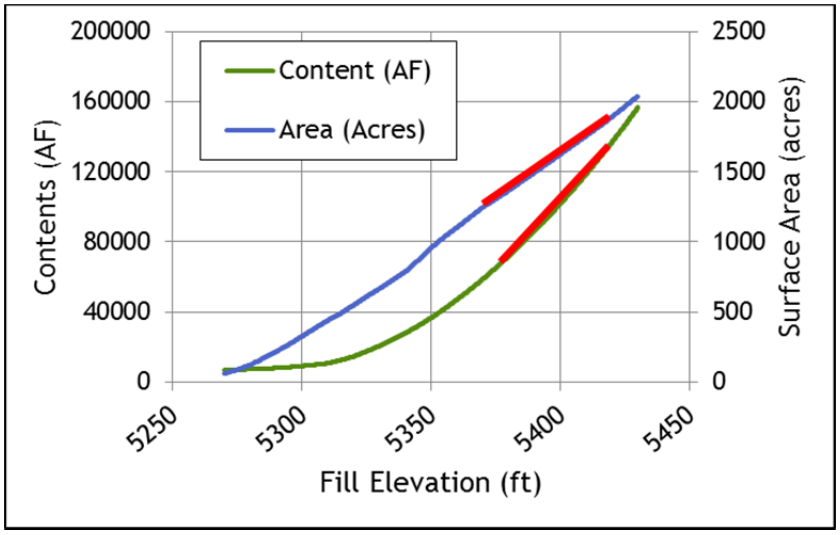

Figure 10. 2005 through September 2010 Water Surface Elevation Range Shown (in Red) on Elevation-Area-Volume Relationships

Based on outflow rates and reservoir contents, residence time was estimated on a calendar-year basis. Residence time between 2005 and 2010 varied between 0.76 and 1.0 year (Figure 11), with a residence time of 0.87 years when assessed over the full study period. Residence time based on inflows was also calculated, and the result was similar on a long-term basis (residence time of 0.91 years over the study period). These simple calculations assume complete mixing, which may not be a good assumption for Horsetooth Reservoir during all seasons.

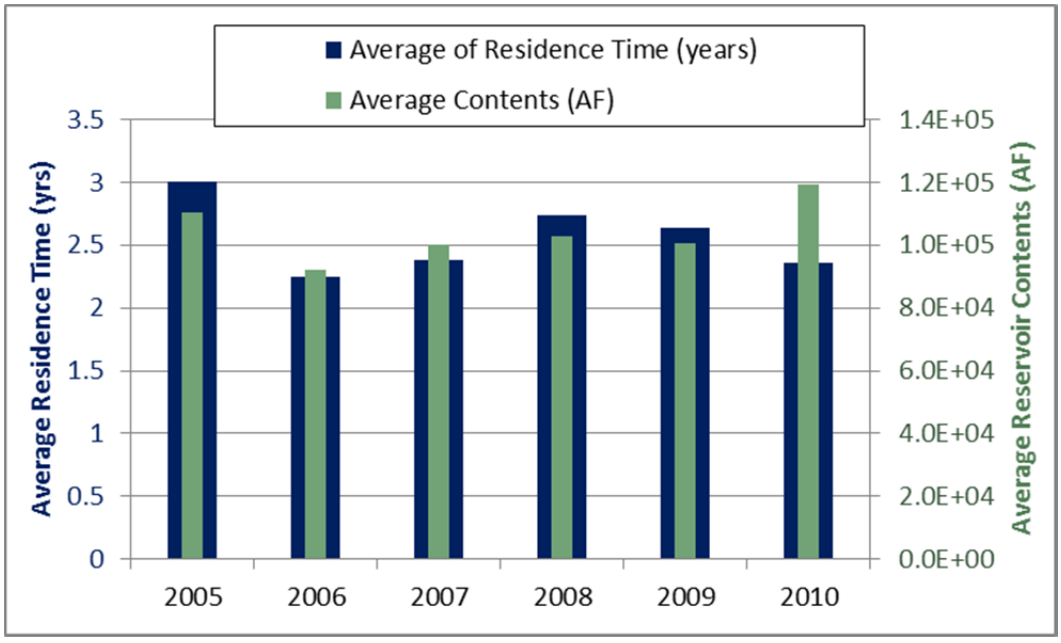

Figure 11. Calculated Calendar-Year Residence Time and Average Reservoir Contents for Horsetooth Reservoir (2005 through September 2010)

2.2 METEOROLOGY

Weather conditions can be a critical driving force in determination of reservoir water quality. Important parameters typically include air temperature, precipitation, wind speed, wind direction, cloud cover, and solar radiation. Weather data are collected at several stations near Horsetooth Reservoir. The following data were compiled for use in this project:

- CoAgMet (Colorado Agricultural Meteorological Network) station FTC01
    - Five-minute data for temperature, solar radiation, and relative humidity;
    - Located roughly 1.5 miles east of the north end of the reservoir.
- Fort Collins Airport
    - Hourly cloud cover data retrieved from hourly data sent to NOAA;
    - Located approximately 8.5 miles south and east of the reservoir.
- Christman Field Site (CSU)
    - Five-minute data for temperature, wind speed, and wind direction;
    - Located 0.5 miles east of the hogback that forms Horsetooth Reservoir.

Air temperature affects water temperature near the surface, and therefore affects reaction rates, growth rates, and stratification. Review of air temperature data show consistent larger patterns from year to year. Figure 12 presents daily minimum and daily maximum air temperatures from 2005 through September 2010. For this period, the highest observed temperature was 40°C (104°F) in 2005, and the lowest was -28°C (-18°F) in 2010.

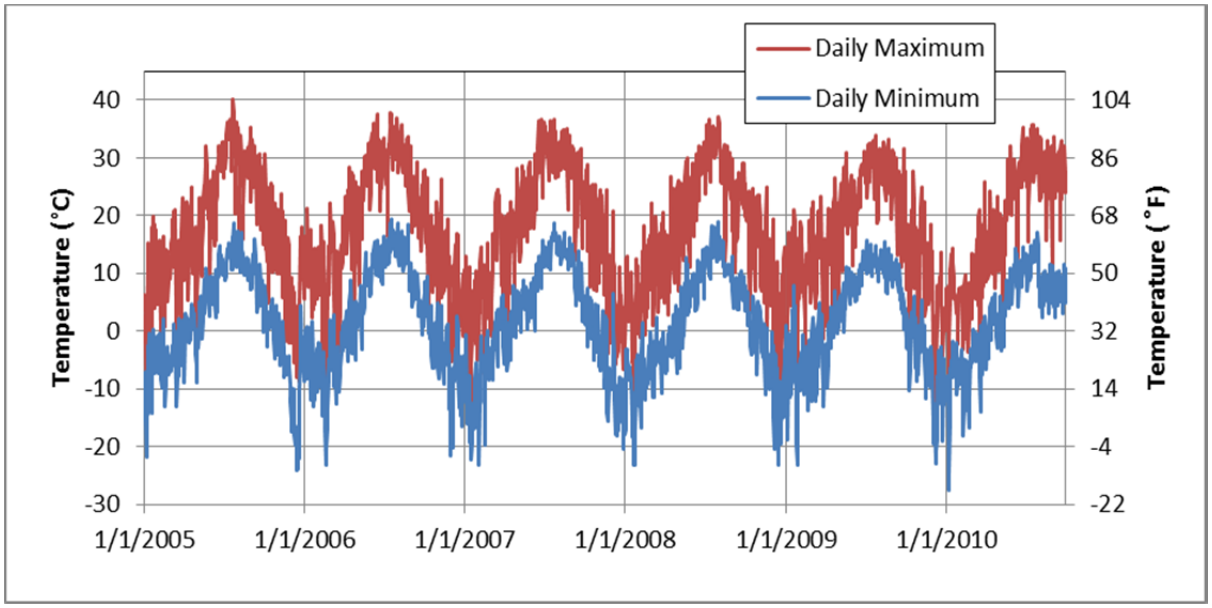

Figure 12. Daily Minimum and Maximum Air Temperature Record, Christman Field Site Data (2005 through September 2010)

Precipitation from 2005 through 2010 averaged 15.2 inches per year. Seasonal precipitation patterns vary from year to year, but typically the winter months of November through February have the lowest precipitation totals of the year (Figure 13). Of the years in focus, 2009 was relatively wet, with 21.8 inches observed for the year, reflecting high totals in April, June, and July.

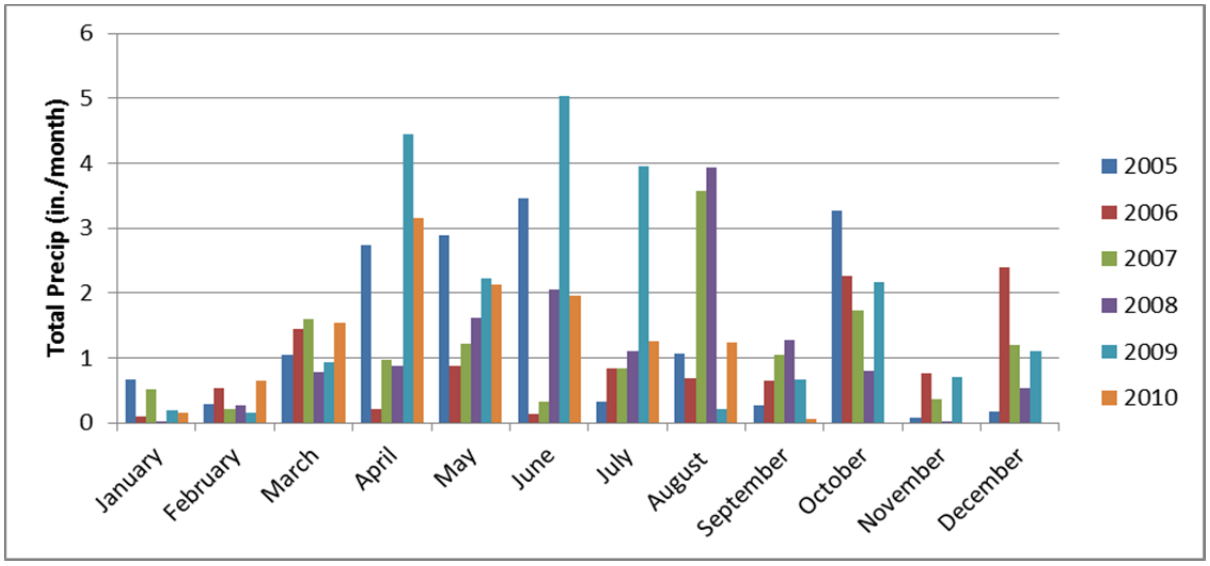

Figure 13. Average Monthly Precipitation Totals (2005 through September 2010)

Wind causes turbulence and mixing in a reservoir, which can affect stratification and distribution of materials in the water column. Wind direction is also important, defining the fetch (or length of water over which the wind is blowing). Wind data show that this area is a fairly windy place. Most days exhibit gusts of at least 10 mph. Upper range gusts reach 45 mph. Winds come from all directions, but most frequently come from the south-southwest, and less frequently from the north or northeast. Average daily wind speeds follow a generally consistent pattern from year to year, with lower average wind speeds observed in summer and fall (Figure 14).

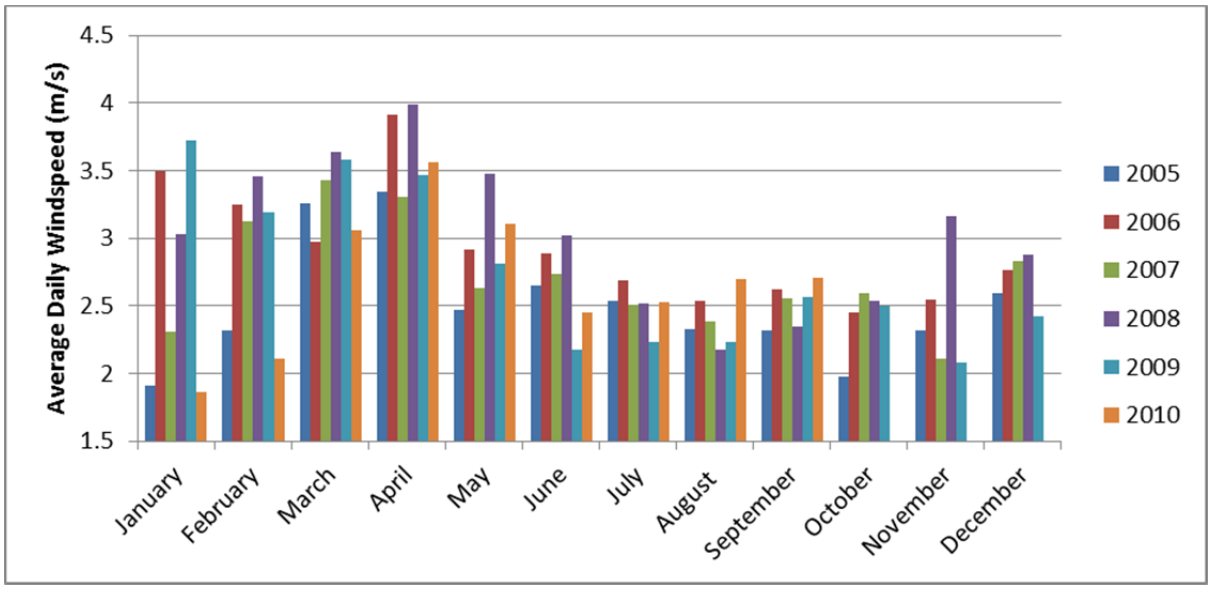

Figure 14. Average Monthly Wind Speed (2005 through September 2010)

Solar radiation is a measure of the radiant energy emitted by the sun. In combination with cloud cover, it can directly affect algal growth and water temperature, which in turn affects reaction rates and stratification. Each year, solar radiation is greatest in the summer months of June through September. Figure 15 presents the cumulative solar radiation data for each year of the focus time period. The highest summer cumulative solar radiation was observed in 2010, and the lowest was observed in 2006. Solar radiation in June of 2009 was low relative to other years, but by the end of the summer, cumulative values were similar to other years.

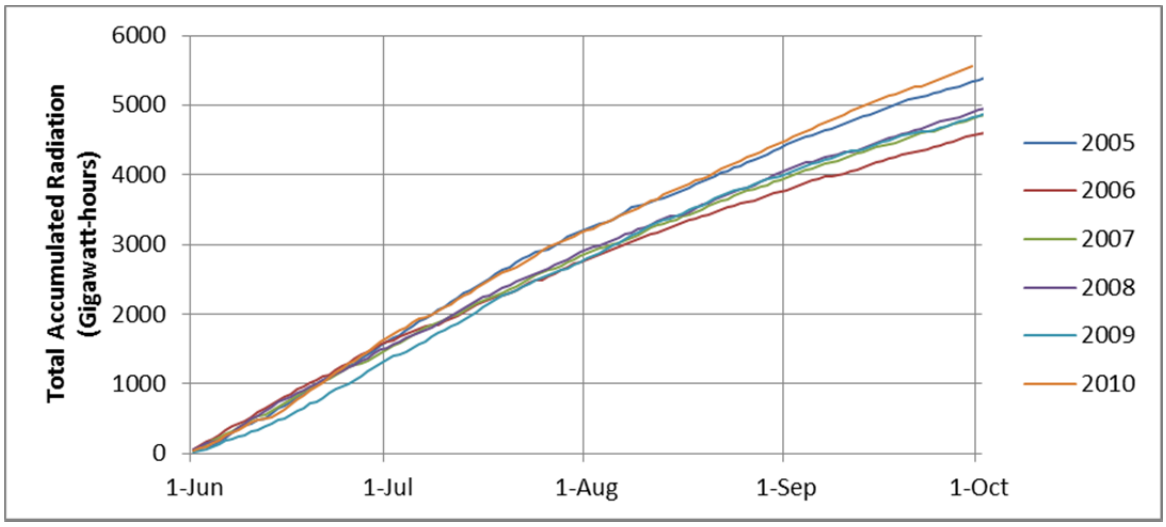

Figure 15. Cumulative Summertime Solar Radiation, June through September, 2005-2010

Cloud cover affects the amount of short wave solar radiation that reaches the reservoir, which in turn affects water temperatures and photosynthetic growth rates. In the absence of site-specific solar

radiation data, incident solar radiation can be estimated based on altitude, latitude, and cloud cover. Cloud cover data were compiled to provide options in modeling. The cloud cover data show variability over the years, but generally summer months exhibit less cloud cover, as shown in Figure 16.

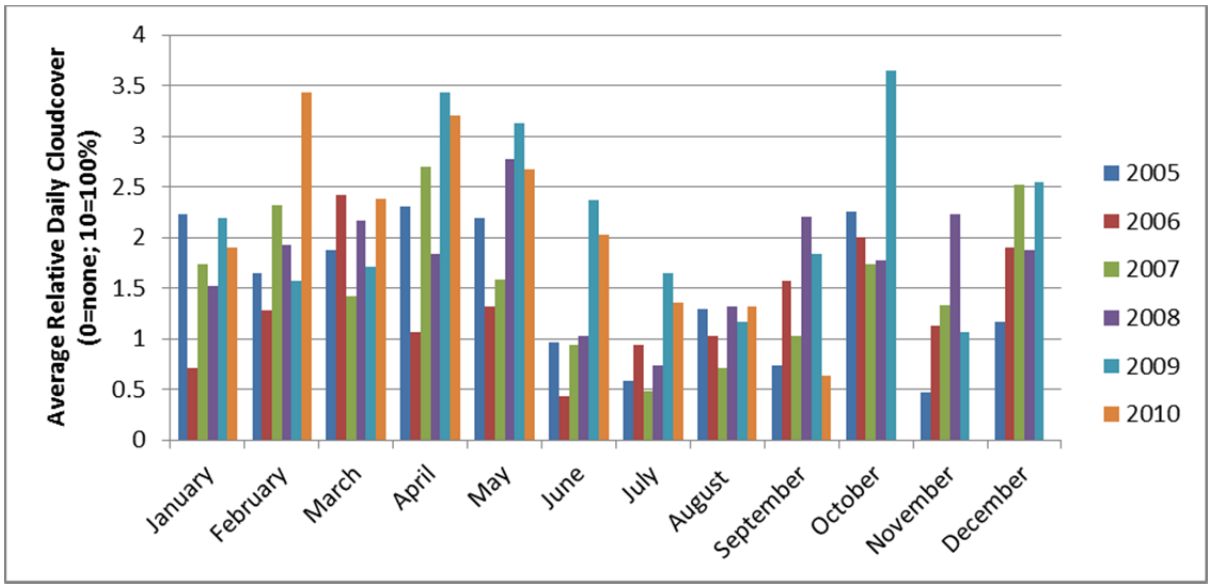

Figure 16. Average Relative Cloud Cover by Month, 2005 through September 2010

2.3 WATER QUALITY

Available water-quality data for inflow from Hansen Feeder Canal, in-reservoir sampling sites, and outflow from Soldier Canyon were compiled and reviewed to develop an understanding of seasonal patterns and system dynamics. Inflow and in-reservoir sampling stations are shown on Figure 17. Data from the following data sources were compiled into a single database by Northern Water for use in this project:

- Northern Water,
- USBR,
- USGS, and
- City of Fort Collins.

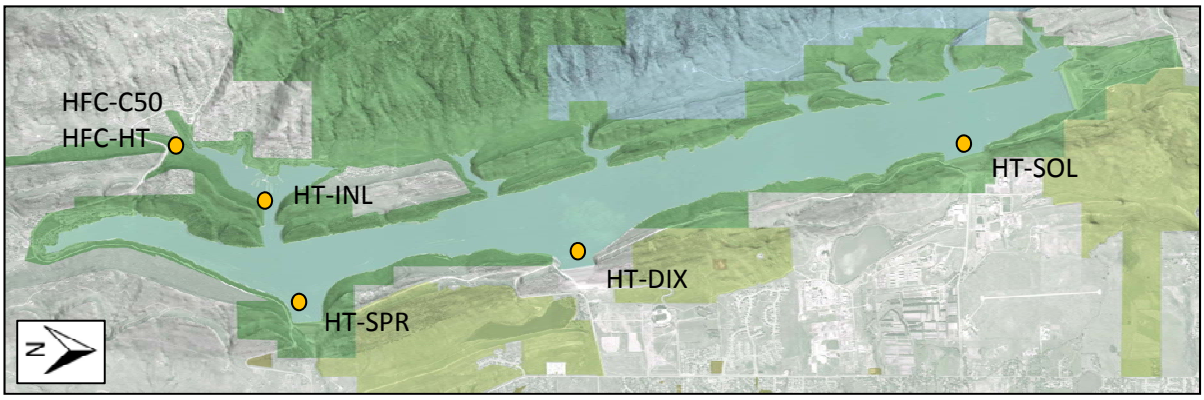

Figure 17. Water-Quality Sampling Locations on Horsetooth Reservoir

The following subsections present an overview of findings from the review water-quality data. As noted previously, presentation of the complete observed dataset is beyond the scope of this report, so the discussion and figures focus on summary findings relevant to development of the model. The discussions focus on stratification patterns, dissolved oxygen, manganese, total organic carbon, nutrients, and chlorophyll *a*. Inflow, in-reservoir, and outflow data are discussed, where available and relevant.

2.3.1 Temperature and Stratification

Review of temperature profile data from water-quality sampling locations in the reservoir indicates that the reservoir follows a classic stratification-turnover pattern for a dimictic water body. Figure 18 presents the thermal stratification and turnover in 2009, as observed at the Spring Canyon sampling station (HT-SPR) and at the Soldier Canyon sampling station (HT-SOL), respectively. The black areas at the bottom of each figure are included to allow for representation of the changing water depth of each location over the year. Stratification begins to develop in late April/early May at both locations. Through the summer, warming from above causes the depth of the metalimnion to gradually deepen until the reservoir turns over in October. From year to year, the reservoir is typically stratified for 140 to 180 days. Review of the temperature data indicate that turnover typically occurs sooner, by one or two weeks, at Soldier Canyon, possibly reflecting the hydrodynamic effects of bottom withdrawals at the north end of the reservoir in the fall.

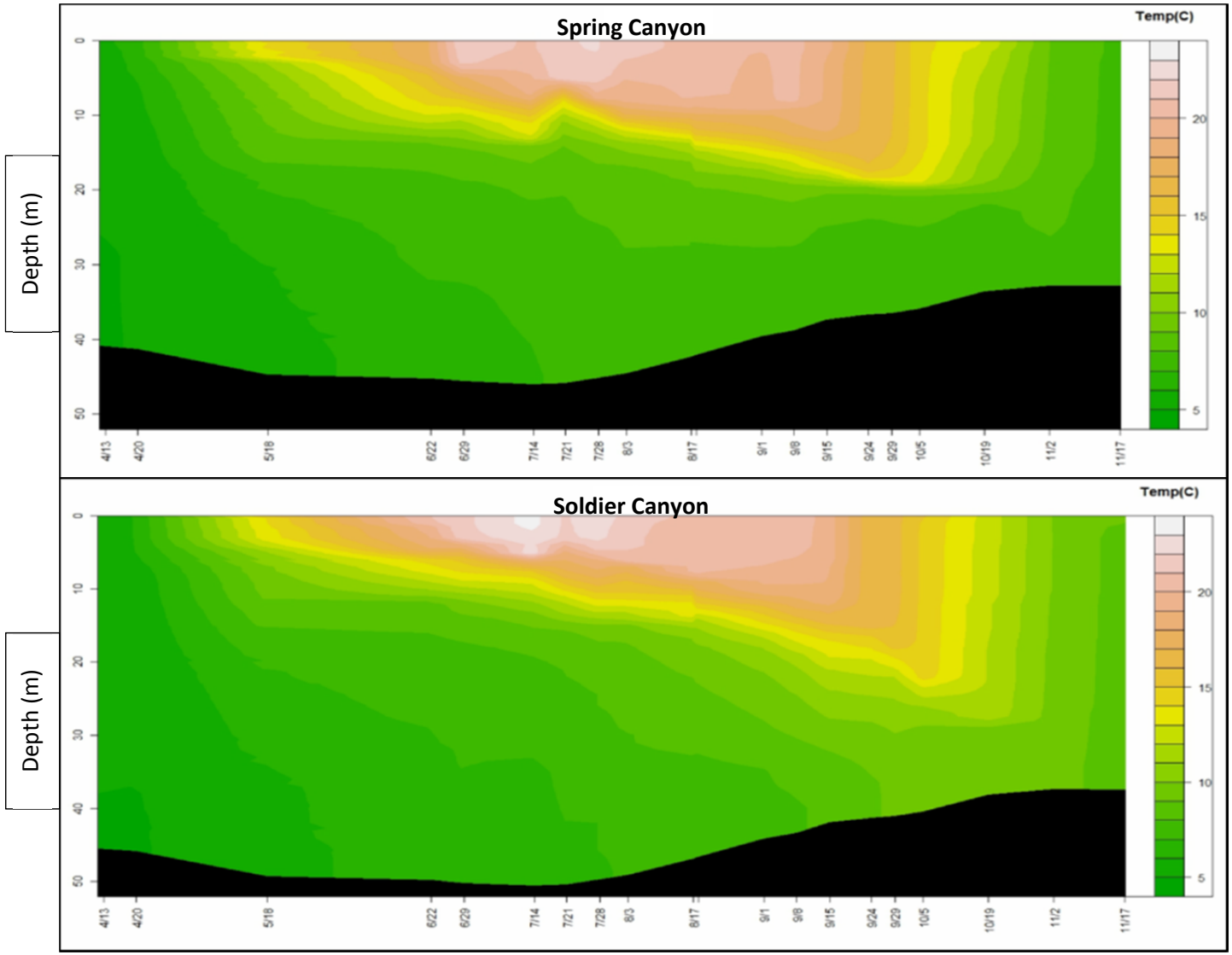

Figure 18. Temperature Isopleths of 2009 at Spring Canyon and Soldier Canyon

The temperature of water flowing in from Hansen Feeder Canal will determine the depth/stratum at which it enters the reservoir during stratification because water temperature is a primary determinant of fresh water density. Inflow water temperatures in the Hansen Feeder Canal follow typical seasonal patterns (Figure 19). Overlaying the time series temperature for 2009 on the Spring Canyon isopleth plot (Figure 20) gives a good indication of where inflow water will go after entering the reservoir during stratification. As shown on Figure 20, during stratification, the temperature of the Hansen Feeder Canal water generally matches that of the metalimnion throughout the stratified period. Based on this, inflow during stratification would likely "plunge" to the depth of the metalimnion after entering the reservoir.

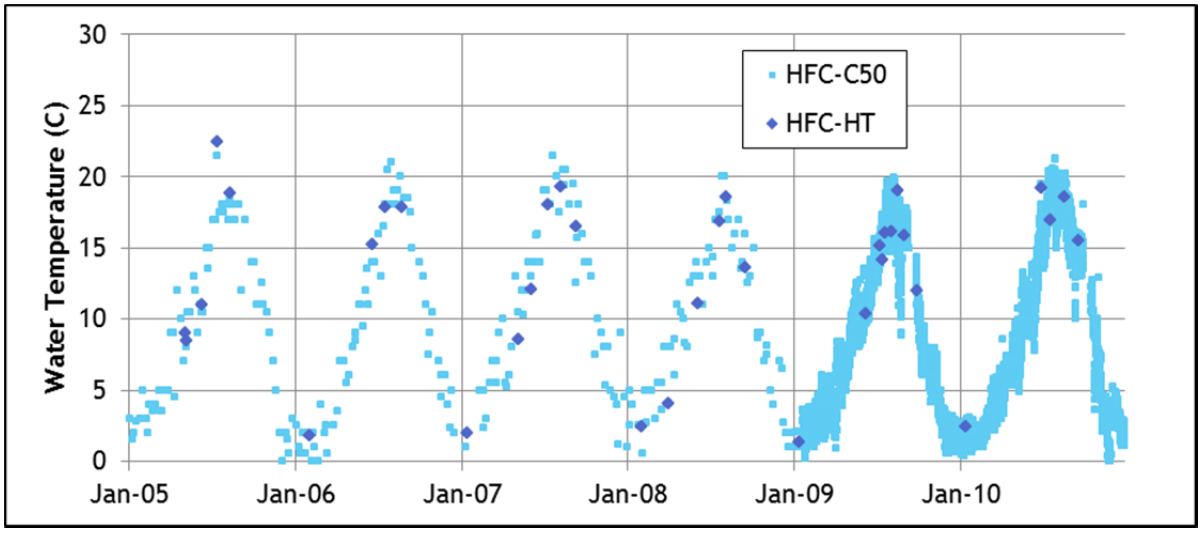

Figure 19. Hansen Feeder Canal Inflow Temperature Record, 2005 through 2010
Note: HFC-C50 observation frequency increase to every four hours in 2009.

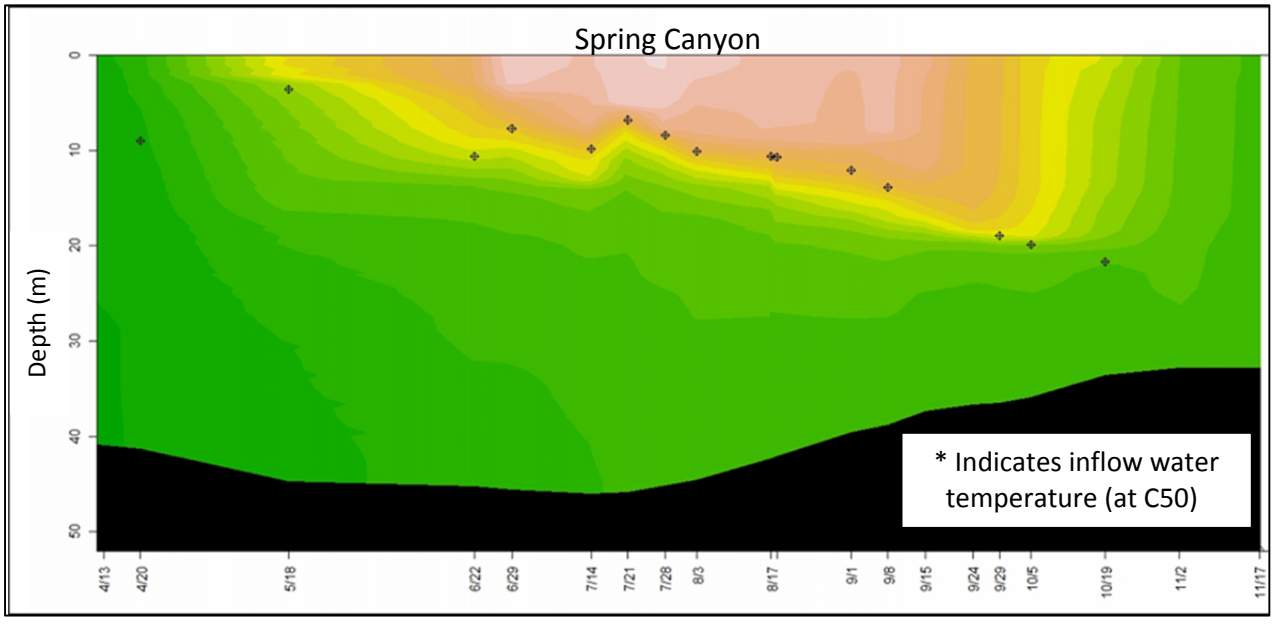

Figure 20. Spring Canyon 2009 Isolpleth with Indicators of Hansen Feeder Canal Inflow Temperatures

While the temperature data indicate that Hansen Feeder Canal inflows enter the reservoir at the metalimnion during stratification, specific conductivity data give an indication of the extent to which mixing decreases this signal across the reservoir. Water in the Hansen Feeder Canal has lower specific conductivity than in-reservoir water for much of the stratified period. Figure 21 shows the specific conductivity data record for Hansen Feeder Canal inflows, which generally follows a consistent seasonal pattern reflecting reduced specific conductivity from snowmelt runoff each year. The effects of operational changes to Hansen Feeder Canal composition are apparent in the more recent four-hour frequency records (since 2009).

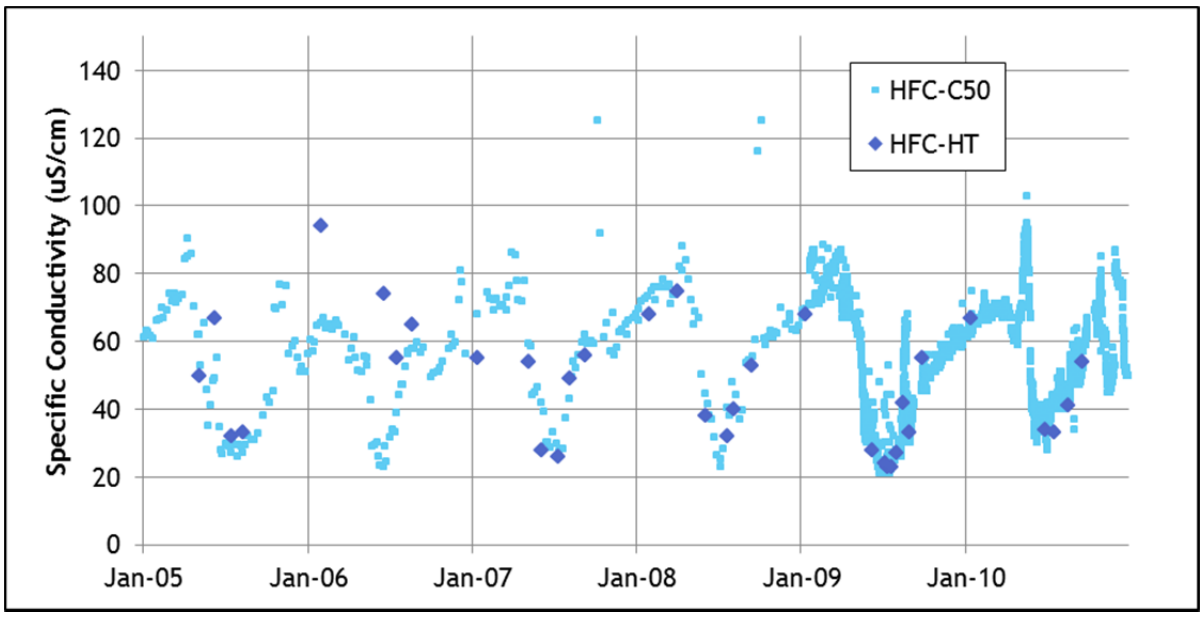

Figure 21. Hansen Feeder Canal Inflow Specific Conductivity Record, 2005 through 2010
Note: HFC-C50 observation frequency increase to every four hours in 2009.

The lower conductivity signal of the inflow is apparent in the metalimnion in isopleths generated from specific conductivity profile data (Figure 22). While the low conductivity signal in the metalimnion during stratification is diminished by the time it reaches Soldier Canyon due to mixing, the data do indicate that the inflow through the metalimnion during stratification extends, at least to some extent across the reservoir to Soldier Canyon. Additionally, the effects of operations are apparent in this specific conductivity signal. First, when higher rate outflows to the Hansen Supply Canal at the Horsetooth Dam began in mid-July of 2009, the metalimnion low-conductivity signal became stronger at the north end of the reservoir at Soldier Canyon (see blue line on Figure 22). Next, when the regularly-scheduled two-week shutdown of the Hansen Feeder Canal occurred in 2009 (Sept. 11 through Sept. 25), there was a corresponding shift in the specific conductivity pattern in the metalimnion (see red line on Figure 22).

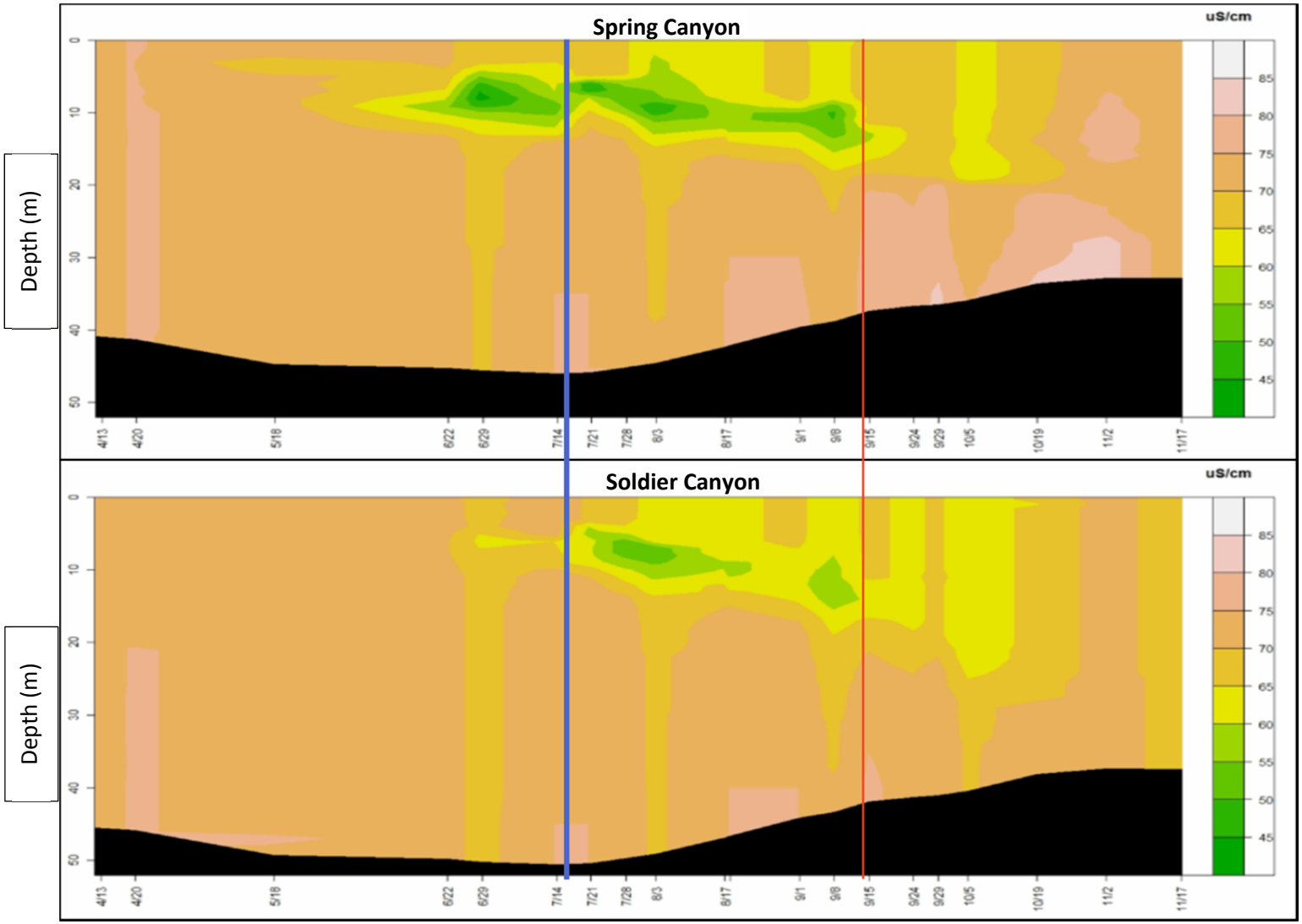

Figure 22. Specific Conductivity Isopleths of 2009 at Spring Canyon and Soldier Canyon
Blue line indicates increase in outflow rate at Hansen Supply Canal; red line indicates start of two-week maintenance closure of Hansen Feeder Canal

2.3.2 Dissolved Oxygen

Dissolved oxygen in the reservoir exhibits metalimnetic and hypolimnetic depletions during stratification each year. The metalimnetic low develops first, producing a negative heterograde curve, as shown in the August 18, 2009 profiles in Figure 23. Figure 24 shows the metalimnion dissolved oxygen concentration patterns from 2005 through 2010. The magnitude of the annual minimum dissolved oxygen concentration in the metalimnion ranges from roughly 2 mg/L to 4 mg/L. Patterns are fairly consistent across the reservoir, and there is no obvious long-term trend of increasing or decreasing effect over these years since refilling in 2004, though a statistical analysis was not conducted.

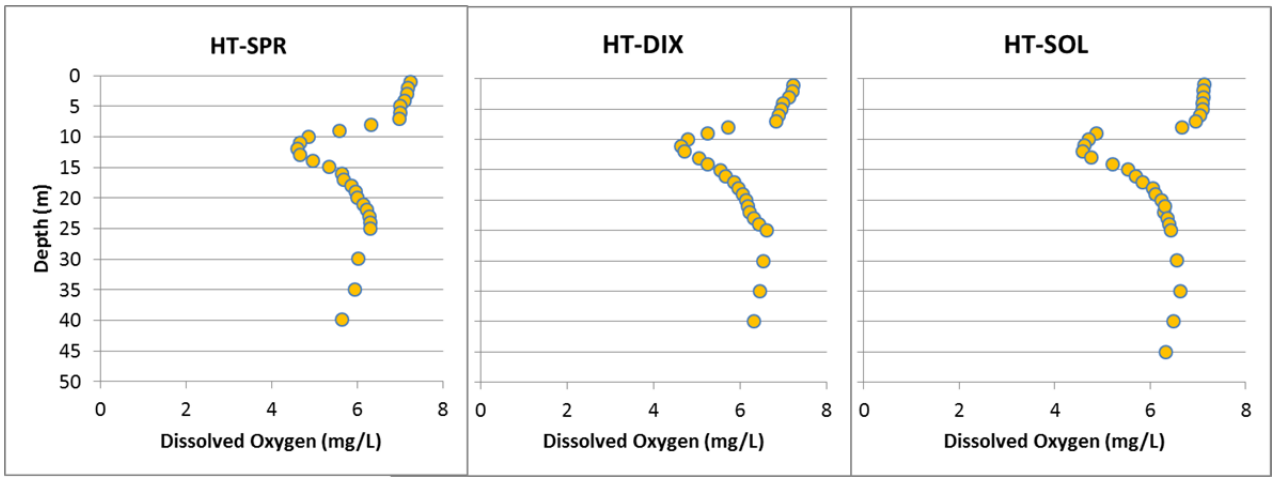

Figure 23. Observed Dissolved Oxygen Profiles from August 18, 2009 at Spring Canyon, Dixon Canyon, and Soldier Canyon

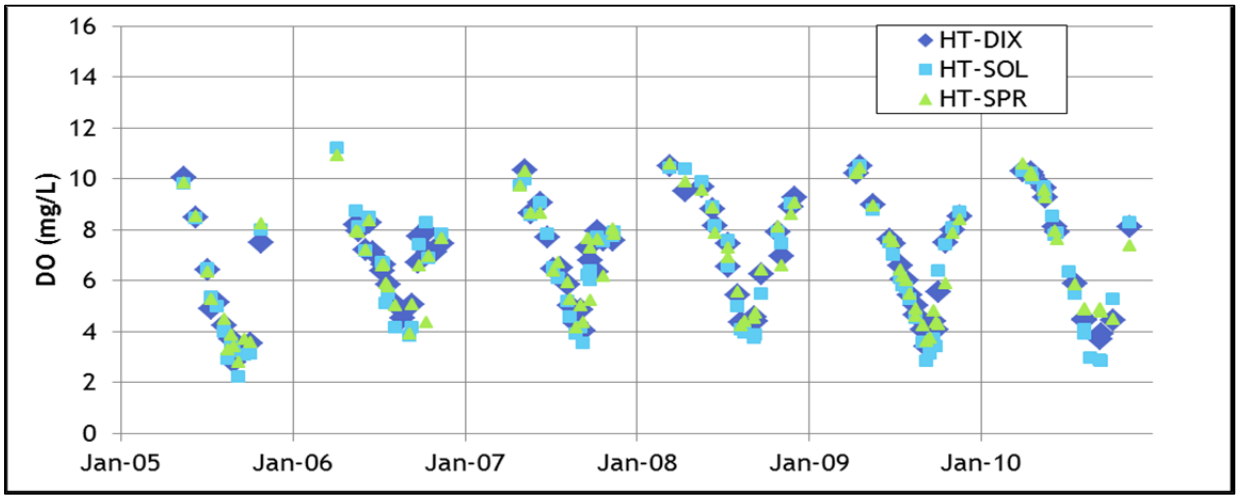

Figure 24. Metalimnetic Dissolved Oxygen Minima Time Series (Minimum Dissolved Oxygen Concentrations between 0 m and 20 m Depth), 2005 through 2010

The hypolimnetic low dissolved oxygen develops throughout stratification across the reservoir. Figure 25 presents the time series of minimum dissolved oxygen concentrations at the bottom of the reservoir. Annual minimum hypolimnetic concentrations across the reservoir vary between 0 mg/L and ~2 mg/L. There is more spatial variability in minima at the bottom of the reservoir than in minima in the metalimnion. Spring Canyon tends to exhibit the lowest hypolimnetic dissolved oxygen concentrations, followed by Dixon Canyon, then Soldier Canyon. From year to year, the patterns are fairly consistent, and there is no obvious long-term trend in this six-year, post-drawdown dataset.

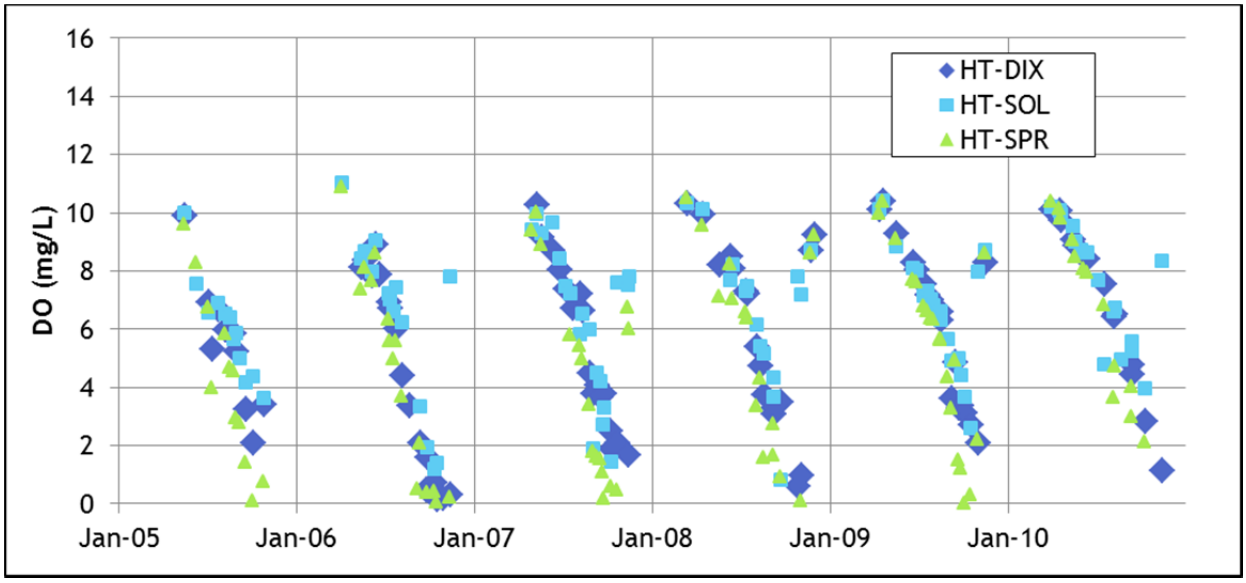

Figure 25. Hypolimnetic Dissolved Oxygen Minima Time Series (Minimum Dissolved Oxygen Concentrations between 30 m and the Bottom), 2005 through 2010

Isopleths of dissolved oxygen concentrations for 2009 at Spring Canyon and Solider Canyon are presented in Figure 26. This figure shows the distinct metalimnetic and hypolimnetic low dissolved oxygen concentrations and the differences, particularly in hypolimnetic dissolved oxygen across the reservoir. The duration and magnitude of hypolimnetic low dissolved oxygen concentrations are greater each year at Spring Canyon, as compared to Soldier Canyon. This difference may reflect the hydrodynamic mixing effects of withdrawals from the bottom of the reservoir at Soldier Canyon and Horsetooth Dam. There may also be spatial differences in sediment oxygen demand. Spring Canyon may have higher organic matter content in sediment due to settling of inflow suspended solids from Hansen Feeder Canal.

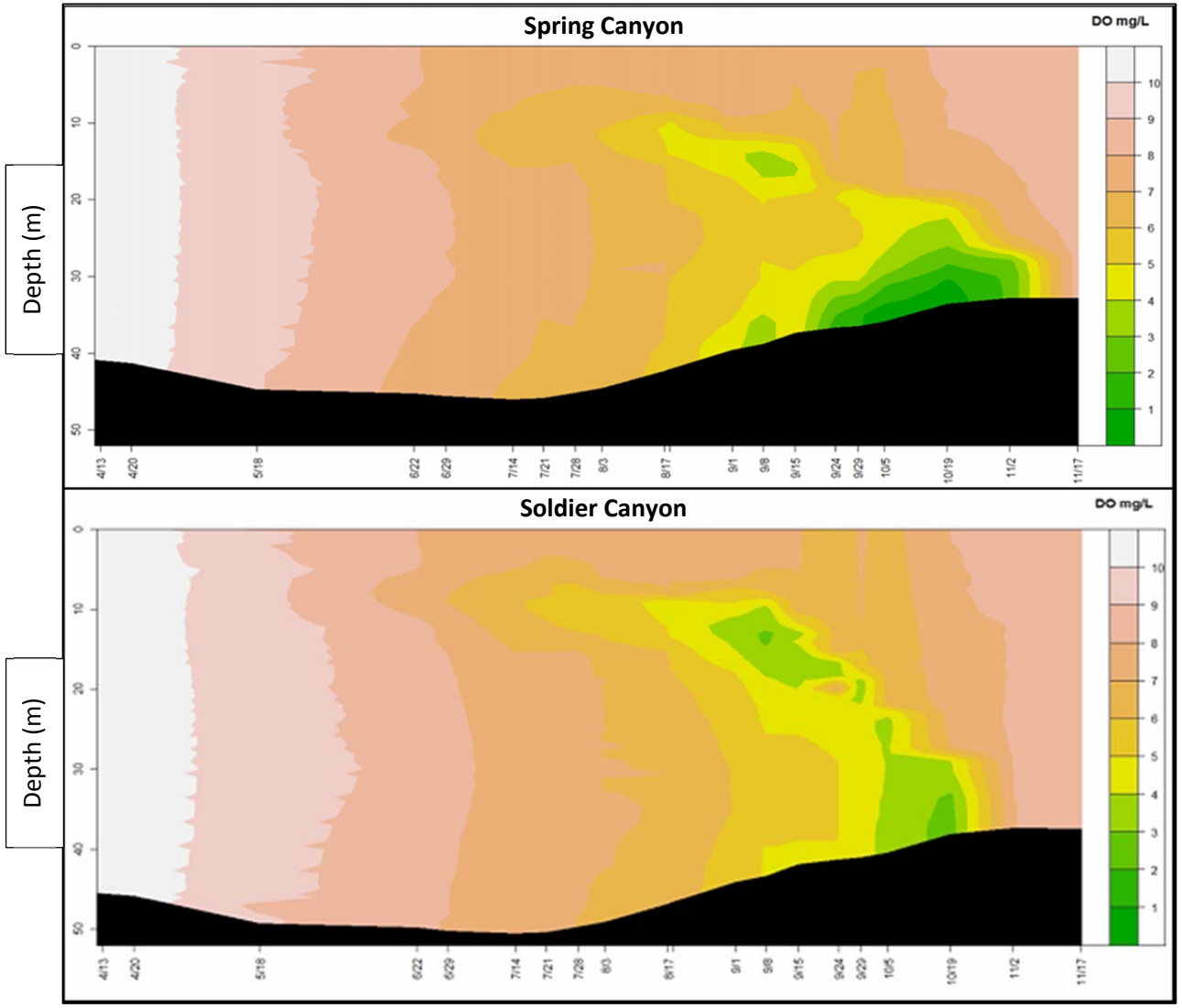

Figure 26. Dissolved Oxygen Isopleths of 2009 at Spring Canyon and Soldier Canyon

2.3.3 Manganese

Dissolved manganese concentrations in outflow from Horsetooth Reservoir have periodically been problematic for water treatment facilities. Figure 27 presents manganese concentrations in the outflow at Soldier Canyon as measured by the City of Fort Collins Utilities.

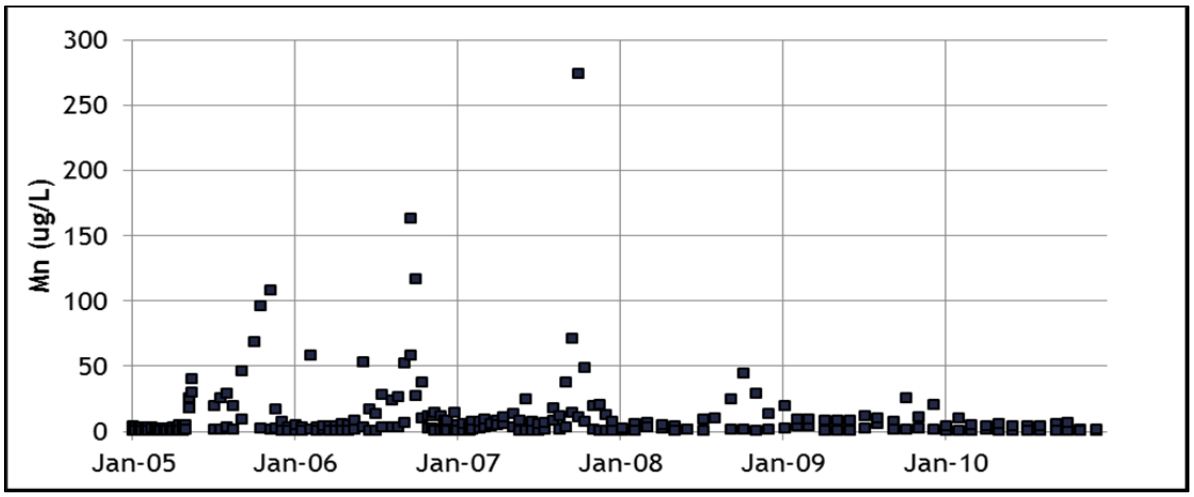

Figure 27. Dissolved Manganese Concentrations in Outflow from Soldier Canyon, 2005 through 2010

Inflow dissolved manganese concentrations are consistently well below peak outflow concentrations. Figure 28 shows inflow dissolved manganese concentrations, which tend to vary seasonally between non-detect and 10 ug/L, averaging 3.4 ug/L.

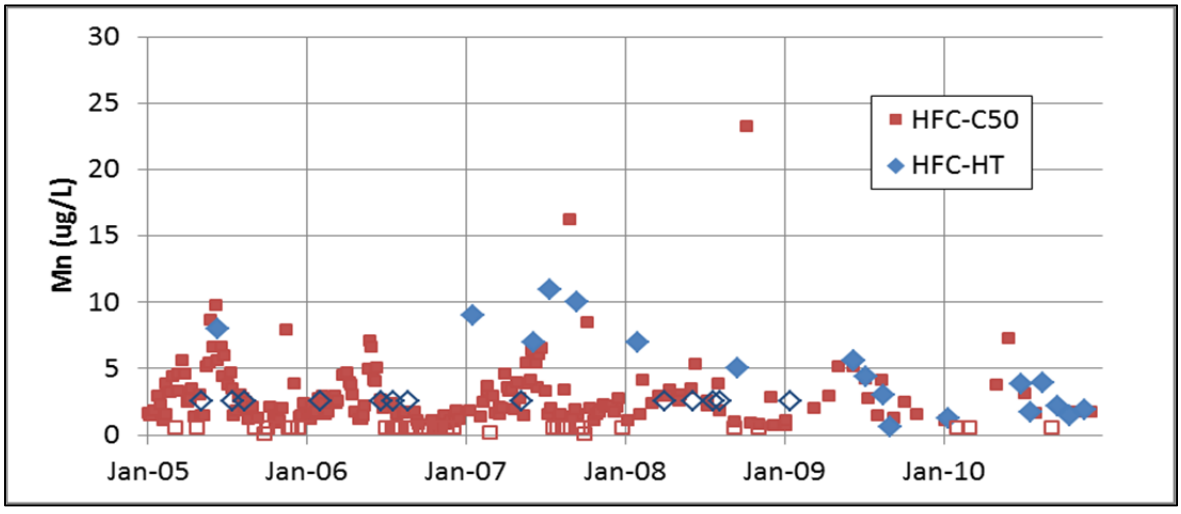

Figure 28. Dissolved Manganese Concentrations in Hansen Feeder Canal Inflow, 2005 through 2010
Hollow symbols present non-detect results at half the reported detection limit.

Manganese can be released from sediments under anoxic conditions. Review of grab sample data from the bottom of the reservoir show elevated manganese concentrations developing seasonally with

reducing conditions during stratification, averaging 90.6 ug/L from 2005 through 2010. Figure 29 shows dissolved manganese concentrations at the bottom of the reservoir. The observed seasonal pattern matches that in the Soldier Canyon outflow data (Figure 27). Based on this information, manganese concentration concerns in the outflow are assumed to be directly related to hypolimnetic oxygen depletion, as opposed to direct inflow loading.

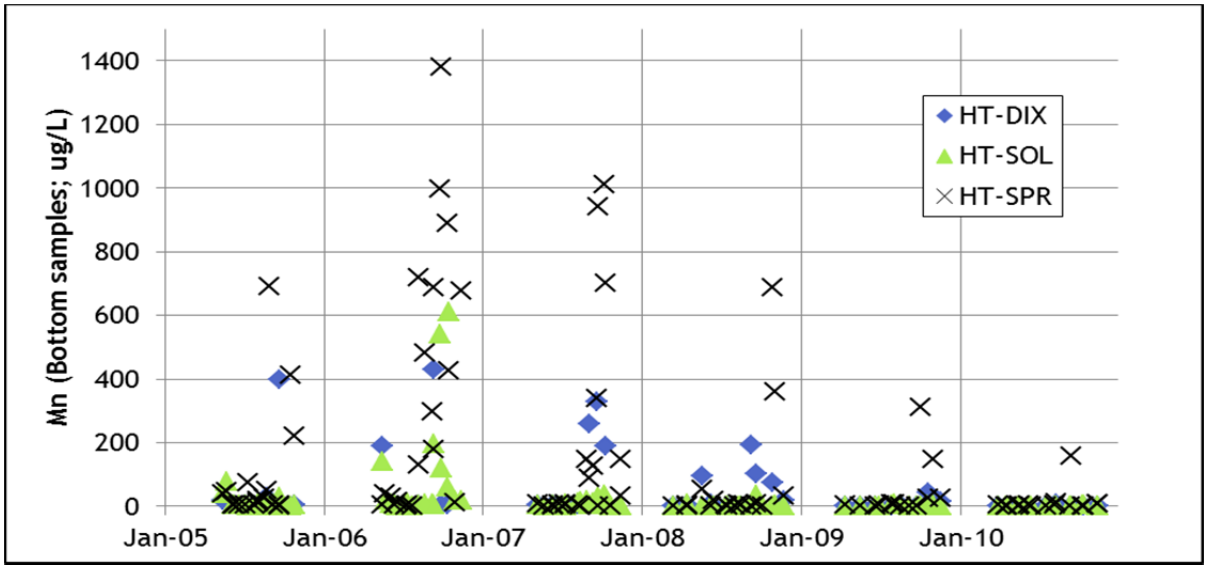

Figure 29. Dissolved Manganese Concentrations at the Bottom of the Reservoir, 2005 through 2010

2.3.4 Total Organic Carbon

Total organic carbon (TOC) concentrations in water entering the reservoir via the Hansen Feeder Canal typically range between 3 mg/L and ~7 mg/L, peaking in May or early June (Figure 30). The seasonal peak is a reflection of the increased contribution of runoff from the Big Thompson watershed each year (Billica and Oropeza, 2010). The baseline values between 3 and 4 mg/L between these seasonal peaks largely represent water quality from the trans-mountain diversion (Adams Tunnel). As noted in Section 1.1, studies (Haby and Loftis, 2007; Hydros, 2011) have shown statistically-significant trends of increasing TOC concentrations in water at the east end of the Adams Tunnel. It is also worth noting that in 2010, peak concentrations were markedly higher (peaking at 13.4 mg/L) than those seen the previous four years.

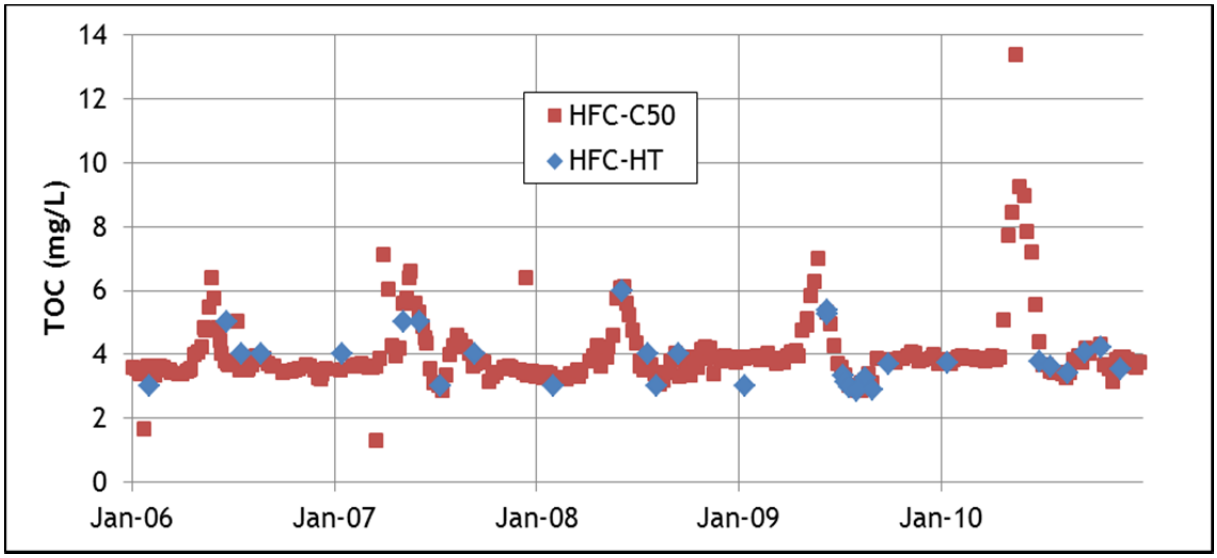

Figure 30. Total Organic Carbon in Inflow from Hansen Feeder Canal, 2005 through 2010

Concentrations of TOC across the reservoir are fairly consistent from Inlet Bay to Soldier Canyon. Observed concentrations at the top (1 m) and bottom (1 m above the sediment) of the reservoir are presented on the same vertical scale in Figure 31 and Figure 32, respectively. These plots show a more pronounced seasonal concentration pattern as well as a wider concentration range in the 1 m samples as compared to the bottom samples. Still, all peak concentrations at 1 m are lower than inflow peak concentrations. Additionally, these figures show that the increased peak inflow TOC concentrations in 2010 correspond (same year) to the highest annual peak concentrations both at the top and bottom of the reservoir.

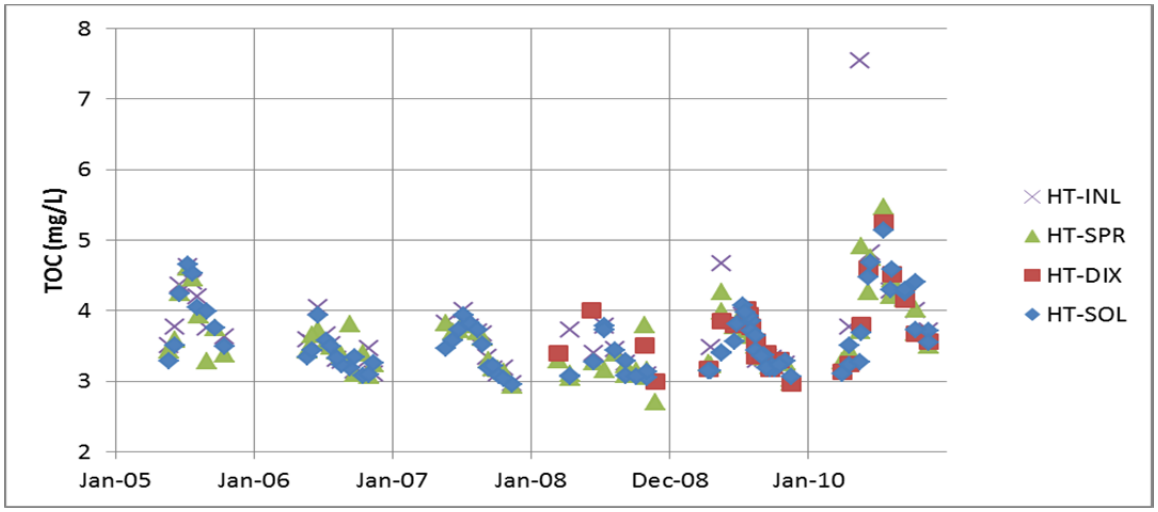

Figure 31. Observed TOC Concentrations across Horsetooth Reservoir in 1m Grab Samples, 2005 through 2010

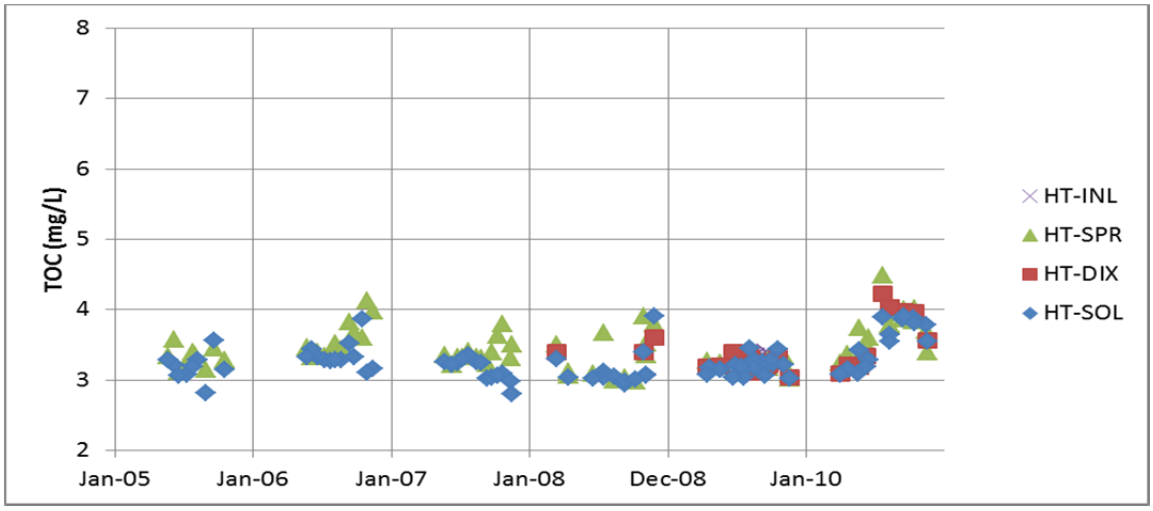

Figure 32. Observed TOC Concentrations across Horsetooth Reservoir in 1m Grab Samples, 2005 through 2010

In 2009, TOC concentration data were collected at 15 m (roughly corresponding to the metalimnion for much of stratification). These data at Spring Canyon and Soldier Canyon are presented in Figure 33. These data show that metalimnion TOC concentrations in August and September are more comparable to bottom TOC concentrations than those at 1 m.

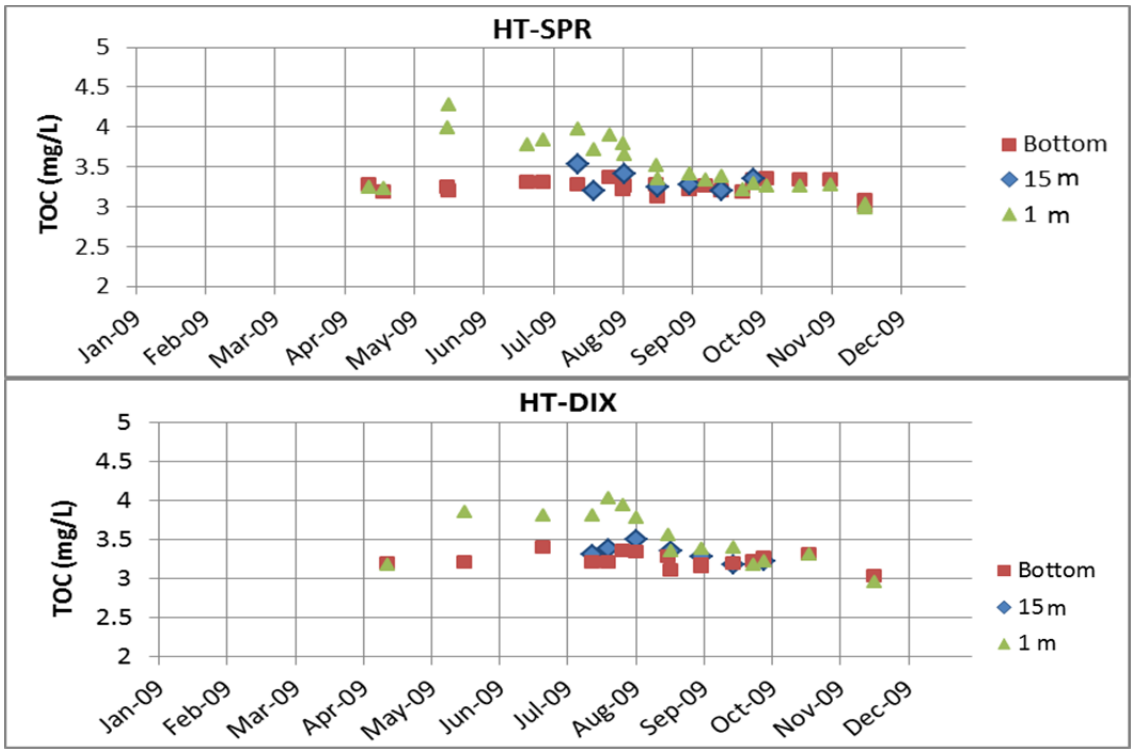

Figure 33. Observed TOC Concentrations in the Metalimnion at Spring Canyon and Soldier Canyon Compared to Top and Bottom, 2009

Soldier Canyon outflow TOC data from the City of Fort Collins Utilities show a fairly narrow range of concentrations, generally between roughly 3 mg/L and 3.5 mg/L from 2005 through 2009 (Figure 34). In 2010, there is an increase in outflow TOC concentrations to 4.2 mg/L halfway through the year. This change likely reflects the increase in inflow TOC concentrations in the spring of the same year.

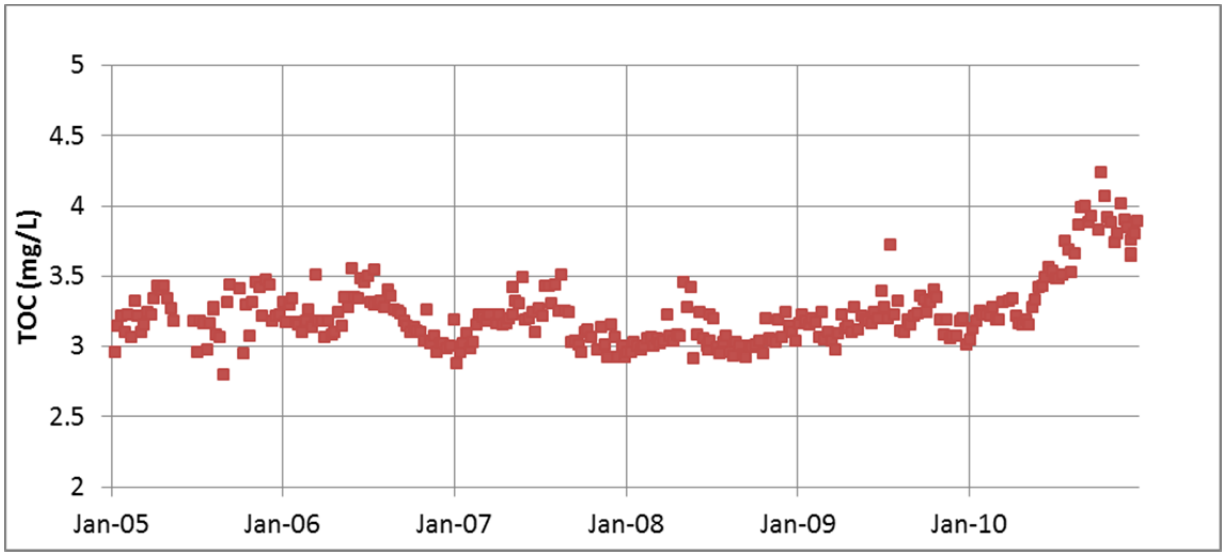

Figure 34. Observed TOC Concentrations in Outflow from Soldier Canyon, 2005 through 2010

2.3.5 Chlorophyll *a*

Observed chlorophyll *a* concentrations[3] in the inflow to Horsetooth Reservoir at Hansen Feeder Canal are presented in Figure 35. Concentrations range from 0.6 to 11 ug/L and show variable timing for peaks. This lack of clear patterns may reflect a combination of factors including, water source mixing, data collection frequency, and algal control activities in canals upstream of the observation location. Further, this data set does not exhibit any obvious trending over the six year period.

[3] All observed chlorophyll *a* concentrations presented in this document are corrected for pheophytin.

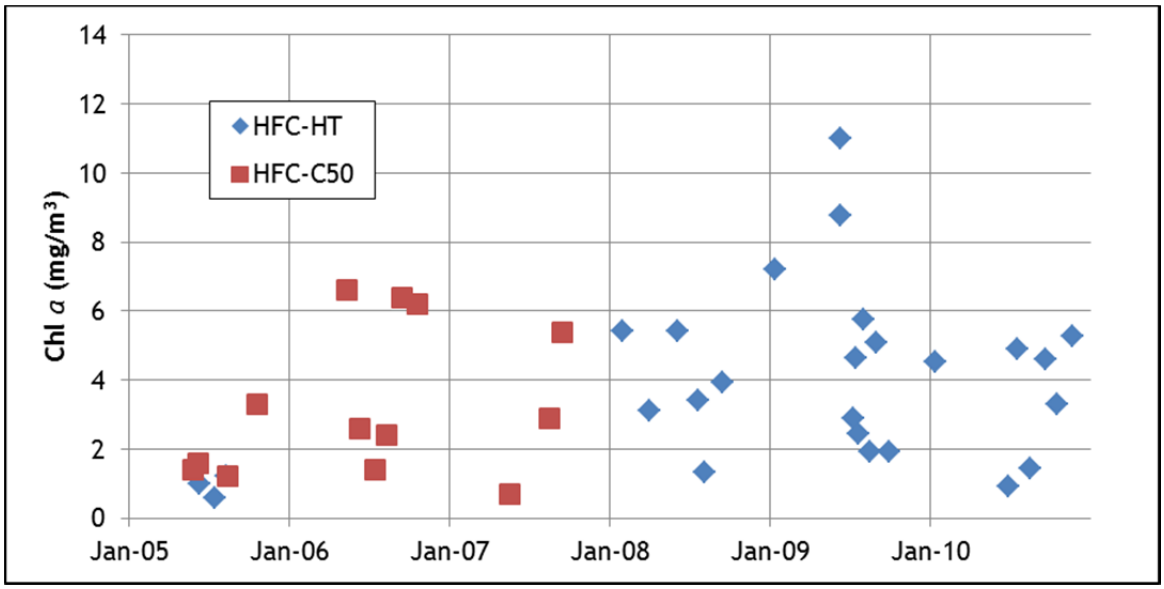

Figure 35. Observed Inflow Chlorophyll a Concentrations in Hansen Feeder Canal, 2005 through 2010

Figure 36 presents chlorophyll *a* concentrations across the top of the reservoir in 0 to 5 m composite samples. Interestingly, the concentration range in this dataset (0.1 to 12 ug/L) is similar to that noted for the inflows. This figure also shows that patterns and concentration ranges are fairly consistent across stations. The highest annual observed chlorophyll *a* concentrations in the reservoir can occur at Spring Canyon, Dixon, Canyon, or Soldier Canyon. As seen in the inflow, there is no obvious trending over the six year period, though a statistical analysis was not conducted.

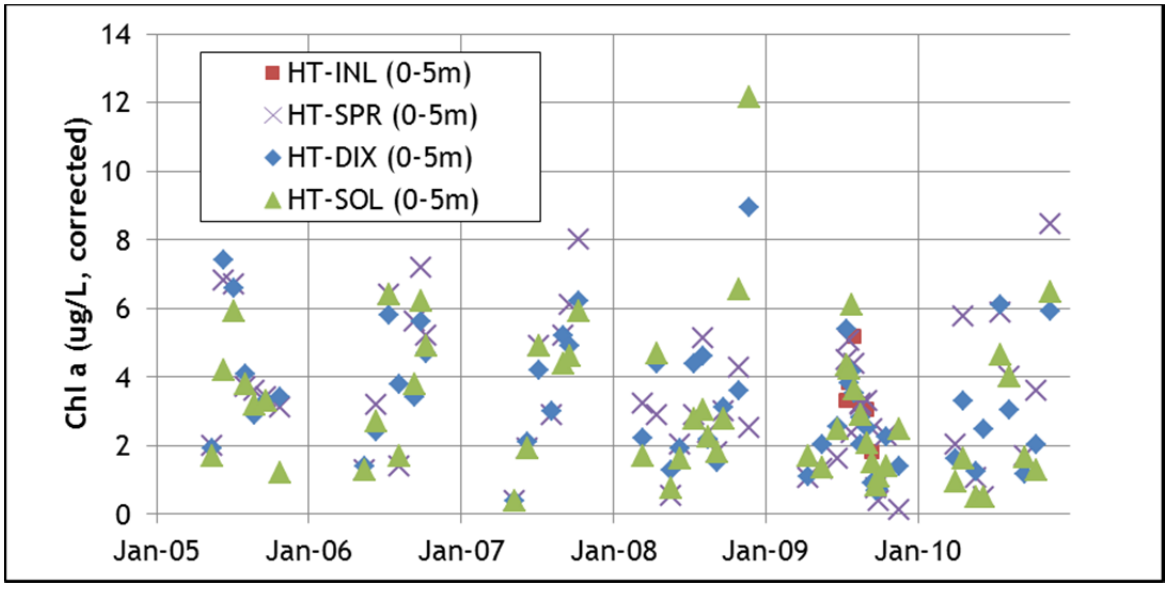

Figure 36. Observed Chlorophyll a Concentrations across Horsetooth Reservoir (0 to 5 m Composite Samples), 2005 through 2010

In 2009, more detailed chlorophyll *a* sampling was conducted, with greater vertical resolution across the reservoir. Figure 37 presents 2009 observed chlorophyll a concentrations across the reservoir from the top to a depth of 25 m. These figures show good matching of temporal and vertical chlorophyll *a* concentrations and patterns at the three sampling stations. Each location also shows decreasing chlorophyll *a* concentrations with depth, with an apparent step change located approximately between 10 and 15 m.

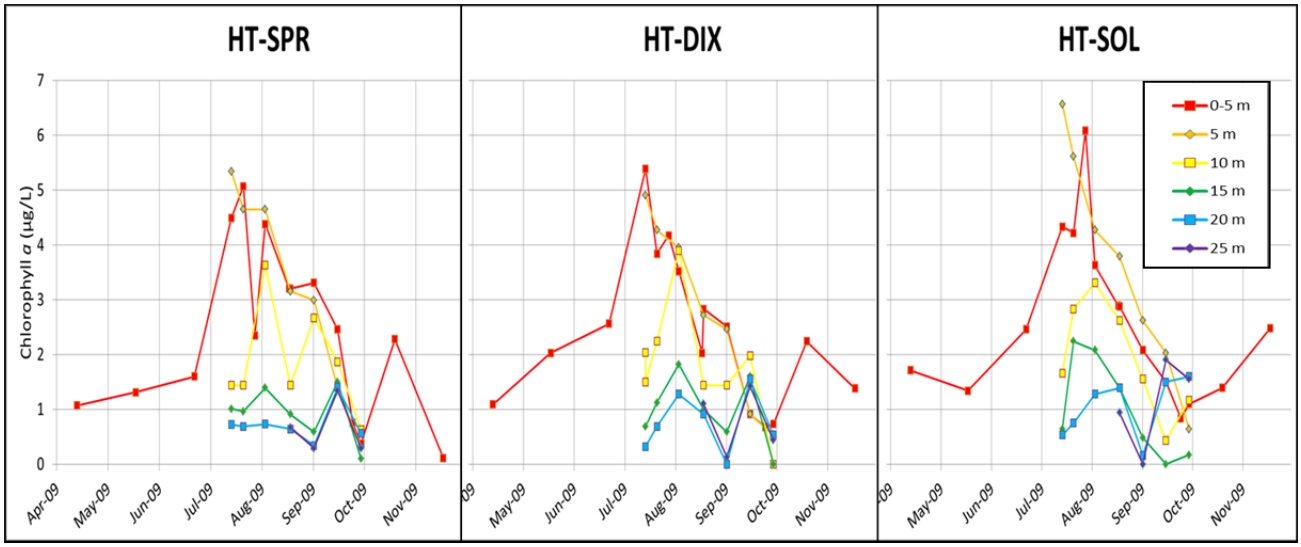

Figure 37. Observed Chlorophyll *a* Profile Data across the Reservoir from 2009

2.3.6 Nutrients

The following subsections present a brief discussion of observed inflow and in-reservoir concentrations of nutrients from 2005 through 2010. The discussions focus on inorganic species of orthophosphate (PO4), nitrate (plus nitrite), and ammonia.

2.3.6.1 Orthophosphate

Inflow concentrations of PO4 show variable seasonal patterns with concentration peaks in summer and with peaks also occasionally observed at other times of the year (Figure 38). The average concentration of PO4 entering Horsetooth Reservoir from 2005 through 2010 was 5.1 ug/L, compared to the average inflow total phosphorus (TP) concentration of 22.0 ug/L.

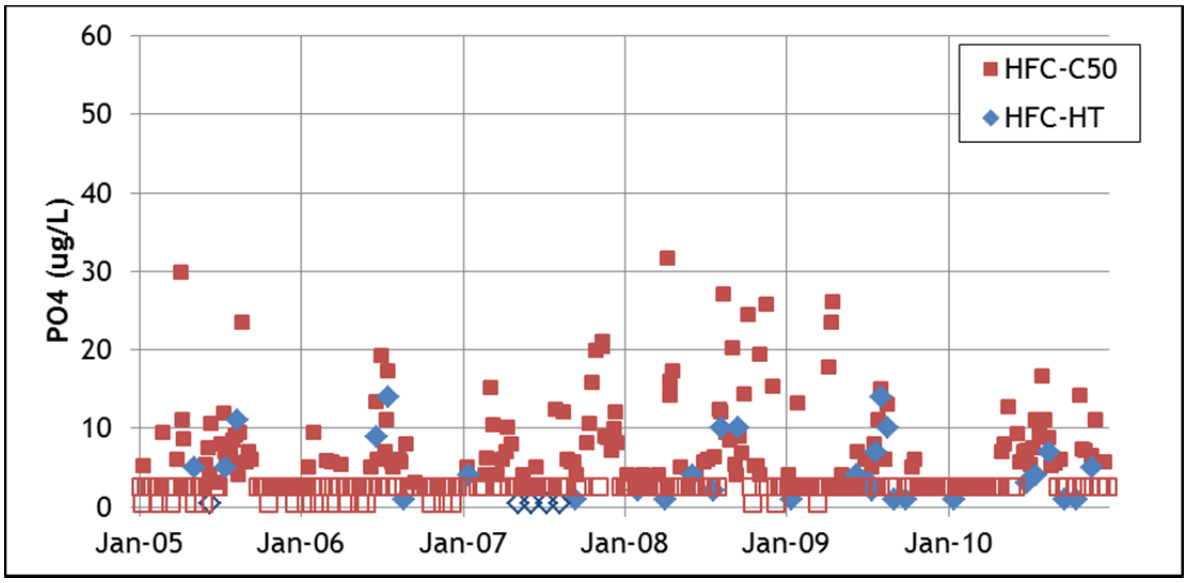

Figure 38. Observed Orthophosphate Concentrations Entering the Reservoir from Hansen Feeder Canal, 2005 through 2010

Hollow symbols present non-detect results at half the reported detection limit.

At the top of the reservoir, PO4 concentrations are generally lower than inflow concentrations, ranging from 0.5 to 9 ug/L (Figure 39). At this depth, PO4 concentrations tend to be the lowest across the reservoir in summer months, likely reflecting algal uptake. Figure 39 also shows that concentration ranges are generally similar across the top of the reservoir, but concentrations in Spring Canyon can be higher shortly after turnover.

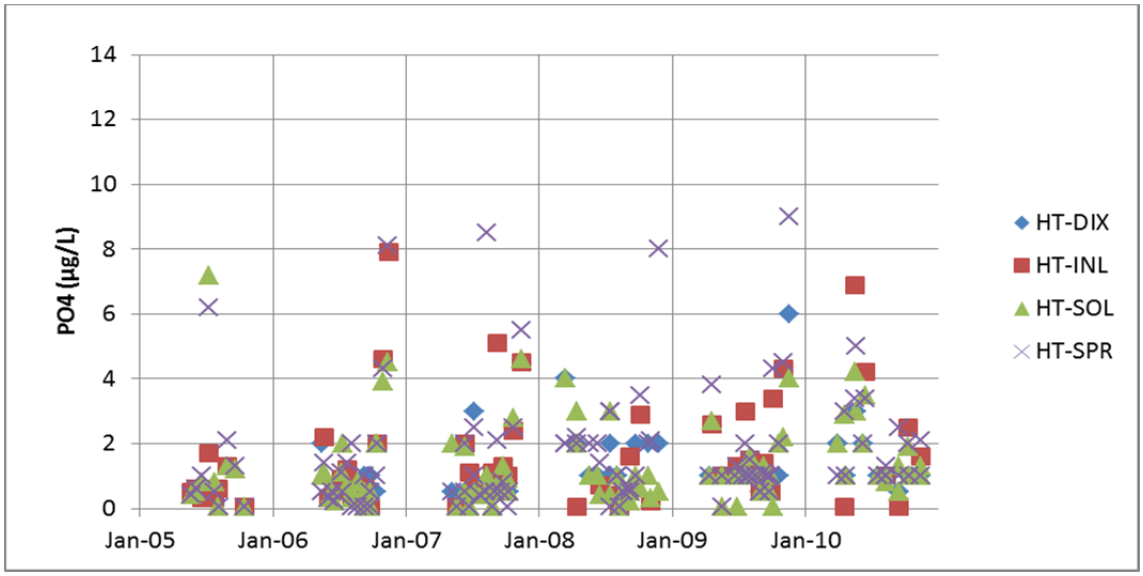

Figure 39. Observed Orthophosphate Concentrations at the Top (1 m) of Horsetooth Reservoir, 2005 through 2010

At the bottom of the reservoir, PO4 concentrations range from 0.5 ug/L to 80 ug/L, with a seasonal pattern reflecting internal loading during anoxic conditions in the sediment (Figure 40). As seen in Figure 40, higher PO4 concentrations are observed at the bottom of Spring Canyon each year, as compared to Dixon or Soldier, matching hypolimnetic dissolved oxygen depletion patterns. Each year, the timing of the peak corresponds to the time immediately before fall turnover.

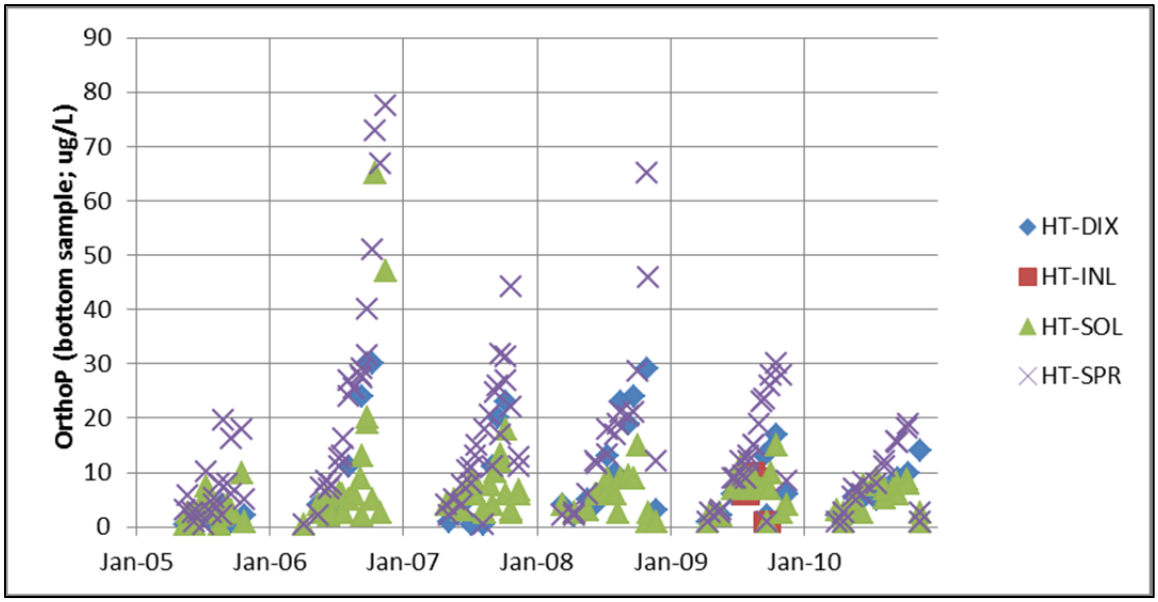

Figure 40. Observed Orthophosphate Concentrations at the Bottom of Horsetooth Reservoir, 2005 through 2010

2.3.6.2 Nitrate and Ammonia

Inflow concentrations of ammonia and nitrate (plus nitrite) show a general seasonal pattern of increased concentrations in summer (Figure 41). Based on TKN data, these nutrients make up a relatively small percentage of the total nitrogen entering the reservoir. From 2005 through 2010, of the average TN inflow, 3% was ammonia, 20% was nitrate, and 77% was organic nitrogen.

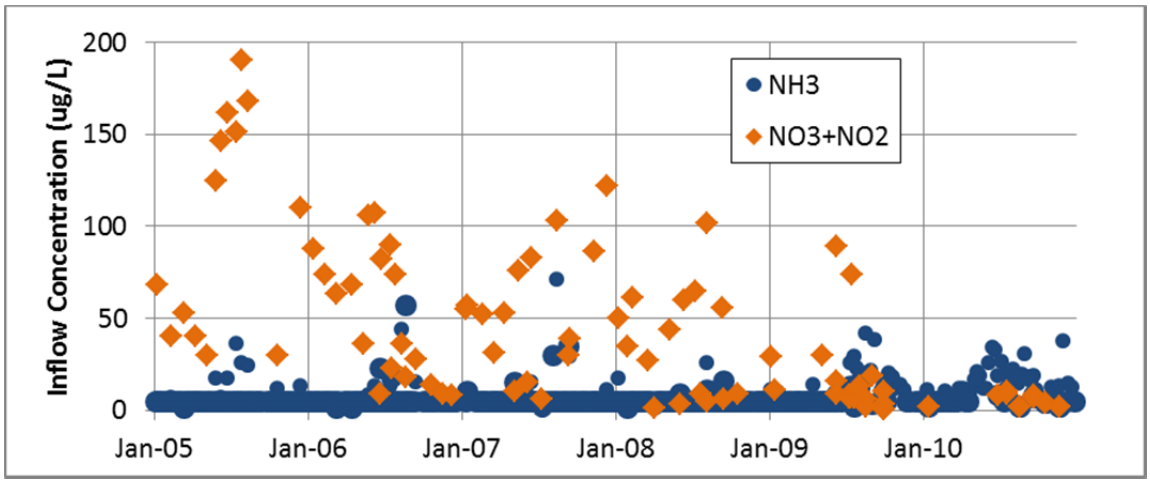

Figure 41. Inflow Concentrations for Nitrate and Ammonia at Hansen Feeder Canal, 2005 through 2010

In the reservoir, summertime concentrations of ammonia and nitrate tend to be the lowest of the year at the top (1 m). Figure 42 shows ammonia and nitrate concentrations at 1 m across the reservoir from 2009. Concentrations are fairly consistent from HT-INL to HT-SOL. This summertime pattern is expected to reflect the effects of algal uptake.

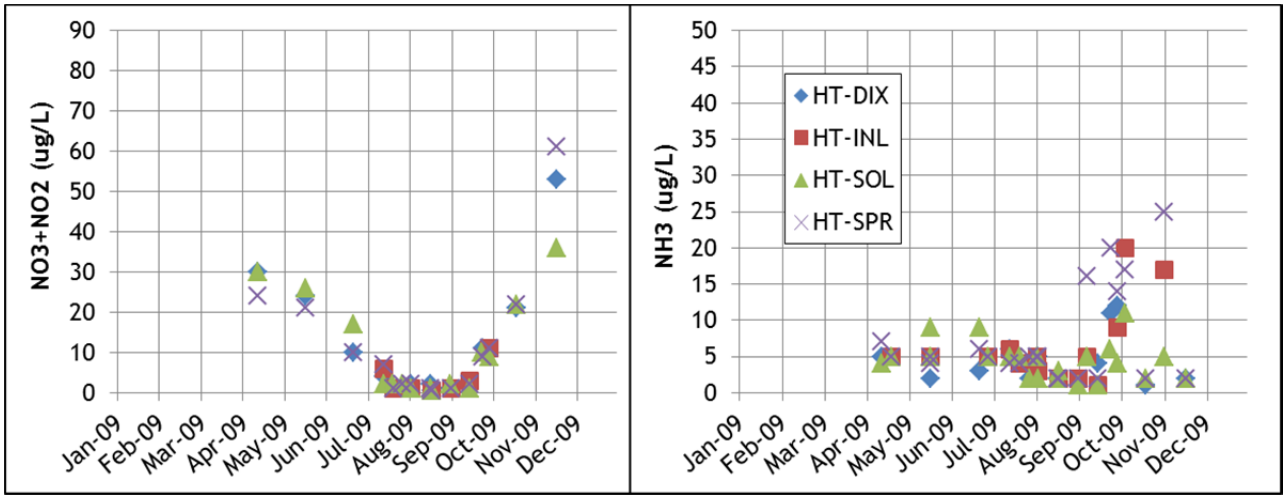

Figure 42. Nitrate and Ammonia Concentrations at 1 m across the Reservoir in 2009

In 2009, profile nutrient data were also collected from July through September. Figure 43 shows nitrate and ammonia concentration at 15 m, which roughly represents the depth of the metalimnion for much of the stratified period. The pattern observed for nitrate is different at 15 m than that observed at 1 m. At 15 m concentrations are higher in July and August. This finding matches the chlorophyll *a*

concentration patterns that show very low algae concentrations at a depth of 15 m (discussed in Section 2.3.5). Ammonia concentrations, however, are still low at 15 m through this summertime period, likely reflecting water-column nitrification[4] of ammonia, which is generated by degradation of organic matter.

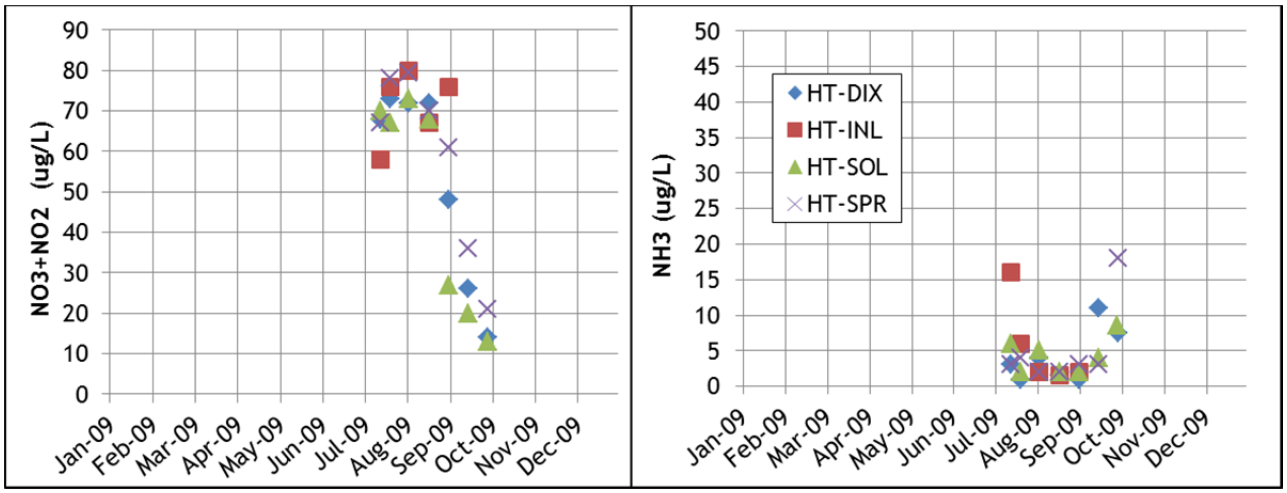

Figure 43. Nitrate and Ammonia Concentrations at 15 m across the Reservoir in 2009

Figure 44 presents bottom nitrate and ammonia concentrations from 2009 across the reservoir. At the bottom of the reservoir, nitrate concentrations show seasonal patterns indicative of nutrient release from anoxic sediments. As with PO4, peak concentrations at the bottom occur just before fall turnover, and the range of bottom concentrations extends much higher than inflow concentrations or concentrations elsewhere in the reservoir. Note that nutrient releases occur from sediments before the onset of anoxic conditions in the overlying water, requiring only anoxia in the sediments. In addition to sediment release of nutrients, nitrate concentrations at the bottom of the reservoir increase with decay of organic matter. Organic matter decays to form ammonia, which is then converted to nitrate through nitrification while oxygen is still present in the hypolimnion. Ammonia concentrations on Figure 43 show some evidence of sediment release also; however, the pattern is not as clear, and the concentration range is lower than that of the inflow. As noted, when oxygen is still present in the hypolimnion, ammonia can be converted to nitrate through nitrification.

[4] Nitrification is the biologically-mediated oxidation of ammonia into nitrite, which is, in turn, rapidly oxidized to nitrate.

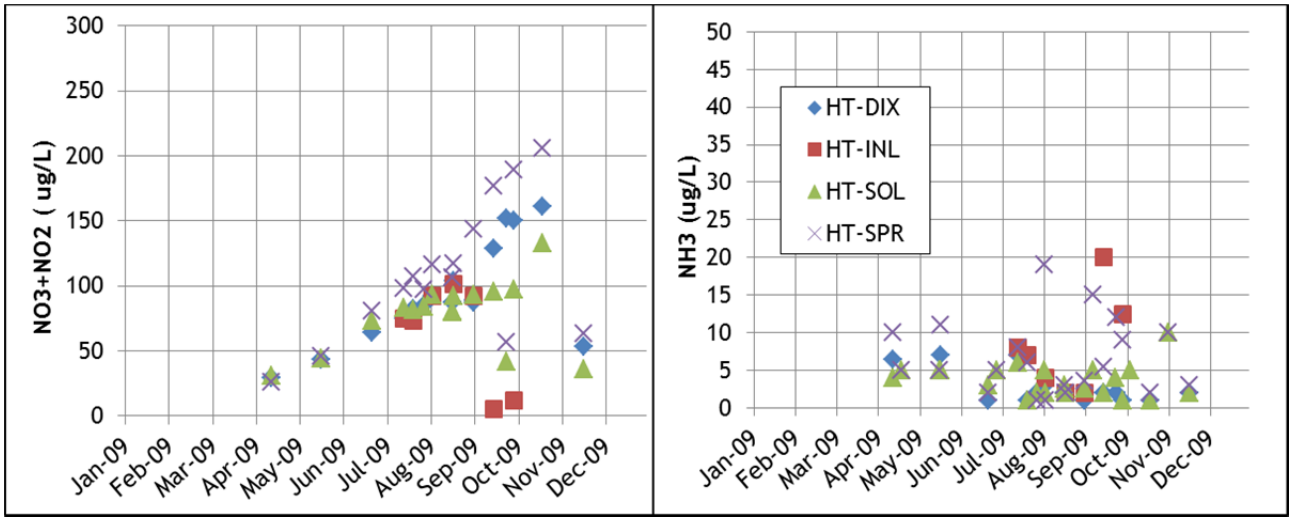

Figure 44. Nitrate and Ammonia Concentrations at the Bottom across the Reservoir in 2009

2.4 SUMMARY OF REVIEW OF EXISTING DATA

Review of the existing data set provided a good foundation for model development. The following highlights summarize key findings from analysis of the observed data that will be in focus during model development and testing:

- The data set is adequate to support development and testing of a numerical model of Horsetooth Reservoir.
- Hydrodynamics and operations appear to be important factors in determining water quality in the reservoir. The inflow water quality is a function of the upstream mixing of water from the Big Thompson watershed and trans-basin water. Further, the specific conductivity signal suggests that inflow and outflow rates affect residence time and mixing/dilution in metalimnion. Finally, bottom withdrawals appear to affect mixing and stratification at Soldier Canyon.
- Horsetooth Reservoir strongly stratifies each year, and inflow from Hansen Feeder Canal enters at the metalimnion during stratification due to inflow water temperature.
- Hypolimnetic dissolved oxygen concentrations vary across the reservoir. Hypolimnetic low DO develops first at Spring Canyon and typically reaches lowest values at Spring Canyon. Nutrient and manganese releases behave in agreement with this pattern. Further, there is no apparent trending with time of hypolimnetic DO concentrations following refilling of the reservoir in 2004.
- Dissolved manganese data show that the source of manganese concentrations of concern is release from bottom sediments under anoxic conditions, as opposed to direct loading from inflows.

- Inflow TOC concentrations show a repeating pattern of elevated concentrations in spring and early summer, corresponding to the period of greater relative contribution of inflows from the Big Thompson Watershed.

- TOC data in the inflow reached higher peak concentrations in 2010 than in any of the previous five years. In-reservoir TOC data show this change both at the top and at the bottom of the reservoir in the same year. An increase in TOC concentrations is also seen in outflow from Soldier Canyon Dam in 2010.

- Chlorophyll *a* concentrations are greatest in the upper portion of the reservoir, with concentrations falling off sharply below ~10 m.

- Nutrients show patterns indicative of summertime algal uptake at the top of the reservoir. Additionally, grab data from the bottom of the reservoir show internal loading from sediments during stratification.

3 MODEL DEVELOPMENT AND TESTING

This section presents the software selected for modeling, model construction, model calibration, and model validation. Model construction includes development of the numerical representation of the reservoir bathymetry and comparison of the model area-elevation-volume relationships with operational records used by the USBR. Model calibration presents the hydrologic, thermal, and water-quality calibration simulation for calendar years 2005 through 2009. The model was validated by simulating January through September 2010 with the calibrated model to assess performance.

3.1 DESCRIPTION OF MODELING TOOL

To meet objectives identified in Section 1.2, the modeling software CE-QUAL-W2 (version 3.6) was applied to simulate Horsetooth Reservoir. CE-QUAL-W2 is a two-dimensional hydrodynamic and water-quality model. The model assumes lateral homogeneity, but simulates variation longitudinally and vertically to the resolution specified. The U.S. Army Corps of Engineers developed the model, and it is currently supported by Portland State University. The model uses Intel FORTRAN V10.1 to compile, and can be operated from a Windows environment. Detailed documentation of the model and associated technical manuals are available at http://www.ce.pdx.edu/w2/.

The model was selected for this application for the following key reasons:

- The model is in the public domain.
- The model is well suited for relatively long and narrow water bodies (Cole and Wells, 2008), and Horsetooth Reservoir fits this description, with inflow on one end and outflow(s) on the other end.
- The model is capable of simulating multiple inflows and outflows.
- The model can simulate ice cover onset, growth and breakup, which could be important for multi-year simulations.
- The model has an excellent reputation and has been applied successfully to more than 450 lakes, including the following reservoirs in Colorado: Dillon, Aurora, Blue Mesa, Morrow Point, and Crystal.
- The model simulates water temperature, DO, TOC (derived from components), nutrients, and algae, including biotic and abiotic reactions and transformations. Most of these reactions are temperature dependent.
- The model can simulate features and effects that are potentially important for Horsetooth Reservoir, including reservoir morphology, meteorological effects, spatially-varied sediment oxygen demand, and complex hydrodynamics.
- The model has good, built-in flexibility for outputting data at key locations in the frequency and formats of interest.

In addition to consideration of model capabilities, it is prudent to consider model limitations in selection and application of modeling software. Upon selection of CE-QUAL-W2, the following limitations were noted:

- The model is laterally-averaged, meaning spatial variation perpendicular to the longitudinal axis cannot be estimated and is not included in the simulation.
- Vertical momentum is not included in the hydrodynamic calculations. The user specifies the vertical turbulence scheme, and eddy coefficients are used to model turbulence. If significant vertical acceleration is occurring in a water body, the model may not be well suited for the application.
- Water-quality interaction calculations are, by necessity, simplified representations of extremely complex aquatic ecosystem dynamics.
- The model is not a true sediment diagenesis model; and as such, SOD is specified as opposed to calculated from organic matter delivery to the sediment. There is, however, a first-order sediment organic matter concentration calculation that can accumulate organic matter in the sediment, and this was used for the Horsetooth application.
- As with all models, this model will be limited by the quality and completeness of input data.

3.2 MODEL CONSTRUCTION

The bathymetric representation of Horsetooth Reservoir in the CE-QUAL-W2 model was defined based on a 10-ft contour map of the reservoir generated by the U.S. Army Corps of Engineers in 1952. The map was imported into GIS and total of 41 cross-section lines were placed over Inlet Bay and the length of the reservoir. These lines were set to identify the longitudinal discretization of the model cells. The contour data were used to estimate the volume of each 10-ft interval between the cross section lines. The volumes at each 10-ft depth interval of coves and bays on the west side of the reservoir were included in the volumes for the adjacent (main reservoir) model cells. Figure 45 presents the contour map and the location of the cross-section lines.

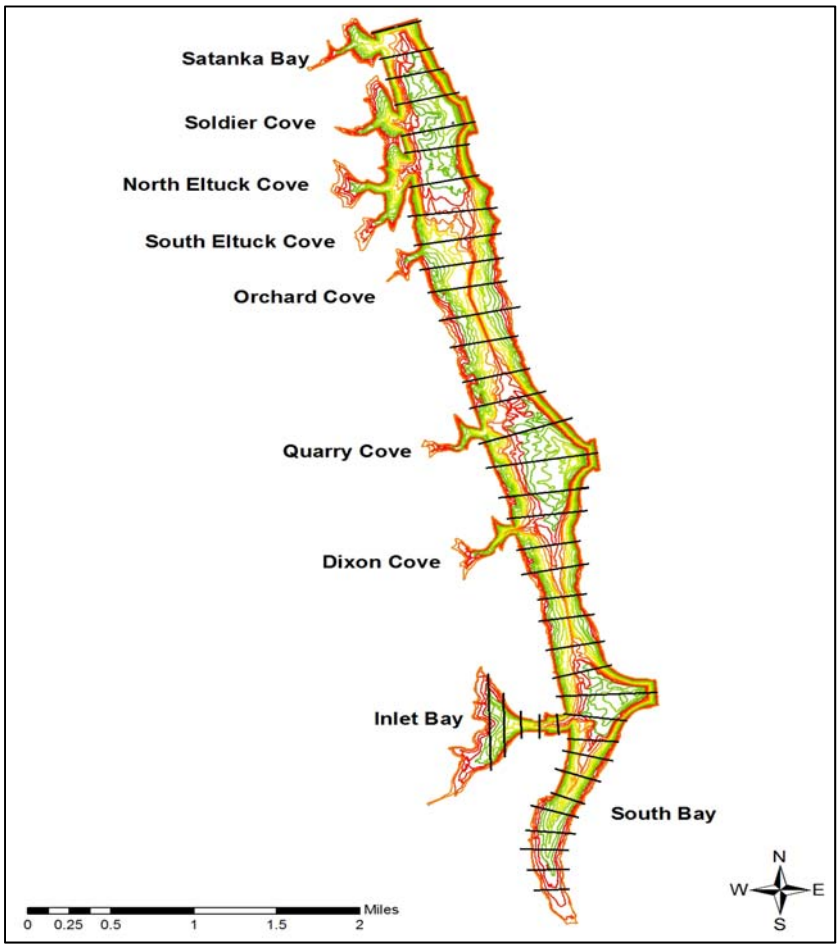

Figure 45. 1952 U.S. Army corps of Engineers 10-ft Contour Map of Horsetooth Reservoir and Cross Section Locations

The decision to not simulate bays and coves as separate branches, but to instead include their volumes into the adjacent mainstem reservoir cells was based on a few considerations. First, these small branches represent only a small percentage of the total volume of the reservoir. Specifically, the GIS analysis indicated that the bays and coves represent a total of 5.5% of the reservoir volume when the reservoir is full. Next, the observed data do not suggest major effects of the bays on water quality at the focus sampling locations near the dams. Further, early simulations with additional simplified branches to represent each bay had long run times relative to the simplified representation. Such simplifications are common in CE-QUAL-W2 applications (e.g., DeGray reservoir described in the model documentation [Cole and Wells, 2008]). Finally, it was anticipated that, in the event that water quality in the reservoir could not be simulated and the lack of resolution in situation of the bays was identified as a potential cause, the bathymetry could be reconstructed to include them.

The resulting model representation of the bathymetry includes two branches (the mainstem reservoir and the Inlet Bay). The main reservoir branch consists of 36 active segments which are oriented according to the azimuth of the thalweg for each. The Inlet Bay branch consists of five active segments.

Figure 46 presents the aerial view of the branches and segments. In this figure, colored segments identify ends of branches and connecting segments.

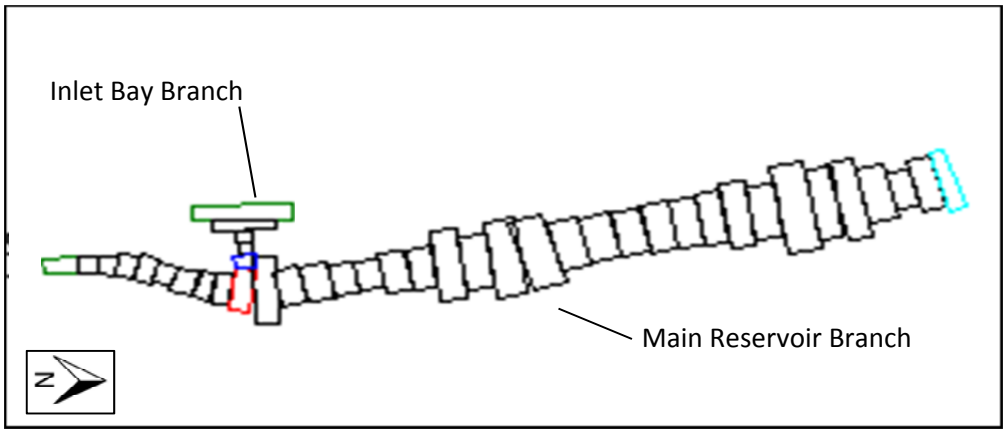

Figure 46. Aerial View of Horsetooth Model Branches and Segments

To define the vertical discretization of the model, the 10-ft cells were bisected to create a vertical resolution of 5 ft (~1.5 m) for each segment. Vertical resolution was set at 1.5 m based on best professional judgment, weighing the need to capture critical processes, including a distinct metalimnion, against computational inefficiency of a large number of cells. While the model is capable of managing layer thicknesses that vary vertically, the 1.5 m uniform layer thickness seemed a good fit for this system with fairly wide-ranging annual water levels and the need to capture the metalimnion from initial formation to turnover. Figure 47 presents the vertical cell discretization for each branch of the model. Note in this figure that the direction of flow is from right to left, which is the opposite of that presented in Figure 46. As in Figure 46, green and blue outlined cells indicated upstream and downstream segments. The red outlined cells indicate the location of the inflow connection from the Inlet Bay branch.

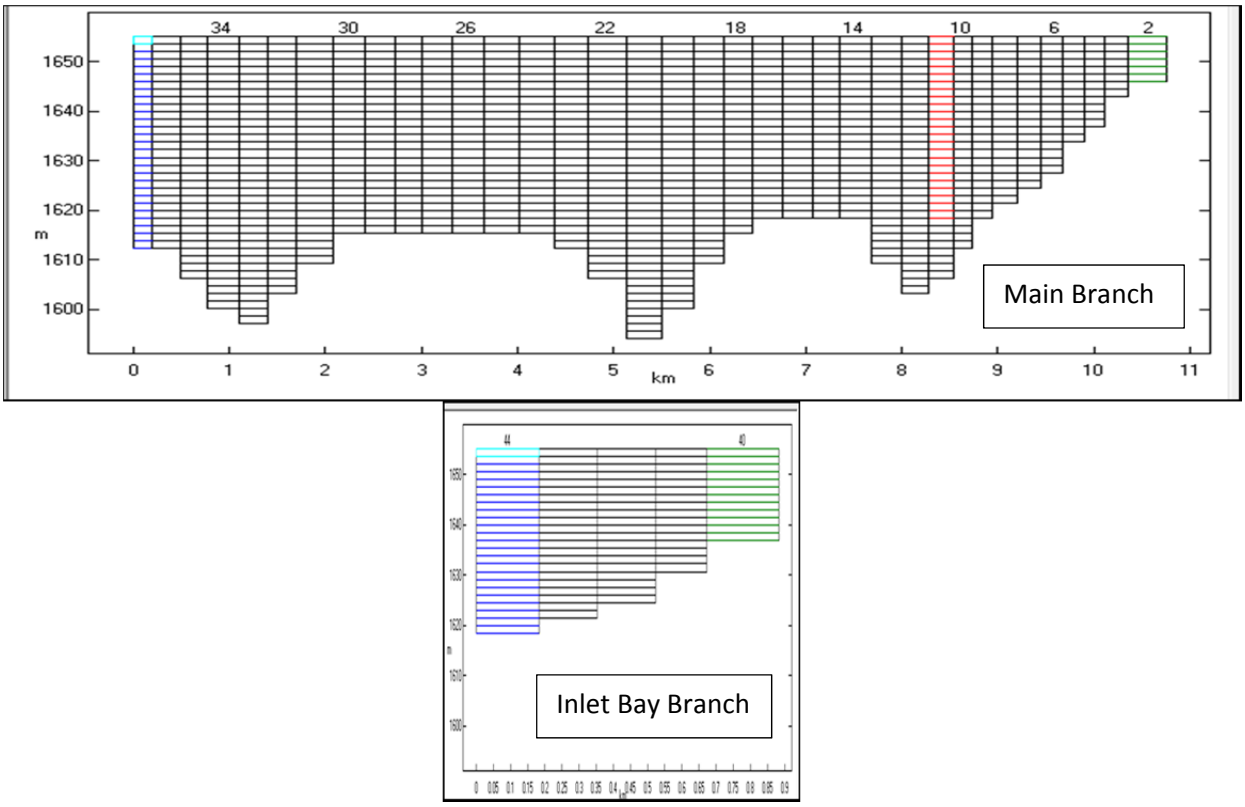

Figure 47. Profile Views of Horsetooth Model Branches

In addition to specification of the segment lengths and thicknesses, the width of each segment was specified to generate the appropriate volume at each depth. Figure 48 shows example views of width designation, looking at cross-section views in the direction of flow.

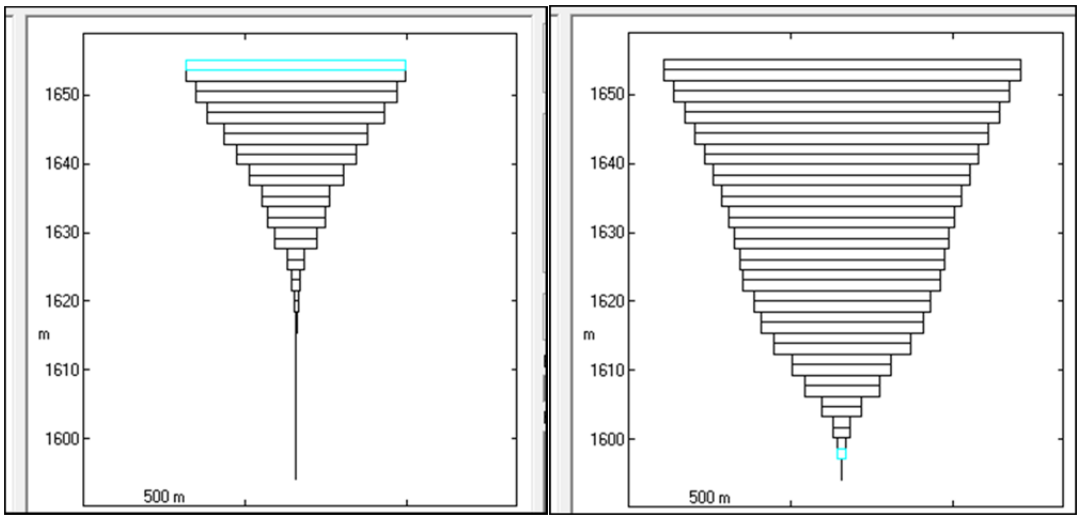

Figure 48. Example Cross-Section Views of Main Reservoir Branch Segments of the Horsetooth Model

Elevation-to-volume relationships were developed from the model cells by adding up cell volumes at each 1.5 m cell depth interval over the entire model. These points were compared to the relationship developed from GIS analysis of the 1952 contours and to the elevation-to-volume relationship used by Northern Water and the USBR in management of the reservoir. The elevation-volume estimates were no more than 0.1% different from the GIS –based relationship and no more than 2% different from the Northern Water and USBR curve[5]. In the range of the 2005 through 2010 operations, the maximum difference between the model and the USBR curve was 1%. The surface area-to-elevation relationship was also evaluated that same way. Figure 49 presents the USBR volume-elevation relationship, the GIS-estimated points, and the model bathymetry points. Figure 50 presents the comparison for surface area-to-elevation.

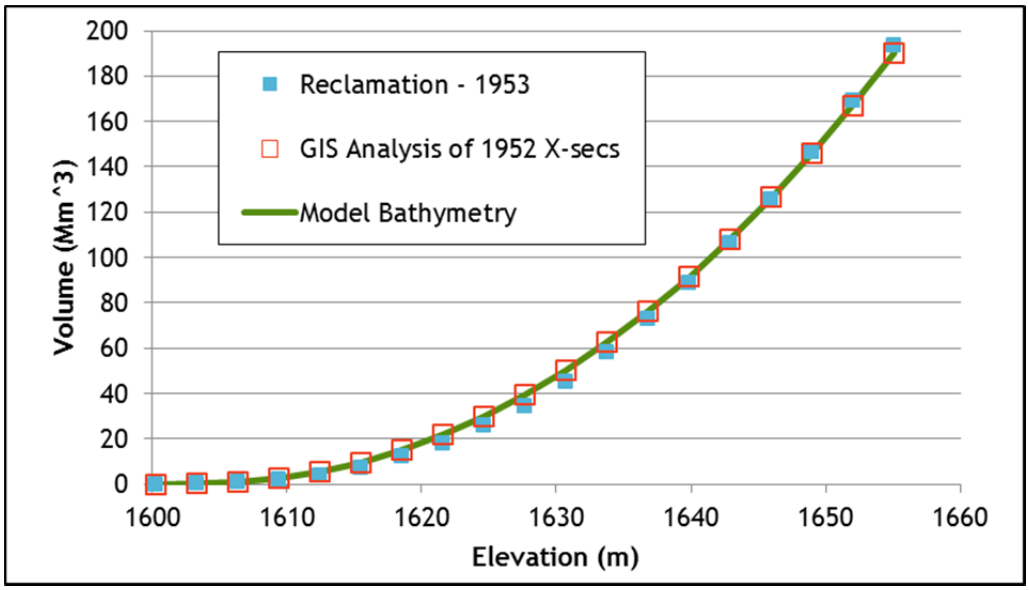

Figure 49. Horsetooth Model Volume-Elevation Compared to GIS Estimates and the USBR 1953 Curve

[5] The USBR elevation-area-volume curves were built in 1953. These were most likely generated using the 1952 contour data that were used in this GIS analysis. It is expected that the GIS analysis differs slightly from the 1953 curve because more primitive spatial analysis was likely completed in 1952 (e.g., planimeter or other manual tool).

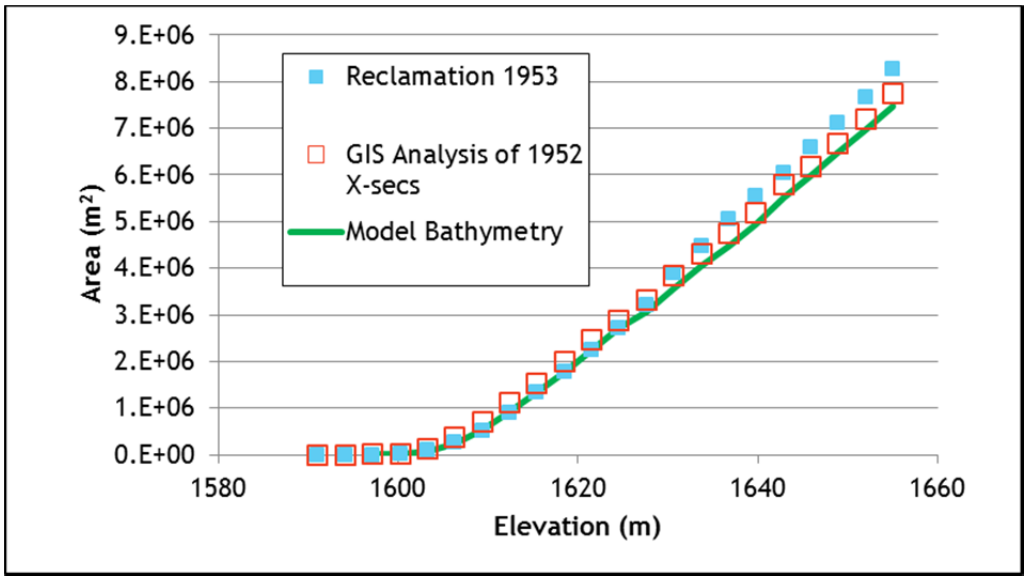

Figure 50. Horsetooth Model Surface Area-Elevation Compared to GIS Estimates and the USBR 1953 Curve

Following bathymetry development, outlet works were placed in the model at the location of the Soldier Canyon Dam outlet and the Horsetooth Dam outlet. These outlet works were set up to use the selective withdrawal algorithm in the CE-QUAL-W2 code. This algorithm calculates a time-varying withdrawal zone for each outlet based on outflow, outlet geometry, and upstream density gradients. Figure 51 shows the locations of the outlet structures on the longitudinal profile view of the reservoir. As in Figure 47, this figure is oriented such that flow is from right to left (blue arrow).

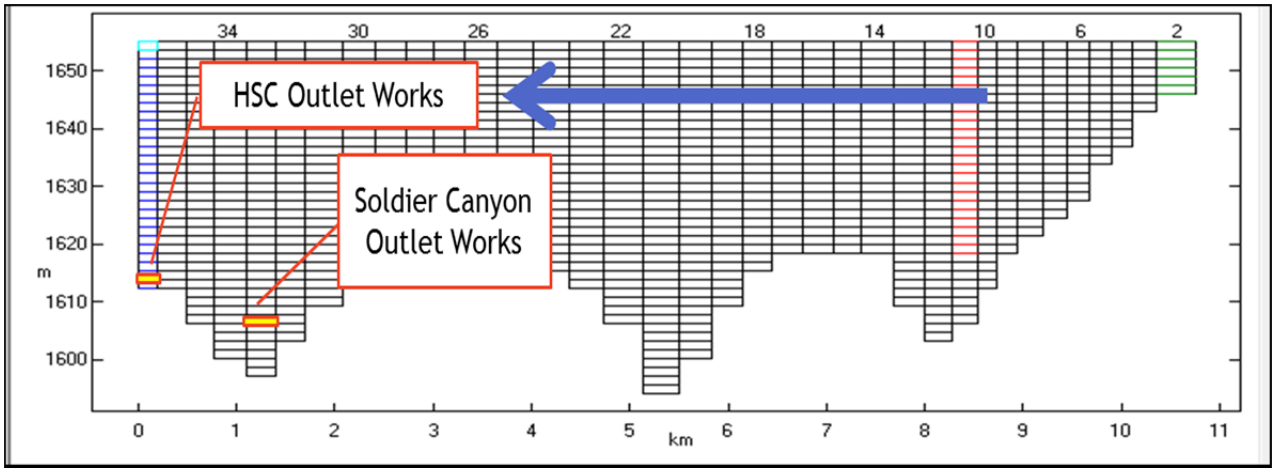

Figure 51. Outlet Works in Horsetooth Reservoir Model

3.3 CALIBRATION

This section presents calibration of the Horsetooth Model. Calibration is the process in which model coefficients are adjusted to produce a reasonable match between observed and simulated results. The process is iterative and not prescriptive. In calibration of this model, the focus was on capturing concentration ranges, seasonal patterns, spatial patterns, and year-to-year differences by visual review of graphical comparisons of observed and simulated results. This approach[6], as opposed to simply calibrating to minimize residuals, is more likely to result in development of a model that captures the water-quality mechanisms at work in the reservoir.

Calibration was achieved by adjusting conceptually-relevant coefficients within reasonable ranges. Reasonable ranges of coefficient settings were defined by model guidance documents and literature. The calibration focused on the observed record from January 2005 through December 2009 and was completed in three main steps. First, the hydrology was simulated and compared to observations. Next, water temperatures were calibrated. Finally, water quality was simulated and calibrated to the observed record. The following subsections present the calibration approach and results for hydrology, temperature, and water quality. This section is supported by Appendices A, B, C, and D which present calibration and validation results plotted against observed data.

3.3.1 Hydrology

A water balance for the calibration period (January 2005 through December 2009) was provided by Northern Water. This balance included daily values for the following terms which were input into the model:

- Hansen Feeder Canal inflows,
- Outflows from Soldier Canyon,
- Outflows from Horsetooth Dam,
- Estimated seepage from the reservoir, and
- Evaporation losses.

Seepage and evaporation values were input as distributed terms over all active segments. Seepage was input at a constant rate of 7 AF/day to close the water balance. The model has a capability to estimate evaporation, based on water levels, water temperatures, and meteorological inputs; however, USBR-estimated evaporation values from the balance provided by Northern Water were input as user-defined terms. USBR-estimated evaporation values were calculated as 0.73 x pan evaporation. As stated in Section 2.1, evaporation and seepage comprise only a small percentage of the total annual water

[6] In other words, a simulated line through an observed pattern may produce smaller residuals; however, this modeling effort attempted to simulate the pattern rather than favor minimization of residuals.

balance, as 4% and 2%, respectively. Precipitation was also input into the model to complete the water balance.

The results of the hydrology simulation were compared to daily water surface elevation values from the Northern Water balance and from the observed record (Figure 52). The average daily error for the model simulation relative to the observed water levels was 0.1 m, ranging from a maximum positive error of +0.37 m to a maximum negative error of -0.44 m. For comparison, the error in the water balance generated by Northern Water was in the same range, with average error of 0.04 m, and a range of +0.53 m to -0.61 m).

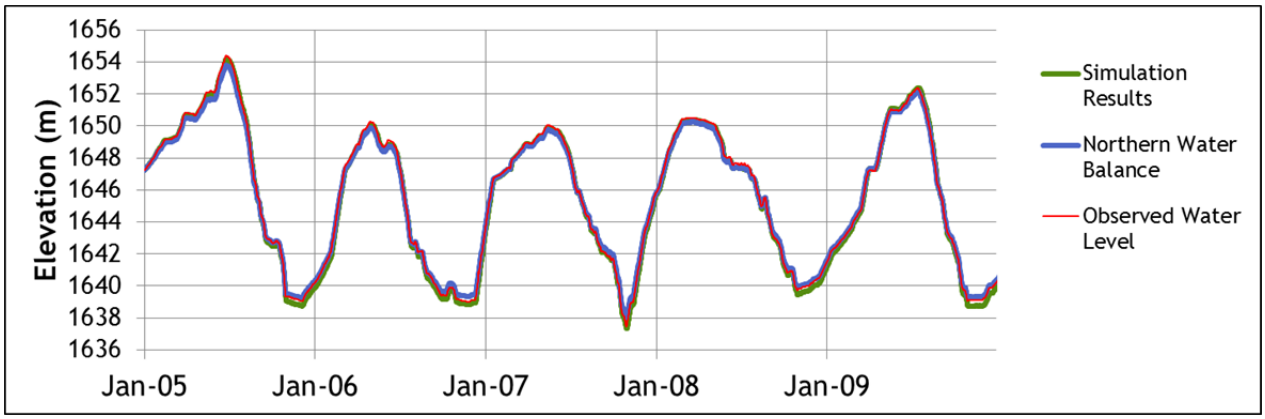

Figure 52. Hydrology Calibration Simulation – Daily Water Surface Elevation

Simulated daily reservoir contents were also assessed against USBR estimates. As discussed in Section 3.2, the USBR estimates reservoir contents from the elevation-volume relationship developed in 1953 from the 1952 U.S. Army Corps of Engineers 10-ft contour map. For model development, a new curve was estimated from the same 1952 contours, using GIS techniques. These curves do not match perfectly, and there is no way at this time to determine which provides a better estimate of reservoir contents based on water elevation. Figure 53 compares the daily reservoir contents estimated by the model to those estimated by the USBR curve and observed water levels. In spite of the differences discussed above, the results compare well, with an average difference of less than 0.1% in the daily contents over the calibration period. Average contents for the full period were 104,000 AF.

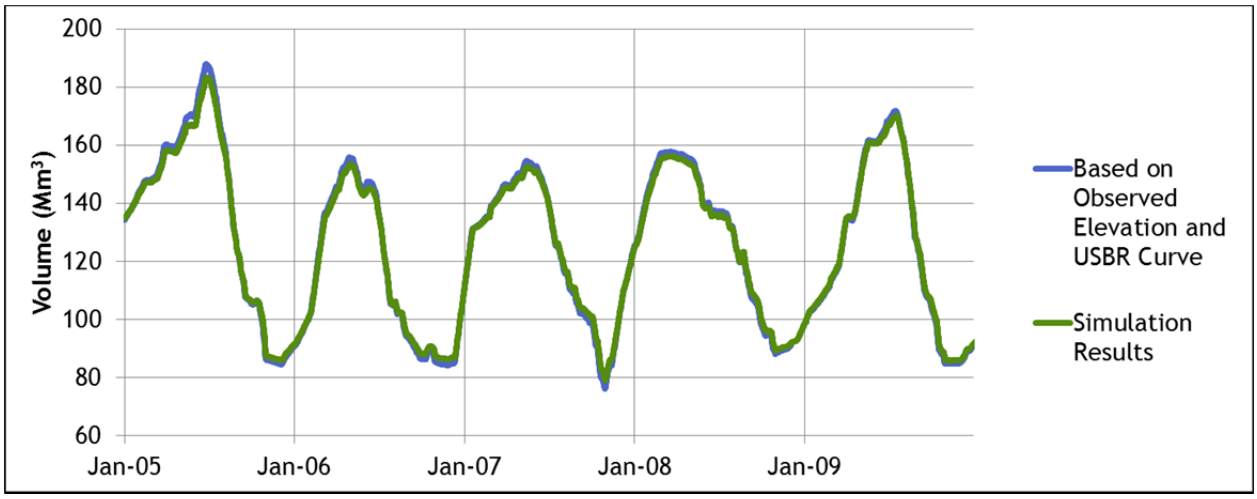

Figure 53. Hydrology Calibration Simulation – Daily Reservoir Volume

Based on these results, the input water balance and the physical representation of the reservoir by a grid of laterally averaged cells discussed in Section 3.2 was deemed a reasonable representation of the reservoir hydrology to support proceeding to the next phase of calibration – water temperature.

3.3.2 Water Temperatures

As discussed in Section 2.3.1, Horsetooth Reservoir stratifies strongly each year, turning over in the fall. Water temperature is simulated as part of the hydrodynamic simulation in CE-QUAL-W2 because of its effect on water density. The following subsections presents the approach to and results of the calibration of water temperature.

3.3.2.1 Approach

Calibration of water temperature focused primarily on adjustment of key coefficients and comparison of output to temperature profile data from HT-INL, HT-SPR, HT-DIX, and HT-SOL for the full calibration period. Conceptually, it is recognized that the thermal response in the reservoir is typically determined by the following major controls:

- Air Temperatures,
- Wind,
- Solar Radiation (long and short wave),
- Inflow Water Temperatures, and
- Hydrodynamics, including bathymetry and water velocity.

Within the model, there are a variety of setting and coefficients that affect the simulated response of water temperature. The key temperature-related coefficients in CE-QUAL-W2 are:

- Hydrodynamic settings
    - Longitudinal eddy viscosity
    - Longitudinal eddy diffusivity
    - Bottom roughness
- Meteorological-related settings
    - Wind sheltering
    - Shading
- Heat exchange settings
    - Air-water/evaporation
    - Water-sediment
- Absorption/reflection settings
    - Absorption of solar radiation in surface layer
    - Extinction coefficients (pure water, organic solids, inorganic solids).

For this model of Horsetooth Reservoir, a subset of key terms and setting were the most sensitive and critical for calibration of water temperatures. First, input of observed solar radiation, as opposed to model-generated solar radiation, made an improvement in the simulation. Originally, the model was set up to estimate solar radiation based on elevation, latitude, and input cloud cover. In an effort to improve simulation results, local observed shortwave solar radiation data were sought, and the CoAgMet FC01 station was located[7]. Figure 54 shows the model generated solar radiation plotted with the observed data from FTC01. Comparison of the ranges of these values shows some underestimation at the upper end by the model and failure to capture some observed variability.

[7] The Christman Field Site also had solar radiation data; however, the data were not suitable for use in the model. The Christman Site uses a pyranometer (pointed upwards), which measures global solar radiation. The model needs input of shortwave solar radiation. When two pyranometers are associated, one oriented upwards and the other downwards, the net short wave radiation is measured.

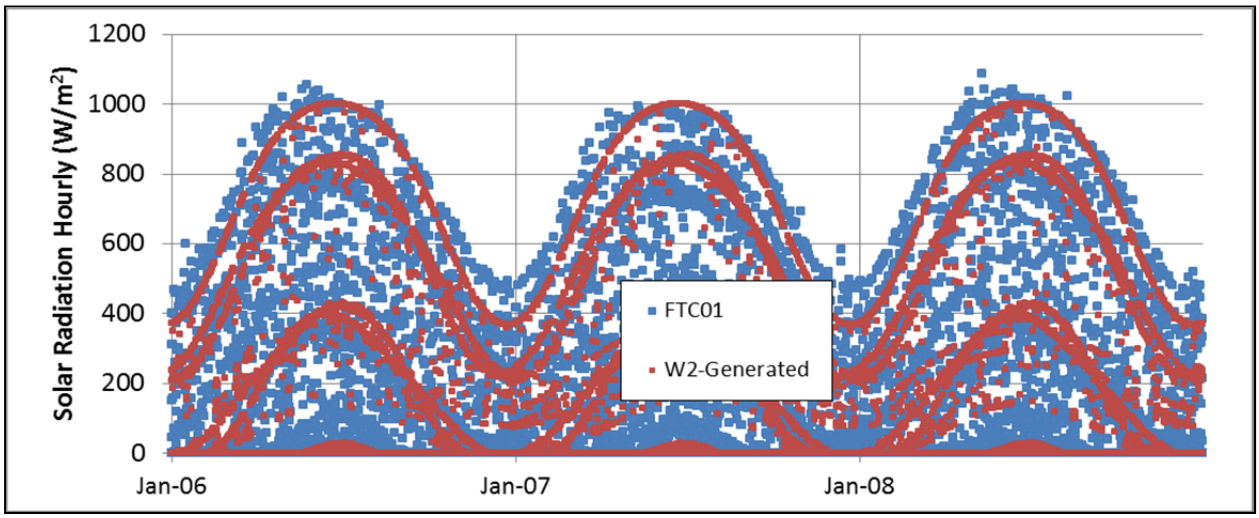

Figure 54. Comparison of Model-Generated and Observed (CoAgMet FTC01) Solar Radiation

Next, adequately capturing the effects of wind on water temperature created a challenge for calibration. Horsetooth Reservoir is located at the edge of the foothills which is a very dynamic and complicated location in terms of wind patterns. Winds coming from over the mountains can form mountain waves, which can result in strong downslope winds (Figure 55). Where these winds reach the ground and where rotors develop can vary from event to event due to atmospheric stratification and other factors. There are also upslope winds and the complicating factors of the existence of barriers to wind in some areas, including the hogback that helps to form Horsetooth (Figure 55). All of this complexity makes it difficult to accurately extrapolate wind data from the Christman Field Site (located 0.5 miles east of the reservoir) to the surface of the reservoir over the 6.5 miles from north to south. Wind direction at the reservoir may also vary from that observed at the Christman field Site, which would affect energy transferred to the reservoir as the fetch varies strongly with wind direction for this system.

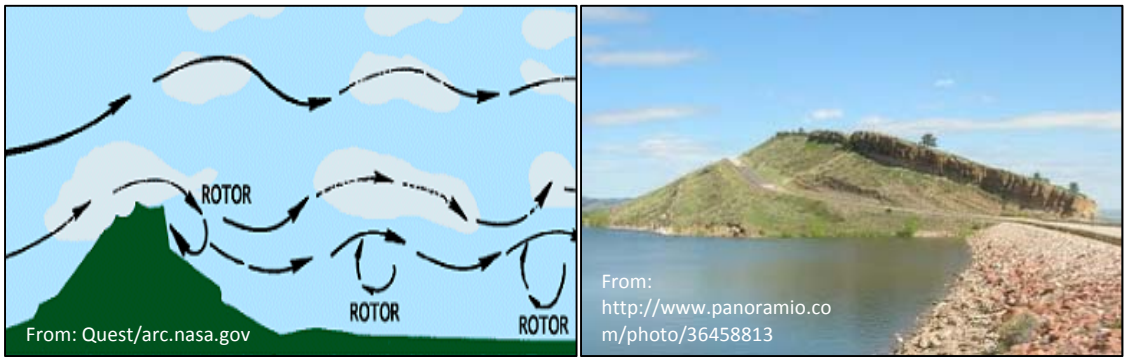

Figure 55. Mountain Wave Schematic and Photo of Hogback near Dixon Dam

Through calibration, wind sheltering coefficients were applied to the Christman wind data to improve the calibration. Wind sheltering coefficients can be used to increase or decrease input wind speeds. After numerous simulations, calibrated coefficient settings ranged from 0% change to 20% sheltering. These settings were applied consistently (same values on a seasonal basis) for each year. Ideally, wind

speed and direction would be collected at the reservoir at more than one location, perhaps on each dam. Data could be collected for a year at these locations and compared to assess the need to continue data collection at more than one location. Such data could improve the calibration; however, for the current purposes of the model, additional wind data collection is not deemed critical, since the calibration was able to adequately capture key responses.

Some of same physical features that cause complexity in estimation of wind over the reservoir can also cause shading over parts of the reservoir at certain times of the day/year. Without input of shading information, the model assumes there is no shading, and the input time-series solar radiation signal reaches 100% of the reservoir at all times. Shading can be specified in the model as a constant percent for each segment, or by inputting barrier distances and heights on either side of each segment and allowing the model to assess shading by input azimuth and calculated angles of the sun throughout the day and year. Both methods were tested, and ultimately, the model was calibrated by applying a uniform 5% shading across the reservoir to account for its position slightly closer to the mountains (relative to the CoAgMet FTC01 location used for solar radiation).

3.3.2.2 Results

In spite of the uncertainties and calibration challenges discussed above, the water temperature calibration for the reservoir is good. The model appropriately simulates formation and breakdown of stratification from year to year. Figure 56 shows model output for the five year calibration simulation at the HT-SOL location. This figure shows color profiles for each day of the simulation, and also includes representation of the changing water level.

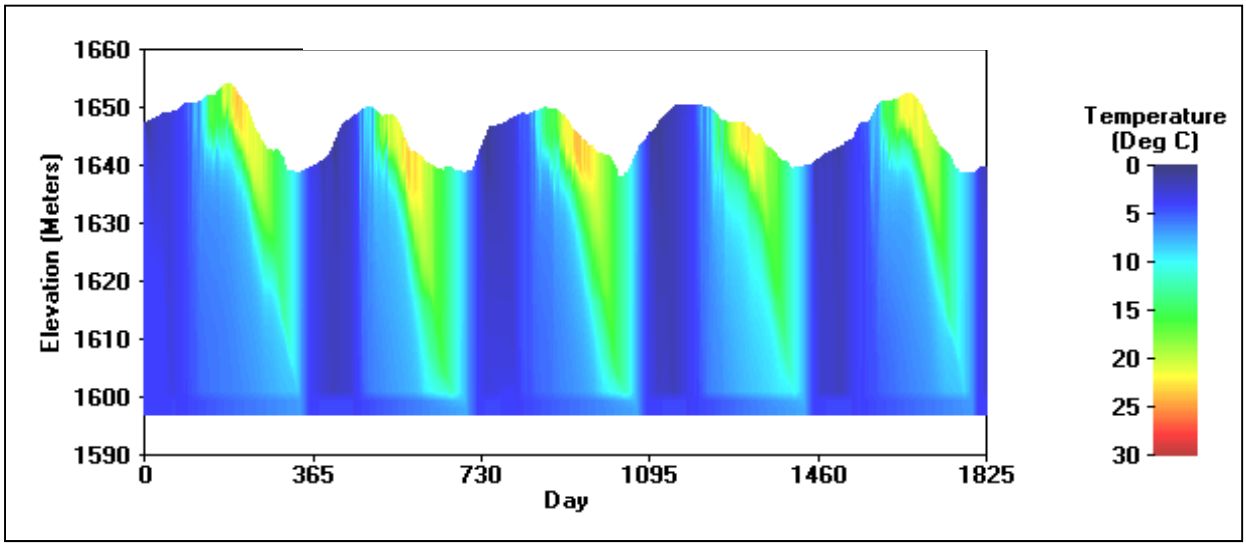

Figure 56. Calibration Period Thermal Simulation at Soldier Canyon (HT-SOL), 2005 through 2010

For a more detailed assessment of the temperature calibration, model results were compared to observed temperature profiles. For the calibration period of 2005 through 2010, the observed data set includes a total of 312 observed profiles. Model output was retrieved at each sampling location at noon on the day of each observed profile for direct comparison. Appendix A presents the full set of observed

and simulated profile plots for the calibration period. Subsets of these plots from 2009 are presented here in the main report to support the discussion.

Figure 57 presents results from HT-SOL for four dates over 2009. These plots show how the model is successfully simulating the formation of stratification, matching the hypolimnion and epilimnion temperatures, and capturing the metalimnion depth. These figures also presents absolute mean error (AME)[8] and root mean squared error (RMSE) for each profile in units of degrees Celsius (°C). Figure 58 presents observed and simulated 2009 profiles from locations across the reservoir on September 29, 2009. This is a dynamic time near the end of the stratified period in 2009, and Figure 58 shows that the model is capturing the spatial variability across the reservoir. Specifically, stratification is not as strong at HT-SOL at this time when the metalimnion is deepening across the reservoir and flows out of Horsetooth Dam to the Hansen Supply Canal are high. This simulated difference appears to be accurately reflecting the hydrodynamic effects of outflows on stratification that were noted in review of the observed dataset (Section 2.3.1).

[8] AME is one quantitative assessment of the difference between observed and simulated results (residuals). For each profile, the absolute value of differences between each observed-simulated pair are calculated then averaged. RMSE is another quantitative assessment of residuals, and is often considered a measure of accuracy of prediction of individual points. RMSE is calculated by squaring the residuals, summing these squared values, dividing by the number of values, then taking the square root of that number.

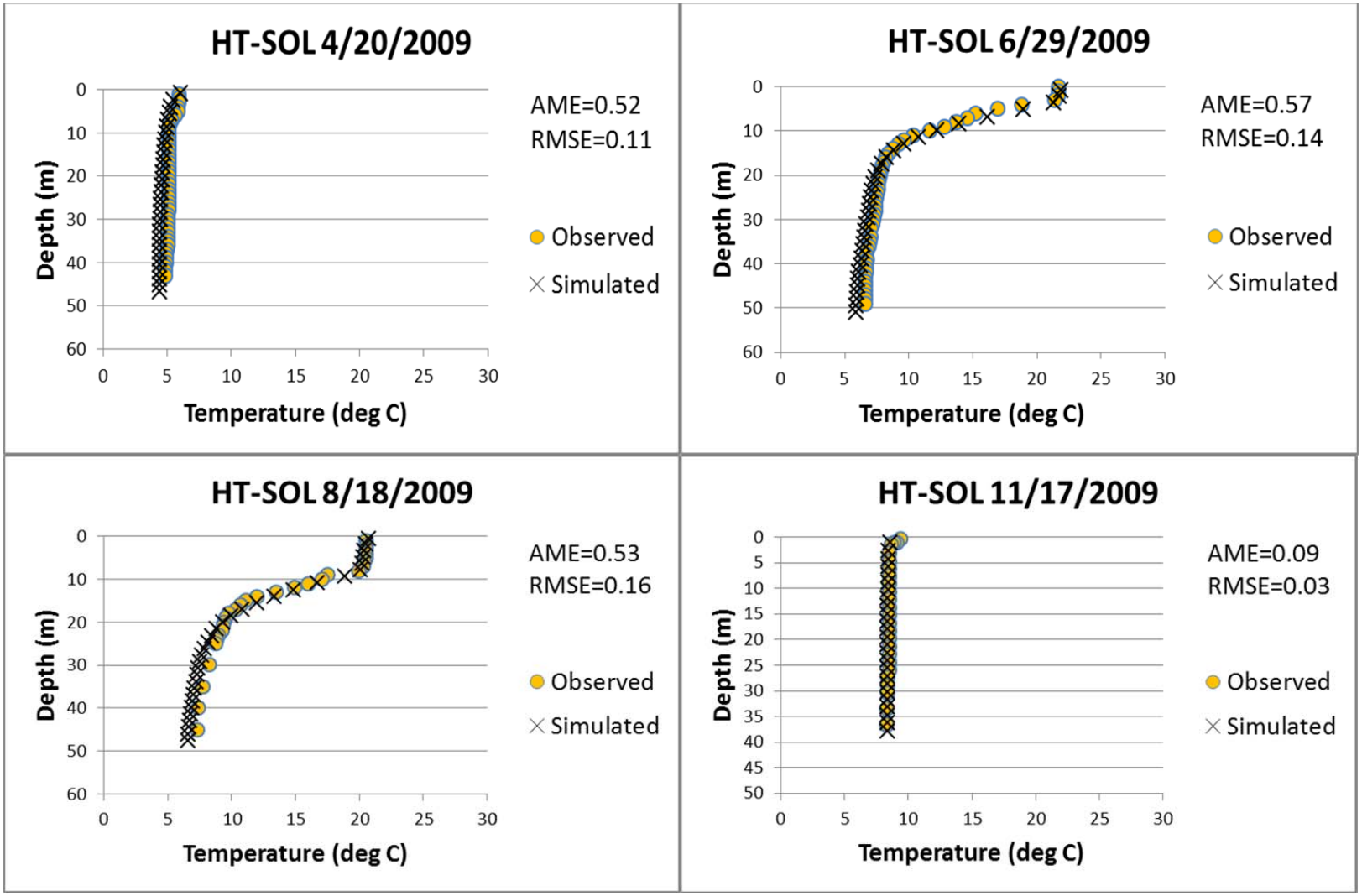

Figure 57. Comparison of Observed and Simulated Temperature Profiles at HT-SOL in 2009

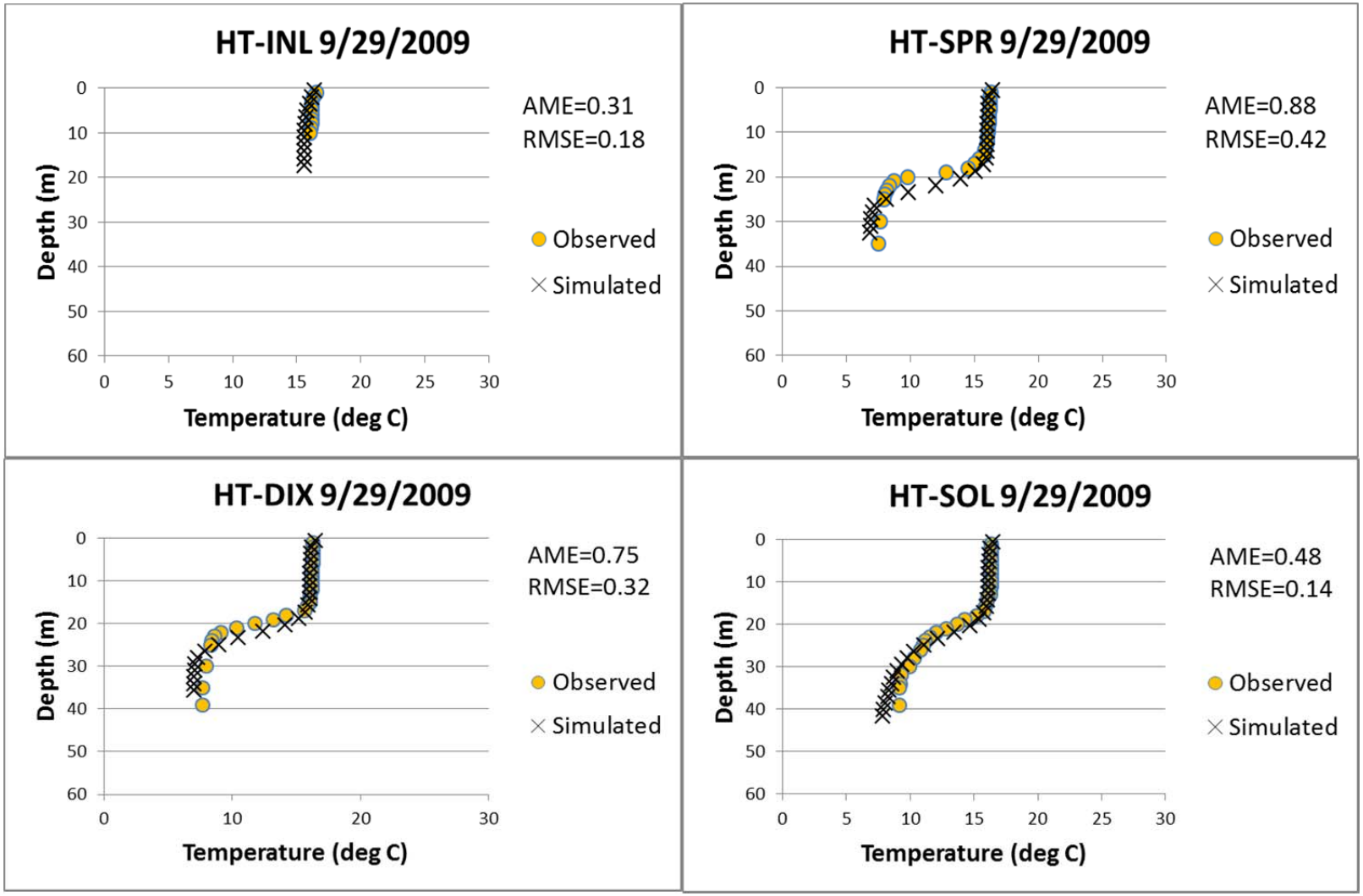

Figure 58. Comparison of Observed and Simulated Temperature Profiles across the Reservoir on September 29, 2009

Calibration was reviewed for all profiles in the calibration period (plots presented in Appendix A). The AME for the full set of 312 calibration profiles is 0.6°C, ranging from 0.02°C to 2.1°C for individual profiles. The RMSE for the full set of calibration profiles is 0.2°C, ranging from 0.012°C to 1.0°C for individual profiles. As presented in the tables in Appendix A, AME and RMSE values do not show any obvious trending with time through the model simulation period. Most importantly, the model does a good job of capturing the timing of water temperature changes, the depth and thickness of the metalimnion over time, and spatial variations across the reservoir for all of the years of the calibration period. Good simulation of water temperature is critical to support simulation of water-quality parameters of interest (e.g., nutrients, TOC, algae, and DO) and relevant reactions and transformations that vary strongly as a function of temperature and stratification. These good results in temperature calibration also give additional confidence that the hydrodynamic simulation is performing well.

3.3.3 Water Quality

The modeling objectives were the basis for defining focus parameters and match locations for the water-quality calibration. The overriding objective is to create a modeling tool that can simulate the effects of hydrodynamics, operations, and inflow water quality on key in-reservoir water-quality parameters (dissolved oxygen and TOC). Through this process an understanding must be developed of the causes of low metalimnetic and hypolimnetic dissolved oxygen. The model must also be able to simulate TOC concentrations at the outlet works at Soldier Canyon, a key concern for water treatment. Based on this and the existing conceptual understanding of the reservoir, the following focus parameters were identified for the water-quality calibration:

- Nutrients – Simulation of algal uptake patterns and sediment release patterns for ammonia (NH3), nitrate plus nitrite (NO3+NO2), and orthophosphate (PO4) across the reservoir.
- TOC – Simulation of TOC concentrations in top and bottom measurements across the reservoir as well as outflow concentrations observed at Soldier Canyon outlet works.
- Algae – Simulation of algal growth patterns as measured by chlorophyll *a* concentrations in the 0-to-5 m composite measurements across the reservoir.
- Dissolved Oxygen – Simulation of top and bottom concentrations across the reservoir as well as individual profiles.

The following subsections present the calibration for nutrients, TOC, chlorophyll *a*, and dissolved oxygen. Each discussion presents an overview of how the model conceptualizes each parameter, a plot of inflow inputs, a discussion of the calibration approach taken, and a presentation of the calibration results (graphical and numerical). Findings and uncertainties are also discussed.

3.3.3.1 Nutrients

Inorganic nutrients are simulated in the model as state variables of nitrate (plus nitrite), ammonium, and orthophosphate. Figure 59, Figure 60, and Figure 61 present kinetic diagrams from the model documentation of gain and loss mechanisms simulated in the model, excluding advection and diffusion. As indicated with black-line slashes in these figures, macrophytes and epiphyton were not included in the simulation for Horsetooth Reservoir.

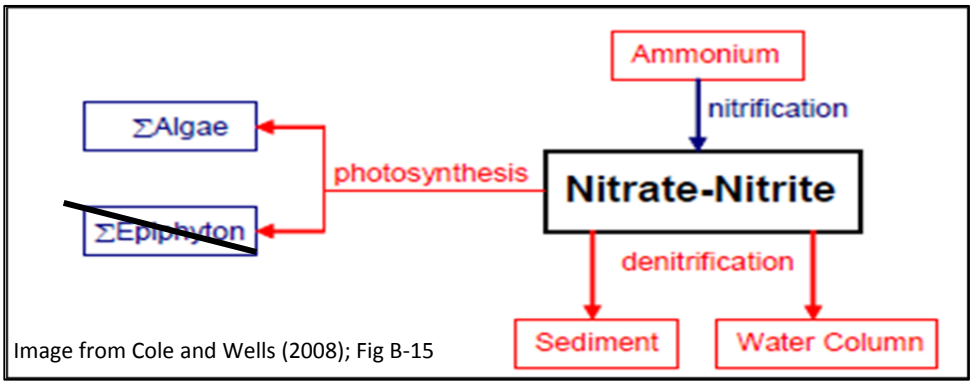

Figure 59. Kinetic Diagram of Gain and Loss Mechanisms for Nitrate-Nitrite in the Model

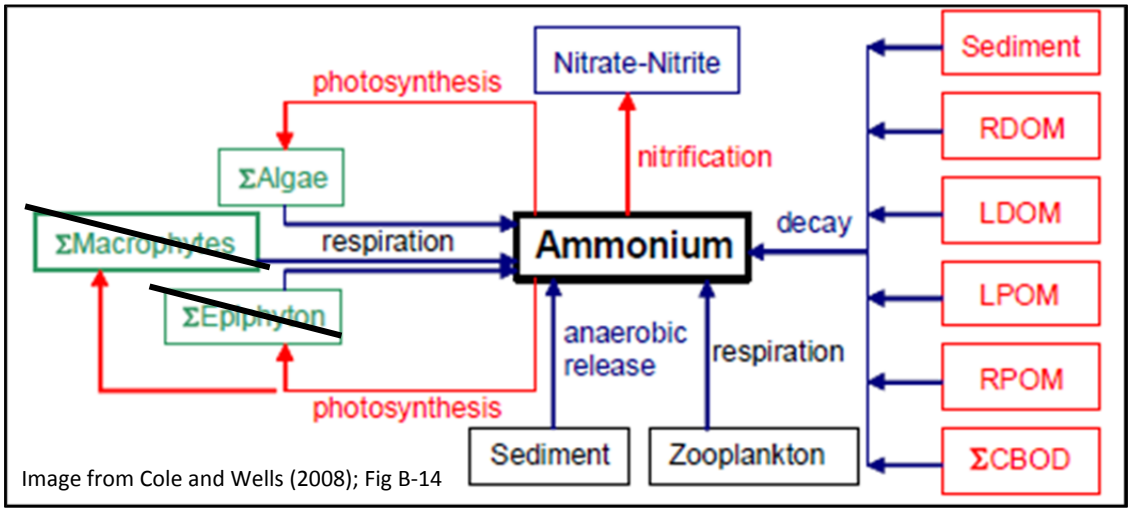

Figure 60. Kinetic Diagram of Gain and Loss Mechanisms for Ammonium (NH4+) in the Model

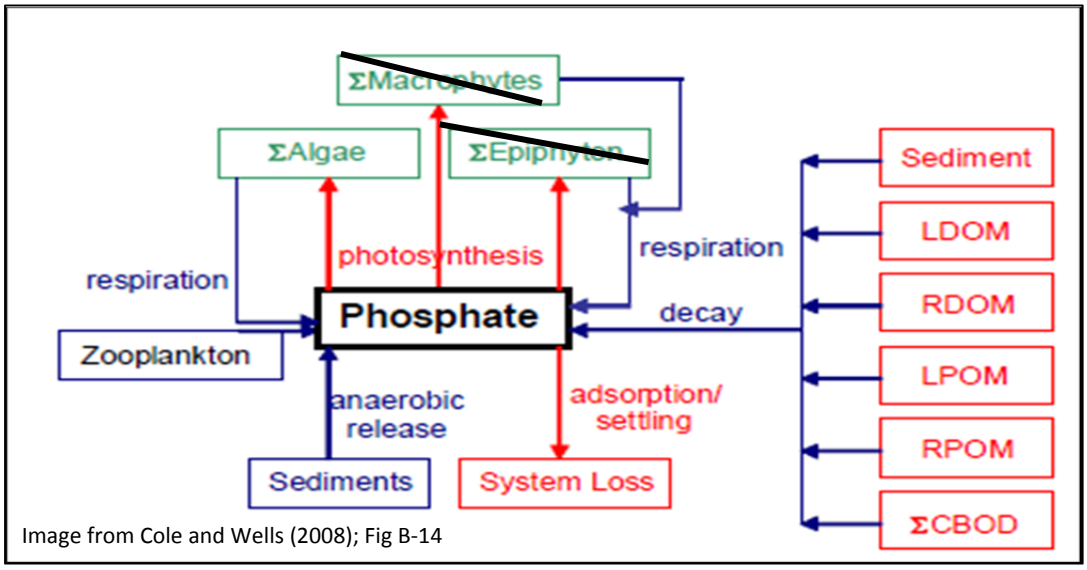

Figure 61. Kinetic Diagram of Gain and Loss Mechanisms for Phosphate in the Model

As shown in Figure 59, Figure 60, and Figure 61, nitrate, ammonia, and orthophosphate are subject to the following reactions and gain/loss mechanisms in the model:

- Nitrate can be produced from ammonia through nitrification and lost by denitrification (microbially-facilitated process of nitrogen reduction). Nitrate can also be taken up by algae as part of photosynthesis.

- Ammonia is a product of the decay of organic matter (all forms of sediment organic matter or water column organic matter). Ammonia can also be simulated to enter the water column by anaerobic release from the sediments and as a product of algal or zooplankton respiration. Ammonia can be converted to nitrate via nitrification or taken up by algae through photosynthesis.

- Phosphate is simulated as a product of decay of organic matter in the water column. Phosphate is also simulated to be released from the sediment under anaerobic conditions and as a product of algal and zooplankton respiration. As with ammonia and nitrate, phosphate is consumed by algae through photosynthesis. Phosphate can also be lost via adsorption and settling if this function is enabled in the model; however, use of this function is not recommended because the model does not have a true diagenesis approach to tracking settled nutrient mass into the sediments (Cole and Wells, 2008). Further, this mechanism is not expected to be significant in this system because available sites for phosphorus adsorption onto inflowing inorganic suspended solids would be extremely limited, so little sorption would take place when inorganic suspended solids enter into a reservoir (Cole and Wells, 2008).

3.3.3.1.1 Inflow Nutrient Concentrations

Figure 62 presents the input inflow concentrations of nitrate, ammonia, and phosphate for the calibration period from 2005 through 2009 in mg/L (input units for the model). Inflow concentrations range up to 274 ug/L, 75 ug/L, and 32 ug/L for nitrate, ammonia, and phosphate, respectively. For all values reported below the detection limit, a value equal to half of the detection limit was used.

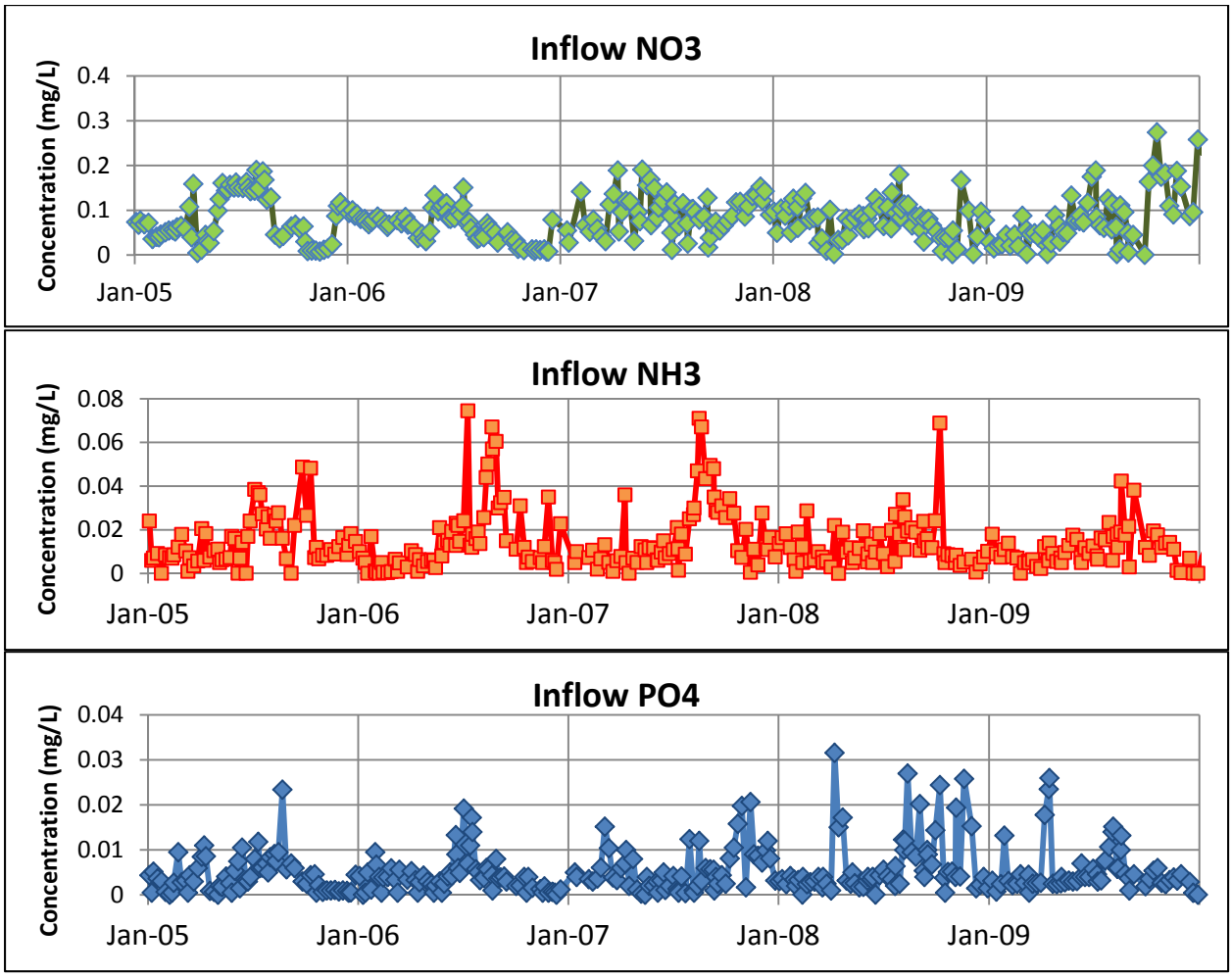

Figure 62. Calibration Period Input - Inflow Nutrient Concentrations

3.3.3.1.2 Calibration of Nutrient Concentrations

Calibration of the model for nutrients required adjustments of algal growth, ammonia and phosphorus release rates from sediment (in coordination with the hypolimnetic dissolved oxygen calibration), nitrification/dentrification rates, and organic matter degradation rates. Due to the importance of multiple major mechanisms for each parameter, the calibration required an integrated and iterative approach (as opposed to a step-wise approach).

Through hundreds of simulations, much was learned about how the system works for the calibration period. At the top of the reservoir, nutrient concentrations are largely controlled by inflow concentrations as modified by algal uptake. Algal uptake is important in both summer and winter. Each summer, across the reservoir, nitrate and orthophosphate are largely consumed from the upper layer of the reservoir by algae, whereas ammonia concentrations are more variable in this period, possibly suggesting algae are not strongly NH3 preferring. At the bottom of the reservoir, the nutrient concentrations are largely a function of release of nitrate and ammonia from the sediments. Ammonia is, in turn, converted to nitrate in the lower water column when adequate oxygen is still available.

Figure 63, Figure 64, and Figure 65 present simulated and observed nitrate, ammonia, and phosphate concentrations at the top (simulated average of the top 1.5 m compared to observed grabs at 1 m) of the reservoir for the calibration period (2005-2009). These figures present results at HT-SPR. Calibration results across the reservoir, show similar results (all calibration results are presented in Appendix B). The model is successfully capturing the range of observed concentrations. The model is also simulating the overall seasonal patterns of reduced summer concentrations attributable to algal consumption. All three parameters were sensitive in the upper water column to algal growth patterns and organic matter decay rates.

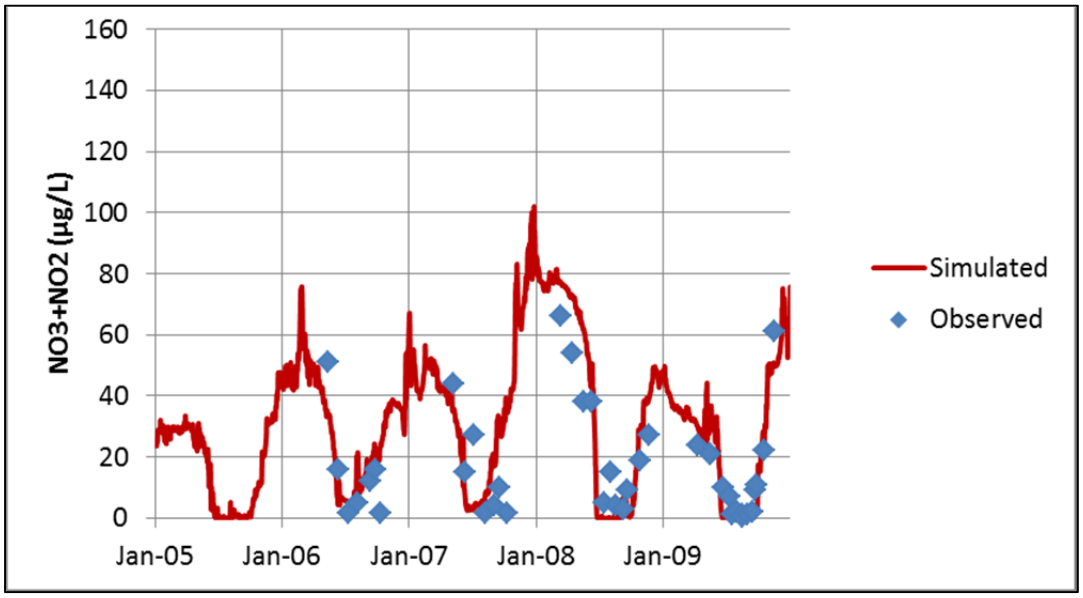

Figure 63. Comparison of Observed and Calibrated Nitrate Concentrations at the Top of the Reservoir at HT-SPR, 2005 through 2009

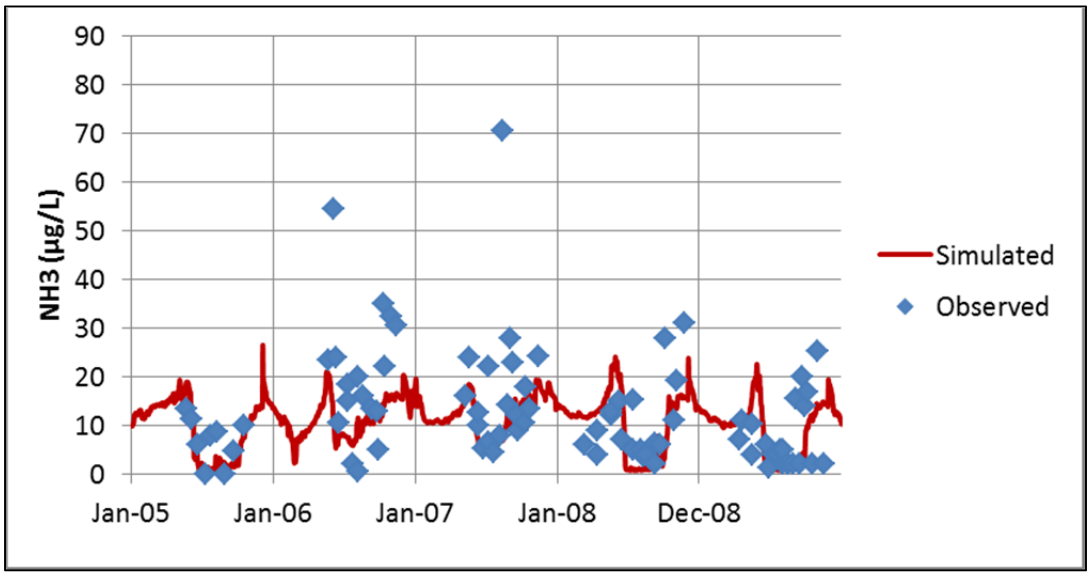

Figure 64. Comparison of Observed and Calibrated Ammonia Concentrations at the Top of the Reservoir at HT-SPR, 2005 through 2009

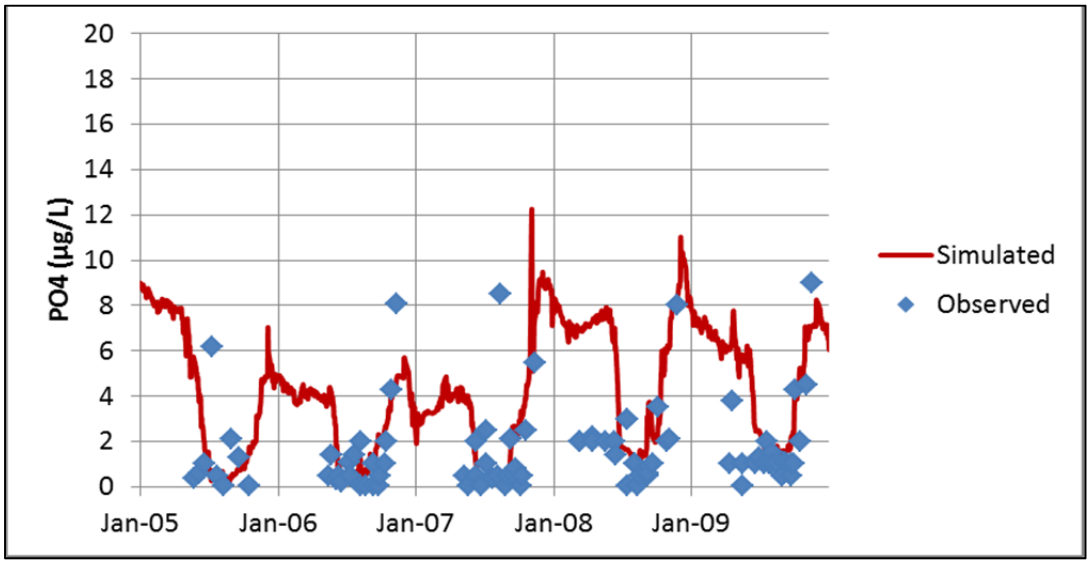

Figure 65. Comparison of Observed and Calibrated Phosphate Concentrations at the Top of the Reservoir at HT-SPR, 2005 through 2009

Figure 66, Figure 67, and Figure 68 present simulated and observed nitrate, ammonia, and phosphate concentrations at the bottom of the reservoir (simulated average of the bottom 1.5 m compared to observed grabs at 1 m from bottom) for the calibration period (2005-2009). The model is successfully capturing the range and timing of observed concentrations. The model is also capturing the patterns of variation in peak concentrations between the Inlet, Spring, Dixon, and Soldier locations. Generally, the observed data show greater sediment nutrient releases at Spring Canyon and less at Soldier Canyon, with the least occurring at the Inlet (which is shallow relative to the other locations). The Spring Canyon

location is likely to receive (by settling) more of the particulate organic matter that enters the reservoir from the Hansen Feeder Canal (as compared to Dixon Canyon or Soldier Canyon). Calibration of nutrient concentrations at the bottom of the reservoir required adjustment of release rates and sediment organic matter decay rates, and were extremely sensitive to the sediment oxygen demand. One challenge in calibration was setting the nitrification rate high enough that ammonia released from sediment would be converted to nitrate, but not too high so that ammonia at the surface of the reservoir was reduced below observed levels.

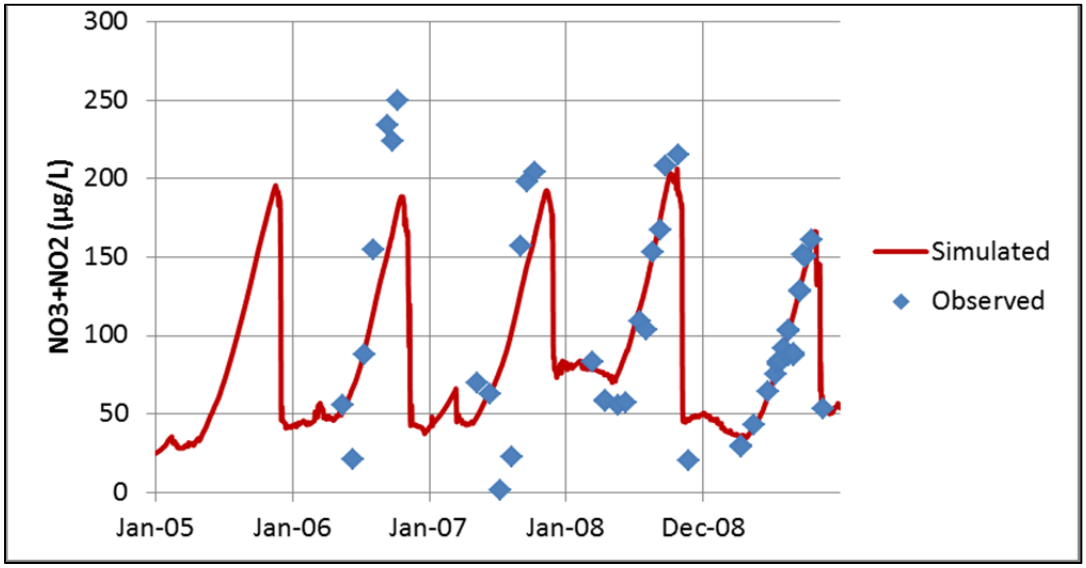

Figure 66. Comparison of Observed and Calibrated Nitrate Concentrations at the Bottom of the Reservoir at HT-DIX, 2005 through 2009

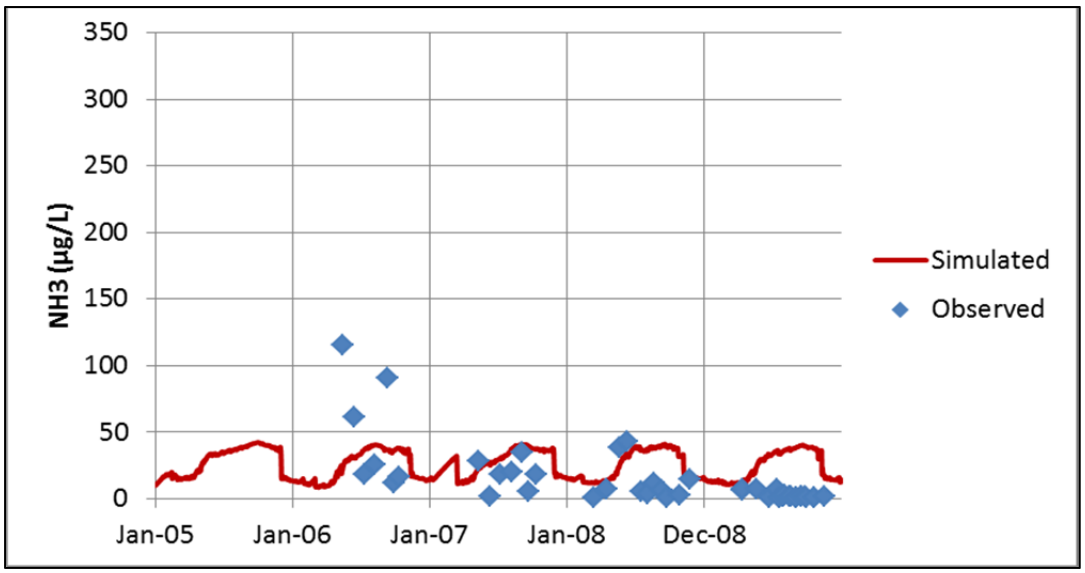

Figure 67. Comparison of Observed and Calibrated Ammonia Concentrations at the Bottom of the Reservoir at HT-DIX, 2005 through 2009

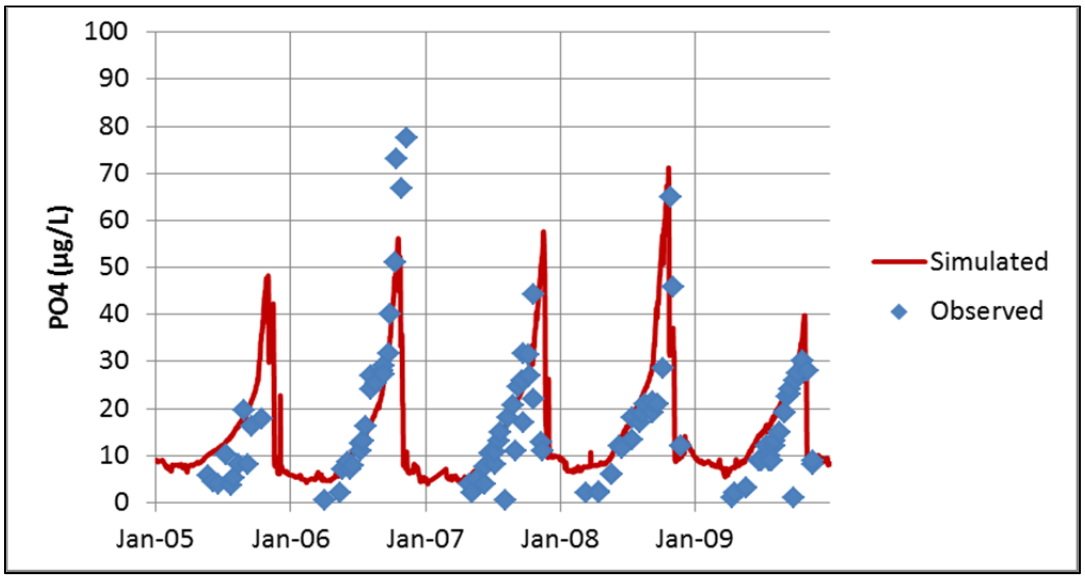

Figure 68. Comparison of Observed and Calibrated Phosphate Concentrations at the bottom of the Reservoir at HT-DIX, 2005 through 2009

3.3.3.1.3 Nutrient Calibration Summary

The calibrated model successfully simulates observed seasonal patterns and concentrations ranges of nitrate, ammonia, and orthophosphate at the top and bottom of the reservoir. All three parameters are largely controlled in the upper water column by algal growth patterns and organic matter decay rates. Nutrient concentrations at the bottom of the reservoir are also somewhat sensitive to algal growth patterns during de-stratified periods, but capturing the larger seasonal concentration patterns and ranges at depth is primarily dependent on adequate simulation of hypolimnetic dissolved oxygen concentrations.

3.3.3.2 Total Organic Carbon

As discussed above, the simulation of TOC in the reservoir focused on matching observed patterns and concentration ranges at the top and bottom of the reservoir as well as in the observed outflow at Soldier Canyon. In reality, TOC is not a single chemical, but a continuum of aliphatic and aromatic organic molecules with varying molecular compositions and degradation rates. This continuum of TOC molecules is simulated in the model as fractions of dissolved and particulate organic matter. The dissolved and particulate fractions are further subdivided into labile (more easily degraded) and refractory (more resistant to degradation) fractions. As such, TOC is simulated as four separate state variables in the model:

- LDOM – Labile dissolved organic matter,
- RDOM – Refractory dissolved organic matter,
- LPOM – Labile particulate organic matter, and

- RPOM – Refractory particulate organic matter.

These four state variables are subject to different gain and loss mechanisms. Note: TOC also includes algae and zooplankton. Figure 69 and Figure 70 present kinetic diagrams of the gain and loss mechanisms (excluding reservoir inflow and outflow terms) simulated in the model for or each organic matter state variable. As with the kinetic diagrams presented for nutrients, the black-line slashes in the labile fraction figures indicate that epiphyton and macrophytes were not simulated in the Horsetooth model.

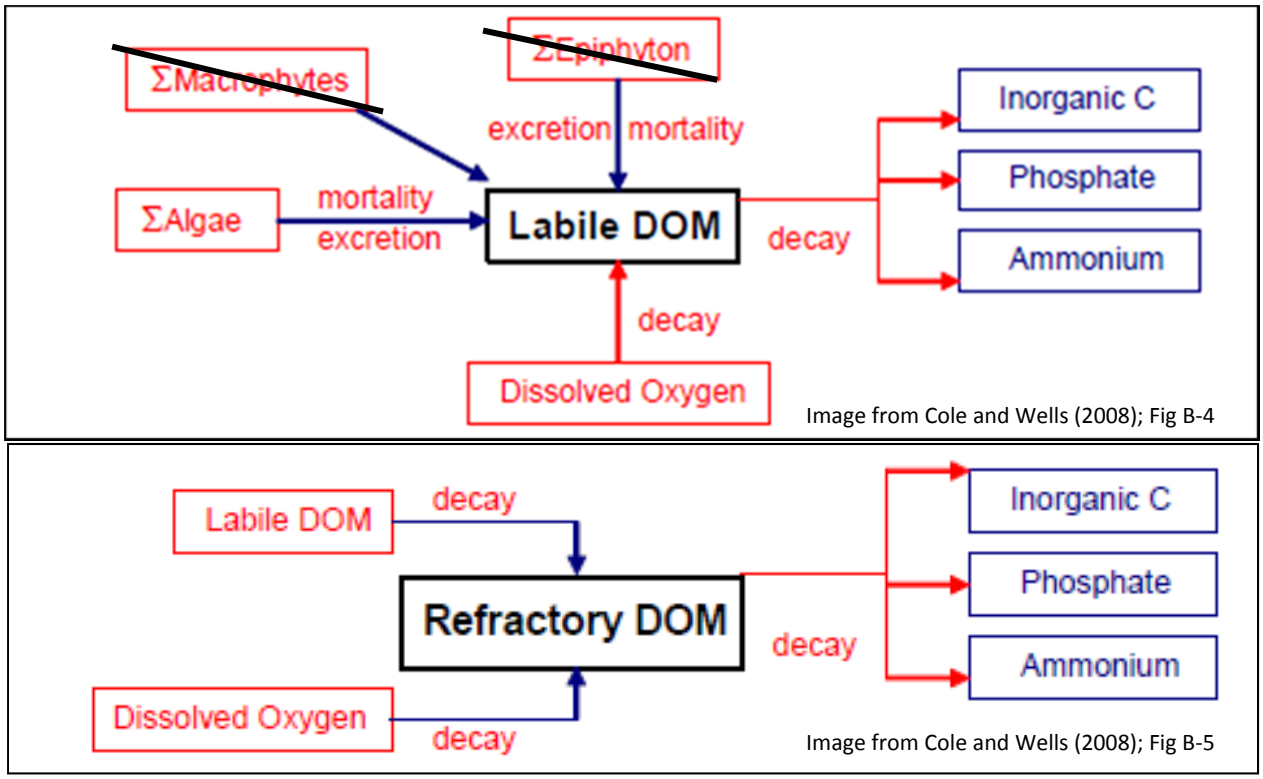

Figure 69. Kinetic Diagram of Gain and Loss Mechanisms for Labile and Refractory Dissolved Organic Matter in the Model

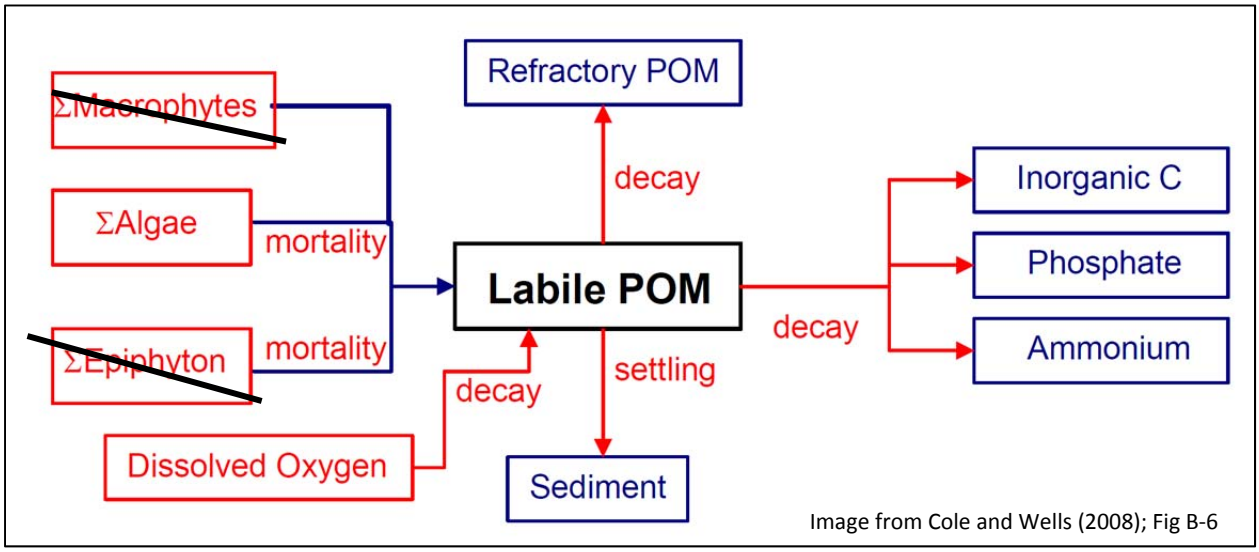

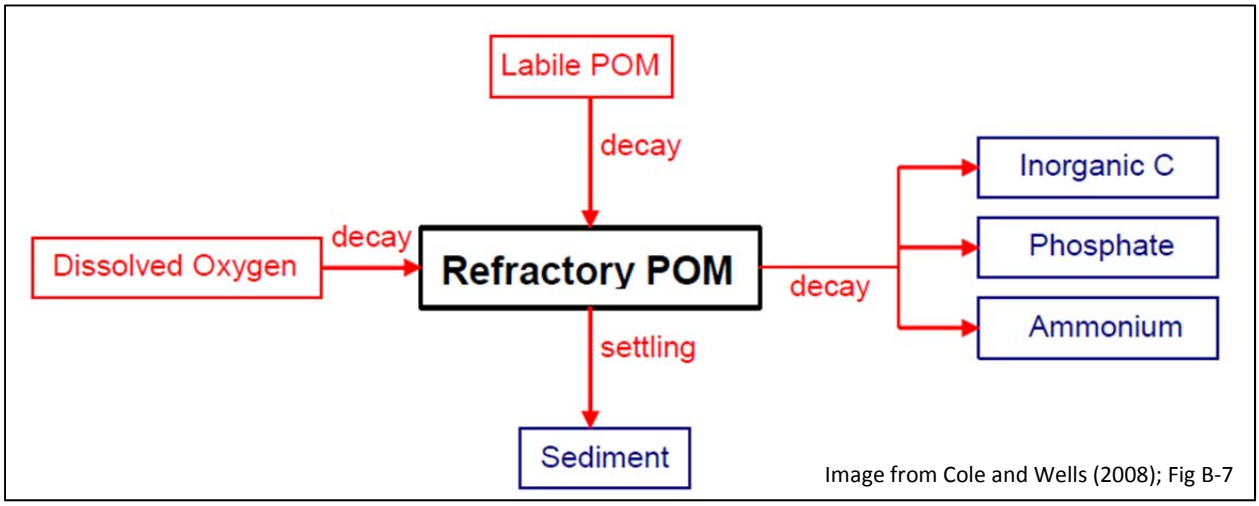

Figure 70. Kinetic Diagram of Gain and Loss Mechanisms for Labile and Refractory Particulate Organic Matter in the Model

As shown in Figure 69 and Figure 70, the TOC fractions are subject to the following reactions and gain/loss mechanisms in the model:

- LDOM is produced by algal excretion or algal decay. LDOM is subject to aerobic decay, producing inorganic carbon, phosphate, and ammonium.
- RDOM can be produced through decay of LDOM. Aerobic RDOM decay is, by definition, slower than LDOM decay; however, the byproducts are the same: inorganic carbon, phosphate, and ammonia.
- LPOM is produced with the death of algae. LPOM is subject to aerobic decay, producing inorganic carbon, phosphate, and ammonium. Because it is particulate, it is also subject to settling and can be lost to sediment.

- RPOM can be produced through decay of LPOM. Aerobic RPOM decay is, by definition, slower than LPOM decay; however, the byproducts are the same, inorganic carbon, phosphate, and ammonia. Because it is particulate, it is also subject to settling and can be lost to sediment.

3.3.3.2.1 Inflow Total Organic Carbon Concentrations

As described above, the model simulates TOC as the total of four fractions (in addition to algae and zooplankton); therefore, the model requires input of concentrations for each fraction. Currently, only observed TOC concentrations are available at the inflow, so assumptions were required to define the inflow concentrations of each of the four fractions. Six grab sample analyses from samples collected in July, August, and September of 2009 included both dissolved and total organic matter concentrations. These data showed consistently high percentages of dissolved organic matter, with an average of 96% dissolved. Based on this, it was assumed that all inflow TOC is 4% particulate and 96% dissolved.

There are no direct data to support assignment of labile and refractory fractions. The contributing watershed for the Hansen Supply Canal includes a wide variety of sources of organic matter that would all be expected to have different labile and refractory fractions, some varying seasonally. Sources of organic matter include the C-BT inflows. The C-BT inflows can include allochtonous organic matter (generally more refractory watershed runoff sources) and autocthonous organic matter (generally more labile material produced within a water body). Ratios would depend on operations, runoff patterns for that year, and time of the year. Other sources of organic matter to the Hansen Supply Canal include east slope wastewater treatment plants, runoff in the upper Big Thompson watershed, and organic matter produced/modified in east slope reservoirs upstream of Horsetooth Reservoir.

It was decided that time-variation of assumed labile-to-refractory fractions would be limited to two seasons and would be consistently assigned from year to year. The seasons were set to April through June (generally covering the east slope runoff period) and July through March (representing more trans-basin water sources). While this is expected to be an oversimplification that may miss shorter term and year-to-year differences in reservoir response attributable to the fractionation patterns, data do not exist to support more complex temporal breakdown of the TOC input. Recognizing the important role of inflowing organic matter fractionation on reservoir water quality and outflow, collection of additional data to support modeling and corresponding applications is being discussed with Northern Water.

Assignment of the labile-to-refractory fractions for the two seasons was part of the calibration. Generally, labile fractions were set to be low, with even lower fractions in the east slope spring runoff period (April-June). This pattern of greater refractory fractions during runoff is typical and matches the general (non-quantitative fractionation) findings of Beggs (2010) who completed a study of the humic and fulvic material in the watershed and Hansen Supply Canal. Through calibration, values of 10% labile during runoff (April-June) and 20% over the rest of the year were assigned. Figure 71 presents the resultant fractionation applied seasonally to the observed inflow TOC to develop model inputs.

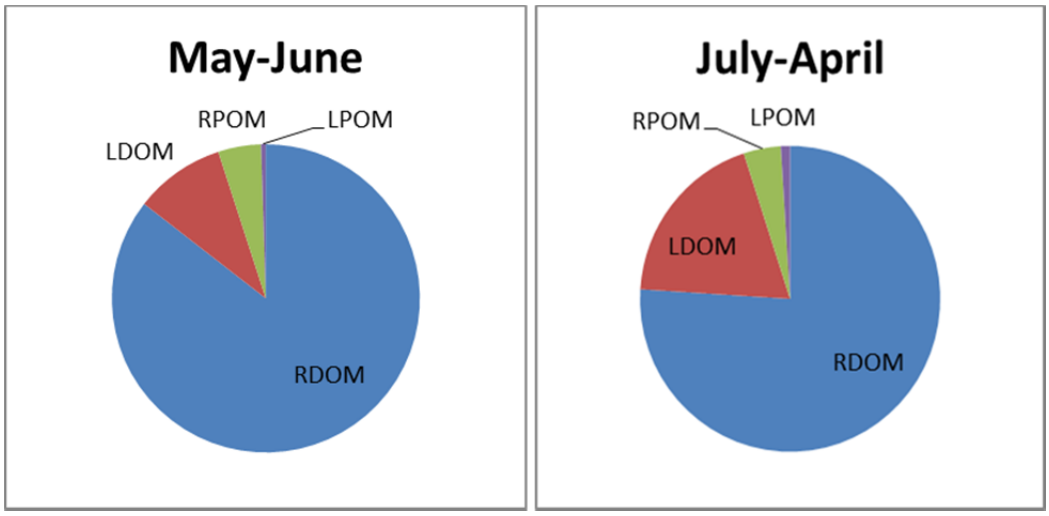

Figure 71. Pie Charts of Assigned Fractionation of TOC for Model Input at Hansen Feeder Canal

Figure 72 and Figure 73 present the results of application of this seasonal fractionation to inflow TOC data. Dissolved organic matter fractions represent the majority of inflow TOC, and the seasonal TOC pattern is reflected clearly in the RDOM inflow concentrations. Note: inflowing algal and zooplankton organic carbon were subtracted from the TOC total before fractionation of the inflow.

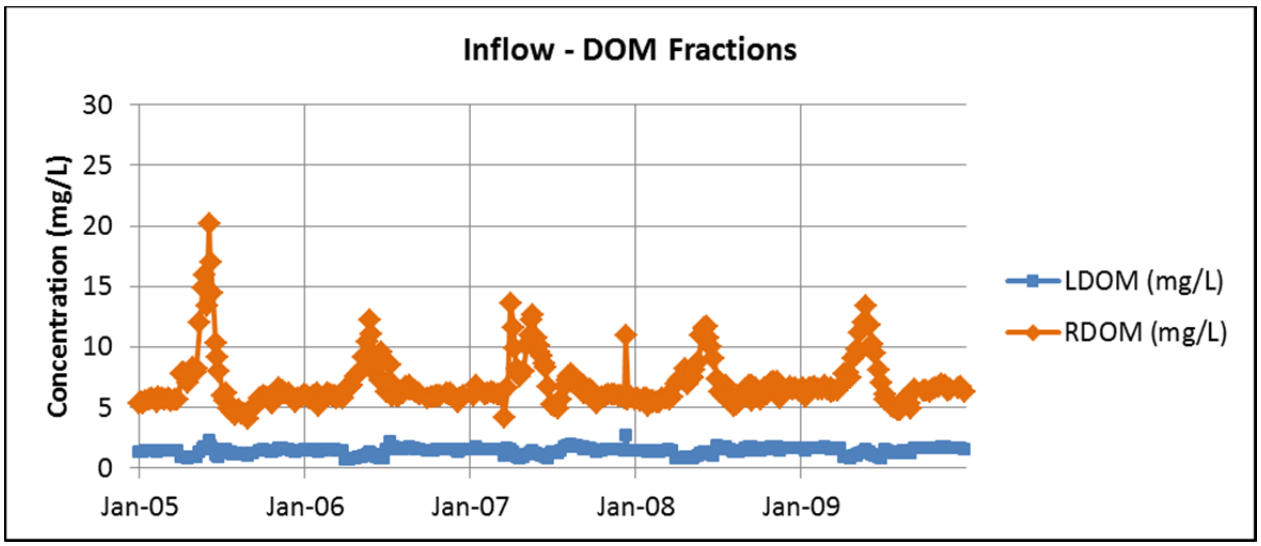

Figure 72. Inputs for Hansen Feeder Canal Dissolved Organic Matter Concentrations, 2005 through 2009

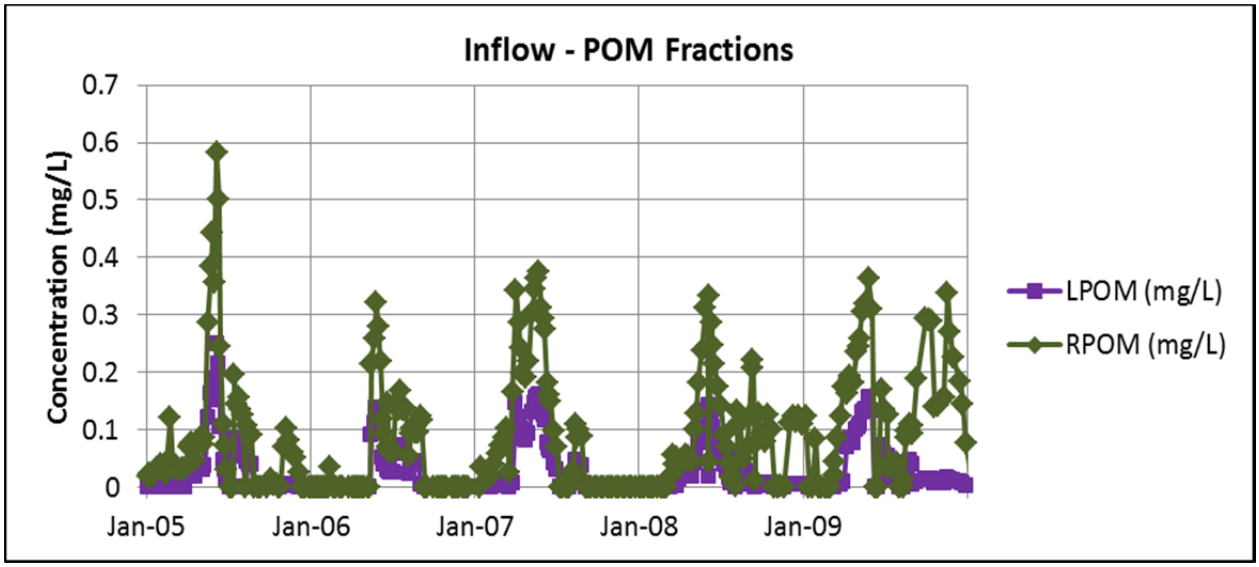

Figure 73. Inputs for Hansen Feeder Canal Particulate Organic Matter Concentrations, 2005 through 2009

3.3.3.2.2 Calibration of Total Organic Carbon Concentrations

Calibration of the model for TOC simulation required adjustments of inflow fractionation, as discussed above, as well as calibration of decay rates and Arrhenius temperature rate multipliers for the various fractions. The model allows setting of decay rates for labile and refractory fractions as well as sediment organic matter decay rates. The rate of labile decay to refractory organic matter is also a variable for both dissolved and particulate organic matter. To set these decay rates, the CE-QUAL-W2-recommended 100-to-1 ratio for labile-to-refractory decay rates was honored in calibration. Because dissolved oxygen is consumed in conjunction with TOC decay, calibration of TOC was conducted in coordination with the dissolved oxygen calibration. The TOC calibration was also closely tied to the simulation of algae/zooplankton, which is part of the TOC total and also produces organic matter through excretion and mortality.

Figure 74 presents simulated and observed TOC concentrations at the top of the reservoir (simulated average of the top 1.5 m compared to observed grabs at 1 m) for the calibration period of 2005 through 2009. Figure 75 presents simulated and observed TOC concentrations at the bottom of the reservoir (simulated average of the bottom 1.5 m compared to observed grabs at 1 m from bottom). Winter TOC concentrations at the top of the reservoir are consistently slightly over-predicted (on the order of 0.2 mg/L TOC), and peak concentrations at HT-SOL are consistently slightly under-predicted (on the order of 0.5 mg/L). Overall, however, the model successfully simulates major seasonal patterns and concentrations ranges across the reservoir for this complicated multi-variable term, in spite of uncertainty in inflow fractionation. At the top of the reservoir, TOC concentrations were a function of inflow concentrations and decay rates, with peak concentrations related to algal growth patterns. At the bottom of the reservoir, there is less seasonal variation than at the top, and the model is successfully simulating this difference. Average AME and RMSE values across the top and bottom of the reservoir were between 0.2 mg/L and 0.3 mg/L for the calibration period.

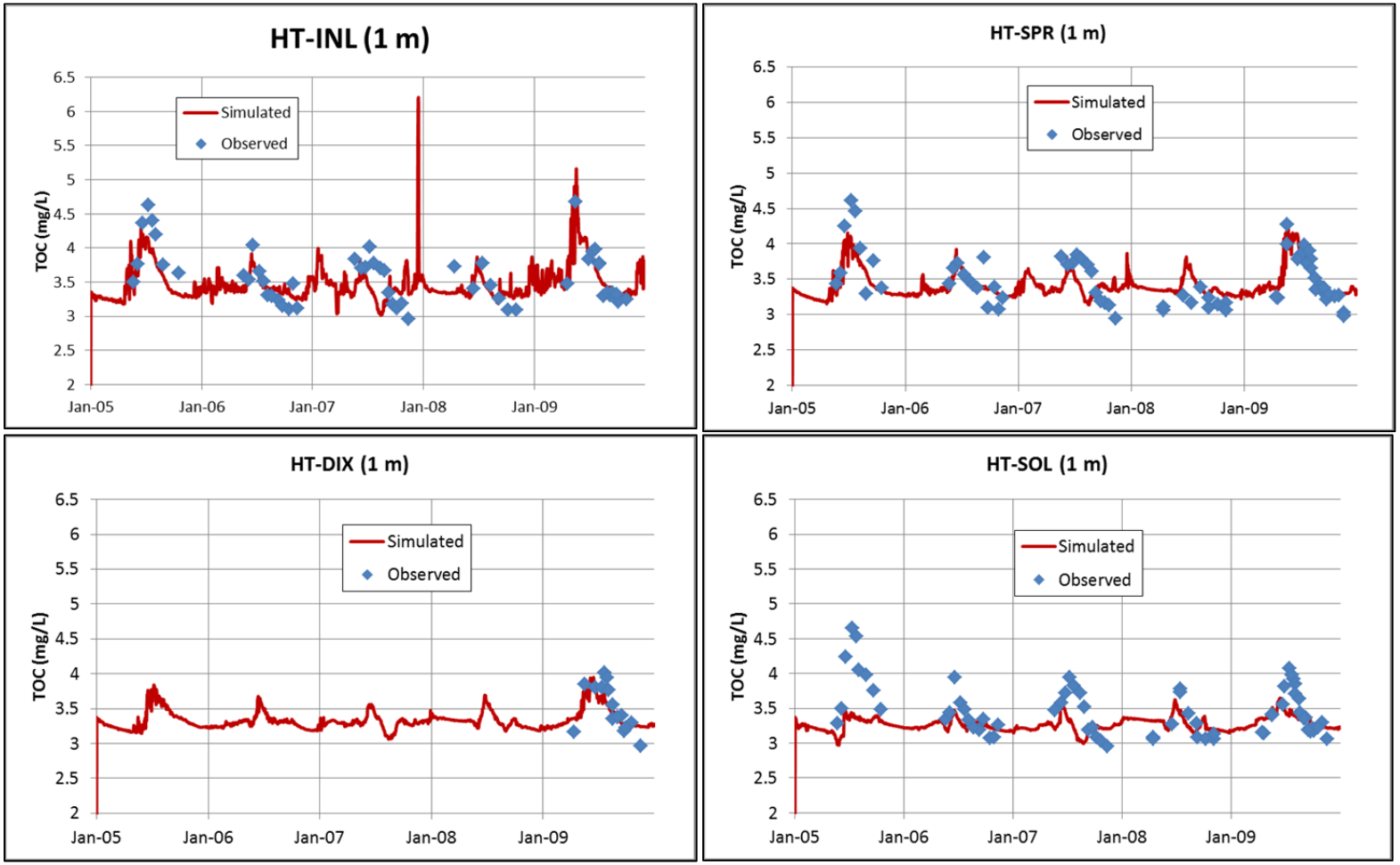

Figure 74. Simulated and Observed TOC at the Top of the Reservoir, 2005 through 2009

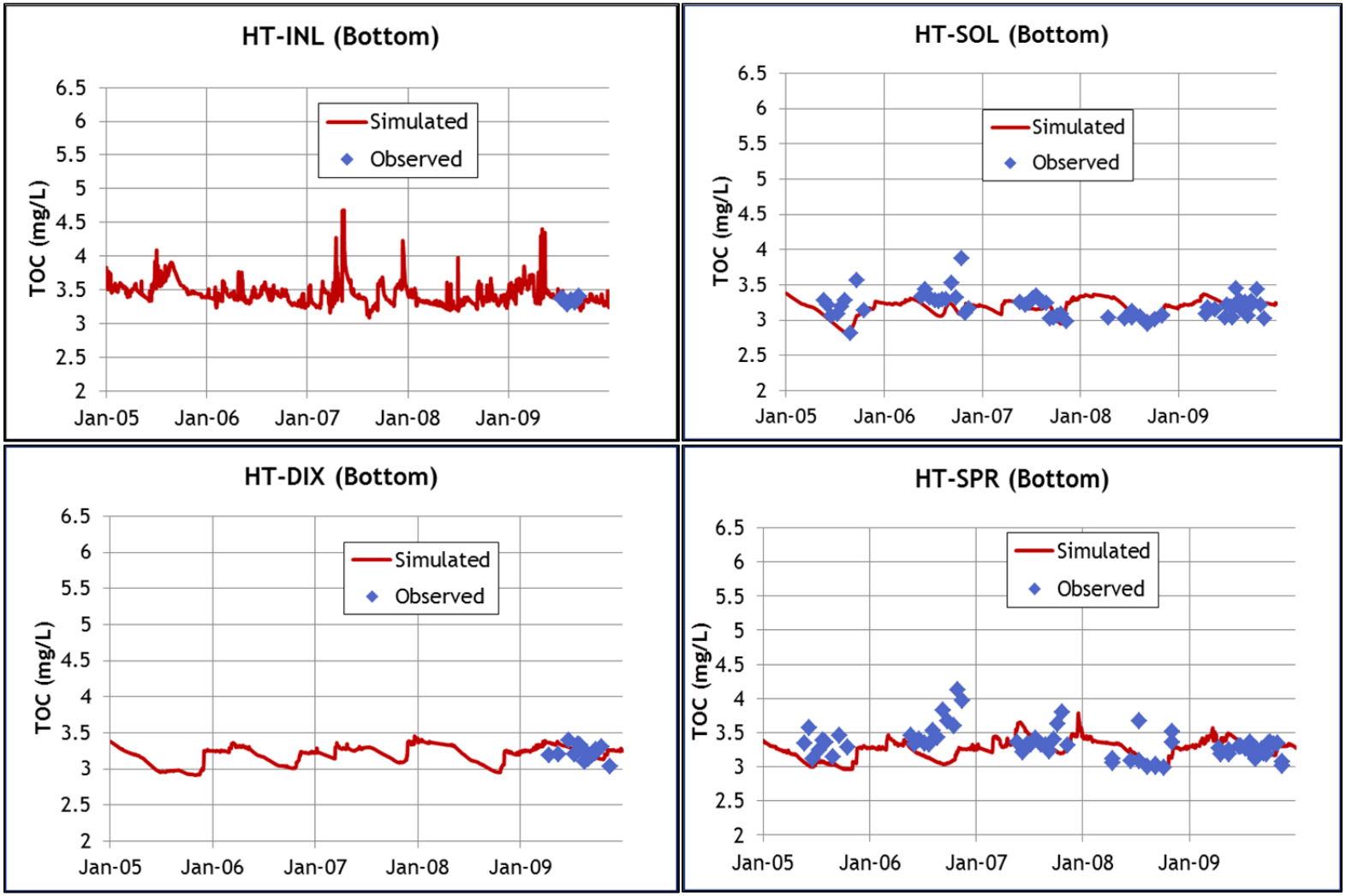

Figure 75. Simulated and Observed TOC at the Bottom of the Reservoir, 2005 through 2009

Figure 76 presents the observed and simulated TOC outflow concentrations at Soldier Canyon. The outlet works at Soldier Canyon are located near the bottom of the reservoir, and observed outlet concentrations are generally similar to observed concentrations at the bottom of the reservoir in Soldier Canyon, though not exactly the same. The outlet works can pull water from all levels of the water column, depending on outflow rates and the water temperate density profile. The selective withdrawal algorithm in the model simulates the hydrodynamics of this withdrawal, and review of simulated spatial withdrawal patterns indicates that there are times when water is being pulled from all levels of the reservoir. As such, comparison of simulated and observed data for the Soldier Canyon outlet provides a check on simulation of TOC as well as on the hydrodynamics of the outlet works, given the concentration differences between TOC at the bottom and TOC at the top of the reservoir. As shown in Figure 76, the model is successfully simulating the tight range of observed concentrations (between 3 and 3.5 mg/L for most of the simulation period). AME and RMSE values for the calibration period were 0.1 mg/L and 0.2 mg/L TOC, respectively.

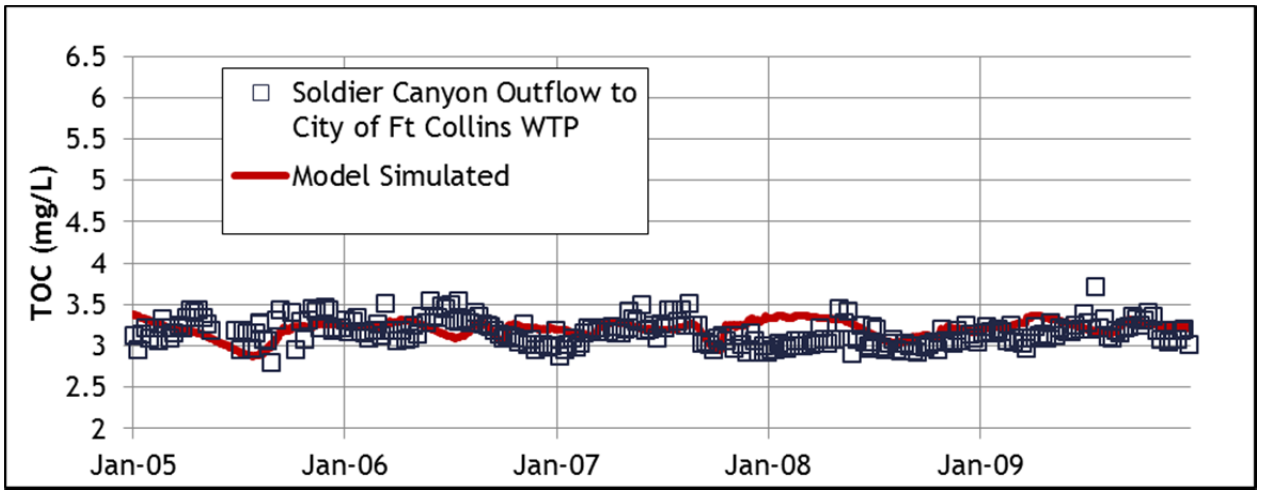

Figure 76. Observed and Simulated TOC Concentrations in the Outflow at Soldier Canyon, 2005 through 2009

3.3.3.2.3 Total Organic Carbon Calibration Summary

The calibrated model successfully simulates observed seasonal patterns and concentration ranges of TOC at the top and bottom of the reservoir. The model also performs well simulating the outflow TOC concentrations observed at Soldier Canyon. TOC concentrations are largely controlled in the upper water column by organic matter decay rates and algal growth patterns. The assumption of labile and refractory TOC fractionation of the inflow is also important, affecting TOC concentrations both at the top and bottom of the reservoir. As discussed above, this has been identified as a data gap for inflows at Hansen Feeder Canal and a remaining uncertainty in the calibration. Northern Water is taking this data need into consideration, evaluating possible approaches to collect additional data to reduce this uncertainty.

3.3.3.3 Algae

CE-QUAL-W2 simulates each specified algal group as a state variable. Figure 77 presents a kinetic diagram of the gain and loss mechanisms (excluding reservoir inflow and outflow terms) simulated in the model for algae. Algae grow under the right conditions (includes model settings for optimal light and temperatures) by consuming ammonium, phosphate, silica, and inorganic carbon. Algae produce oxygen through photosynthesis, but also consume oxygen through respiration. Through excretion, algae produce labile organic matter. Algae are subject to mortality, and when they die they become part labile dissolved organic matter and part labile particulate organic matter. Algae can also be consumed by zooplankton. Algae are subject to settling and are assumed in the model to be non-motile.

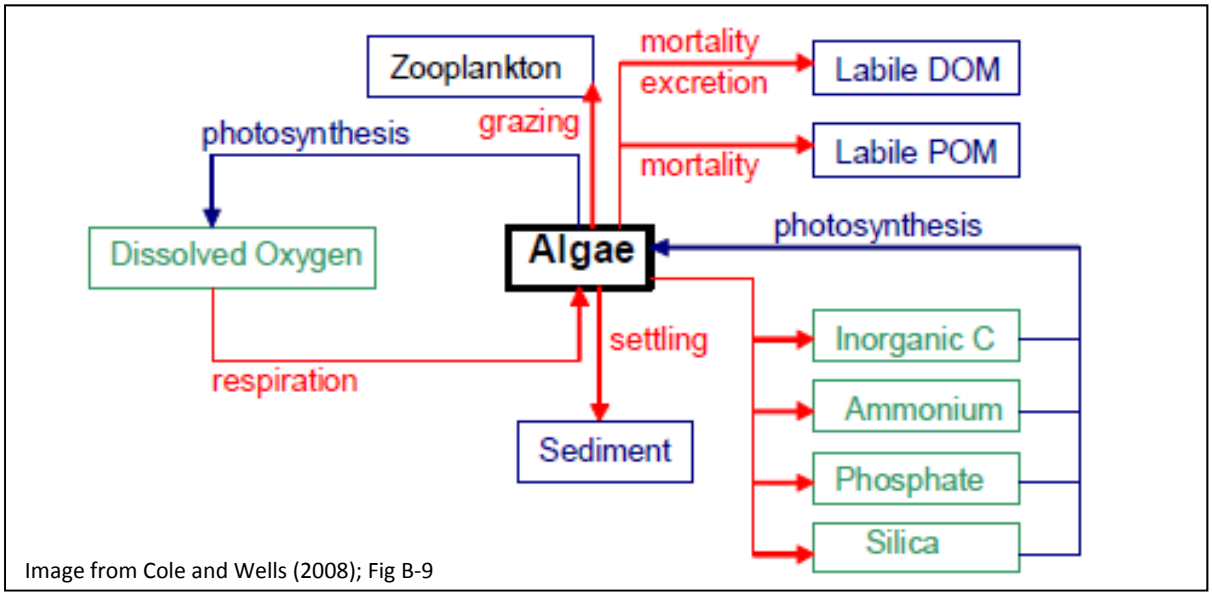

Figure 77. Kinetic Diagram of Gain and Loss Mechanisms for Algae in the Model

The model is capable of simulating multiple algal groups. In reality, hundreds of species of algae occur in Horsetooth Reservoir, but the model requires simplification into groups by general behavior and composition. Typically, algae are simulated by species group (e.g., diatoms, green algae, cyanophyta [blue-green algae], etc.), with inclusion of groups based on what has been observed in the reservoir. Figure 78 shows the biovolume of each major algal group observed in the reservoir in the 0-5 m composite samples at HT-SPR (note: patterns are similar across the reservoir). Diatoms dominate over all other algae groups each year and throughout the seasons. Diatoms are boom-bust type algae that can grow quickly to dominate other species when nutrients become available. They have silica-based cell walls, and their growth can be limited by light, inorganic nutrient concentrations, or even silica. Generally, diatoms are non-motile. This pattern of diatom dominance at HT-SPR is also observed at the other sampling stations across the reservoir.

Figure 78 also presents chlorophyll *a* concentrations at HT-SPR over the calibration period (secondary axis). Estimation of observed algal biomass is commonly based on chlorophyll a concentrations[9], and for model calibration, the simulation of algae in the reservoir is focused on matching observed patterns and concentrations ranges of chlorophyll *a* at the top of the reservoir. Chlorophyll *a* is a pigment used in oxygenic photosynthesis, and is present in live algae. The chlorophyll *a* concentration data track the diatom biomass pattern fairly well, further supporting the finding of dominance of diatoms for the calibration period. Based on these findings, two algal groups were designated in the model. One group targeted simulation of summertime diatom populations, and the other was specified to allow for simulation of observed algal growth, as needed, under conditions outside the optimal range for the diatom group.

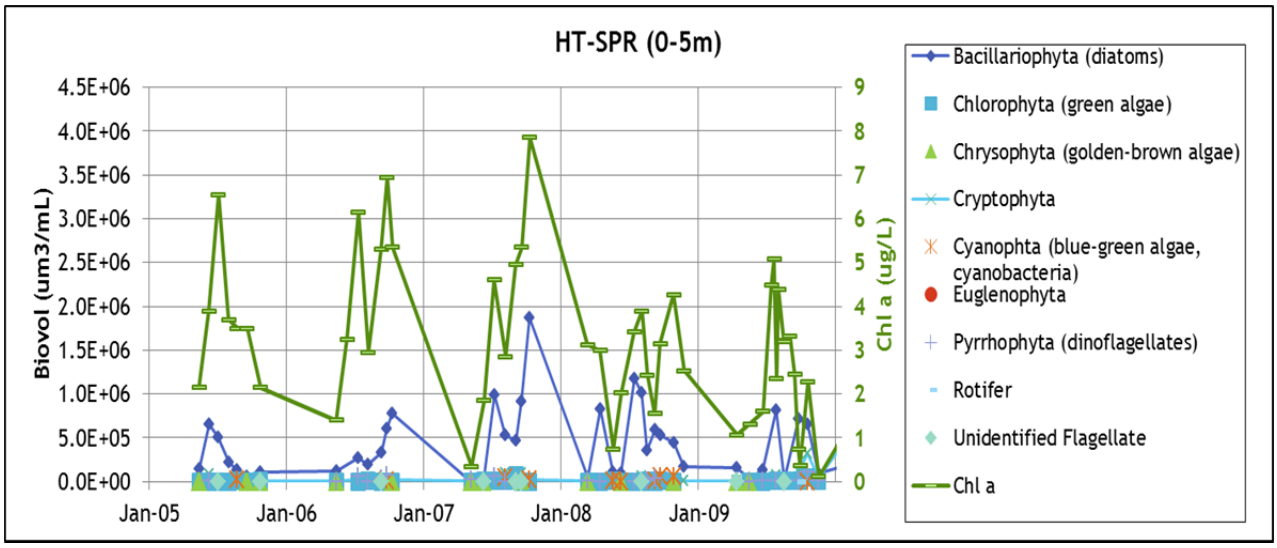

Figure 78. Biovolume of Algal Types Observed in Horsetooth Reservoir at HT-SPR, 0 to 5 m Composite Samples, 2005 through 2009

3.3.3.3.1 Inflow Algae Concentrations

Assignment of inflow algal concentrations as mg/L of organic matter was based on observed chlorophyll *a* concentrations in Hansen Supply Canal. The amount of chlorophyll *a* in a single algal cell varies by species, water column conditions, seasons, etc. The model requires a simplification of this complexity and simulates a constant chlorophyll *a*-to-algal organic carbon ratio for each algal group. Based on the

[9] Chlorophyll *a* in this discussion refers to chlorophyll *a* concentrations corrected for pheophytin. Pheophytin is a natural degradation product of chlorophyll that has an absorption peak in the same spectral region as chlorophyll a, and corrected chlorophyll a concentrations attempt to remove pheophytin from the reported chlorophyll *a* concentration.

range for this ratio of 10 to 50 ug chlorophyll *a* per mg carbon (with higher values being typical of more eutrophic conditions), provided by Chapra (1997), a central value of 25 ug chlorophyll *a* per mg carbon was assumed. Further, a ratio of 0.45 for carbon to organic matter was assumed to complete the conversion of chlorophyll *a* concentration to algae organic matter concentration. Figure 79 presents the resulting inflow algal concentrations (as mg/L-OM) for the calibration period.

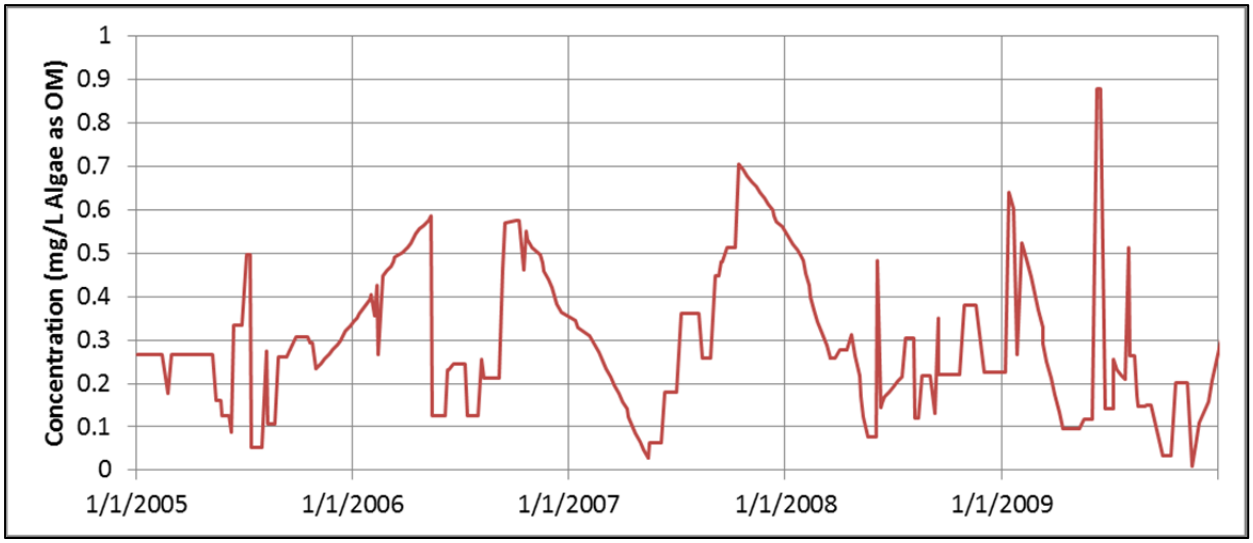

Figure 79. Inflow Algae Concentrations (as mg/L OM), 2005 through 2009

3.3.3.3.2 Calibration of Algae

The simulation of algae in the reservoir is focused on matching observed patterns and concentration ranges of chlorophyll *a* at the top of the reservoir. Calibration involved modification of algal growth rates and temperature multipliers, excretion and mortality rates, and settling rates. The calibration was conducted in coordination with calibration of TOC and nutrients because of the interdependences of settings and responses.

Figure 80 presents the simulated and observed chlorophyll *a* concentrations (simulated results converted back to chlorophyll a from organic matter masses) for the calibration period of 2005 through 2009 at HT-SPR. Note that these results compare the top layer from the model with 0 to 5 m composite samples from the observed record. Results at locations across the reservoir are similar to those presented here for HT-SPR and are presented in Appendix B. Average AME and RMSE values across the reservoir were 1.7 ug/L and 2.1 ug/L chlorophyll *a*, respectively. In spite of the necessary simplifications for modeling of a constant chlorophyll *a*-to-carbon ratios and subgrouping of algal species, the model is capable of simulating the observed ranges and seasonal patterns. The model simulates the first and second chlorophyll *a* peaks observed in most years. Through calibration, it was noted that collection of chlorophyll *a* data in winter months, to the extent possible, could help the simulation of algae, as well as TOC and nutrients.

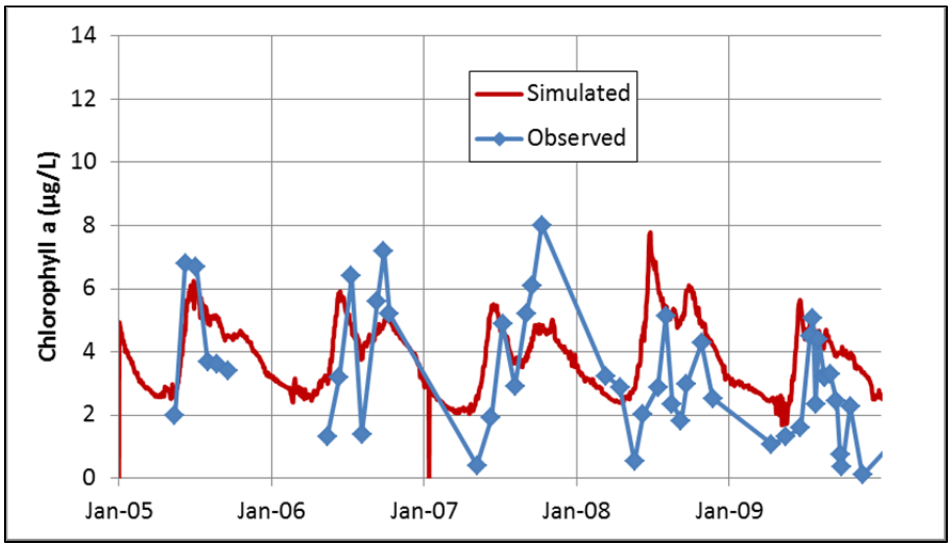

Figure 80. Simulated and Observed Chlorophyll *a* Concentrations at HT-SPR, 2005 through 2009

3.3.3.3.3 Algae Calibration Summary

Simulation of algae in a water-quality model is a complicated undertaking. By necessity, CE-QUAL-W2 requires a series of simplifying assumptions for inputs, allowing the user to specify algal groups, composition, and behavior as kinetic rate parameters. Algal growth in the model was found to be strongly dependent on water temperatures, light, and inorganic nutrient concentrations. The calibrated model successfully simulates observed seasonal patterns and concentration ranges of chlorophyll *a* at the top of the reservoir. Due to limited observed data, there is some remaining uncertainty about algal growth in winter months. Additional winter sampling, when possible is recommended. As algal species in the reservoir change, further refinement to the model would be necessary to capture the characteristics of the changing population.

3.3.3.4 Dissolved Oxygen

Calibration of dissolved oxygen concentrations in the model focused on simulating a seasonal negative heterograde curve (metalimnetic low DO) and matching the pattern and magnitude of hypolimnetic dissolved oxygen depletion each year. Simulation of observed differences across the reservoir was also a goal. Figure 81 presents a kinetic diagram of the gain and loss mechanisms (excluding reservoir inflow and outflow terms) simulated in the model for dissolved oxygen. As noted previously, the black-line slashes in this figure indicate that macrophytes and epiphyton were not included in the simulation for Horsetooth Reservoir. Dissolved oxygen enters the reservoir through reaeration and with inflowing water. Dissolved oxygen is also generated as a product of photosynthesis by algae. Sinks for dissolved

oxygen are respiration (by algae and zooplankton), nitrification, sediment oxygen demand[10], and organic matter decay in the water column.

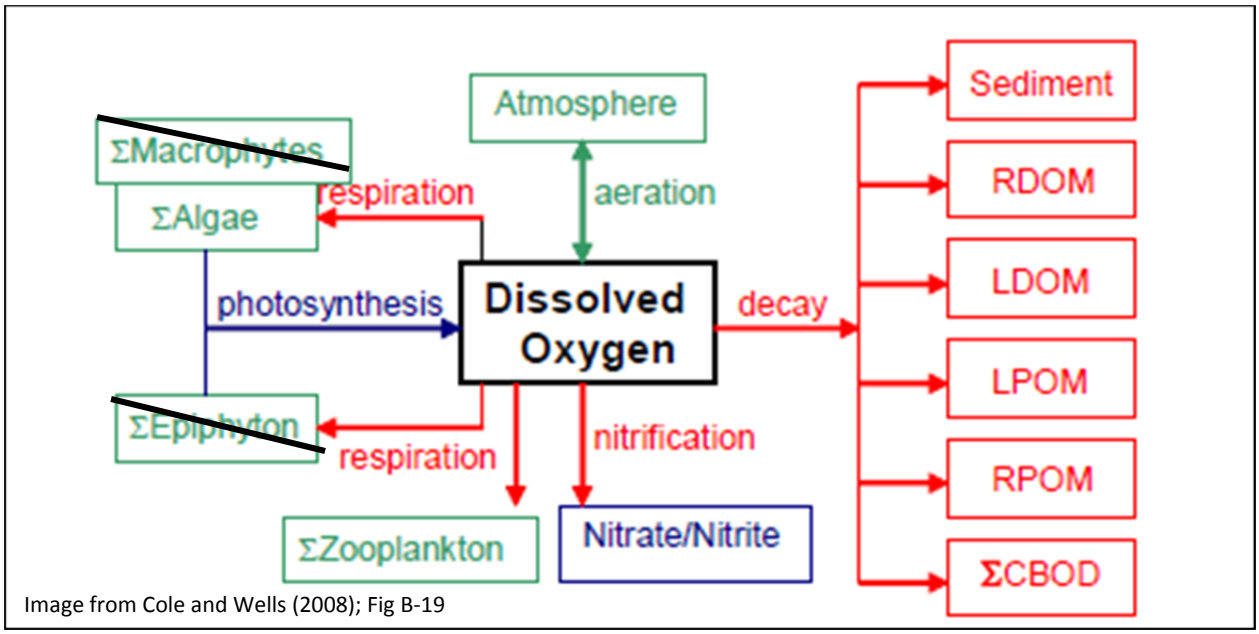

Figure 81. Kinetic Diagram of Gain and Loss Mechanisms for Dissolved Oxygen in the Model

3.3.3.4.1 Inflow Dissolved Oxygen Concentrations

Dissolved oxygen concentrations observed in Hansen Feeder Canal at the inflow point to Horsetooth Reservoir were input into the model. These data, shown in Figure 82, were collected at a higher frequency (every four hours) in 2009 and 2010. These data show a typical seasonal pattern reflective of temperature effects on dissolved oxygen saturation. The higher-frequency dataset from 2009 and 2010 was evaluated to see whether there were any patterns of under-saturation in this source of water and dissolved oxygen load to the reservoir. Figure 83 presents at plot of dissolved oxygen concentrations and temperature in the Hansen Feeder Canal relative to the theoretical dissolved oxygen saturation. From this figure, it can be seen that dissolved oxygen concentrations are generally close to saturated in the inflow, varying by ~1 mg/L below saturation and ~2 mg/L above saturation at times. Based on this, any oxygen depletion observed in the reservoir must be simulated by mechanisms occurring within the reservoir.

[10] Consumptions of oxygen in the sediments (sediment oxygen demand) is attributable to decay (oxidation) of organic matter in bottom sediments. Oxidation of organic matter can occur through biological, biochemical, and chemical processes. Oxygen is also consumed through nitrification of ammonia (a product of degradation of organic matter) to nitrate.

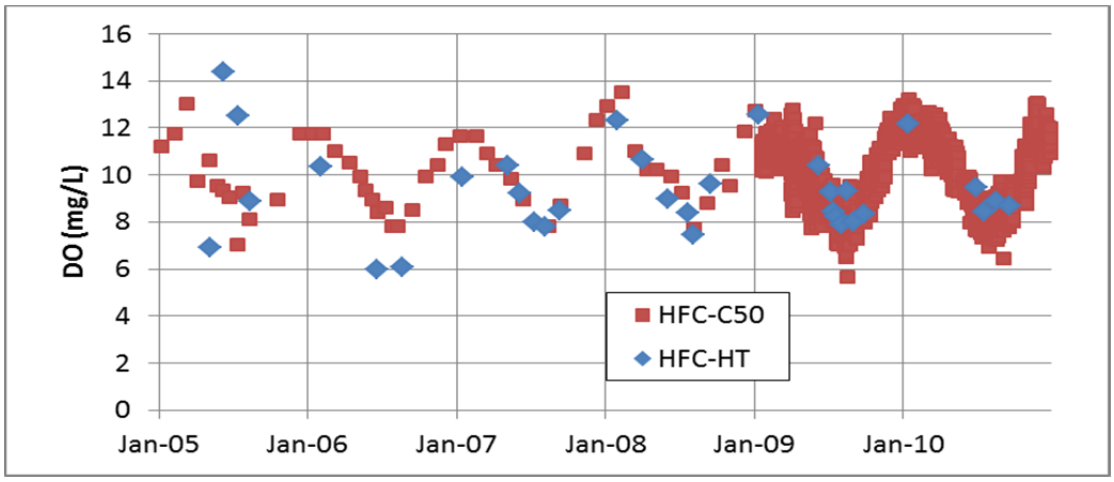

Figure 82. Observed Hansen Feeder Canal Dissolved Oxygen Concentrations Entering Horsetooth Reservoir, 2005 through 2010

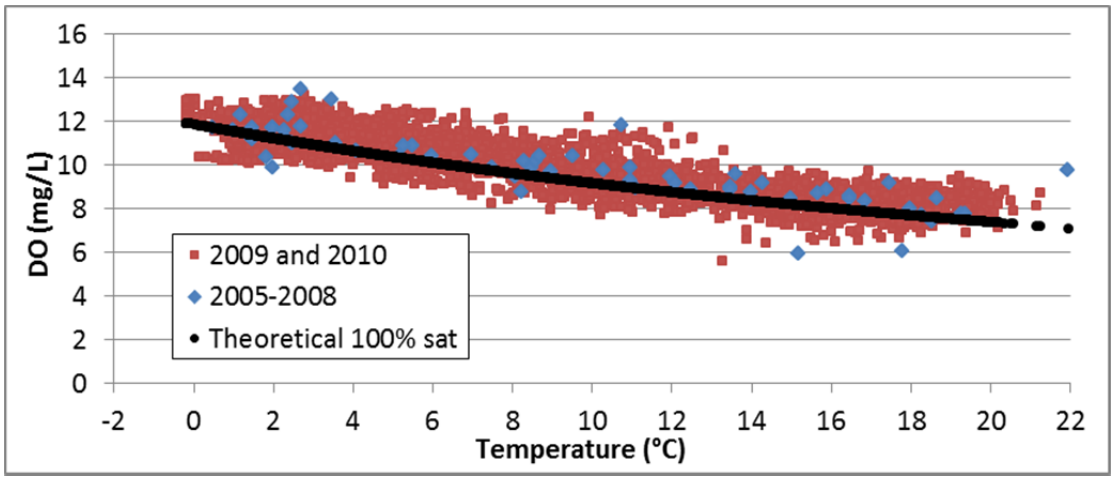

Figure 83. Assessment of Dissolved Oxygen Saturation of Inflows to Horsetooth Reservoir, 2009 and 2010 Data

3.3.3.4.1 Calibration of Dissolved Oxygen Concentrations

Calibration of the model for dissolved oxygen required adjustment of sediment oxygen demands and careful coordination with calibration of nutrients and TOC. Sediment oxygen demand was set in the model to decrease with increasing distance from the inflow location along the mainstem. As noted in the review of observed data (Section 2.3.2), this pattern is expected to reflect the settling of inflow solids from Hansen Feeder Canal.

Figure 84 presents simulated and observed dissolved oxygen concentrations from the top of the reservoir (observations at 1 m compared to simulation results from the top layer of the model) at the HT-SOL location. Results across the reservoir are very similar and are presented in Appendix B. Dissolved oxygen at the top of the reservoir is primarily controlled by reaeration (which is a function of

temperature and wind), organic matter decay, and algal activity. Figure 84 shows a good match of the seasonal pattern and concentration ranges.

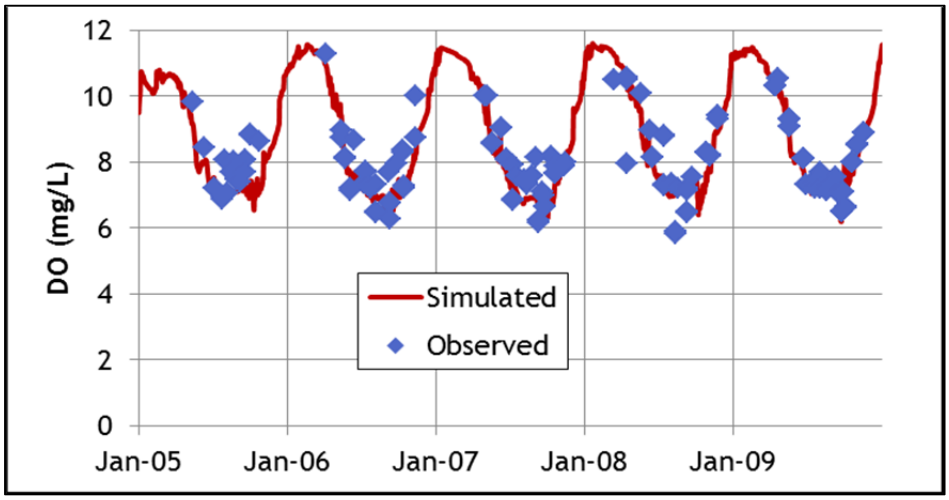

Figure 84. Observed and Simulated Dissolved Oxygen Concentrations at the Top of the Reservoir at HT-SOL, 2005 through 2009

Observed data from profiles were also compiled at a depth of 15 m, as a surrogate of metalimnion concentrations for much of the stratified period. Figure 85 presents a comparison of observed and simulated dissolved oxygen concentrations at 15 m at HT-SOL. At this depth dissolved oxygen concentrations can respond to reaeration when the reservoir is not stratified, but is primarily controlled by water column and contacting sediment reactions. The results show a good match of the seasonal pattern and concentration ranges at this depth. Results across the reservoir are similar to HT-SOL and are presented in Appendix B.

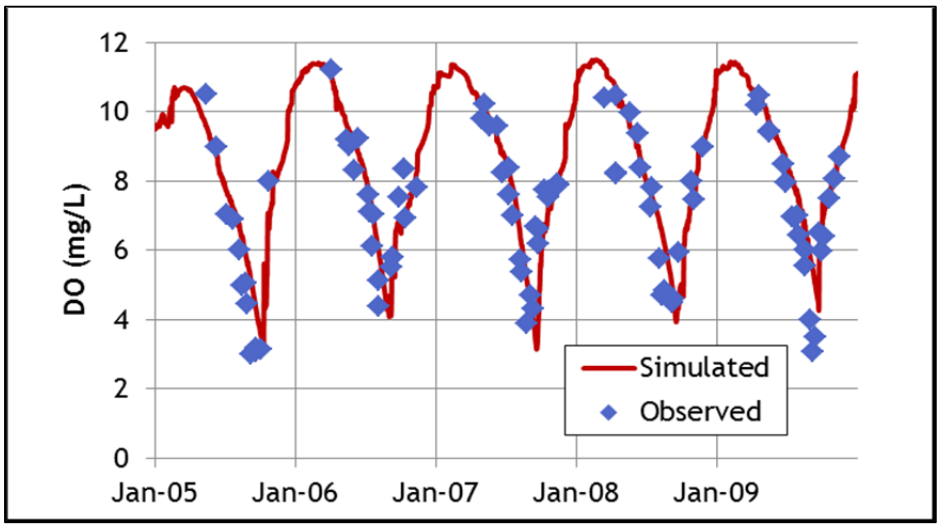

Figure 85. Observed and Simulated Dissolved Oxygen Concentrations at a depth of 15 m in the Reservoir at HT-SOL, 2005 through 2009

The model is also able to capture the hypolimnetic dissolved oxygen concentrations, as observed at the bottom of the reservoir. At the bottom of the reservoir, dissolved oxygen depletions are primarily controlled by reactions in the sediment compartment and lower water column, in addition to the duration and timing of turnover. Figure 86 presents simulated and observed dissolved oxygen concentrations at HT-SPR and HT-SOL to show spatial variation across the reservoir. The timing and extent of oxygen depletions are well represented by the model simulation from year to year. Further, the lesser dissolved oxygen depletion observed in Soldier Canyon each year (as compared to Spring Canyon) is reflected in model results.

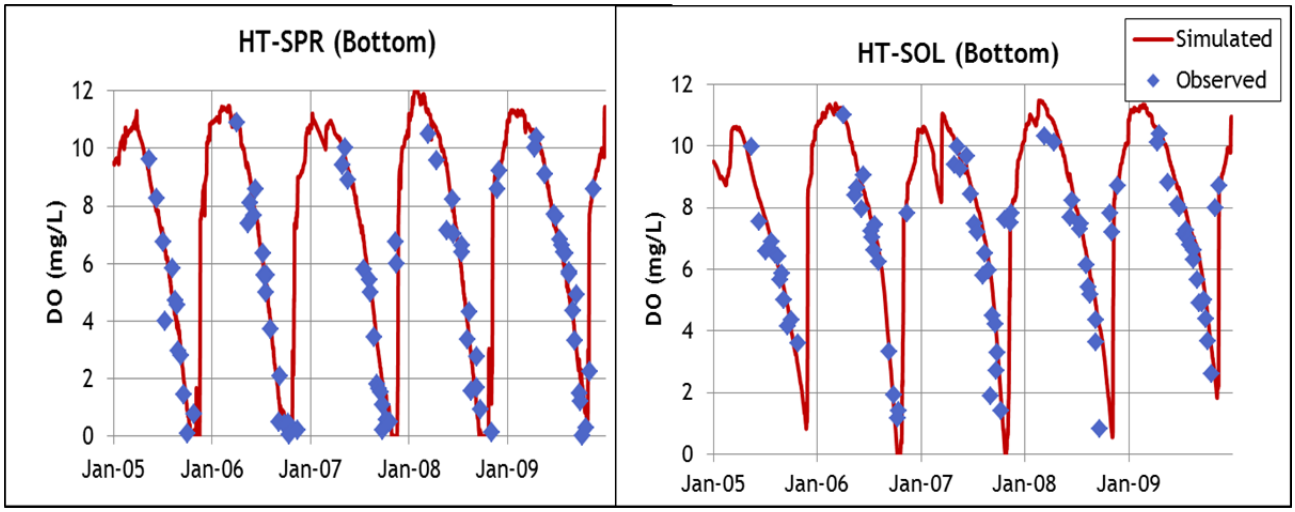

Figure 86. Observed and Simulated Dissolved Oxygen Concentrations at the Bottom of the Reservoir, HT-SPR and HT-SOL, 2005 through 2009

Simulated dissolved oxygen results were also compared to observed profile data. Simulation of dissolved oxygen concentrations to match observed profiles is challenging, as numerous competing mechanisms are at work, all of which are subject to a range of estimates and assumptions. Even so, the model performed well simulating dissolved oxygen profile results. As reflected in Figure 84, Figure 85, and Figure 86, the model predicts development of metalimnetic low dissolved oxygen concentrations as well as hypolimnetic dissolved oxygen depletions. Figure 87 shows observed and simulated dissolved oxygen concentration profiles on four dates in 2009 at HT-DIX. The model is also simulating differences in the dissolved oxygen profile across the reservoir similar to observed differences. Specifically, the greater dissolved oxygen depletions at HT-SPR (relative to HT-DIX and HT-SOL) prior to turnover are apparent in Figure 88.

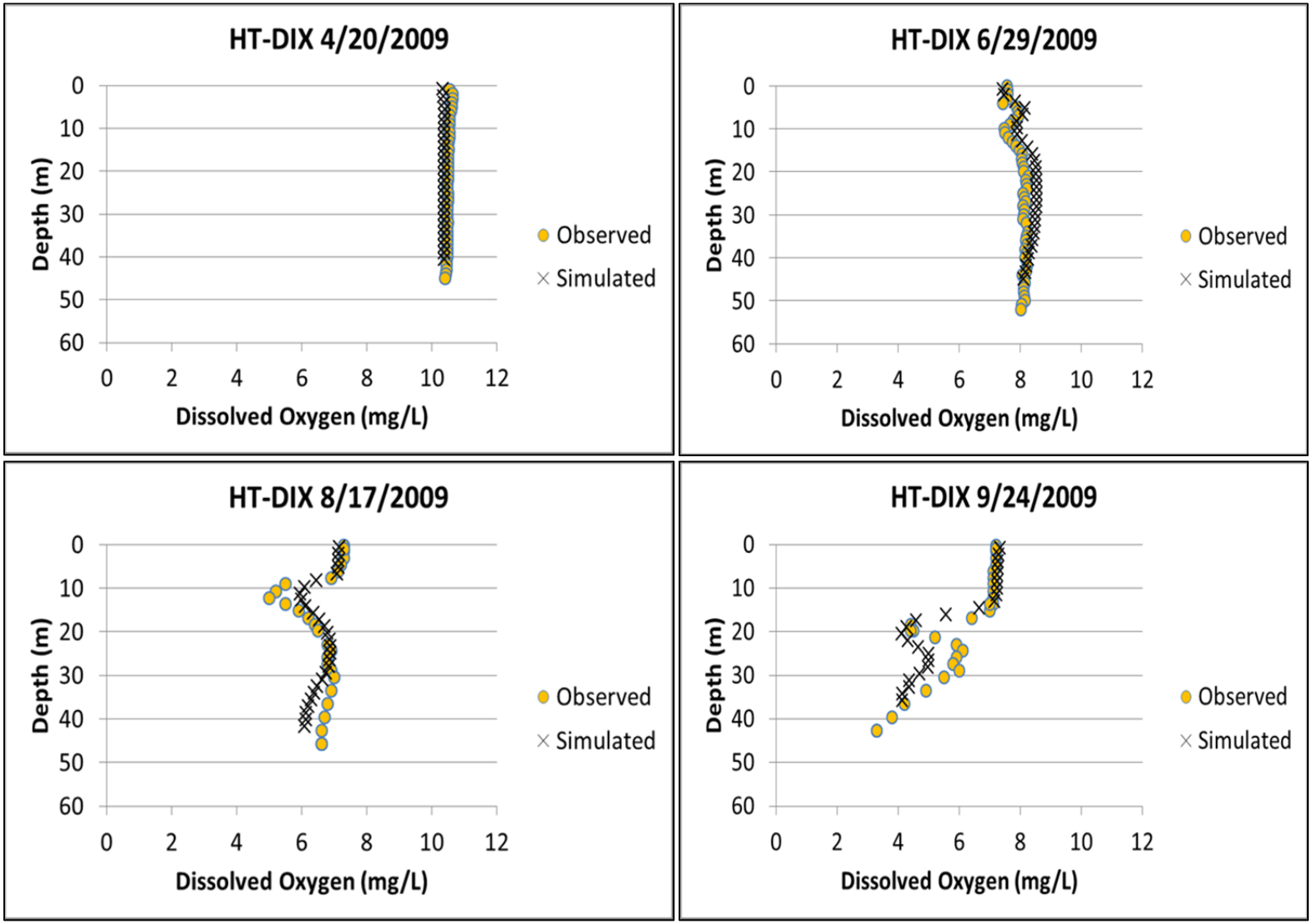

Figure 87. Select Observed and Simulated Dissolved Oxygen Profiles at HT-DIX in 2009

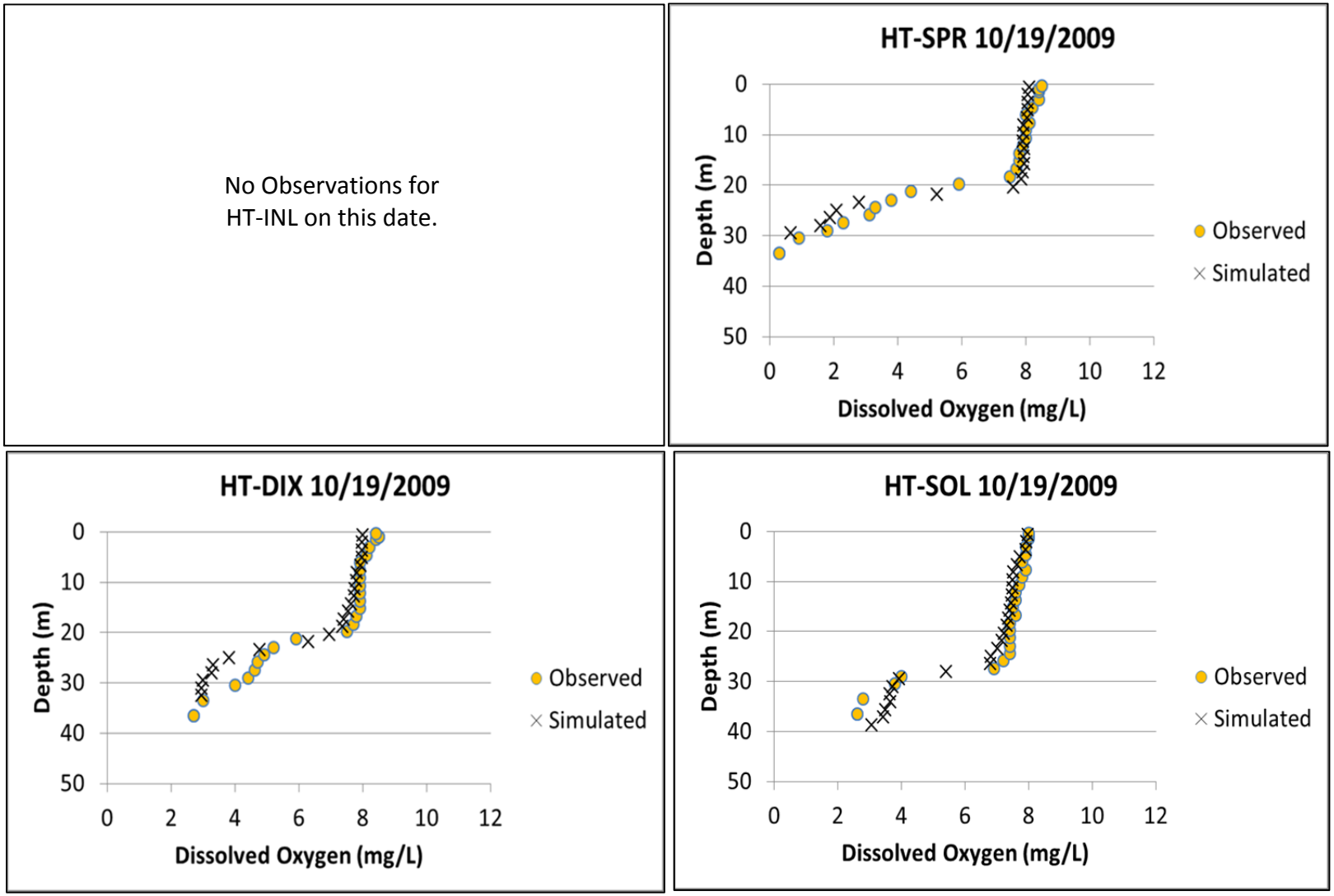

Figure 88. Observed and Simulated Dissolved Oxygen Profiles across the Reservoir on October 19, 2009

The complete set of observed and simulated dissolved oxygen profiles is presented in Appendix C. The magnitude and timing of formation of the metalimnetic low is under-predicted in some years and over predicted in others. This is expected to be related, at least in part, to the uncertainty in the composition of inflowing organic matter. Further, the dissolved oxygen profile matches in the first half of 2005 were the worst of the full period, possibly reflecting the challenge of setting appropriate initial conditions throughout the reservoir in January of 2005 without any observations. In spite of periodic timing/magnitude mismatches, the model is capturing the metalimnetic and hypolimnetic responses, spatial patterns, and differences from year-to-year.

AME and RMSE results are also presented in Appendix C. These results show an overall AME of 0.6 mg/L and RMSE of 0.8 mg/L for the full calibration period. These values compare well to compiled calibration results in Cole and Wells (2008) from various CE-QUAL-W2 lake applications, most of which have considerably shorter simulation periods. The AME and RMSE results also show general improvement from year to year, possibly reflecting improved data quality (inputs and comparison observations). Further, the AME and RMSE values are very consistent across the sampling locations, indicating no systematic spatial error bias.

3.3.3.4.1 Dissolved Oxygen Calibration Summary

The model simulates the metalimnetic low dissolved oxygen observed from year to year in Horsetooth Reservoir as well as the hypolimnetic depletions. The model also simulates that spatial variation in hypolimnetic dissolved oxygen concentrations apparent in the observed record. One remaining uncertainty in the simulation of metalimnetic low DO in particular is the composition (degradability) of the inflowing TOC fractions.

3.4 VALIDATION

The calibrated model was validated against the observed record of January 2010 through September 2010. All inputs were prepared using the same approaches and assumptions described for calibration in Section 3.3. Conditions in the validation period were largely similar to those of the calibration period with one important exception. Specifically, peak inflow TOC concentrations and TOC loading were higher in 2010, as compared to 2005 through 2009. Figure 89 shows that the relative increase in TOC mass loading was greater than the relative increase in inflow volumes to the reservoir in water year[11] 2010. As discussed in Section 2.3.4, the signal of these higher inflow TOC concentrations is apparent in the observed record at the top and bottom of the reservoir, as well as in the outflow from Soldier Canyon (see Figure 31, Figure 32, and Figure 34).

[11] A water year refers to the 12-month period of time from October 1 (of the previous calendar year) to September 30. Water years were used for this analysis of data because the water balance dataset provided by Northern Water for this investigation was complete through September 30, 2010.

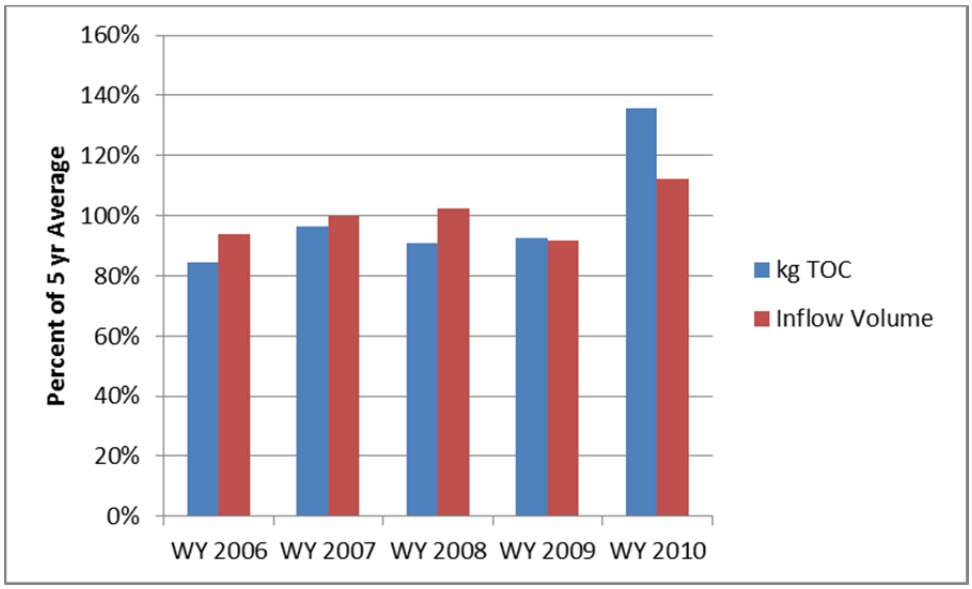

Figure 89. Relative TOC Loading to Horsetooth Reservoir, Water Year 2006 through Water Year 2010

Validation simulation results were worked up in the same manner as the calibration run results and are presented in Appendices A through C. AME and RMSE values presented in Table 1 show that validation results compare well with calibration results. More importantly, as with the calibration period, validation results simulate concentrations ranges and seasonal patterns for nutrients, TOC, DO, and chlorophyll *a*. The following discussion of validation results focuses on TOC, which had a different observed response in 2010 than in previous years, as described above.

Table 1. Goodness of Fit Summary Statistics for Temperature, TOC, Chlorophyll a, and DO for Calibration and Validation Model Runs

		AME	RMSE
Temperature Profiles	Calibration Run*	0.6°C	0.2°C
	Validation Run**	0.6°C	0.2°C
TOC (Top/Bottom)***	Calibration Run	0.2/0.2 mg/L TOC	0.3/0.2 mg/L TOC
	Validation Run	0.2/0.2 mg/L TOC	0.3/0.3 mg/L TOC
Chlorophyll *a* (Top)***	Calibration Run	1.7 ug/L Chl *a*	2.1 ug/L Chl *a*
	Validation Run	1.7 ug/L Chl *a*	2.1 ug/L Chl *a*
Dissolved Oxygen Profiles	Calibration Run	0.6 mg/L DO	0.8 mg/L DO
	Validation Run	0.6 mg/L DO	0.7 mg/L DO

AME and RMSE results include all four sampling stations.
* 2005 through 2009
** 2005 through September 2010

Simulated TOC concentrations for the combined calibration and validation period are presented in Figure 90 (top of the reservoir) and Figure 91 (bottom of the reservoir). These results show that the model is successfully simulating increased TOC concentrations in 2010 at the top and bottom of the reservoir from HT-INL to HT-SOL. At the top of the reservoir, the wintertime over-prediction (by ~0.2 mg/L TOC) and the summer time peak under0prediction (by ~0.5 mg/L TOC) at HT-SOL was simulated again in 2010. These differences are expected to be primarily related to algal growth and secondarily to uncertainty in inflow TOC fractionation (degradability). While TOC is not a key concern the top of the reservoir, future model refinements could focus on improving this consistent mismatch. Overall, the model is performing well across the reservoir, simulating the range and seasonal patterns of TOC concentrations and replicating the increase in TOC concentrations in 2010 in response to increasing inflow concentrations.

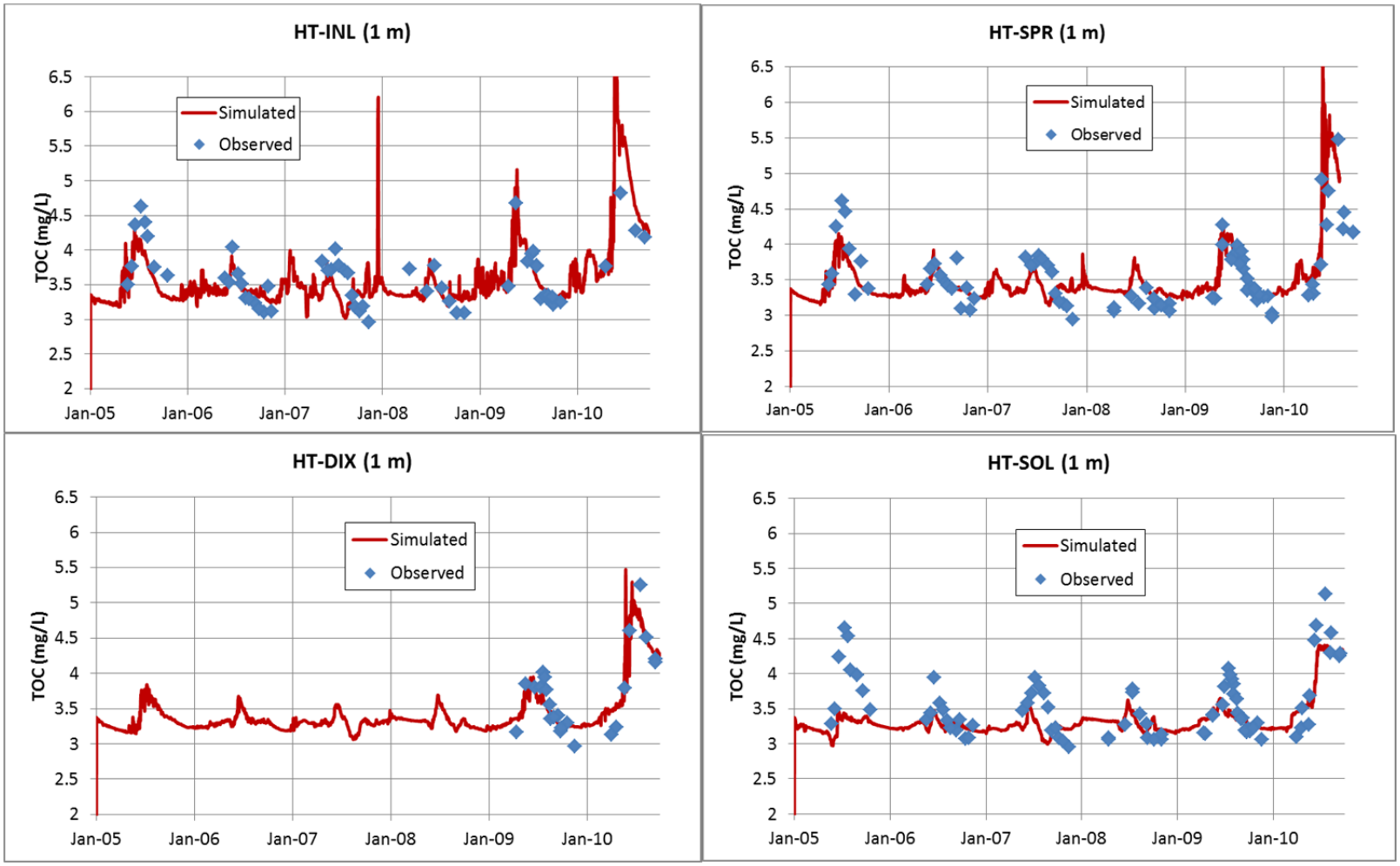

Figure 90. Simulated and Observed TOC at the Top of the Reservoir, 2005 through September 2010

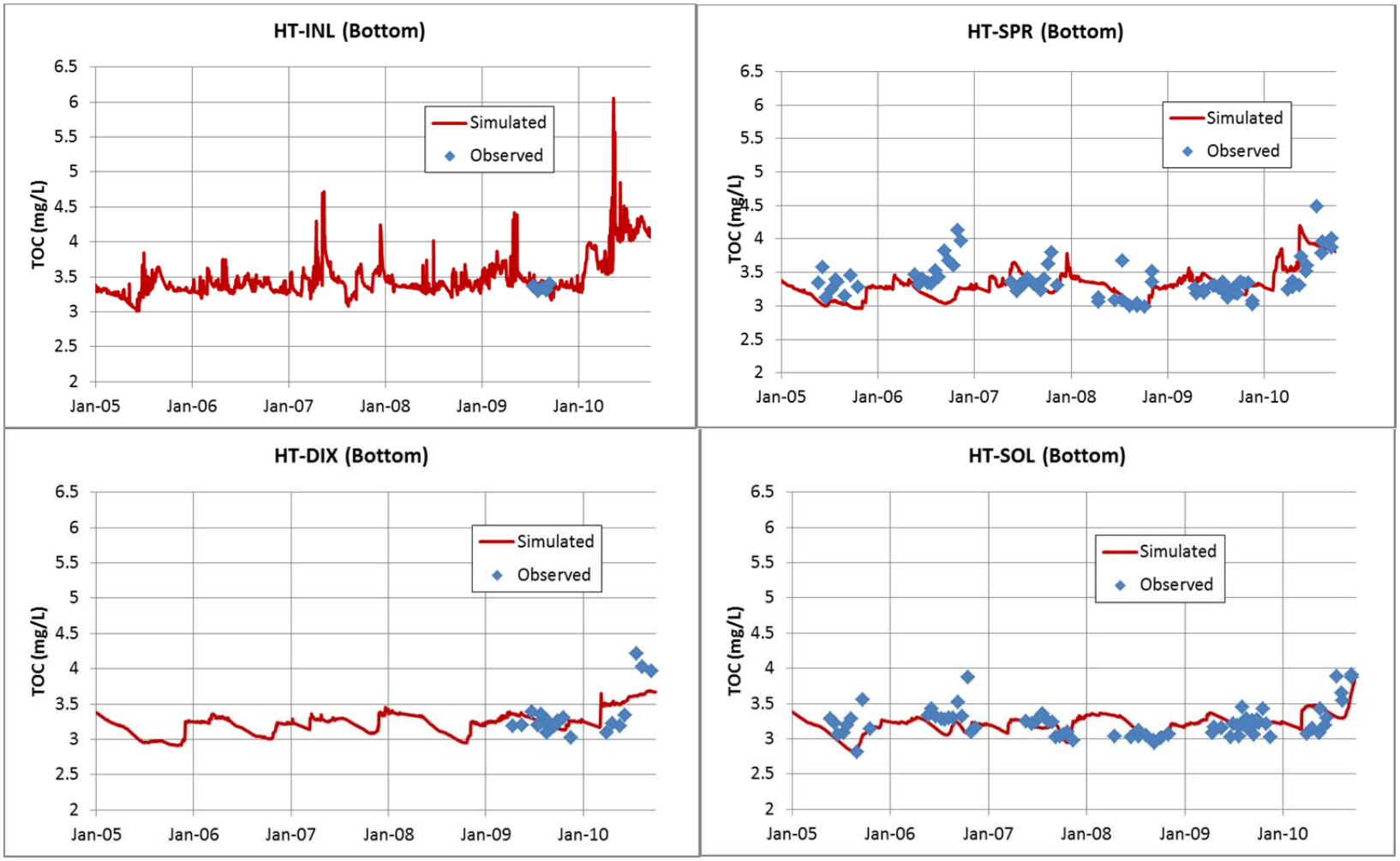

Figure 91. Simulated and Observed TOC at the Bottom of the Reservoir, 2005 through September 2010

Simulated TOC concentrations in the outflow from Soldier Canyon Dam were also compared to observed data to assess whether the model was able to simulate the observed same-year increase response of TOC concentrations in 2010. These observations and simulation results are presented in Figure 92. The model continued to perform well simulating TOC concentrations in outflow from Soldier Canyon, including replication of the magnitude of increased TOC concentrations. Table 2 presents a summary of AME and RMSE results for this key simulation target for the calibration period and the validation period. By these measures of fit, the validation period was simulated as well as the calibration period for this parameter/location.

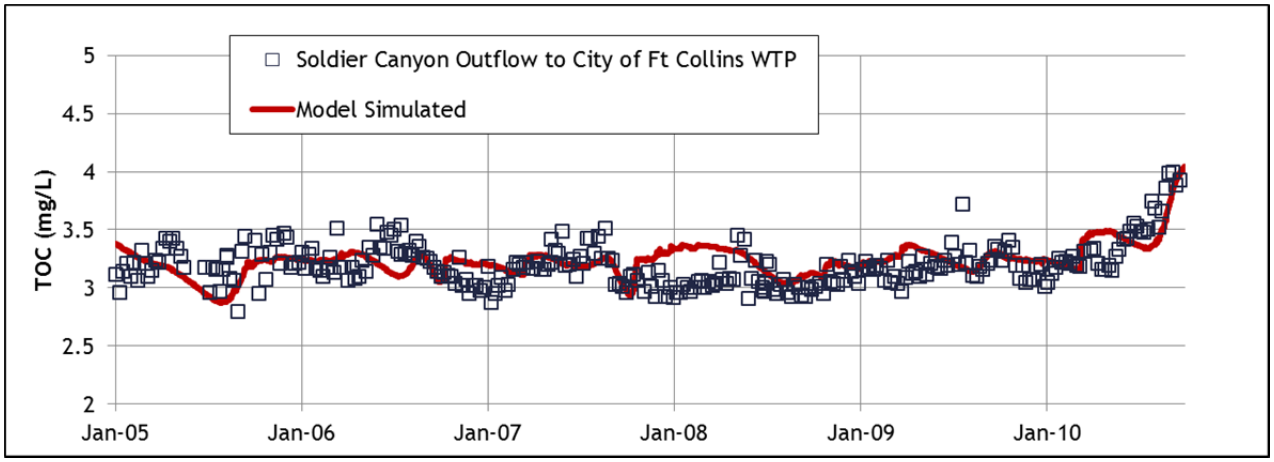

Figure 92. Observed and Simulated TOC Concentrations in the Outflow from Soldier Canyon, 2005 through September 2010

Table 2. Goodness of Fit Summary Statistics for TOC in Outflow from Soldier Canyon

	AME (mg/L TOC)	RMSE (mg/L TOC)
Calibration	0.1	0.2
Validation	0.1	0.2

4 PRELIMINARY MODEL APPLICATION

The calibrated and validated model was applied to two sets of preliminary applications to assess model responses and to learn more about the reservoir. The following subsections present results of an analysis of dissolved oxygen response in the model and results of preliminary scenario simulations.

4.1 DISSOLVED OXYGEN SENSITIVITY ANALYSIS

This section presents the results of a limited sensitivity analysis conducted to further assess dissolved oxygen response in the model. The goal of this analysis was to evaluate the importance of select model settings and inputs on simulated dissolved oxygen concentrations. The analysis focused on more uncertain model settings and inputs, informed by the understanding of system response developed through the calibration effort. This analysis purposefully does not include variation of well-measured settings and inputs or those that may be evaluated under the Modeling Scenarios portion of the project (Section 4.2). Additionally, this analysis does not attempt to be an exhaustive, classic sensitivity analysis of the model or the modeling software. The results of this effort were reviewed to meet the following purposes:

- Prioritize additional data needs/management,
- Check for unexpected simulation system response that could indicate a problem with the model, and
- Improve the conceptual system understanding.

A two-step approach was developed to conduct this focused sensitivity analysis. First, detailed model output was reviewed to evaluate the major sources and sinks of epilimnetic, metalimnetic, and hypolimnetic dissolved oxygen across the reservoir in the calibrated model. This analysis, termed the "dissolved oxygen flux analysis", was used to support selection of parameters to vary in sensitivity runs. The second step was to conduct a limited series of runs focused on these selected parameters.

This analysis focuses on dissolved oxygen at 1m, 15m (as representative of the metalimnion during much of the stratified period), and the bottom at HT-SPR, HT-DIX, and HT-SOL over the combined calibration and validation period (January 2005 through September 2010). The findings from each step of this analysis are presented in the following subsections.

4.1.1 Dissolved Oxygen Flux Analysis

CE-QUAL-W2 can be configured to provide output of kinetic fluxes simulated within the model, providing insight into the relative importance of forcing functions in the corresponding simulation. This output can be specified to the resolution of a single by model cell or for the entire water body. For dissolved oxygen, this kinetic flux output includes accounting for the following sources and sinks:

- Algal production (DOAP) – dissolved oxygen source,

- Algal and zooplankton respiration (DOAR) – dissolved oxygen sink,
- Organic matter decay (DOOM), particulate (DOPOM) and dissolved (DODOM) – dissolved oxygen sink,
- Nitrification (DONITR) – dissolved oxygen sink,
- Reaeration (DOREAR) – dissolved oxygen source or sink, and
- Sediment oxygen demand (DOSOD) – dissolved oxygen sink.

Note: This list of source and sink terms does not include advection [inflow and outflow] or diffusion of dissolved oxygen into or out of the cell(s) of interest. As such, these terms cannot be assessed as a balance, but rather serve as a tool for assessment of relative importance.

The Horsetooth model was configured to output this diagnostic information for the full simulation. Average daily dissolved oxygen flux for the entire reservoir was output on a monthly basis. Additionally, instantaneous hourly fluxes were output for the observation locations at three depths (top, 15 m, and bottom). These data were reviewed to better understand what is driving the simulated dissolved oxygen response. The discussion starts with full reservoir fluxes and then presents results for the three depths.

4.1.1.1 Full-Reservoir Simulated DO Fluxes

Average daily fluxes for the full reservoir for the full simulation period (January 2005 through September 2010) are presented in Figure 93. Positive values on the bar chart represent net sources of dissolved oxygen to the reservoir; negative values represent net sinks. Further, fluxes attributable to decay of particulate organic matter (DOPOM) and dissolved organic matter (DODOM) are presented in a lighter shade to indicate that they are a subset of the flux attributable to total organic matter decay (DOOM). From this figure, it is clear that both photosynthesis (DOAP) and reaeration (DOREAR) are both important source terms. Among the dissolved oxygen sink terms, sediment oxygen demand (DOSOD) consumes the most dissolved oxygen, followed by degradation of organic matter (DOOM). Degradation of dissolved organic matter, as opposed to particulate organic matter, comprises the majority (75%) of the DOOM sink term. Algal respiration (DOAR) and nitrification (DONITR) also consume significant amounts of dissolved oxygen; however they are of lesser importance on the full-reservoir scale than SOD and organic matter decay by more than a factor of five.

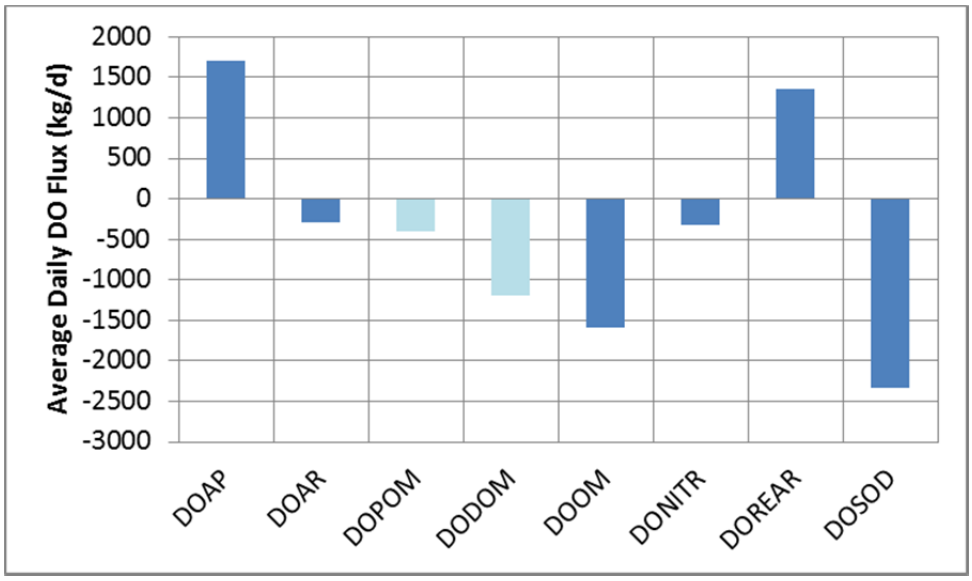

Figure 93. Simulated Average Daily DO Flux for Horsetooth Reservoir, 2005 through September 2010

A closer look at the monthly output for the full reservoir dissolved oxygen fluxes (Figure 94) provides insights into seasonality. First, the reaeration term (DOREAR) varies between source and sink each year, bringing oxygen into the reservoir when the system is under-saturated at the surface and releasing oxygen when the system had excess oxygen for the given water temperature. Next, algal respiration (DOAR) is a source of oxygen to the system primarily in summer months, as would be expected based on algal growth patterns. Through the first part of summer each year, DOAR is greater in magnitude than the other source term, DOREAR.

The two major sink terms for dissolved oxygen (decay of organic matter in the water column [DOOM] and sediment oxygen demand [DOSOD]) follow similar seasonal patterns, with peak fluxes simulated in mid to late summer. The peak sediment oxygen demand flux is typically in September. Interestingly, in 2010 DOOM is a greater oxygen sink term for the full reservoir than DOSOD in June and July, reflecting the increased TOC loading that year. The more minor (on a reservoir-wide basis) oxygen sink terms of nitrification and respiration also show a consistent seasonal pattern, typically peaking in the same month as organic matter decay.

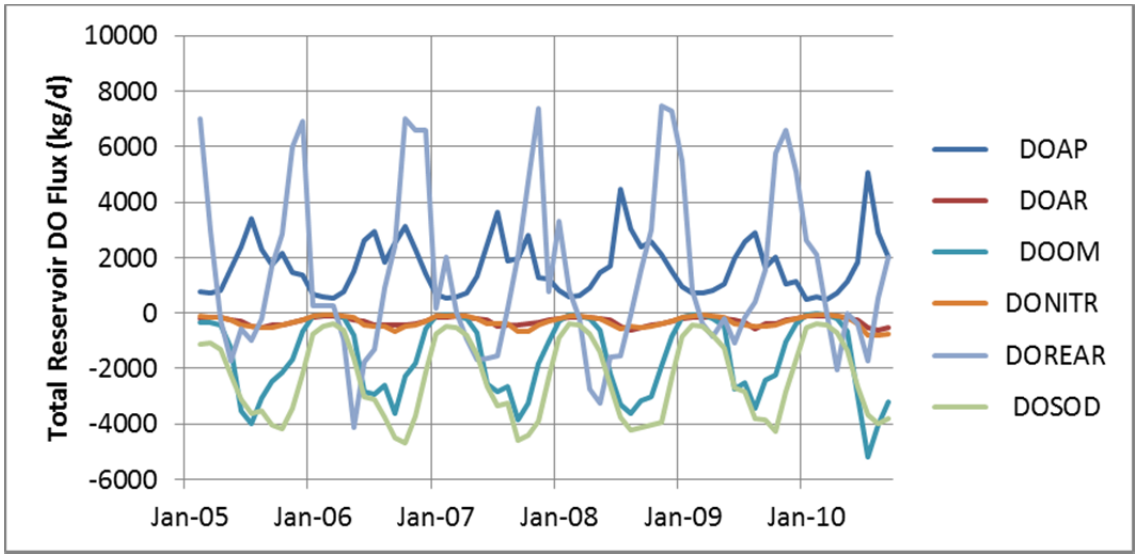

Figure 94. Simulated Monthly Dissolved Oxygen Fluxes for Horsetooth Reservoir, 2005 through September 2010

For a look at spatial variation of these dissolved oxygen fluxes in the model, results were reviewed in individual model cells at the top of the reservoir, at a depth of 15 m, and at the bottom of the reservoir. The following discussions present results from Spring Canyon and Soldier Canyon at each of these depths. These results are presented on a purely relative scale (as opposed to units of kg/day), recognizing the different and variable cell sizes for focus locations. For each of these discussions, presentation of results focuses on the period of July through September, when the reservoir is stratified and dissolved oxygen depletion conditions in the metalimnion and hypolimnion become a concern.

4.1.1.2 Top of the Reservoir Simulated DO Fluxes

Simulated relative dissolved oxygen sink terms at the top of the reservoir at HT-SPR and HT-SOL are presented in Figure 95. These results have been normalized by cell volume to allow for comparison and are presented on a purely relative scale. Results are limited to the strongly stratified period from July through September, recognizing that dissolved oxygen conditions of concern occur during stratification.

As shown in Figure 95, at the top of the reservoir, both algal photosynthesis and reaeration are important dissolved oxygen source terms (positive values). During this period of July through September, reaeration is the dominant source term. At the top of the reservoir, decay of organic matter is the major sink term (negative values) for dissolved oxygen during the stratified period. This pattern is consistent from HT-SPR to HT-SOL. Decay of dissolved organic matter consumes more oxygen than decay of particulate organic matter. Decay of particulate organic matter, however, has a greater relative effect at HT-SOL as compared to HT-SPR, though decay of dissolved organic matter still dominates at both locations. Nitrification effects are an order of magnitude less than organic matter decay effects. Interestingly, sediment oxygen demand is second in relative importance for dissolved oxygen losses at the top of the reservoir, although respiration is a close third. This is a reflection of the sediment in contact with water in the top layer of the model.

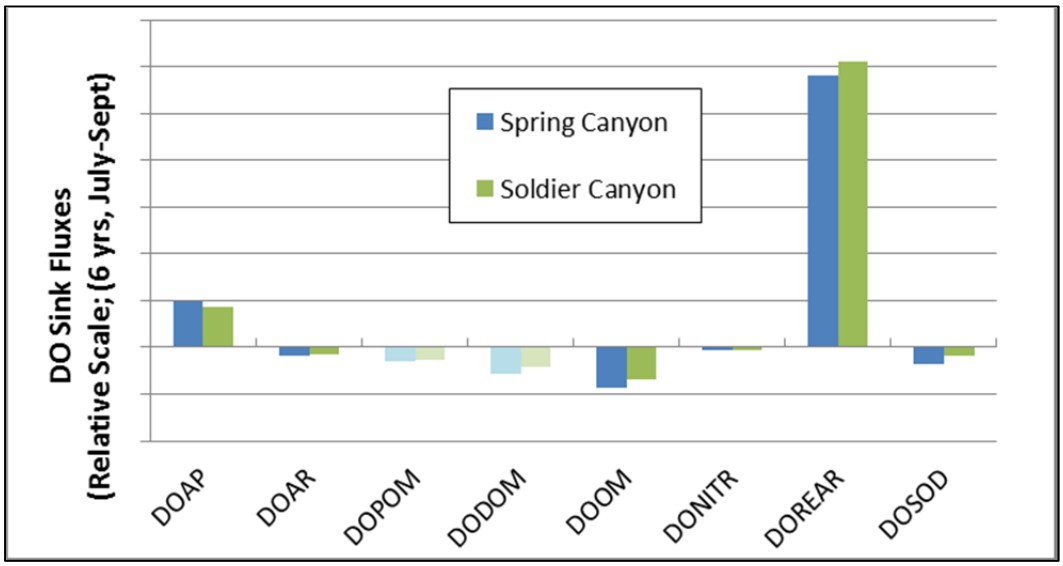

Figure 95. Simulated Dissolved Oxygen Fluxes in the Top Model Layer at HT-SPR and HT-SOL, July through September Results for 2005 through 2010

4.1.1.3 Simulated DO Fluxes at 15 m

Simulated relative dissolved oxygen sink terms at a depth of 15 m at HT-SPR and HT-SOL are presented in Figure 96. A depth of 15 m was chosen because it is a reasonable representation of the metalimnion through much of the stratified period. These results have been normalized by cell volume to allow for comparison and are presented on a purely relative scale. Results are limited to the strongly stratified period from July through September, recognizing that dissolved oxygen conditions of concern occur during stratification.

Dissolved oxygen source terms of algal photosynthesis and reaeration are not shown on this figure because they were zero or insignificant at 15 m. While reaeration at the surface may results in increased dissolved oxygen at this depth at times, the flux output does not include diffusive (or advective) fluxes. As for algal photosynthesis, algae are not simulated to be growing significantly at 15 m. There are some living algae at this depth, as indicated by chlorophyll *a* concentrations, but they are not producing oxygen in the model. At a depth of 10 m, algal photosynthesis is simulated to be occurring. This agrees with profile observations of chlorophyll *a* collected in 2009. As presented in Section 2.3.5, observed chlorophyll *a* concentrations drop off sharply between 10 m and 15 m.

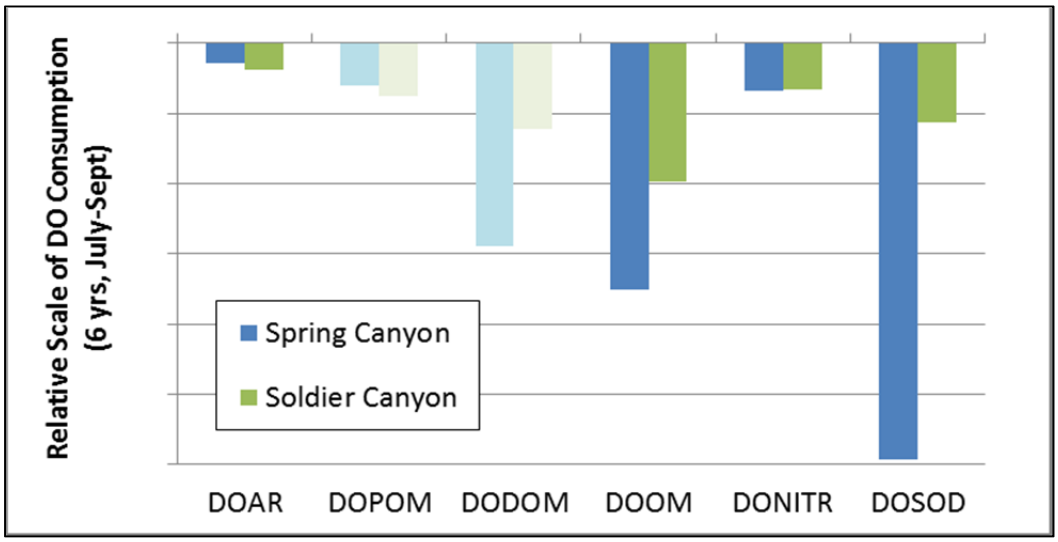

Figure 96. Simulated Dissolved Oxygen Fluxes at a Depth of 15 m at HT-SPR and HT-SOL, July through September Results for 2005 through 2010

Among the dissolved oxygen sink terms, decay of organic matter is important during stratification at 15 m. Again, decay of dissolved organic matter dominates the DOOM term; though particulate organic matter decay is not insignificant. HT-SPR, relative to HT-SOL, exhibits a greater decay of dissolved organic matter at 15 m. This is likely due to the fact that HT-SPR is closer to the source of inflowing organic matter. Interestingly, decay of particulate organic matter does not show as large of a spatial difference. This is likely an indication that the DOPOM term is primarily associated with decay of algae across the reservoir. Sediment oxygen demand is also important in determination of dissolved oxygen at 15 m, with greater effects at HT-SPR. DOSOD effects at the metalimnion reflect the surface area of sediment in contact with metalimnetic water. Given the shape the reservoir, sediment from bays and even the rises between the canyons can be in contact with the metalimnion at times. This effect is a shelf or cove effect, as illustrated in Figure 97. Finally, nitrification is again a relatively small sink terms for dissolved oxygen at 15 m.

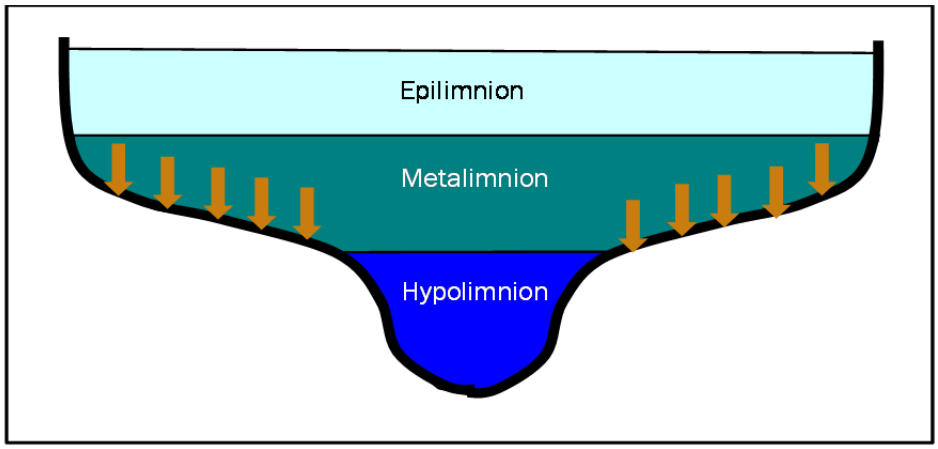

Figure 97. Conceptual Figure of Shelf or Cove Effects of Sediment Demand on the Metalimnion

4.1.1.4 Simulated DO Fluxes at the Bottom of the Reservoir

Simulated relative dissolved oxygen sink terms at the bottom at HT-SPR and HT-SOL are presented in Figure 98. These results have been normalized by cell volume to allow for comparison and are presented on a simple relative scale. Results are limited to the strongly stratified period from July through September, recognizing that dissolved oxygen conditions of concern occur during stratification. Dissolved oxygen source terms of algal photosynthesis and reaeration are not shown on this figure because they do not contribute dissolved oxygen at this depth. (Reminder: Flux terms do not include advective or diffusive fluxes.)

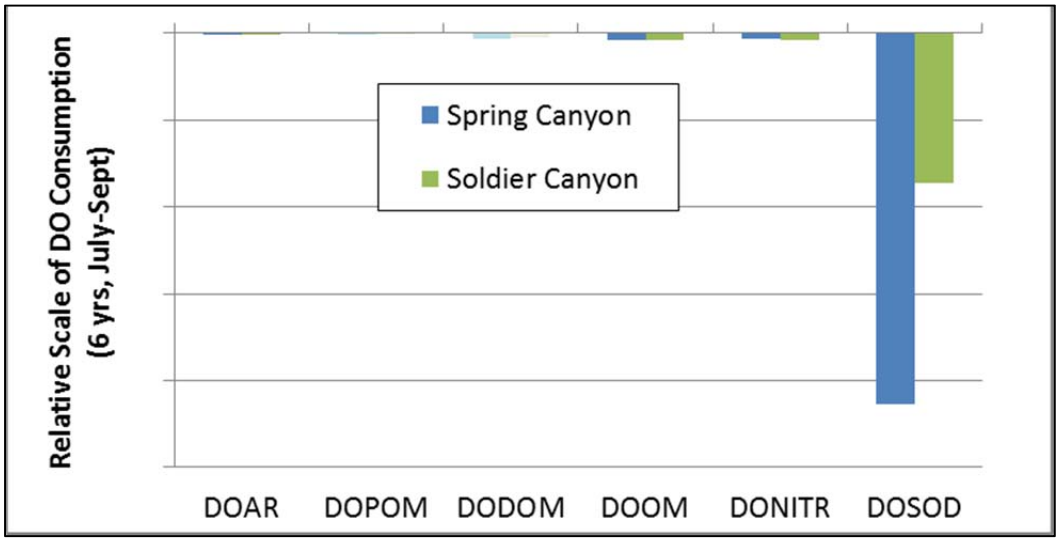

Figure 98. Simulated Dissolved Oxygen Fluxes in the Bottom Model Layer at HT-SPR and HT-SOL, July through September Results for 2005 through 2010

Sediment oxygen demand is the primary sink of dissolved oxygen at the bottom of the reservoir. DOSOD consumes oxygen at the bottom of the reservoir year round, through it is lowest in winter months. In the model, sediment oxygen demand is higher at HT-SPR and lower at HT-SOL, which is expected to reflect proximity of HT-SPR to the inflow source and settling. The combined effect of decay of organic matter and nitrification on dissolved oxygen is two orders of magnitude less than that of sediment oxygen demand. Finally, algal respiration is minimal at the bottom of the reservoir in the stratified period.

4.1.2 Dissolved Oxygen Sensitivity Runs

To further evaluate the model and the simulated reservoir response, a limited set of model runs was defined to look at the effects of select settings on the dissolved oxygen results. Settings to be modified were selected based on current understanding of the simulated response and identified uncertainties. As discussed above the purpose of these simulations was to improve system understanding, highlight data collection needs, and further test model performance. In all, a total of 17 model runs were completed. Analysis of results focused exclusively on dissolved oxygen concentrations. Model runs included varying:

- Inflow labile-to-refractory TOC ratio,
- Nitrification Rates
- Organic matter decay rates,
- Algal settling rates,
- Sediment oxygen demand, and
- Reaeration rates.

4.1.2.1 Inflow Labile-to-Refractory TOC Ratio

As discussed in Section 3.3.3.2.1, a consistent assumed seasonal ratio was applied to observed TOC concentration data to generate the required model input for inflows from Hansen Feeder Canal. Specifically, it was assumed that inflowing TOC is 10% labile during runoff (April-June) and 20% labile over the rest of the year. It is recognized that this assumption is an oversimplification of the actual temporal variability of the system. Two model runs were completed as a first look into the sensitivity of this assumption on simulated dissolved oxygen concentrations. For the first run, the assumed ratio was doubled (20% labile, April-June; 40% labile July-March). For the second run, the assumed ratio was halved (5% labile, April-June; 10% labile July-March).

Figure 99 and Figure 100 present simulated dissolved oxygen concentrations at 15 m and at the bottom of the reservoir at HT-SOL (other locations show similar results). The plots are focused on 2009 to allow adequate resolution to see effects. At the top of the reservoir, increased labile fractions do result in lower dissolved oxygen concentrations, but the effects are small, presumably due to the dominance of reaeration at this level. At 15 m, the effects are more pronounced, and occur during the period of stratification. Simulated dissolved oxygen concentrations in the metalimnion are 1 to 1.5 mg/L lower during stratification for the case of increased fractions of labile material in the inflow. Similar effects were simulated at the bottom of the reservoir. Based on these findings, data collection to improve time series estimates of labile-to-refractory fractions in inflow TOC could help improve the model.

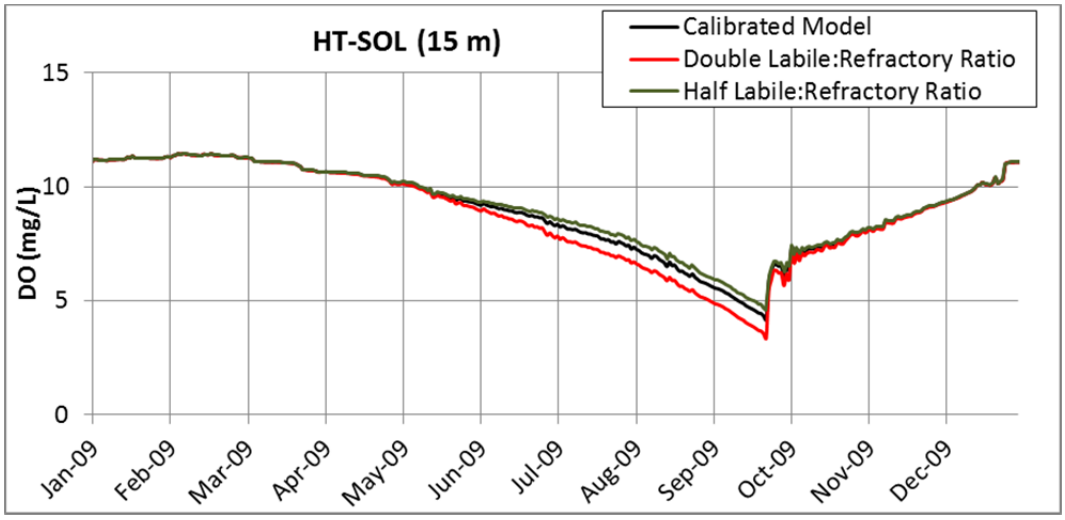

Figure 99. Simulated Dissolved Oxygen Concentrations at 15 m at HT-SOL in 2009 for Different TOC Composition Assumptions

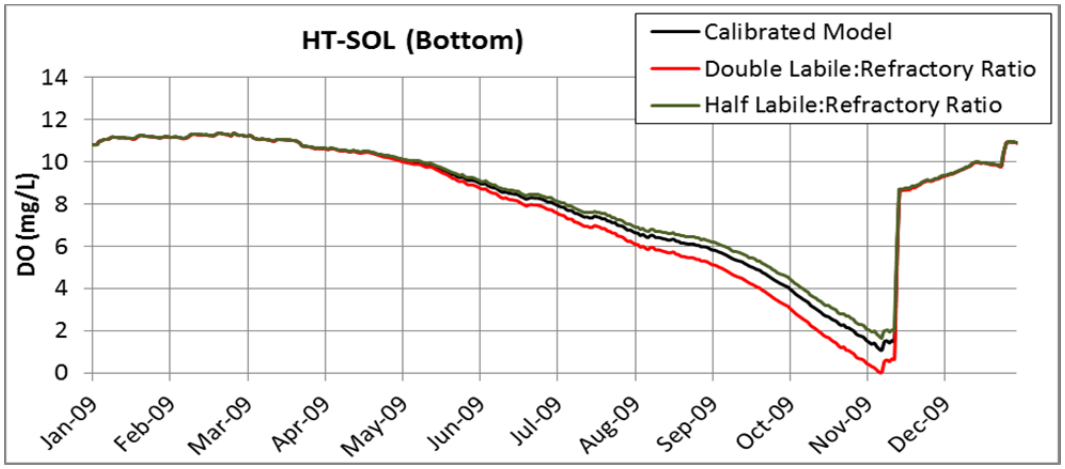

Figure 100. Simulated Dissolved Oxygen Concentrations at the Bottom at HT-SOL in 2009 for Different TOC Composition Assumptions

4.1.2.2 Nitrification Rate

Nitrification is the biologically-mediated oxidation of ammonia (Figure 101). The reaction consumes oxygen and produces nitrite, which is quickly converted to nitrate. As discussed in Section 4.1.1, nitrification in Horsetooth Reservoir is not one of the top two dissolved oxygen sink terms at any depth in the reservoir; however, it is not an insignificant term. Two model runs were conducted varying nitrification rates (doubling and halving) to assess the effect on simulated dissolved oxygen concentrations. Associated temperature rate multipliers were not varied.

$$NH_3 + 2O_2 \rightarrow NO_3 + H_2O + H^+$$

Figure 101. Nitrification Reaction (Simplified)

Figure 102 and Figure 103 present simulated dissolved oxygen concentrations at 15 m and at the bottom of the reservoir at HT-SOL (other locations show similar results). The plots are focused on 2009 to allow adequate resolution to see effects. At the top of the reservoir, effects of changes in nitrification rates are minimal, presumably due to the dominance of reaeration at this level. At 15 m, small effects are apparent in lower dissolved oxygen concentrations during stratification. The change in minimum dissolved oxygen concentration at this depth is <0.1 mg/L. Similarly small effects are apparent at the bottom of the reservoir. These changes at the bottom of the reservoir correspond to an increase of 1 or 2 days per year of hypoxia (<2 mg/L) across the reservoir. Based on these findings, uncertainty in nitrification rate settings is not a critical concern in terms of dissolved oxygen simulation, and setting of a reasonable rate to best match observed ammonia and nitrate concentrations should be sufficient.

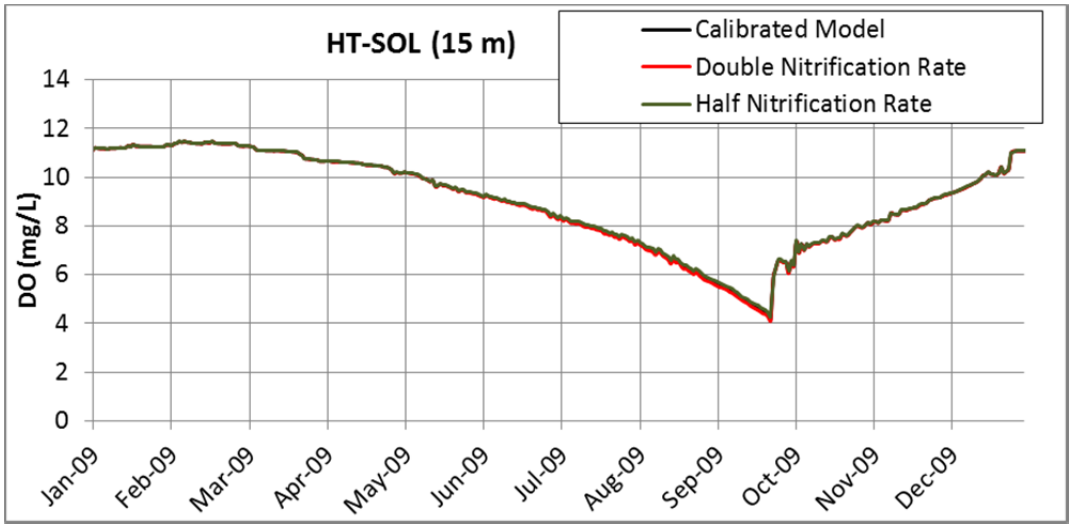

Figure 102. Simulated Dissolved Oxygen Concentrations at 15 m at HT-SOL in 2009 for a Range of Nitrification Rates

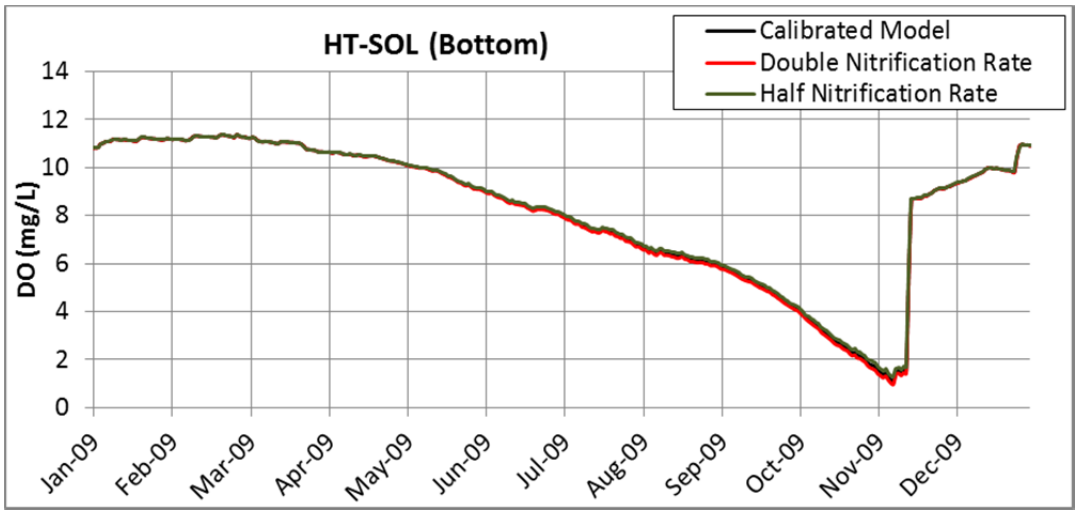

Figure 103. Simulated Dissolved Oxygen Concentrations at the Bottom at HT-SOL in 2009 for a Range of Nitrification Rates

4.1.2.3 Organic Matter Decay Rates

The next settings varied in the dissolved oxygen sensitivity analysis were decay rates for three fractions of organic matter. Decay of organic matter consumes oxygen and produces inorganic carbon, orthophosphate, and ammonia. Decay rates for labile dissolved organic matter (LDOM), labile particulate organic matter (LPOM), and refractory dissolved organic matter (RDOM) were each varied by doubling and halving the calibrated values, for a total of six model runs.

- LDOM makes up ~10 to ~20% of the inflowing TOC (depending on season), and has a decay rate roughly 100 times greater than RDOM.
- LPOM makes up less than 1% of the inflow TOC, but has a relatively high decay rate and is also an in-reservoir product of algal mortality.
- RDOM makes up ~80 to ~90% of the inflowing TOC (depending on season), and has a decay rate that is roughly one hundredth that of LDOM.

Halving and doubling each of these decay rates produced only very small (<<0.1 mg/L) effects on dissolved oxygen concentrations at any time at the top of the reservoir. At 15 m, however, there is an effect in the expected direction (increased rate, decreased dissolved oxygen) for changes in each of the terms, with the largest effect simulated for changes in RDOM rates. As seen in other simulations, the effect was limited to the stratified period. Results varied across the reservoir as shown in Figure 104, Figure 105, and Figure 106. Specifically, the effect of LDOM rates decreased across the reservoir (Figure 104), presumably due to increased distance from the inflow source of the readily degraded term. In contrast, the effects of RDOM rates

increased across the reservoir (Figure 105). Interestingly, reduction in rates showed a greater effect for LDOM and LPOM, as compared to increases in rates for those terms, suggesting an upper limitation, possibly related to remaining concentrations.

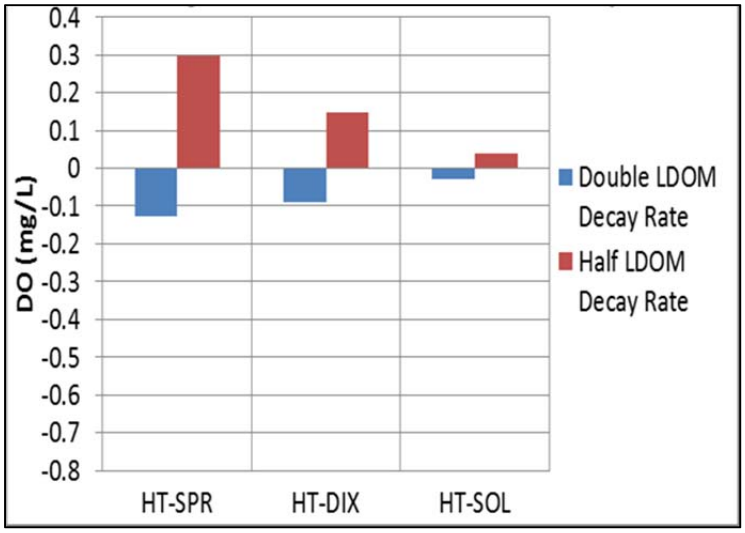

Figure 104. Simulated Change in Minimum Dissolved Oxygen Concentration at 15 m for Changes in LDOM Decay Rates

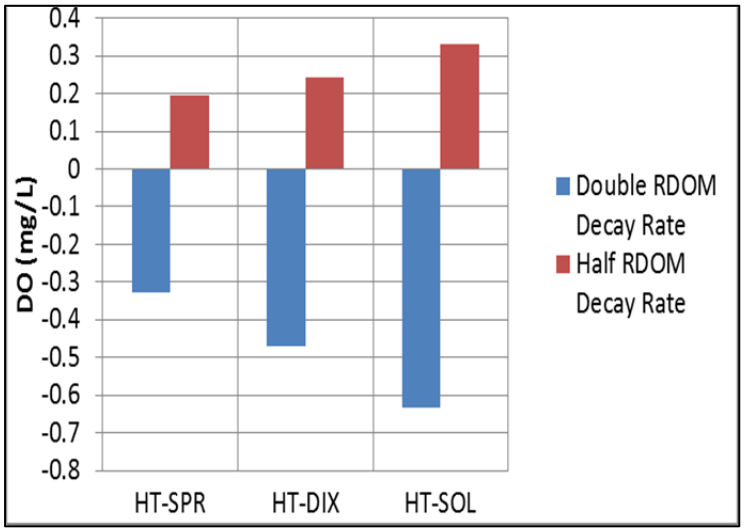

Figure 105. Simulated Change in Minimum Dissolved Oxygen Concentration at 15 m for Changes in RDOM Decay Rates

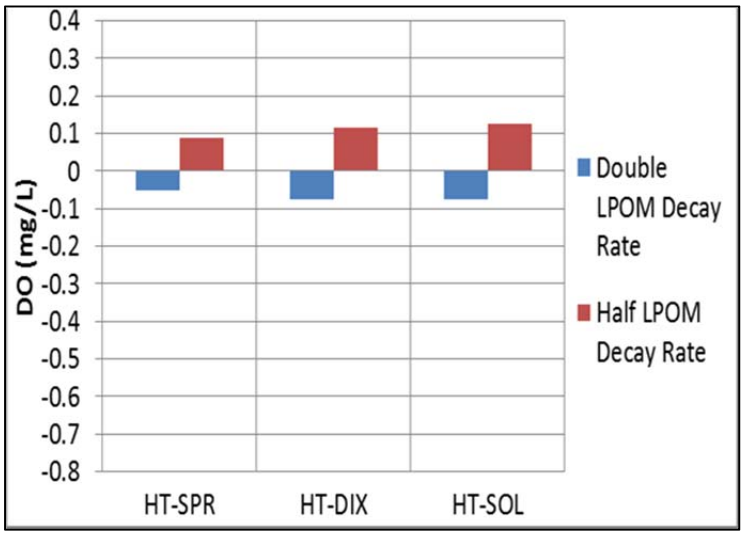

Figure 106. Simulated Change in Minimum Dissolved Oxygen Concentration at 15 m for Changes in LPOM Decay Rates

Simulated effects of LDOM and RDOM decay rate changes on dissolved oxygen at the bottom of the reservoir were very similar to those simulated at 15 m. For LPOM, however, a different result was simulated. As shown in Figure 107, for a doubling of the calibrated LPOM decay rate, there was a small increase in simulated dissolved oxygen at the bottom of the reservoir at the end of stratification. This result seems counterintuitive, but it suggests that, at the higher decay rate, LPOM is decaying before it can settle to the bottom of the reservoir.

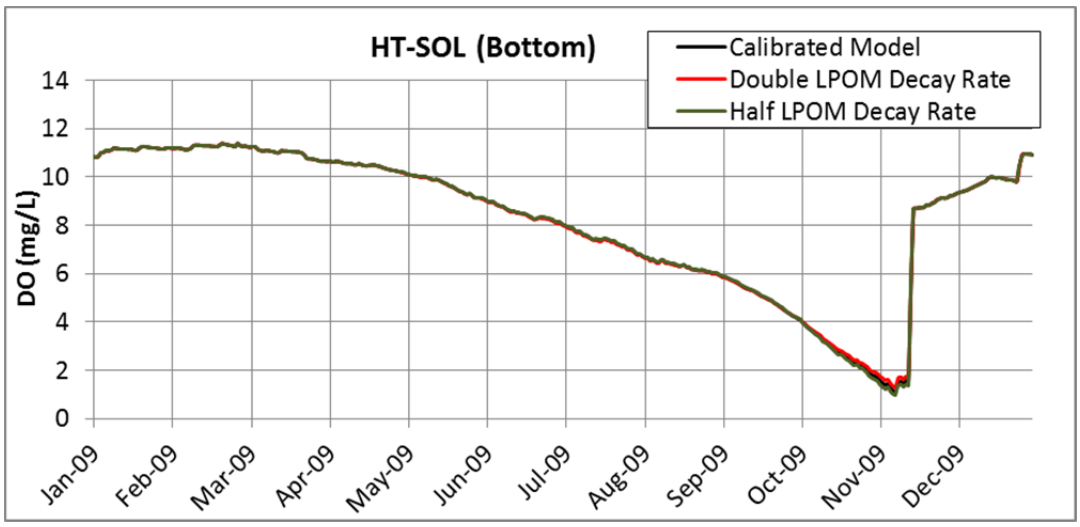

Figure 107. Simulated Dissolved Oxygen Concentrations at the Bottom at HT-SOL in 2009 for Changes to LPOM Decay Rates

4.1.2.4 Algal Settling Rates

Calibrated algal settling rates were varied by a factor of 0.5 and 2 to assess effects on simulated dissolved oxygen concentrations. As seen for other dissolved oxygen sensitivity runs, minimal effects on dissolved oxygen were simulated at the top of the reservoir. Minimal effects were also simulated at 15 m (very small increases in dissolved oxygen concentrations for decreases in algal settling). The bottom of the reservoir was slightly more sensitive, showing maximum increased dissolved oxygen concentrations on the order of 0.5 mg/L (Figure 108). These effects occurred during summertime stratification.

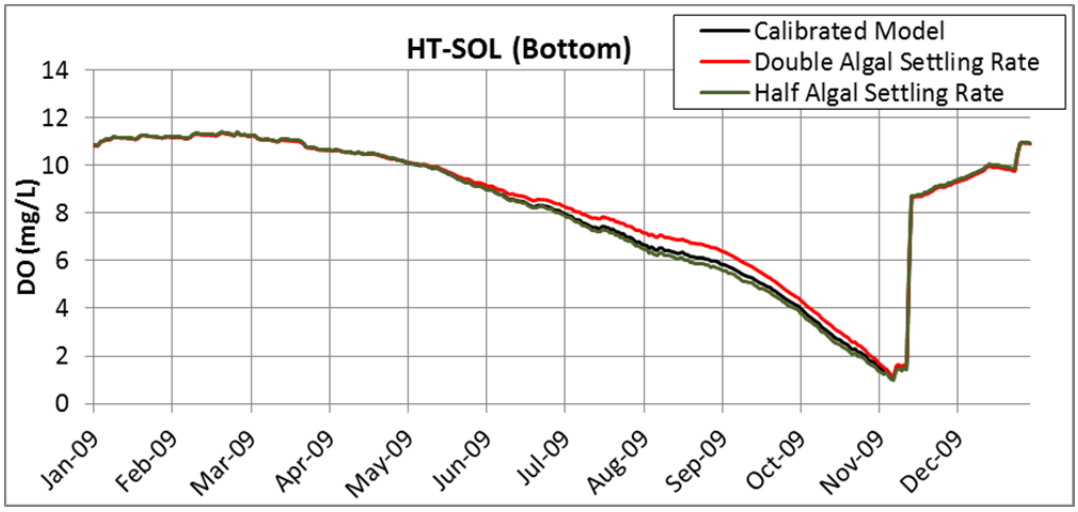

Figure 108. Simulated Dissolved Oxygen Concentrations at the Bottom at HT-SOL in 2009 for Changes to Algal Settling Rates

4.1.2.5 Sediment Oxygen Demand

Sediment oxygen demand (SOD) refers to the overall oxygen demand from sediment by biological, biochemical, and chemical processes. Originally, calibrated SOD values were halved and doubled; however, the doubling of SOD was considered unrealistic in some areas, so a run with a 50% increase in SOD was conducted. Sediment oxygen demand is a sensitive term in the Horsetooth Reservoir Model. At the bottom of the reservoir, large changes to dissolved oxygen concentrations were simulated for these modifications (Figure 109), significantly affecting the duration of the period of hypoxia and anoxia.

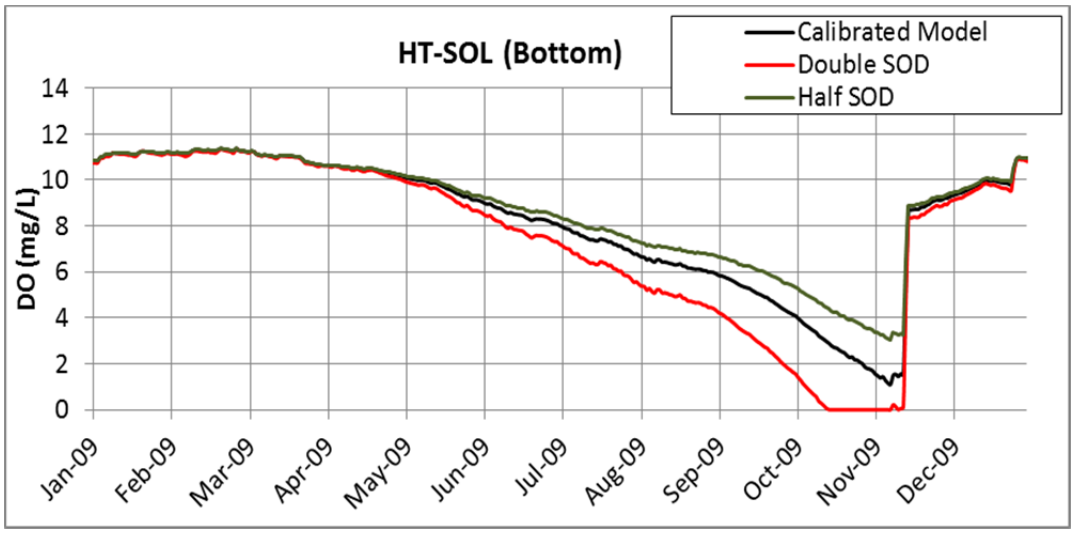

Figure 109. Simulated Dissolved Oxygen Concentrations at the Bottom at HT-SPR in 2009 for Changes to Sediment Oxygen Demand

There was also a significant, though lesser, effect on dissolved oxygen at 15 m (Figure 110). As simulated at the bottom of the reservoir, the effect was greatest at 15 m during stratification. The effect of a 50% increase (or a 50% decrease) in SOD at 15 m was a decrease (or increase) of the minimum annual dissolved oxygen concentration of ~1 to 2 mg/L.

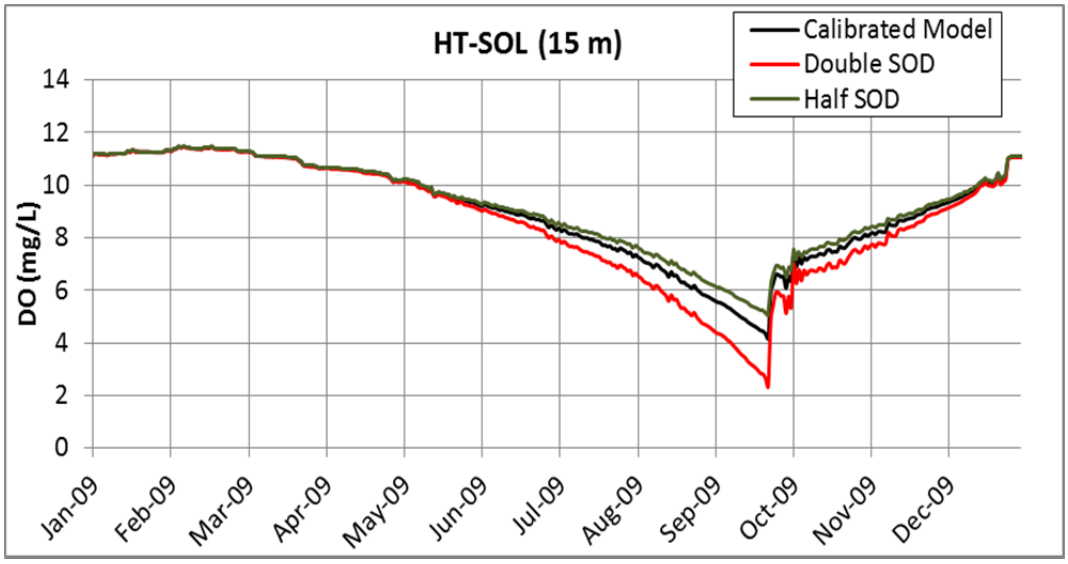

Figure 110. Simulated Dissolved Oxygen Concentrations at 15 m at HT-SOL in 2009 for Changes to Sediment Oxygen Demand

At the top of the reservoir, a slightly different response was simulated to changes in SOD. Effects on dissolved oxygen concentrations were minimal during stratification; however, effects were simulated in the period after stratification. Specifically, increased SOD lowered simulated dissolved oxygen after

turnover (Figure 111). During stratification, the epilimnion is more isolated, and reaeration can keep dissolved oxygen levels at or near saturation. After turnover, however, when waters are still somewhat warm and the reservoir is acting more as a whole, the effects of changes in SOD affect dissolved oxygen at all depths.

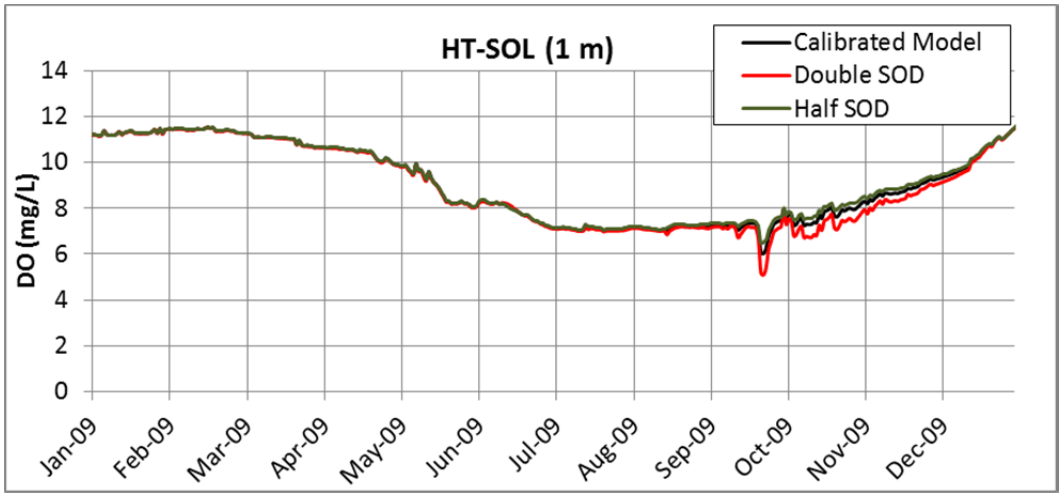

Figure 111. Simulated Dissolved Oxygen Concentrations at 1 m at HT-SOL in 2009 for Changes to Sediment Oxygen Demand

4.1.2.6 Reaeration Rates

The calibrated model applies the Kanwisher (1963) equation to calculate reaeration rates in the reservoir based on wind. CE-QUAL-W2 has a total of 14 lake reaeration equation options that assess wind and reaeration slightly differently. Two equations with responses different to the calibration selection were chosen to run for this analysis:

- Reaeration Equation Option # 4 – Wanninkhof et al. (1991)
- Reaeration Equation Option # 12 – Yu et al (1977)

The simulations results show similar dissolved oxygen concentration ranges at all levels, but there is a shift in the seasonal pattern at the top and at 15 m simulated by the various equations. Figure 112 presents the simulated dissolved oxygen concentrations at HT-SOL at the top of the reservoir for the three equations. Equation #4 and equation #12 show very similar results; however, the equation selected for calibration better matches the observed pattern. In general, the selected calibration equation produces greater reaeration at higher wind values, as compared to the other formulations. This may suggest a need for better input wind data (data collected at the reservoir), as the selected equation could be accounting for a difference between input and at-reservoir actual wind. For now, however, the calibrated equation can continue to be applied with reasonably good results.

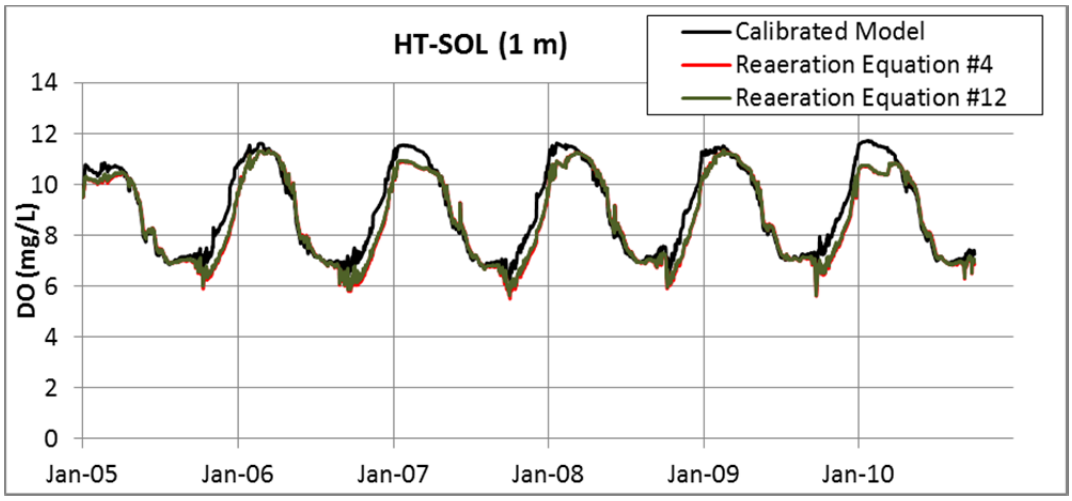

Figure 112. Simulated Dissolved Oxygen Concentrations at 1 m at HT-SOL for Different Reaeration Equations

4.1.3 Dissolved Oxygen Sensitivity Analysis Summary

Based on the result of the analysis presented in Sections 4.1.1 and 4.1.2, the key findings of the dissolved oxygen sensitivity analysis are:

- Dissolved oxygen at the top of the reservoir is relatively insensitive to changes in uncertain parameters because it is largely controlled and maintained near saturation by reaeration mechanisms.
- Metalimnetic low dissolved oxygen is primarily attributable to decay of inflowing dissolved (and to a lesser extent particulate) organic matter. Sediment oxygen demand is also an important control on metalimnetic dissolved oxygen due to direct sediment contact with the metalimnion (shelf and cove effects).
- Hypolimnetic low dissolved oxygen is strongly controlled by sediment oxygen demand and stratification duration each year. Water column organic matter decay and nitrification play only a small role in oxygen depletions at this depth.
- Of the uncertain settings assessed, degradability of the inflowing TOC is the most urgent data need to improve the model.

4.2 MODEL SCENARIOS

A preliminary set of modeling scenarios were simulated with the calibrated and validated Horsetooth Reservoir Model. These scenarios vary inputs related to operations and management, but they do not represent any particular proposed action. The purpose of conducting these simulations was to help inform the conceptual system understanding and support design of future scenarios. The scenarios simulated fall into three categories:

1. Reservoir Residence Time
    - 20% increase in residence time
    - 50% increase in residence time
2. Inflow TOC Concentrations
    - 2006 observed TOC inflow concentrations simulated for all years
    - 2010 observed TOC inflow concentrations simulated for all years
3. Inflow Nutrient Concentrations
    - 10%/ 50%/ 90% increase in PO4, NO3, and NH3
    - 10%/ 50%/ 90% decrease in PO4, NO3, and NH3
    - 50% increase and decrease in PO4 only
    - 50% increase and decrease in NO3 and NH3 only

In all, 14 simulations were completed. Review of results focused on the critical response parameters of chlorophyll *a*, dissolved oxygen (metalimnetic and hypolimnetic), and TOC in the outflow at Soldier Canyon. Additional analysis of run results and additional model runs could be conducted for more detailed investigation of each of these categories; however, that was beyond the scope of this phase of work. The following subsections describe the simulations further and present the key findings. Additional output summary information is provided in Appendix D.

4.2.1 Residence Time Simulations

Two scenarios were run as a preliminary assessment of the effects of increasing reservoir residence times in the reservoir. For these scenarios, increasing residence time was simulated by reducing inflow and outflow rates by a set percentage. Flow rates were reduced by 20% and 50%. Only Hansen Feeder Canal, Hansen Supply Canal, and Soldier Canyon flows were adjusted. No changes were made to inflow concentrations, meteorological inputs, or other settings.

Reducing both inflow and outflow rates for this system by a set percentage causes a few important changes that need to be understood to support evaluation of run results. First, as intended, reducing flow rates increases residence time. Figure 113 shows simulated water age in outflow from Soldier Canyon for the calibrated model and the two residence time scenarios. (Note that water age starts at zero across the reservoir at the start of each simulation, though a steady pattern is reached in the second year.)

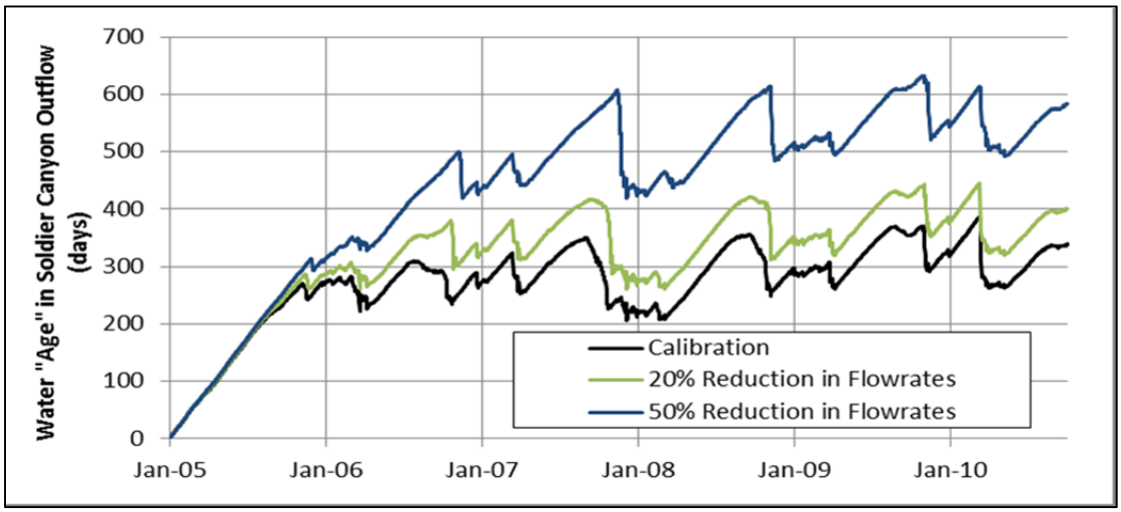

Figure 113. Model Simulated Water Age for Residence Time Scenarios

In addition to increasing residence time, the water levels and corresponding surface area vary over each year. Figure 114 presents simulated water levels for the calibrated model and the two residence time scenarios. As shown on this figure, because of the different timing of inflows and outflows, the net effect of reducing all flow rates is a decrease in spring/early summer water levels and an increase in fall/winter water levels. Decreases in inflow also cause corresponding decreases in inflow loading rates for nutrients and TOC.

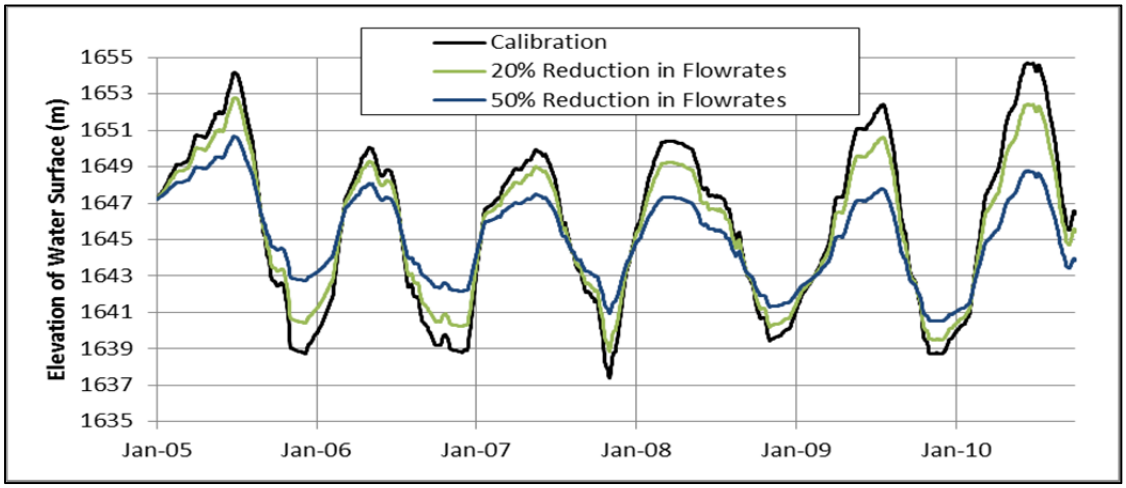

Figure 114. Model Simulated Water Elevation for Residence Time Scenarios

Finally, these changes to water levels and outflow rates can also affect turnover timing in the reservoir. First, water level can affect turnover timing. Typically, shallower water bodies are energetically easier to mix (turnover). While the differences in water level across the simulations is the smallest around the time of turnover (fall) each year (Figure 114), depths prior to turnover affect the heat balance in the system. Next, through analysis of the observed data and through development of the calibrated model,

it is recognized that outflow from the bottom of the north end of the reservoir can affect turnover timing, particularly at Soldier Canyon.

4.2.1.1 Chlorophyll *a*

The simulated changes to residence time produced some changes in peak chlorophyll *a* concentrations in some years (decreases with increased residence time), but overall the changes are relatively small. Figure 115 shows simulated chlorophyll *a* concentrations for the calibration run and the residence time scenarios at the top of HT-DIX. Results were similar across the reservoir. For the July through September period each year, the 20% decrease in flow rates resulted in a 1 to 2 % decrease in chlorophyll *a*. The 50% decrease in flow rates resulted in a 4 to 6% reduction in average chlorophyll *a* concentrations for the July through September period.

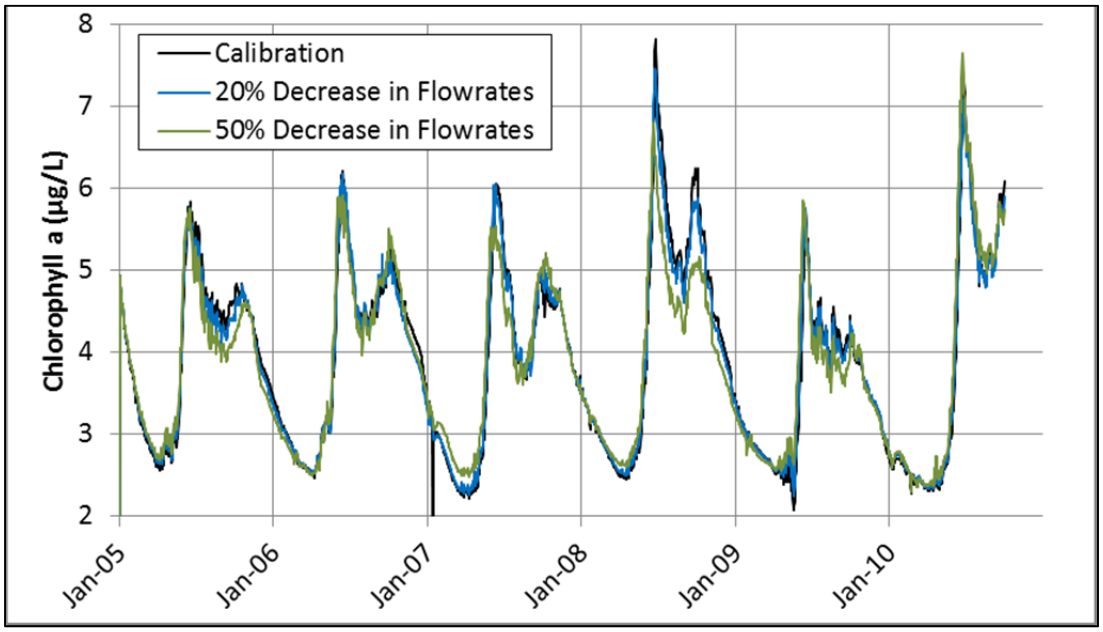

Figure 115. Simulated Chlorophyll a at HT-DIX for Residence Time Scenarios

4.2.1.2 Total Organic Carbon

Simulations increasing residence time resulted in lower TOC concentrations across the reservoir from top to bottom. Figure 116 and Figure 117 present simulated TOC concentrations at the top and bottom of the reservoir at HT-SOL for the calibration run and the residence time scenarios. Results were similar across the reservoir. The 20% reduction in flow rates decreased TOC concentrations over the year by an average of 2%, and the 40% reduction resulted in a 7% reduction in TOC. While there were slightly fewer algae, as discussed above, the change in algae only accounts for a very small fraction of the simulated change in TOC. Longer residence time allows more time for decay of organic matter. For perspective, a doubling of residence time only amounted to a decrease of less than 0.5 mg/L TOC across the reservoir. This is because most of the increased decay is from refractory organic matter, which is very slow to decay.

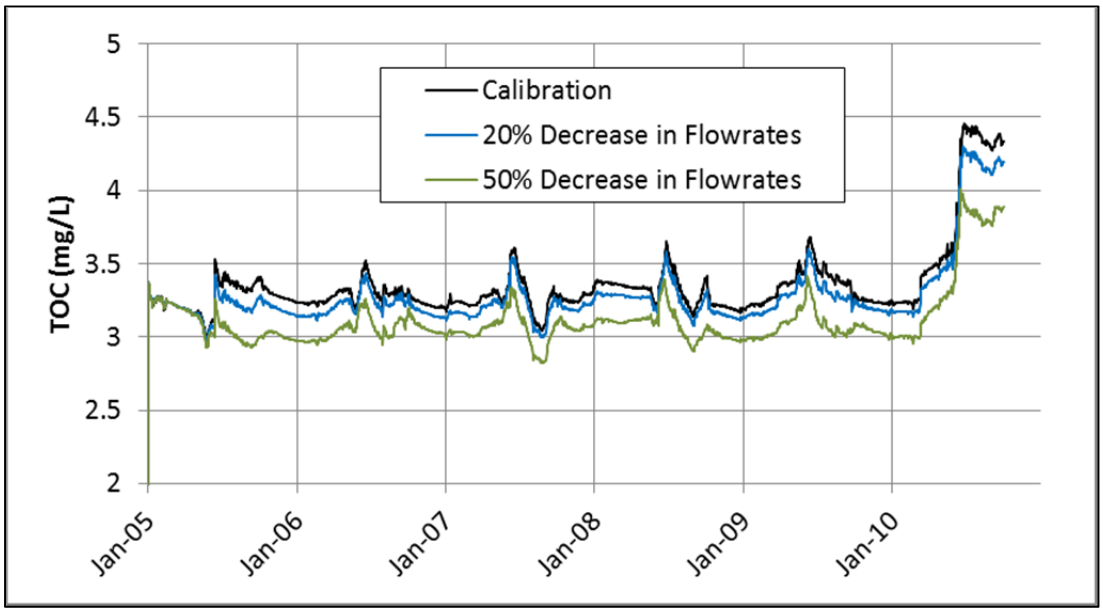

Figure 116. Simulated TOC at the Top of HT-SOL for Residence Time Scenarios

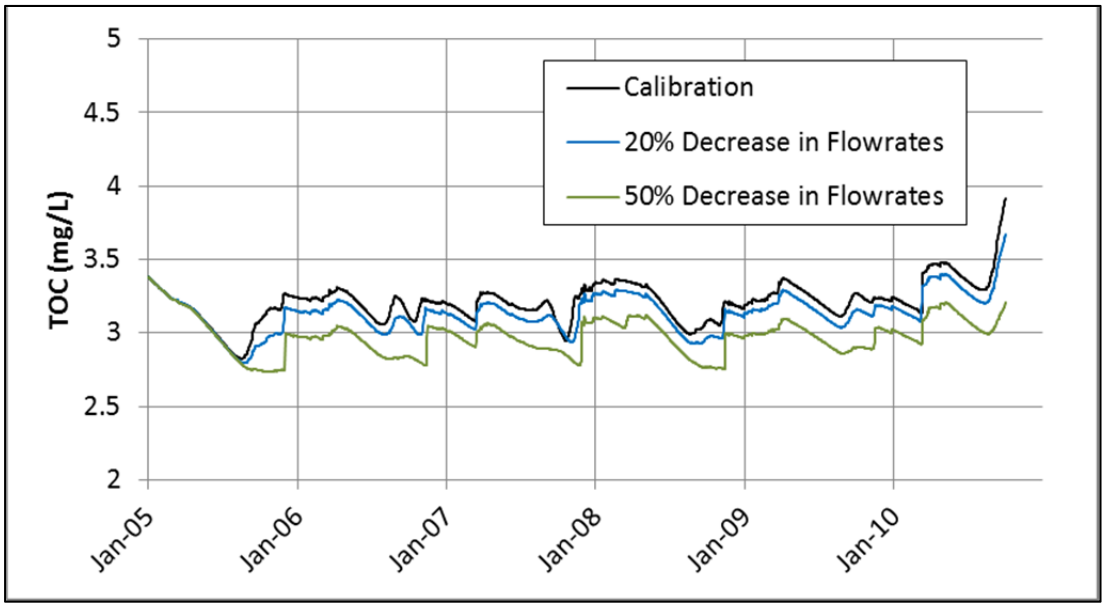

Figure 117. Simulated TOC at the Bottom of HT-SOL for Residence Time Scenarios

4.2.1.3 Dissolved Oxygen

The effect of decreasing inflow and outflow rates on dissolved oxygen concentrations in the metalimnion and epilimnion was largely related to the resulting delay in turnover. Each year of the simulation, turnover was delayed, with duration of delay varying from year to year. In general, the delay relative to the calibration run was longer at Soldier Canyon and shorter at Spring Canyon. Figure 118

and Figure 119 show the simulated dissolved oxygen concentrations at the bottom at HT-SPR and HT-SOL for the residence time scenarios. Average changes in the duration of anoxic condition at the bottom of the reservoir were increases of less than a day per year. On average, the changes in the duration of dissolved oxygen concentrations below 4 mg/L in the metalimnion were increases of less than a day per year.

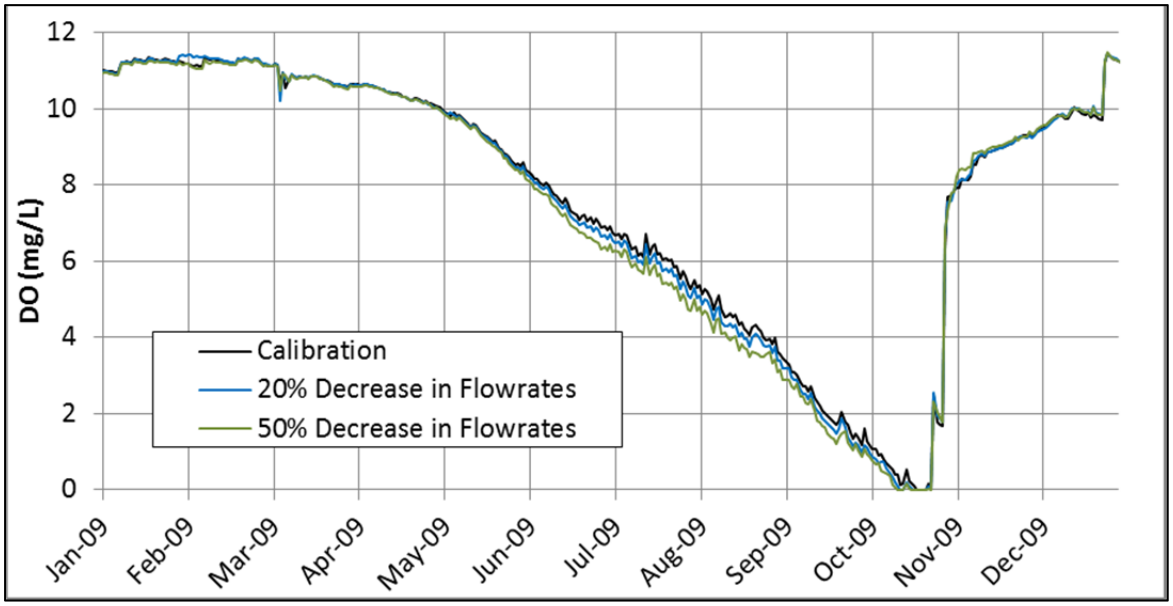

Figure 118. Simulated DO at the Bottom at HT-SPR for Residence Time Scenarios

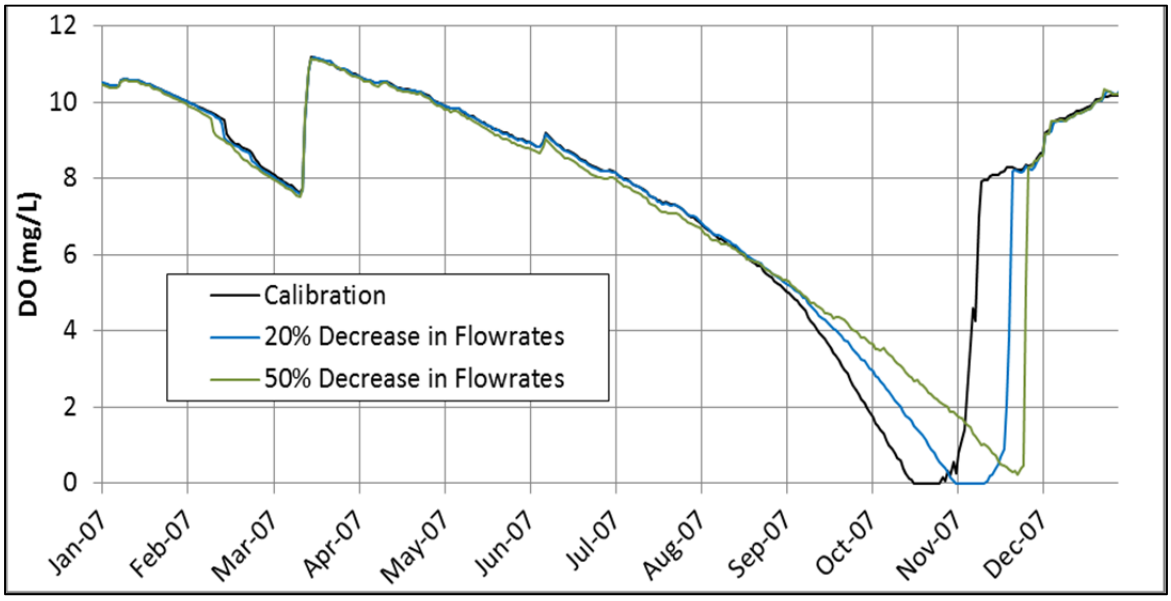

Figure 119. Simulated DO at the Bottom of HT-SOL for Residence Time Scenarios

4.2.2 Inflow Total Organic Carbon Scenarios

Two scenario runs were completed to assess the system response to a realistic range of different inflow TOC concentrations. First, 2006 inflow TOC concentrations were repeated for the full simulation period (2005 through September 2010). Next 2010 inflow TOC concentrations were repeated for the full simulation period. No other inputs were changed for these simulations.

Average TOC concentrations in 2006 were lower than the other simulated years, and 2010 concentrations were higher than the other simulated years. Figure 120 presents input TOC concentrations for each of the TOC Inflow scenarios. Overall, TOC concentrations in the 2006 run were 5% below the 2005-2010 average, with the biggest differences in 2005 and 2010. TOC concentrations for the 2010 run were 11% higher than the 2005-2010 average, with the biggest differences in 2006 through 2009.

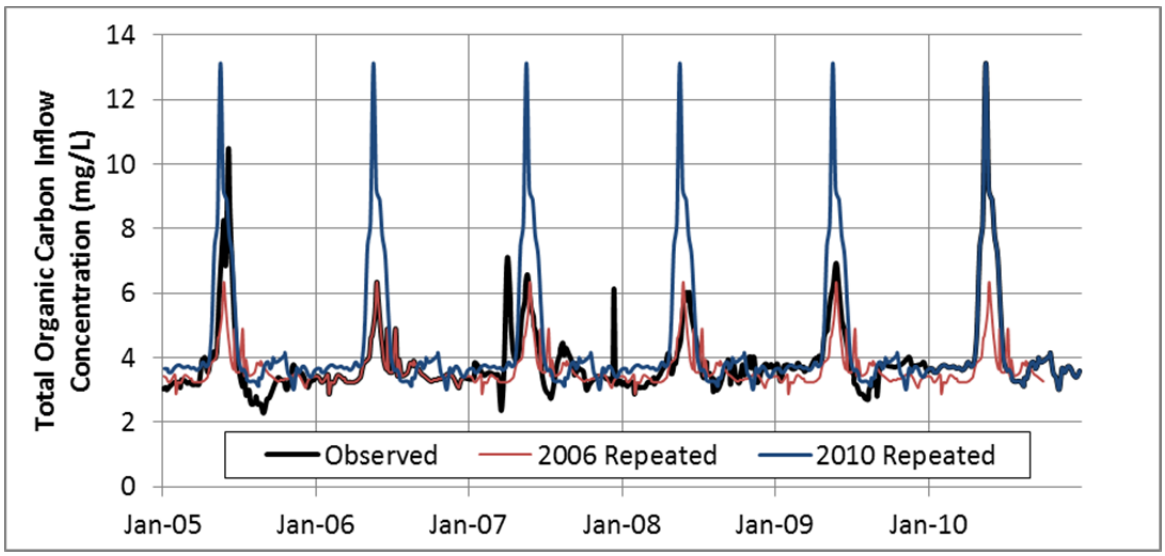

Figure 120. Inflow TOC Concentrations for TOC Inflow Scenarios

To develop model inputs, TOC values were fractionated into LDOM, LPOM, RDOM, and RPOM using the same ratios described in Section 3.3.3.2.1. The average labile and refractory organic matter concentrations for each year of the calibration/validation simulation are presented in Figure 121. Looking at the concentrations on this figure for 2006 and 2010 relative to the other years gives a better understanding of the input simulated. First, the TOC changes reflect larger mg/L changes in refractory organic matter concentrations, as compared to labile organic matter. Next, while average concentrations in 2006 were lowest for refractory fractions of organic matter, 2006 did not have the lowest average labile organic matter concentration of all years, which will be important to keep in mind while reviewing results. Finally, average labile and refractory organic matter concentrations in 2010 are higher than the other years.

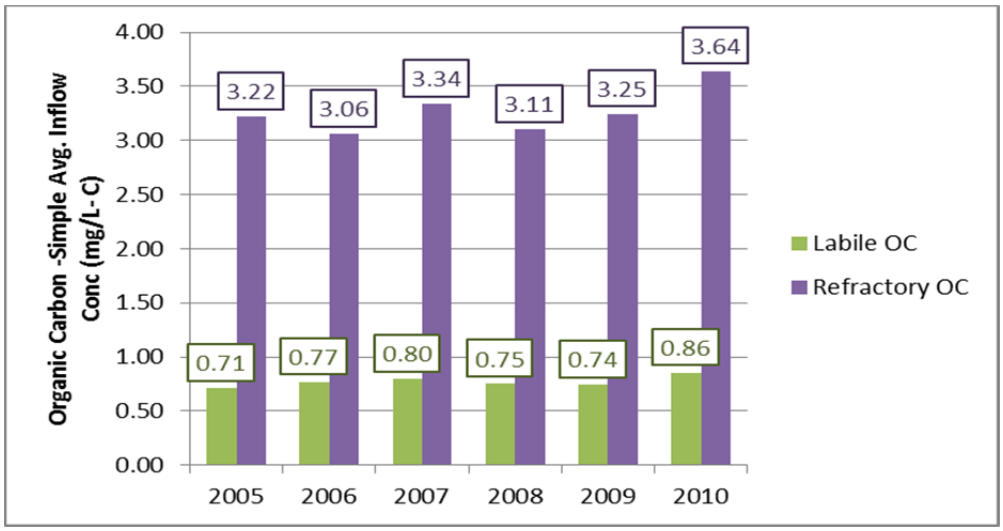

Figure 121. Average Inflow Concentrations of Labile and Refractory Fractions of TOC, 2005 through 2010

4.2.2.1 Chlorophyll *a*

Simulation of increased and decreased TOC resulted in some changes to chlorophyll *a* concentrations at the top of the reservoir. Figure 122 shows simulated chlorophyll *a* concentrations at HT-DIX for the scenarios. Results are similar across the reservoir. The effect varies from year to year and largely reflects the pattern of changes to inflow labile organic matter concentrations. Over the simulation period, the 2006 inflow TOC run produced a 6% decrease in chlorophyll *a* concentrations from July through September. The 2010 inflow TOC run produced a 4% increase in summertime chlorophyll *a* concentrations.

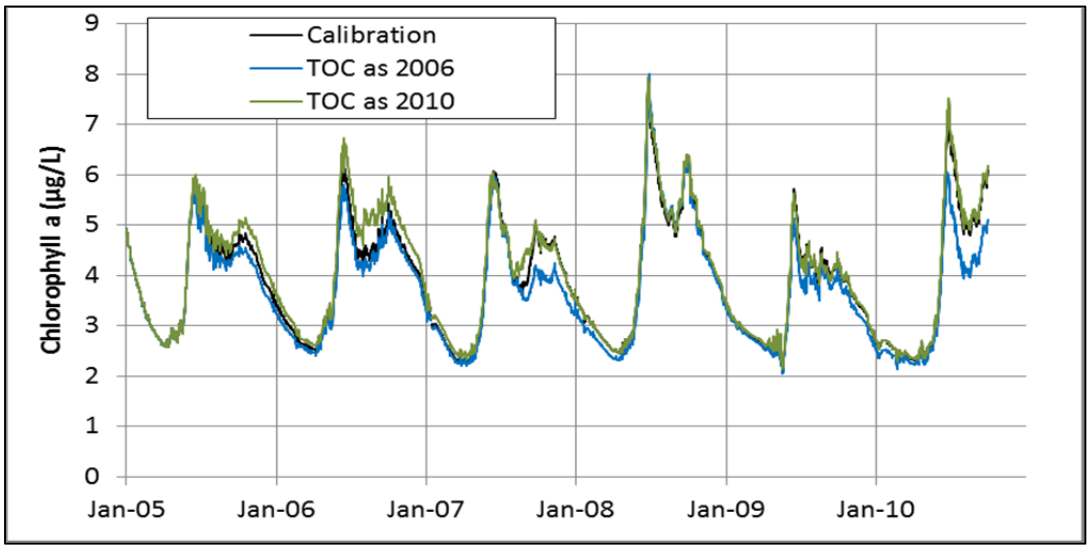

Figure 122. Simulated Chlorophyll *a* at HT-DIX for TOC Inflow Scenarios

4.2.2.2 Total Organic Carbon

The clearest response to changes in TOC inputs was in simulated TOC concentrations. Further, these simulated concentration changes largely reflect the differences in the refractory inputs. Figure 123 and Figure 124 present simulated TOC concentrations at the top of HT-SOL and in the Soldier Canyon outflow. At the top of the reservoir, the 2006 TOC inflow simulation resulted in an average decrease in TOC of 6% TOC over the simulation period. The 2010 TOC inflow simulation resulted in 9% more TOC. Changes were similar in the outflow from Soldier Canyon at -5% and +8%.

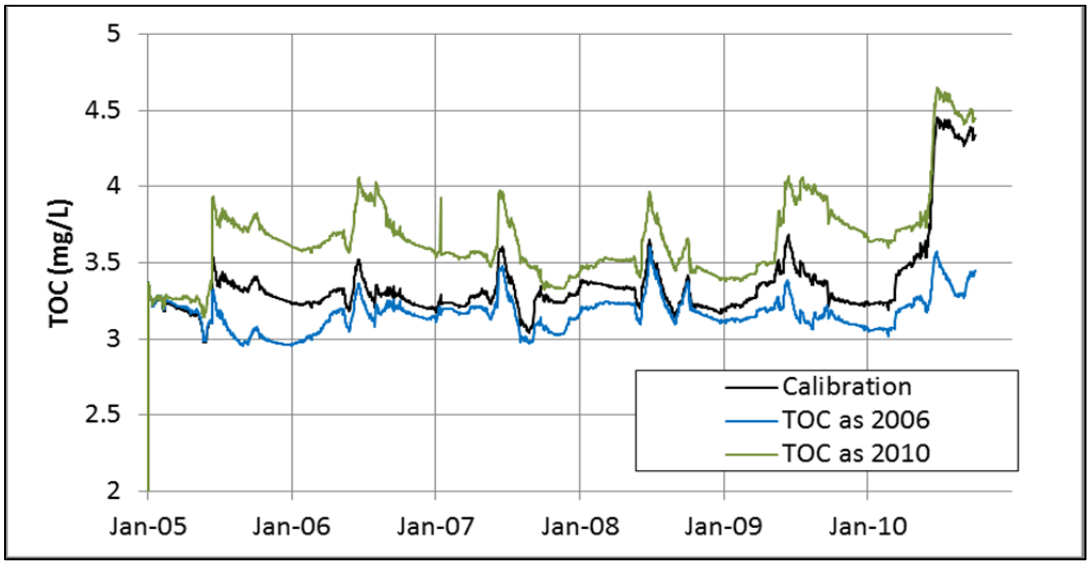

Figure 123. Simulated TOC at HT-SOL at 1 m for TOC Inflow Scenarios

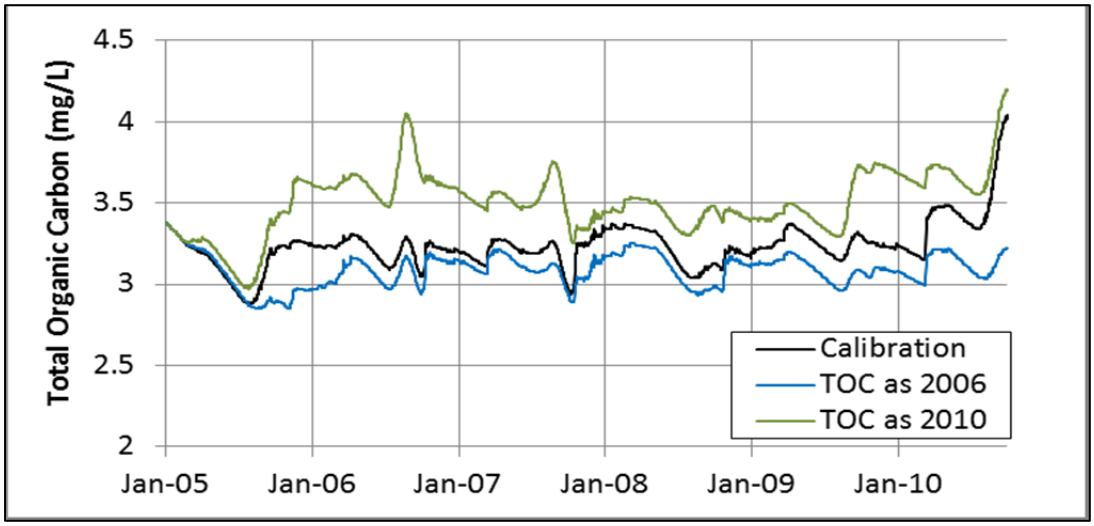

Figure 124. Simulated TOC in Outflow from Soldier Canyon for TOC Inflow Scenarios

Figure 123 and Figure 124 also show some interesting simulation results related to mixing and residence time. On these figures, the simulated concentrations in 2006 for the 2006 TOC inflow scenario do not match the calibration simulation concentrations in 2006. Likewise, simulated concentrations in 2010 for the 2010 TOC inflow scenario do not match the calibrated simulation concentration in 2010. TOC inflow concentrations from the previous year have an effect on concentrations at the top and the bottom in the reservoir in the subsequent year.

4.2.2.3 Dissolved Oxygen

Changing inflow TOC concentrations as simulated for these scenarios had an effect on simulated dissolved oxygen in the metalimnion and the hypolimnion, but the magnitude of the effect was relatively small. Figure 125 and Figure 126 show the simulated dissolved oxygen concentrations at 15 m and at the bottom of the reservoir for the calibrated model and the TOC inflow scenarios (results presented for 2009 at HT-SOL as an example of response simulated across the reservoir). The lower TOC of the 2006 TOC inflow scenario results in higher DO concentrations at the top and bottom of the reservoir, while the 2010 TOC inflow scenario resulted in lower DO concentrations. Over the full simulation period, the simulation periods caused only a one-day change in the number of day per year when DO in the metalimnion was less than 4 mg/L. For the hypolimnion, the average annual simulated change was 2 days of conditions below 2 mg/L DO.

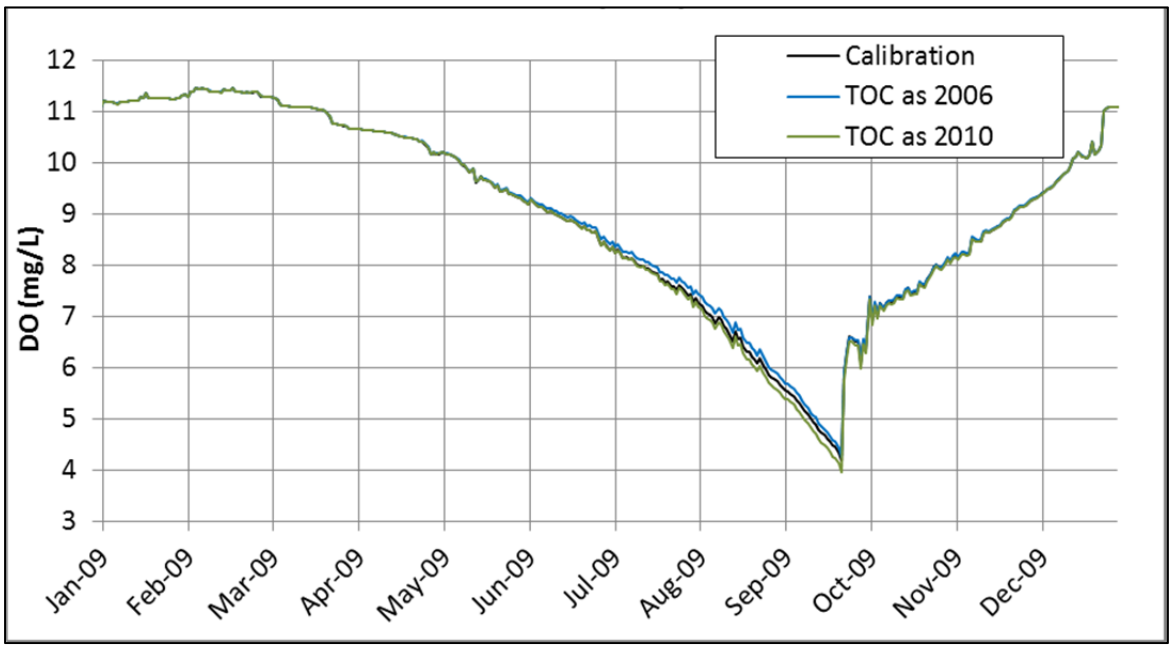

Figure 125. Simulated DO at HT-SOL at 15 m for TOC Inflow Scenarios

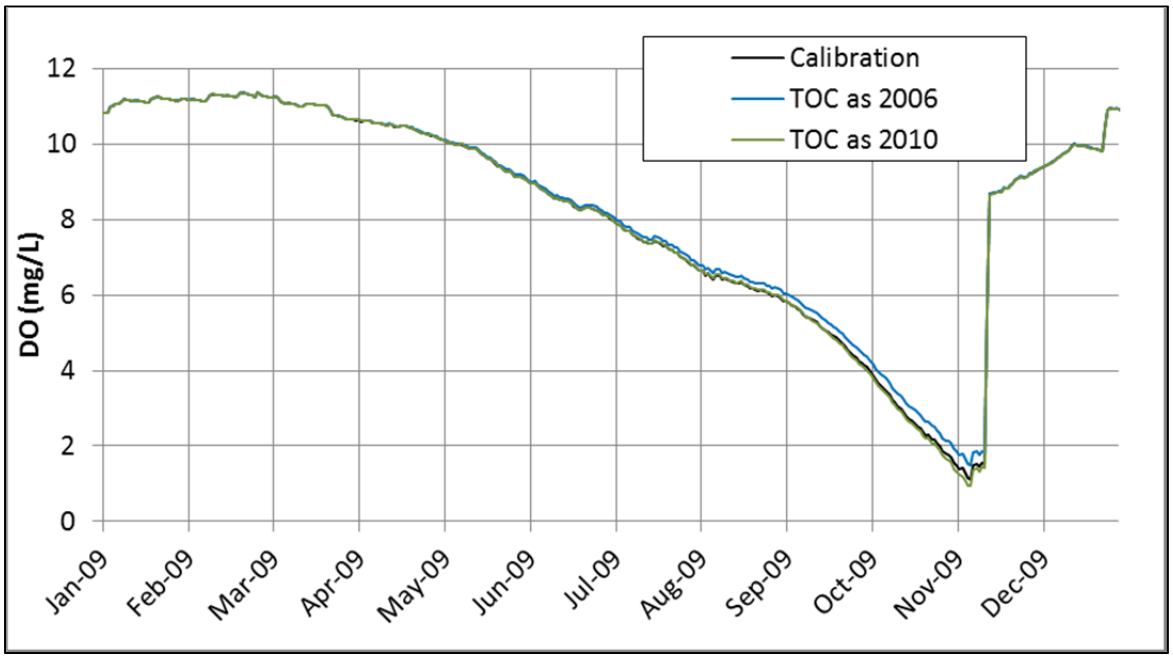

Figure 126. Simulated DO at HT-SOL at the Bottom for TOC Inflow Scenarios

Organic matter decay is expected to be a primary cause of the observed metalimnetic low DO, so a greater response might have been anticipated. However, as discussed above, these scenarios did not simulate large changes in labile organic matter concentrations. Further, there were not changes to meteorological condition and operations which determine the duration of stratification. This simulated response is reasonable considering the observed response in 2010. In 2010, when relatively high organic carbon concentrations entered the reservoir from Hansen Feeder Canal, dissolved oxygen concentrations in the hypolimnion and metalimnion were not markedly lower than those observed in the previous years, largely because much of the increased TOC was refractory.

4.2.3 Inflow Nutrient Concentration Scenarios

Inflow inorganic nitrogen (NH3 and NO3) and phosphorus (PO4) nutrient concentrations were varied together and separately. Concentrations were increased and decreased for all three nutrient species (NH3, NO3, and PO4) by 10%, 50% and 90%, relative to the observed dataset. Additionally, 50% increases and decreases were simulated for PO4 alone, then for NO3 and NH3 combined. No changes were made to other inputs or settings for these simulations.

4.2.3.1 Inflow NO3, NH3, and PO4 Scenarios

Chlorophyll *a*

10%, 50%, and 90% Increases and decreases to inflow inorganic nutrient concentrations (NO3, NH3, and PO4) caused increases and decreases in chlorophyll *a* concentrations across the reservoir. Simulated changes follow the same peak timing simulated for the calibrated model. Figure 127 presents results at

HT-DIX for the 50% nutrient increase and decrease simulations. The patterns shown in this figure are consistent with those simulated across the reservoir.

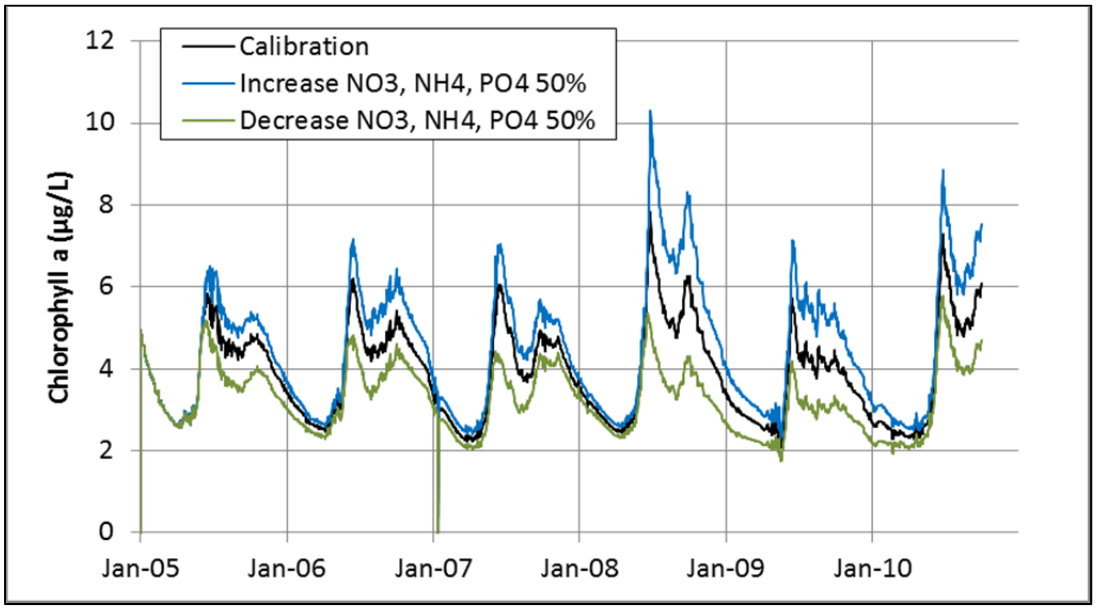

Figure 127. Simulated Chlorophyll a Concentrations at the Top of the Reservoir at HT-DIX for Nutrient Inflow Scenarios

Figure 128 shows simulated average percent changes in chlorophyll *a* across the reservoir for the various simulations. This figure shows that simulated effects on chlorophyll *a* concentrations were proportionately greater in the summertime than at other times of the year. This figure also shows that the magnitude of simulated change in chlorophyll *a* tends to be slightly greater for a 90% decrease in nutrients as compared to a 90% increase. This disproportional response is the results of crossing of a nutrient limitation threshold into a condition of strong nitrogen limitation. With the 90% decrease in NO3, NH3, and PO4, simulated PO4 concentrations are actually higher in the summertime as compared to the calibrated simulation (Figure 129), while NO3 (Figure 130) and NH3 bottom out.

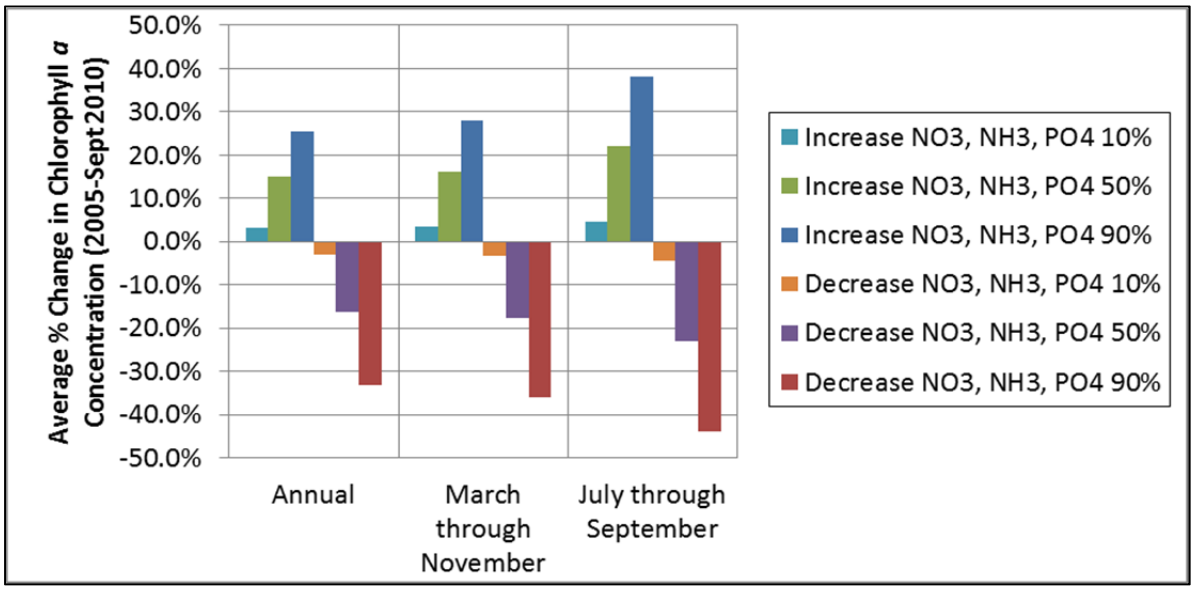

Figure 128. Simulated Average Percent Changes in Chlorophyll a Concentrations at the Top of the Reservoir for Nutrient Inflow Scenarios

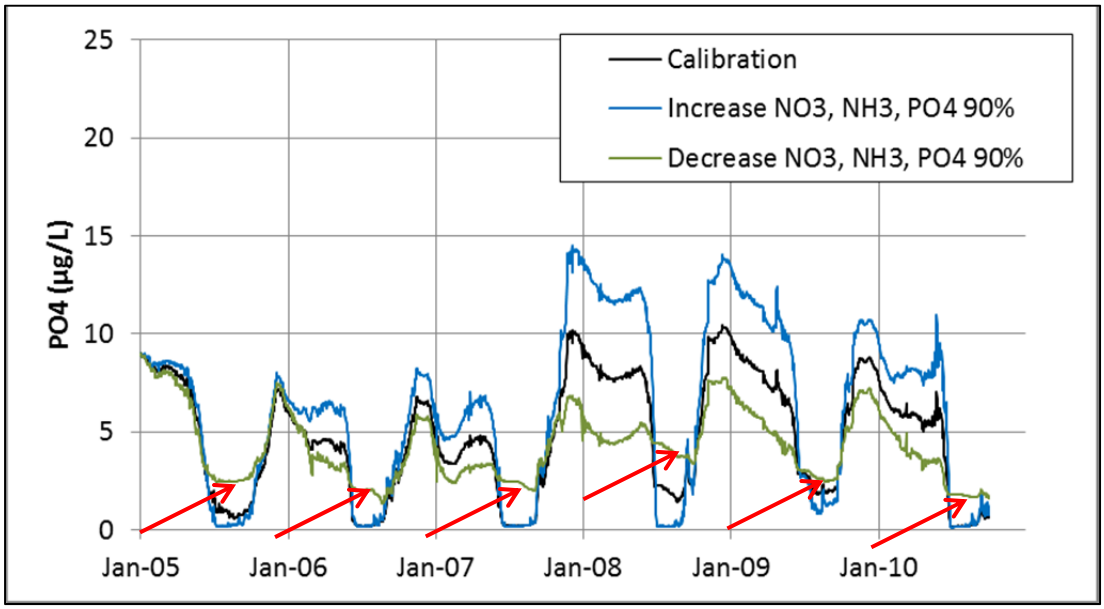

Figure 129. Simulated PO4 Concentrations at the Top at HT-DIX for ±90% Nutrient Inflow Scenarios
(Red arrows indicated summertime PO4 concentrations for the 90% concentration decrease scenario that are higher than the calibration run.)

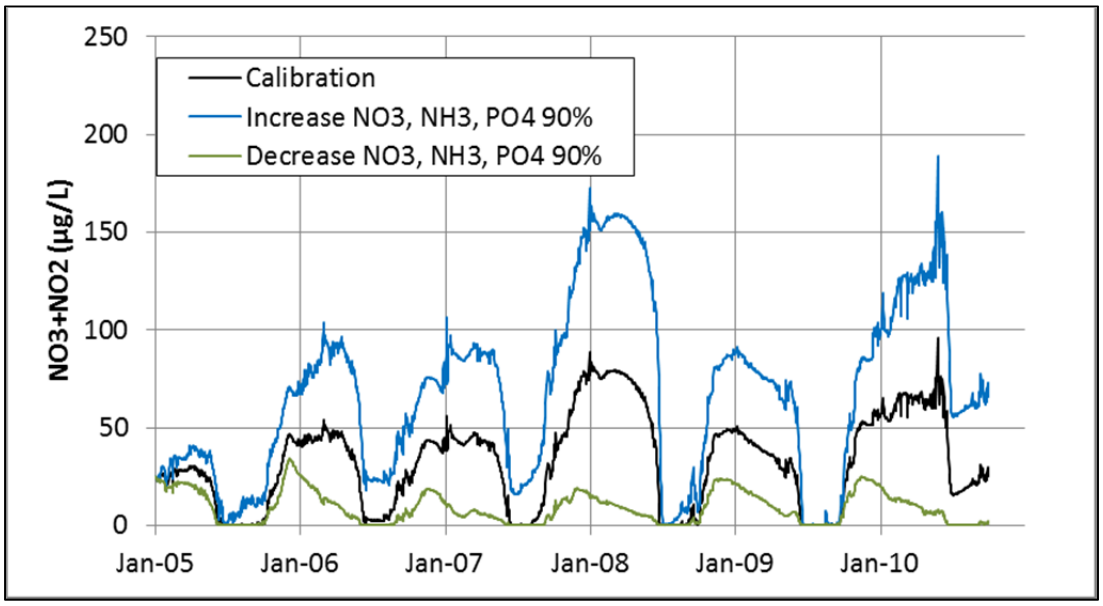

Figure 130. Simulated NO3 Concentrations at the Top at HT-DIX for ±90% Nutrient Inflow Scenarios

Further, between 50% and 90% increases in inorganic nutrients, conditions change enough to cause exceedances of the interim values for chlorophyll *a* standards (CDPHE, 2012b) for direct use water supply (DUWS) reservoirs. The interim value is 5 ug/L chlorophyll *a* (averaged from March through November and not to be exceeded more than once every five years). Figure 131 and Figure 132 present 50% and 90% inflow nutrient simulation results, respectively, compiled using the March-through-November-average metric. Results are shown for chlorophyll *a* concentrations simulated at HT-DIX, but concentrations were generally similar across the reservoir. As shown on these figures, the calibration runs shows no exceedances of the 5 ug/L value in any simulated year. For the 50% increase (Figure 131) in NO3, NH3, and PO4, results show exceedances of this value for one of the six years simulated (2008). For the 90% increase (Figure 132), results show exceedances in four out of the six years simulated (2006, 2008, 2009, and 2010). Further, it should be noted that the effect of increases in nutrient concentrations could be higher since it could be reasonably expected that higher chlorophyll *a* concentrations would enter the reservoir if nutrient concentrations were higher in the Hansen Feeder Canal (inflow chlorophyll *a* concentrations were not changed in these simulations).

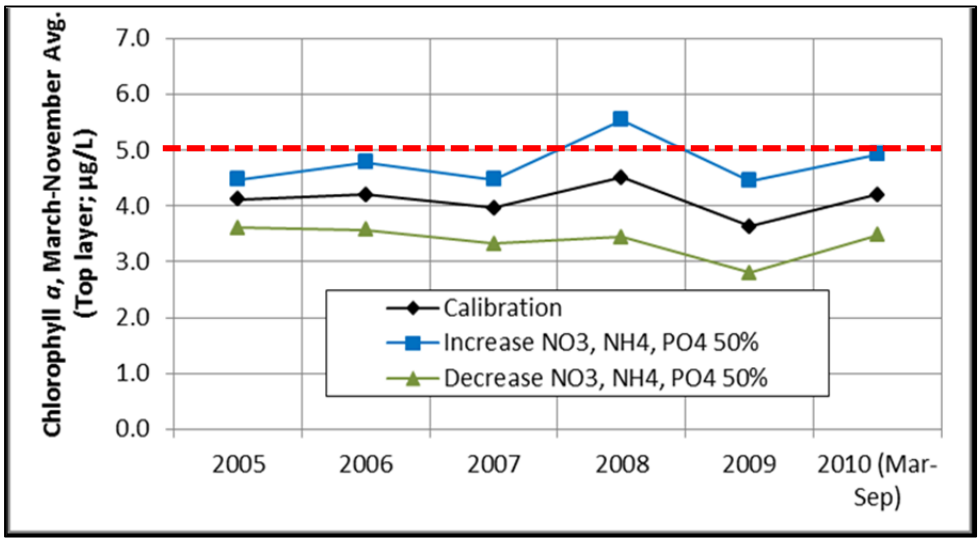

Figure 131. March through November Average Chlorophyll *a* Concentrations Simulated at HT-DIX for ±50% Inflow Nutrient Concentrations

Red line indicates interim DUWS chlorophyll *a* values (CDPHE, 2012).

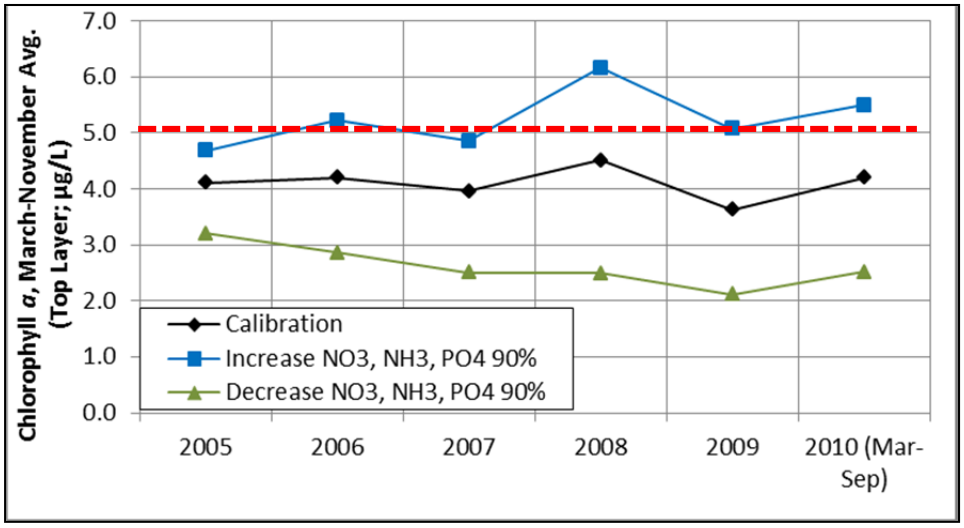

Figure 132. March through November Average Chlorophyll *a* Concentrations Simulated at HT-DIX for ±90% Inflow Nutrient Concentrations

Red line indicates interim DUWS chlorophyll *a* values (CDPHE, 2012).

Dissolved Oxygen

Dissolved oxygen concentrations in the metalimnion and hypolimnion showed relatively small responses to 10% changes in inflow nutrients, but 50% and 90% changes showed greater effects. As anticipated, effects on dissolved oxygen were limited to summer stratification. Figure 133 summarizes the response for each simulation at the bottom of the reservoir and at 15 m.

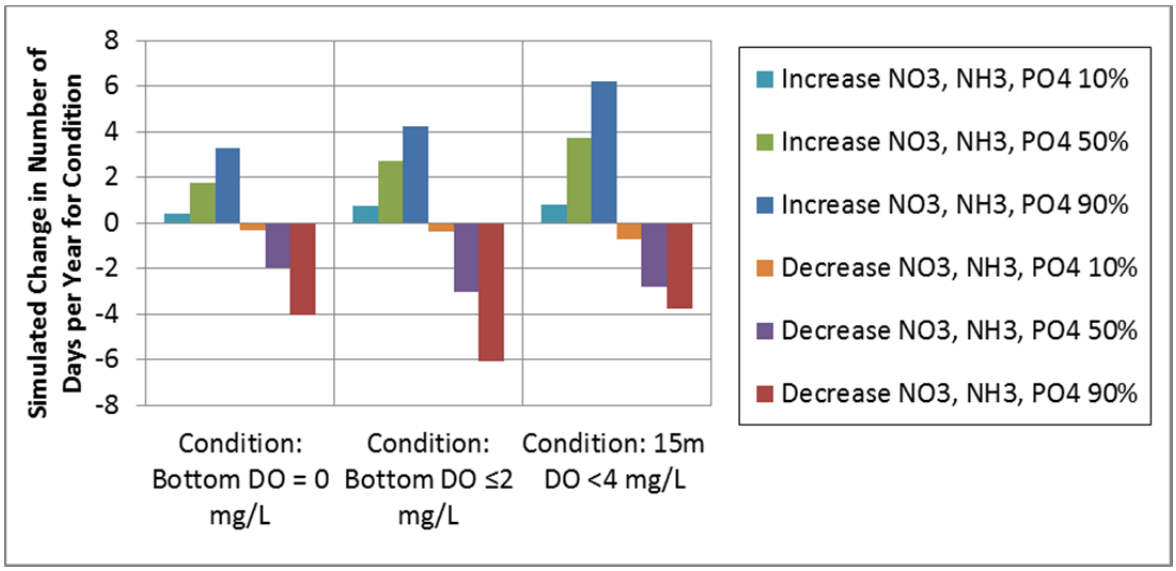

Figure 133. Summary Metrics of Simulated DO Response at 10 m and at the Bottom for Nutrient Inflow Scenarios

Total Organic Carbon

Changes to inflow nutrient concentrations resulted in relatively small changes to simulated TOC concentrations throughout the reservoir. Increasing inflow nutrient concentrations by 90% resulted in less than a 0.2 mg/L increase in TOC across the reservoir. This relatively small change in TOC concentrations reflects the small fraction of the TOC that is attributable to living and dead algae. Further, as described in Section 3.3.3.3, the model simulates produce labile dissolved and particulate organic matter through algal excretion and mortality, which are readily degradable, particularly in warm summertime waters. Figure 134 and Figure 135 show simulated TOC concentrations at the top and bottom at HT-SOL for the ±90% inflow nutrient scenarios. At the top of the reservoir (Figure 134), the greatest effects of the nutrient inflow simulations on TOC tend to occur in the summer months, directly reflecting effects on algal growth. At the bottom of the reservoir (Figure 135), however, the greater effects on TOC are simulated to occur in winter months. This reflects mixing at turnover and slower decay rates in winter months.

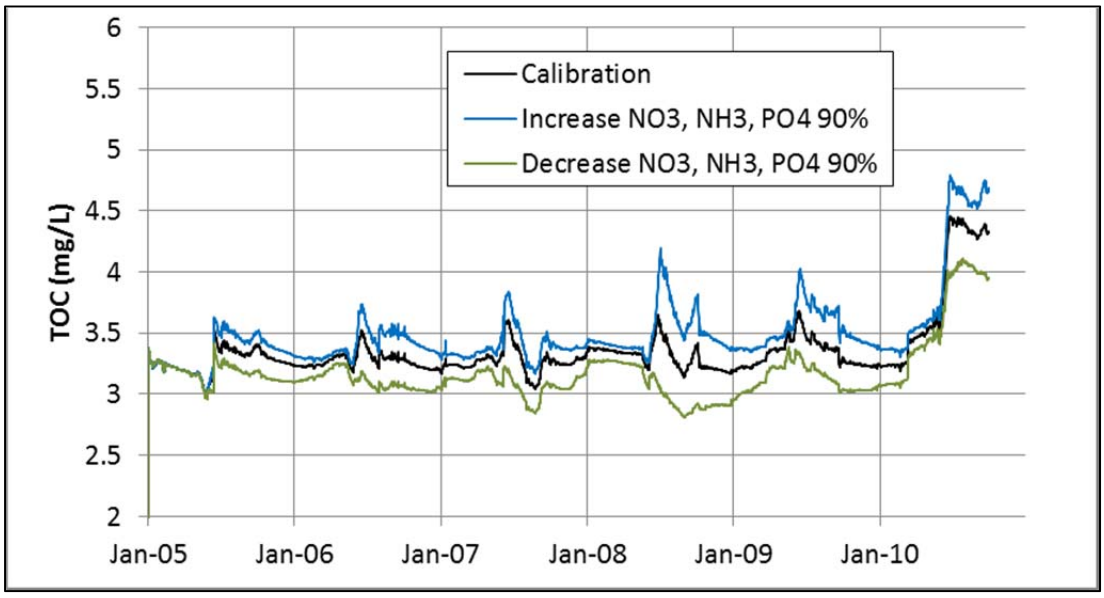

Figure 134. Simulated TOC Concentrations at the Top at HT-SOL for ±90% Nutrient Inflow Scenarios

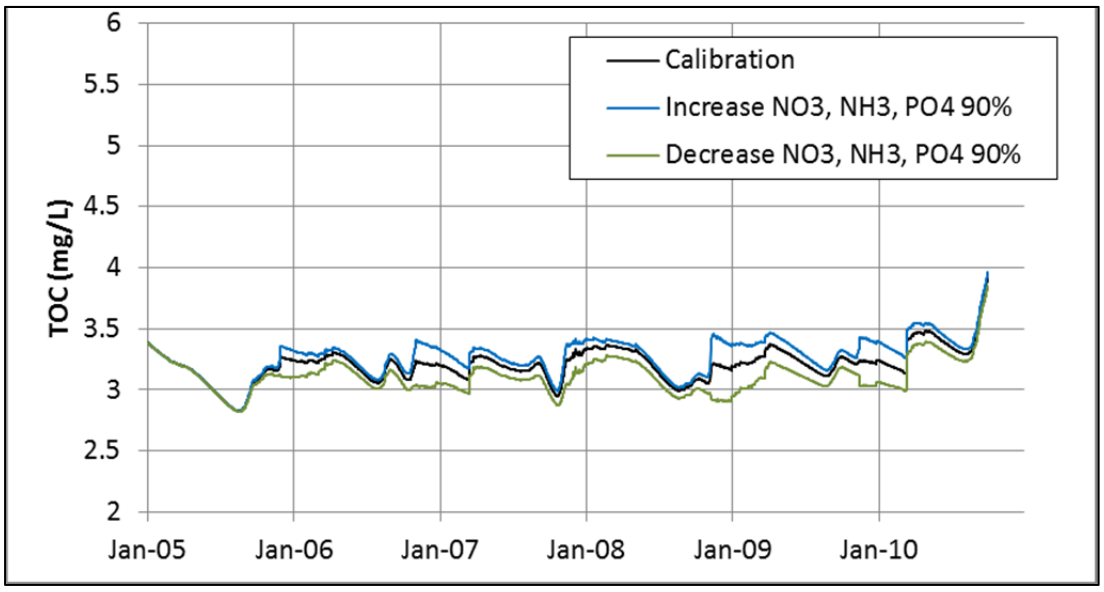

Figure 135. Simulated TOC Concentrations at the Bottom at HT-SOL for ±90% Nutrient Inflow Scenarios

4.2.3.2 Inflow Nitrogen or Phosphorus Scenarios

The modeling scenarios included simulations varying only inorganic nitrogen nutrient species (NO3 and NH3) or only inorganic phosphorus nutrient species (PO4) to assess the relative importance of each on the system. Four runs were conducted, varying concentrations of each by ±50%. For dissolved oxygen and TOC, effects were similar to but lower in magnitude than those simulated for the ±50% runs for

NO3, NH3 and PO4, discussed above. Likewise, increased concentrations of either nutrient resulted in slightly lower dissolved oxygen concentrations in the metalimnion and hypolimnion, as well as small increases in TOC through the reservoir at times.

Chlorophyll *a* results for the individual nutrient scenarios provided some information about nutrient limitations in the reservoir. First, 50% reductions in either inorganic nitrogen or inorganic phosphorus inflows resulted in larger absolute effects on chlorophyll a concentrations than 50% increases. This is apparent in Figure 136, which shows average percent changes in chlorophyll a concentrations at the top of the reservoir for July through September for the individual nutrient scenarios.

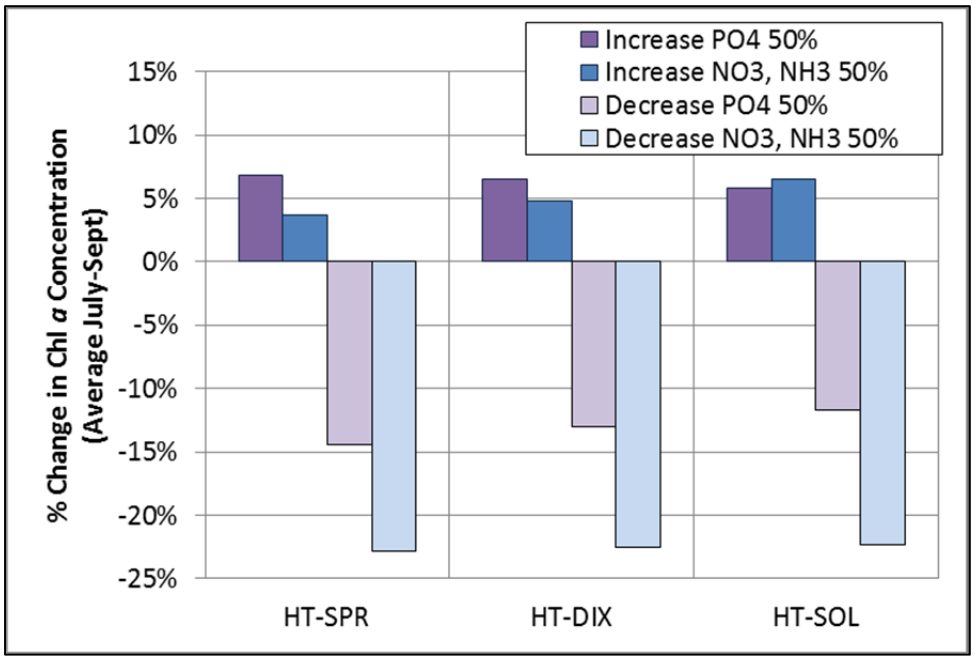

Figure 136. Simulated Average Percent Changes in Chlorophyll *a* Concentrations at the Top of the Reservoir for Individual Nutrient Inflow Scenarios

4.2.4 Model Scenarios Summary

As noted above, review of scenario results focused on in-reservoir response of chlorophyll *a*, dissolved oxygen (metalimnetic and hypolimnetic), and TOC. TOC response in the outflow at Soldier Canyon was also assessed. Additional investigation of modeling results as well as additional modeling runs could be conducted to provide further insights into simulated responses; however, that was beyond the scope of this phase of work. Based on the result of the analysis presented in Sections 4.2.1 through 4.2.3, the key findings of the model scenario simulations are:

Increased Residence Time Simulations

- Increased residence time simulations also included effects on reservoir water levels (due to timing of outflows relative to inflows) and hydrodynamics (due to outflow rates) which resulted

in delayed turnover. The effect was greatest at HT-SOL, closest to the bottom withdrawal locations.

- The increased residence time scenarios produced small reductions in chlorophyll *a* peak concentrations.
- Increased residence times resulted in reduced TOC concentrations throughout the year from top to bottom in the reservoir. The effect was relatively limited though, due to the predominance of refractory organic matter and its corresponding slow decay rate.
- Dissolved oxygen concentrations are slightly higher in the metalimnion and hypolimnion with increased residence time, but the effect is countered by delayed turnover.

Inflow Total Organic Carbon Scenarios

- Changes to inflow TOC need to be understood in terms of changes to labile and refractory fractions of the inflowing organic matter to best predict in-reservoir responses.
- The simulated increased TOC caused small increases in chlorophyll *a* and decreases in dissolved oxygen, which largely reflected the increases in labile organic matter inflows. The opposite pattern was simulated for decreases in inflow TOC.
- Changes to inflow TOC concentrations had direct effects on in-reservoir and outflow TOC concentrations, which largely reflected the changes to inflow refractory organic matter concentrations.
- Inflow TOC concentrations from the previous year have an effect on concentrations at the top and the bottom in the reservoir in the subsequent year.

Inflow Inorganic Nutrient Concentration Scenarios

- Increased (and decreased) inflow nutrient concentrations result in higher (and lower) simulated chlorophyll a concentrations across the reservoir, but do not appear to change the timing of peaks.
- Between a decrease of 50% and 90% of inflow inorganic nutrient concentrations, the reservoir experiences strong nitrogen limitations on algal growth. Under current conditions, the reservoir is considered to be co-limited for nitrogen and phosphorus.
- Between an increase of 50% and 90% of inflow inorganic nutrient concentrations, the model begins to simulate exceedances of the interim DUWS value for the chlorophyll *a* standard.
- Increasing inflow concentrations of inorganic nutrients results in lower metalimnetic and hypolimnetic dissolved oxygen concentrations. The changes, however, are relatively small, reflecting a relatively small role for algae in creating oxygen depletions of concern in the reservoir.

- Simulated changes to inflow concentrations of inorganic nutrients produced only small changes in TOC concentrations throughout the reservoir. This is a reflection of the small fraction of in-reservoir TOC that is algae or dead algae and the relatively rapid decay rate of products of algal mortality and excretion.

5 FINDINGS AND RECOMMENDATIONS

A dynamic, two-dimensional hydrodynamic and water-quality model has been developed using CE-QUAL-W2 version 3.6 to simulate Horsetooth Reservoir. The model was calibrated for a five-year period (2005-2009) and validated using 2010 data. This report documents model development, calibration, validation, and application to a set of preliminary scenarios. This section presents a summary of findings and recommendations generated by this project. All findings presented here are considered preliminary and subject to further development and consideration. With ongoing updates of the model, the conceptual understanding of the system will continue to advance. Also, application of the model to additional scenarios may adjust or refine the understanding of the system and further test the model.

Findings:

1. The two-dimensional model developed for this project successfully simulates Horsetooth Reservoir hydrodynamics and key water-quality constituents. The model is capable of simulating:

    - Nutrient uptake patterns,
    - Sediment releases of nutrients,
    - Algal growth,
    - Total organic carbon concentrations, including Soldier Canyon outlet concentrations,
    - Negative heterograde dissolved oxygen curve (low dissolved oxygen in the metalimnion), and
    - Low dissolved oxygen in the hypolimnion.

2. The observed metalimnetic low dissolved oxygen condition in the reservoir is primarily attributable to degradation of inflowing organic matter from the Hansen Feeder Canal, which enters the reservoir as an interflow at the elevation of the metalimnion. Another process contributing to low metalimnetic dissolved oxygen is sediment oxygen demand from sediments directly in contact with the metalimnion (shelf and cove effects).

3. The observed longitudinal changes in hypolimnetic low dissolved oxygen condition across the reservoir are strongly controlled by sediment oxygen demand and the duration of stratification each year. Sediment oxygen demand is higher in Spring Canyon as compared to Soldier Canyon. This is expected to be attributable to the proximity of Spring Canyon to the inflow from Hansen Feeder Canal and settling of inflow particulate material into that canyon. As a result, observed hypolimnetic dissolved oxygen concentrations are lower in the southern portion of the reservoir than in the north.

4. The composition (specifically degradability) of the inflowing total organic carbon strongly affects dissolved oxygen minima in the reservoir and total organic carbon concentrations in outflow from Soldier Canyon.

5. Both inorganic nitrogen and phosphorus species in the inflow are important to algal growth in the reservoir.

6. Operations affect some key aspects of water quality.

    - Inflow and outflow rates affect mixing in the metalimnion during stratification.

- Residence time and seasonal reservoir water levels affect dissolved oxygen and total organic carbon concentrations.
- Bottom withdrawals influence the duration of stratification, with the greatest effects observed at Soldier Canyon.

Recommendations for Future Work:

1. Overall, the dataset and ongoing monitoring plans for Horsetooth Reservoir are excellent; however, the following primary and secondary data needs were identified to improve the model:

   - Primary data need: Lack of data on the composition of inflowing total organic carbon, in terms of degradability, is a critical data gap. Reservoir water quality is sensitive to the labile-to-refractory breakdown of inflowing organic matter. This composition varies seasonally and likely from year to year. At a minimum, collection of biochemical oxygen demand data at the inflow from Hansen Feeder Canal would be helpful for modeling, but more advanced analyses should also be discussed.
   - Secondary data need: Through calibration, it was noted that collection of chlorophyll *a* data in winter months, to the extent possible, could help improve simulation of algae, total organic carbon, and nutrients throughout the year.
   - Secondary data need: Ideally, wind speed and direction would be collected at the reservoir instead being based on data from a station to the east. Wind is an important control on reservoir reaeration and stratification/turnover. Constructed on a hogback at the edge of the foothills, the reservoir is in a location with complicated and variable wind dynamics that can vary on the ground over short distances, and the data from east of the site is not always representative of conditions over the reservoir.

2. It would be useful to assess system response to the different seasonal pattern of reservoir water levels that occurred in the dry year of 2012. More could be learned about the system, and the model could be further tested and improved with simulation of 2011 and 2012 observed conditions.

3. The model was constructed for use in simulation of operational scenarios, and the following is a list of potential general applications that have been discussed by the technical committee. There are no current plans to conduct these applications, and others may be identified in the future:

   - The model would be well suited for simulation of realistic operation scenarios to improve or manage water quality. This may involve changes to inflows, inflow locations, outflows, locations of outflows (multi-level outlet), or inflow water quality, reflecting changes to reservoir management approaches.
   - The model could be applied to simulate management scenarios for wildfire response to water-quality impacts that could affect Hansen Feeder Canal.
   - The model may be useful to support investigation by the Colorado Parks and Wildlife into concerns about rainbow smelt populations. Prior to this, the model would need a closer look at algae-zooplankton dynamics and effects of inflow algae concentrations on key water-quality concerns in the reservoir.

6 REFERENCES

Beggs, K.M.H. 2010. Doctoral Dissertation: Characterizing temporal and Spatial Variability of Watershed Dissolved Organic Matter and Disinfection Byproduct Formation with fluorescence Spectroscopy. University of Colorado, Department of Civil and Environmental Engineering.

Billica, J.A. and J. Oropeza. 2010. 2009 Horsetooth Reservoir Water Quality monitoring Program Report. Prepared for the City of Fort Collins Utilities. September 13, 2010.

Billica, J.A., J. Oropeza, and G.K. Elmund. 2010. Monitoring to Determine Geosmin Sources and Concentrations in a Northern Colorado Reservoir. In: Proceedings of the National Water Quality Monitoring Council 7th National Monitoring Conference (April 25-29, 2010, Denver).

Billica, J.A. 2013. Personal Communication. Email to Christine Hawley on January 16, 2013.

Chapra, S.C. 1997. Surface Water Quality Modeling. Reissued 2008 by Waveland Press, Inc.

Cole, T.M., and S. A. Wells. 2008. "CE-QUAL-W2: A two-dimensional, laterally averaged, Hydrodynamic and Water Quality Model, Version 3.6," Department of Civil and Environmental Engineering, Portland State University, Portland, OR.

Colorado Department of Public Health and Environment (CDPHE). 2012a. Colorado's 303(D) List of Impaired Waters and Monitoring and Evaluation List. 5 CCR 1002-93 (Regulation 93). Water Quality Control Commission. Amended February 13, 2011; Effective March 30, 2012.

Colorado Department of Public Health and Environment (CDPHE). 2012b. The Basic Standards and Methodologies for Surface Water. 5CCR 1002-31 (Regulation 31). Water Quality Control Commission. Amended June 11, 2012; Effective September 30, 2012.

Ecological Research Associates. 1996. Horsetooth Reservoir Preliminary Limnological Assessment. Prepared for Fort Collins Water Utility. January 4, 1995.

Haby, P.and J. Loftis. 2007. Retrospective Analysis of Water Quality Data in the Big Thompson Watershed 2001-2006. Volume 1: Report. Prepared for The Big Thompson Watershed Forum.

Hydros Consulting Inc. 2011. Big Thompson State of the Watershed, 2010 Report. Developed for The Big Thompson Watershed Forum. February 4, 2011.

INTERA and CH2MHill. 2006. Horsetooth Reservoir Water Balance and TOC Evaluation: Data Inventory and Modeling Assessment, Final Draft Technical Memorandum. Prepared for Fort Collins Utilities. November 27, 2006.

Jassby, A., and C. Goldman. 1998. Horsetooth Reservoir 1996 Water Quality Conditions. Prepared for the City of Fort Collins Water Utility. Prepare by Ecological Research Associates. July 2, 1998.

Jassby, A., and C. Goldman. 1999. Horsetooth and Carter Lake Reservoirs Water Quality Comparisons. Prepared for the City of Fort Collins Water Utility. Prepare by Ecological Research Associates. October, 1999.

Johnson, B. M., J. Butteris, and M. Dodrill. 2006. Final Report: Ecosystem monitoring during Horsetooth Reservoir Refilling. Prepare for USBR. Prepared by CSU Fisheries Ecology Laboratory. April 10, 2006.

Kanwisher, J. 1963. On the Exchange of Gases Between the Atmosphere and the Sea. Deepsea Research with Oceanography; Vol 10. pp 195-207.

Lieberman, D. 2008. Physical, Chemical, and Biological Attributes of Western and Eastern Slope Reservoir, Lake, and Flowing Water Sites on the C-BT Project, 2005 - 2007: Lake Granby, Grand Lake, Shadow Mountain Reservoir, Horsetooth Reservoir, Carter Lake. Prepared for Northern Colorado Water Conservancy District.

Wannikof, R., Ledwell, J. R., and Crusius, J. 1991. Gas Transfer Velocities on Lakes measured with Sulfur Hexafluoride. In Symposium Volume of the Second International Conference on Gas Transfer at Water Surfaces, S. C. Wilhelms and J. S. Gulliver, eds., Minneapolis, MN.

Yu, S.L., T.J. Tuffy, and D.S. Lee. 1977. Atmosphere Reaeration in a Lake; Office of Water Resources and Technology, U.S. Department of the Interior.